The establishment and use of tissue engineered vascular models to investigate the pleiotropic effects of statins

Wanjiku Njoroge
Institute for Science and Technology in Medicine
Keele University

Thesis submitted for the degree of
Doctor of Philosophy

June 2021

Contents

Abstract

Cardiovascular disease (CVD) has been identified as the leading cause of mortality in westernised society. The triggering factor for the majority of cardiovascular diseases is atherosclerosis, defined as an accumulation of fatty materials in the vascular sub-endothelial space. This results in the initiation and propagation of inflammatory responses that result in the narrowing of the vascular lumen, as well as thickening and hardening of arteries. The initiating stimulus in atherosclerosis is elevated levels of low-density lipoprotein (LDL) in circulation, and the cells involved in this process are primarily endothelial cells-which interact with blood-, smooth muscle cells-which facilitate the contraction and relaxation of large diameter blood vessels-, and macrophages, which are immune cells that are able to take up and store lipids. As inflammation progresses, the endothelium becomes dysfunctional and expresses adhesion molecules that facilitate the entry of monocytes into the sub-endothelial space, where they differentiate into macrophages, take up LDL and become foam cells. These lipid rich foam cells are a key component of atherosclerotic plaques, together with dead cells that make up the necrotic core. Statins have been established as the gold standard for the treatment of atherosclerosis, and have been useful in decreasing morbidity and mortality in CVD patients. They function by preventing cholesterol synthesis through inhibition of HMG-CoA, thus lowering amounts of circulating cholesterol. In addition to this function, a number of pleiotropic effects have been associated with statin treatment including, increasing numbers of circulating endothelial progenitor cells (EPCs), reduce inflammation, improve atherosclerotic plaque stability and improve engraftment of MSCs into sites of vascular injury.

To investigate these pleiotropic effects of this ubiquitous drug used in the treatment of the most prevalent disease, we developed tissue engineered blood vessel models that incorporated endothelial cells (Human umbilical vein endothelial cells (HUVECs)) and smooth muscle cells (Human cardiac artery smooth muscle cells (HCASMCs)) to represent the intimal and medial layers of the vasculature and could be used individually (Tissue engineered intimal layer-TEIL and tissue engineered medial layer-TEML) or in concert as a full blood vessel (tissue engineered blood vessel-TEBV). These vessel

models/constructs were subjected to shear stress and used to evaluate the effect atorvastatin has on the homing of endothelial progenitor cells, the production of SDF-1 and expression of its receptor CXCR4. Further to this, the effect of atorvastatin on initiating cholesterol efflux was also investigated with considerations made to examine the role of HUVECs and smooth muscle cells in this process. The experiments conducted for this thesis were able to determine that atorvastatin increases the density of cells attached onto the surface of a lesioned construct. This was observed for the partial blood vessel models (TEIL and TEML) as well as the TEBV. This effect was noted for human mesenchymal stem cells (hMSCs) as well as EPCs. Observations in EPCs were consistent under both high (22.16 dyne/cm^2) and low (2.2 dyne/cm^2) shear stress. We were also able to determine that atorvastatin is more functional when used in conditions of oxidative stress through examination of different lesioning techniques. $FeCl_3$ induced oxidative damage resulted in the recruitment of more cells to the surfaces of the lesioned constructs as well as higher levels of SDF-1, compared to the mechanical lesion which generated a mild surface abrasion. It was also possible to demonstrate that atorvastatin increases secretion of SDF-1 and expression of CXCR4, which are the main cytokine and receptor associated with cell homing and migration. This effect was determined to be both time and dose dependent. Through the use of different blood vessel models, it was determined that the cells in each layer have differing responses to the composite tissue model i.e., observations of cell attachment and SDF-1 production on TEBV were an amalgam of TEIL and TEML responses. Through the use of nanofiber inserts to create a novel HUVEC-RAW264 co-culture system, we were able to demonstrate that atorvastatin triggers consistent cholesterol efflux from cultured foam cells compared to drug free controls, resulting in up to a 13% reduction in amounts off internalised cholesterol, a phenomenon that is affected by HUVEC integrity i.e., lesioned HUVECs promoted cholesterol efflux, especially in the presence of atorvastatin and IFN-γ. Atorvastatin was also able to restrict nitric oxide (NO) production in macrophages and may reverse the effects of the inflammatory cytokine IFN-γ. The models used here proved a useful tool for investigating the effects of atorvastatin, and could prove useful in evaluating cellular responses to a wider array of pharmacologic, or other stimuli.

Acknowledgements

First and foremost, I would like to thank my primary supervisor, Professor Ying Yang for her encouragement and support throughout, I doubt I would have finished without your help. I would also like to thank Dr. Alan Harper for all the help and encouragement. To the members of Ying's group, my second family, thank you so much for all the conversations, laughter and support and for making this experience truly worthwhile. I would like to extend a special thank you to Hati, Matt, Vibin, Jacob, Fatma, Tasmin, Trish and David for offering me friendship and companionship and making my time spent with you all time I will never regret. Sheila, my "bestie", our conversations were a lifeline, thank you for keeping me sane and grounded. I would also like to express my gratitude to the Guy Hilton staff, it was wonderful getting to know you. Finally, I would like to thank my mother, Professor Mary Wambui Ndung'u and father, Captain Njoroge Murimi Kuria for the immeasurable contribution to my pursuit of a doctorate, I would literally be nothing and nowhere without you.

Publications and Conferences

Publications

i. Njoroge W, Hernández ACH, Musa FI, Butler R, Harper AGS, Yang Y. **The Combination of Tissue-Engineered Blood Vessel Constructs and Parallel Flow Chamber Provides a Potential Alternative to In Vivo Drug Testing Models**. Pharmaceutics. 2021;13(3):340. DOI:10.3390/pharmaceutics13030340.

ii. Baig MS, Owida HA, Njoroge W, Siddiqui AR, Yang Y. **Development and evaluation of cationic nanostructured lipid carriers for ophthalmic drug delivery of besifloxacin**. Journal of Drug Delivery Science and Technology, 2020;55. https://doi.org/10.1016/j.jddst.2019.101496.

iii. Gater R, Njoroge W, Owida HA, Yang Y. **Scaffolds mimicking the native structure of tissues. Handbook of Tissue Engineering Scaffolds**. Volume One, Chapter 2. Editors: Mozafari M, Sefat F, Atala A. Woodhead Publishing, 2019

iv. Sandhu K, Njoroge W, Yang Y, Harper AGS and Butler R. **Endothelial Progenitor Cell Identification, Classification and Nomenclature: A Review.** Journal of Blood and Lymph. 2018;8(2):221. DOI: 10.4172/2165-7831.1000221.

v. **TCES (Tissue and Cell Engineering Society) Conference 2018** (poster): Njoroge W, Harper A, Butler R, Sandhu K, Yang Y. **Atorvastatin effect on migration of endothelial cells and bone marrow stem cell homing in a wound model.** https://www.ecmconferences.org/abstracts/2018/Collection4/c4.html (Page 55).

Conferences

i. **ISTM Symposium (2019)** (Oral presentation): Njoroge W, Harper A, Butler R, Sandhu K, Yang Y**. An investigation into the pleiotropic effects of statins: Use of a 3D blood vessel model to evaluate the mechanisms of EPC homing**

ii. **International Symposium on Biomechanics in Vascular Biology and Cardiovascular Disease (BVBCD) (2019)** (poster)**:** Njoroge W, Harper A, Butler R, Sandhu K, Yang Y. **Atorvastatin Effect on Homing of MSCs and EPCs on a 3D Blood Vessel Model**

iii. **Aorta: From Structure to Rupture (2019)** (Attendee)

iv. **ISTM Symposium (2019) ISTM Symposium (2018)** (Poster): Njoroge W, Harper A, Butler R, Sandhu K, Yang Y. **Atorvastatin Effect on Migration of Endothelial Cells and Bone Marrow Stem Cell Homing in a Wound Model**

List of figures

List of abbreviations

- 3-hydroxy-3-methylglutaryl coenzyme A reductase (HMG-CoA)
- 3-Isobutyl-1-methylxanthine (IBMX)
- 5-(and-6) carboxyfluorescein diacetate, succinimidyl ester, mixed isomers (CFSE)
- ABCG1 (ABCG1)
- Acetylated low-density lipoprotein (AcLDL)
- Acid citrate dextrose (ACD)
- Angiopoietin (Ang-1)
- Angiotensin II (AII)
- Antidiuretic hormone (ADH)
- ATP-binding cassette transporters A1 (ABCA1)
- Bare metal stents (BMS)
- Bovine serum albumin (BSA)
- Cell counting kit-8 (CCK-8)
- Chronic obstructive pulmonary disease (COPD)
- Circulating angiogenic cell (CAC)
- Circulating endothelial precursors (CEP)
- Colony-forming Unit Epithelial cell (CFU-EC)
- Copper sulphate (CuSO4.5H2o)
- Dedicator for cytokinesis (DOCK4)
- Deionised water (dH_2O)
- Drug eluting stent (DES)
- Early Outgrowth EPC (CFU-EC, CFU-Hill, CAC)
- Embryonic stem cells (ESCs)
- Endothelial cells (ECs)
- Endothelial colony forming cell (ECFC)
- Endothelial nitric oxide synthase (eNOS)
- Endothelial progenitor cells (EPCs)
- Endothelins (ET-1)
- Extracellular matrix (ECM)
- Foetal bovine serum (FBS)
- Granulocyte-colony-stimulating factor (G-CSF)
- Hepatocyte growth factor (HGF),
- High density lipoprotein cholesterol (HDL-C)
- High proliferative potential-ECFC (HPP-ECFC)
- Human bone marrow stem cells (hMSC)
- Human cardiac artery smooth muscle cells (HCASMC)
- Human Cardiac Artery Smooth Muscle Cells (HCASMCs)
- Human Umbilical Vein Endothelial Cells (HUVECs)
- Hydrochloric acid (HCL)
- Hydroxyapatite (HA)
- Induced pluripotent stem cells (iPSCs)
- Inflammatory bowel diseases (IBDs),
- Insulin-transferrin-selenium (ITS)
- Intercellular adhesion molecule- 2 (ICAM-2)
- Intercellular adhesion molecule-1 (ICAM-1)
- Interferon-gamma (IFN-γ)
- Interleukin (IL)-8, and
- Interleukin-6 (IL-6)
- Iron III chloride (FeCl3)
- Late Outgrowth EPC (ECFC)
- L-glutamine (LG)
- Lipopolysaccharide (LPS)
- Low proliferative potential-ECFC (LPP-ECFC)
- Low serum growth supplement (LSGS)
- Low-Density Lipoprotein (LDL)
- macrophage colony stimulating factor (M-CSF)
- Matrix metalloproteases (MMPs)
- Mesenchymal precursor cells (MPCs)
- Mesenchymal stem cell (MSC)
- Monocyte chemoattractant protein-1 (MCP-1)
- Multiple sclerosis (MS),
- Nitric oxide (NO)
- N-N-dimethyl formamide (DMF)
- Non-essential amino acids (NEAA)
- Oxidised LDL (oxLDL)
- Penicillin/Streptomycin (AA)
- Percutaneous transluminal coronary angioplasty (PTCA/balloon injury)
- Peripheral bone marrow cells (PBMCs)
- Perivascular adipose tissue (PVAT)

- Phosphate buffered saline (PBS)
- Platelet derived growth factor (PDGF) and
- Platelet endothelial cell adhesion molecule-1 (PECAM-1)
- Poly- (Ethylene Glycol) (PEG)
- Poly D, L-lactic-co-glycolic acid (PLGA)
- Poly-caprolactone (PCL)
- Polydimethylsiloxane (PDMS)
- Poly-L, D-lactic acid (96% l/4% d) (PLA)
- Poly-methyl acrylate (PMA)
- Polytetrafluoroethylene (PTFE)
- P-selectin glycoprotein ligand-1 (PSGL-1)
- Rat bone marrow stem cells (rMSC)
- Reactive oxygen species (ROS)
- Rheumatoid arthritis (RA),
- Scavenger receptor A1/II (SR-A1/II), SR-B1
- Scavenger receptor B1 (SR-B1)
- Smooth muscle cells (SMCs)
- Smooth muscle growth supplement (SMGS)
- Sodium hydroxide (NaOH)
- Stromal-derived factor (SDF-1/CXCL12)
- Systemic lupus erythematosus (SLE),
- Three dimensional (3D)
- Tissue engineered (TE)
- Tissue engineered blood vessel (TEBV)
- Tissue engineered intimal layer (TEIL)
- Tissue engineered medial layer (TEML)
- Transforming growth factor-beta (TGF-β)
- Tumour necrosis factor-alpha (TNF-α)
- Two dimensional (2D)
- Vascular cell adhesion protein-1 (VCAM-1)
- Vascular endothelial growth factor receptor-2 (VEGFR2)
- Vascular smooth muscle cells (VSMCs)
- Von Willebrand factor (VWF)

Chapter 1:
Literature Review

1.1 Cardiovascular Disease

Cardiovascular disease has been identified as the biggest killer in the developed world with rising incidences in the developing world. The term cardiovascular disease (CVD) is used to refer to a wide range of conditions that affect the heart and blood vessels. These include coronary heart disease which results from the build-up of an atherosclerotic plaque in the coronary arteries, stroke resulting from obstructed blood supply to the brain, transient ischaemic attacks which are temporary disruptions to blood flow to the brain, peripheral arterial disease which refers to blockage of vessels in the limbs, and aortic disease which are conditions that affect the aorta, such as aortic aneurism (Biscetti *et al.*, 2019). Atherosclerosis has been identified as a starting point for most cardiovascular disease and is the underlying cause of 50% of all deaths in westernised societies (Lusis, 2000; Biscetti *et al.*, 2019). The main risk factors that lead to the development of atherosclerosis include smoking, high blood pressure, family history of cardiovascular disease, high cholesterol (dyslipidaemia), diabetes, a sedentary lifestyle, obesity and age (Libby *et al.*, 2019). There is also some evidence that suggests that psychosocial factors such as depression, anxiety, social isolation and chronic life stress also contribute to the development of CVD (Rozanski, Blumenthal and Kaplan, 1999; Parvin Zafar, 2015). Because it is a disease of the vasculature, it is important to first understand the structure and function of blood vessels.

1.2 Anatomy and Physiology of Blood Vessels

The walls of arteries and veins are made up of three layers 1) the intima, 2) the media and 3) the adventitia (figure 1-1). As the diameter of the vessel decreases, the thickness of the three layers also decreases. The arteries, capillaries and veins have differences in the amounts of the tissue components present. The constant factors in most arterial anatomy are the endothelial cells (ECs), collagen fibres, elastic fibres and smooth muscle cells (SMCs) and the lumen through which blood flows. (Patton and Thibodeau, 2018). Together, their thicker walls and smaller diameters give arterial lumens a more rounded appearance in cross section than the lumens of veins (Klabunde, 2011).

The presence of intercellular clefts between adjacent endothelial cells as well as the presence, size and

number of pores through their cytoplasmic membranes facilitate the diffusion and movement of substances and cells into or out of the blood. The collagen fibres in blood vessels are woven together to provide extra re-enforcement. The fibres are formed from a number of collagen isoforms that aggregate into collagen fibres that are several micrometres in diameter (Patton and Thibodeau, 2018). Under physiological conditions, the collagen fibres are not very extensible and are capable of stretching only 2% or 3%. Their main role is to keep the lumen of the vessel open as well as contributing to maintaining overall tension and strengthening of the vessel wall. The elastic fibres within the vessel are mainly made from elastin which is a small insoluble protein polymer. Once secreted into the extracellular matrix (ECM), the fibres form a rubber-like network that is highly elastic and capable of stretching up to 100% under physiological conditions (Patton and Thibodeau, 2018).

In large arteries, the elastic fibres are organised in a concentric pattern and allow for recoil after distension and this property of elastic fibres plays an important role in the maintenance of passive tension in the vessel. This kind of tension is necessary in maintaining normal blood pressure levels throughout the cardiac cycle (Patton and Thibodeau, 2018).

1.1.1 Intimal Layer

The first layer, the intima (*tunica intima*) (figure 1) is the innermost, and thinnest, layer of the blood vessel and is comprised of an endothelium which is continuous throughout the entire vascular system, including the lining of the chambers of the heart. The endothelium in arteries provides a completely smooth lining compared with that of veins which also forms semilunar valves that facilitate one-way blood flow. The luminal surface of quiescent endothelial cells is anticoagulant and non-thrombogenic, such that platelets and leukocytes do not adhere to it and it helps maintain the inactive state of the blood coagulation system. Damage to the endothelial lining and exposure of blood to the collagenous fibres beneath is one of the primary causes of clot formation. The macromolecules of the basal lamina, synthesized by the endothelial cells, are strongly thrombogenic, and activated endothelial cells promote thrombus formation. The endothelium is physiologically vital to activities such as regulating capillary exchange and altering blood flow (Pearson, 2000; Félétou, 2011; Patton and Thibodeau,

2018). It regulates blood flow by producing endothelins (ET-1) which cause constriction of the smooth muscle within the vessel wall, elevating blood pressure. Production and release of endothelin is stimulated by angiotensin II (AII), antidiuretic hormone (ADH), thrombin, cytokines, reactive oxygen species, and shearing forces acting on the vascular endothelium. ET-1 release is inhibited by prostacyclin and atrial natriuretic peptide as well as by nitric oxide. The unregulated production of ET-1 has been linked to both hypertension and cardiovascular disease (Klabunde, 2011). Under microscopic view, the entirety of the lumen and the tunica intima of a vein will appear smooth, whereas those of an artery will normally appear wavy because of the partial constriction of the smooth muscle in the tunica media.

Endothelial cells also play a vital role in regulating vascular homeostasis by modulating permeability, maintaining vascular tone and responding to a variety of stimuli through the production of bioactive substances. The intimal surface of healthy endothelium is both anticoagulant and antithrombotic: endothelial cells secrete a variety of molecules that are necessary for the regulation of blood coagulation and platelet functions. Vessel damage or exposure to certain cytokines or pro-inflammatory stimuli shifts the balance towards a pro-coagulant/pro-thrombotic phenotype of the endothelial cells. Haemostasis processes are classified as either primary, which mainly involve platelets, or secondary, predominantly related to fibrin formation or blood coagulation, although the two processes are strongly interconnected (Félétou, 2011; Zhao *et al.*, 2016).

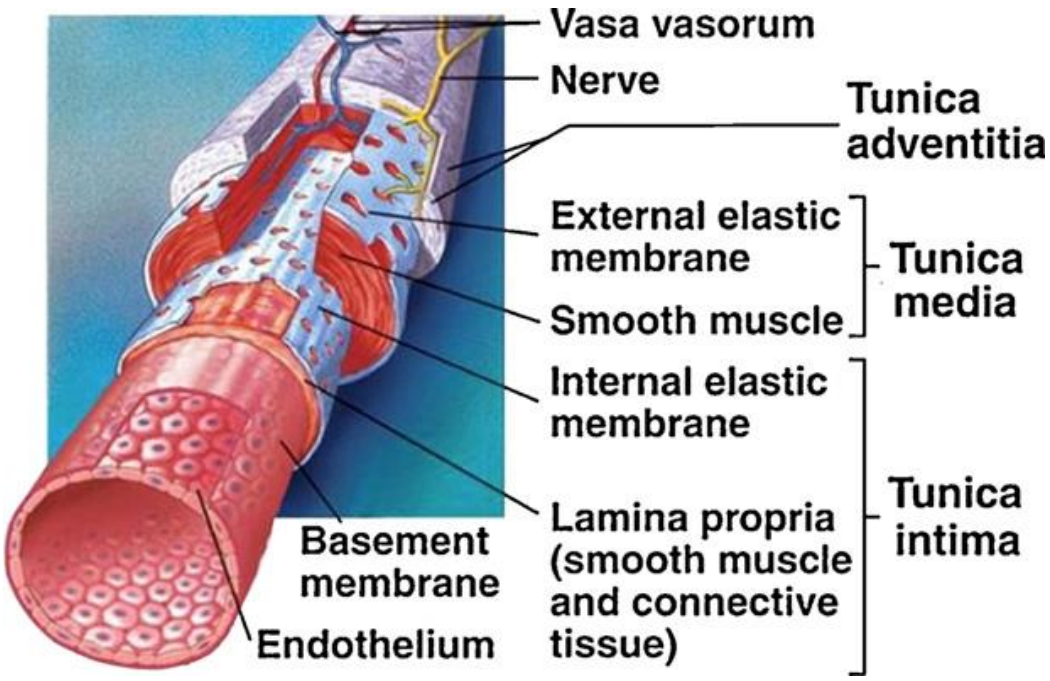

Figure 1-1: Vascular anatomy (Chen, Liang and Thouas, 2013). This image shows the different layers that comprise a blood vessel, with the intima in contact with the blood and the adventitia on the outermost surface. The elastic lamina provides the vessel with the elasticity needed to withstand blood flow under pressure. The collagen and proteoglycans are synthesised

1.1.2 Medial Layer

The second layer is the media (*tunica media*) (figure 1-1) which is the middle layer comprised of a layer of circularly arranged smooth muscle tissue together with a layer of elastic connective tissue (elastin sheets) and supported by a framework of collagenous fibres that also binds the tunica media to the intima and adventitia (Patton and Thibodeau, 2018). The smooth muscle cells in the media layer permits the change of blood vessel diameter. Contraction and relaxation of the circular muscles decrease and increase the diameter of the vessel lumen, respectively. This layer is innervated by autonomic nerves and supplied with blood by small vessels knows as *vasa vasorum* as the walls of the larger vessels are too thick to allow the diffusion of nutrients (Zhao, Vanhoutte and Leung, 2015; Patton and Thibodeau, 2018). This layer is thicker in arteries compared to veins and is absent in capillaries. Separating the tunica media from the outer tunica externa in larger arteries is the external elastic membrane or lamina. This structure is not usually seen in smaller arteries, nor is it seen in veins (Patton and Thibodeau, 2018). SMCs in the vessel wall produce a complex ECM that will ultimately define the mechanical properties of the adult vascular system. These properties include: *1*) a highly resilient wall

where a large proportion of the energy input during systolic inflation will be recovered by elastic recoil during diastole, *2*) low hysteresis (the energy lost during an inflation-deflation cycle), and *3*) nonlinear elasticity characterized by stiffening with increasing pressure to protect the wall from rupture (Wagenseil and Mecham, 2009; Basatemur *et al.*, 2019).

1.1.3 Adventitial Layer

The third layer is the adventitia (*tunica adventitia*) (figure 1-1) and is the outermost layer of a blood vessel which is found in the larger blood vessels. This layer is made of tough, fibrous connective tissue and its main role is to hold the vessel open and to prevent the tearing of the vessel during body movements (Patton and Thibodeau, 2018). The adventitia also contains nerve endings, perivascular adipose tissue (PVAT) and connective elements (fibroblasts and collagen fibres) that assure adherence to the surrounding organs. Components of the adventitia are also involved in vascular development and remodelling, immune surveillance and inflammatory cell trafficking, and signal exchanges between the blood vessel and its residential tissue (Wagenseil and Mecham, 2009; Patton and Thibodeau, 2018). This layer is thicker in veins than arteries where it is slightly thinner than the media and also contains groups of smooth muscle fibres. (Patton and Thibodeau, 2018).

1.3 Pathophysiology of Cardiovascular Disease

Atherosclerosis is characterised by the accumulation of fatty and fibrous material within the intimal layer of arteries (Herrington *et al.*, 2016; Libby *et al.*, 2019). This accumulation of fatty material is initiated by elevated levels of cholesterol in the blood which in turn lead to endothelial activation and inflammation. Consequently, atherosclerosis can be defined as a chronic inflammatory disease (Libby *et al.*, 2019; Qiu *et al.*, 2020), with endothelial cells, leukocytes and smooth muscle cells being the major players in the development of disease (Parvin Zafar, 2015; Qiu *et al.*, 2020).

1.1.4 Role of Low-Density Lipoprotein (LDL)

Studies into the pathogenesis of atherosclerosis have identified LDL particles as the cause of atherosclerosis (Libby *et al.*, 2019), with their accumulation into the sub-endothelial space leading to the formation of atherosclerotic plaques (Lillis *et al.*, 2015). Passage of LDL into the sub-endothelial

space is facilitated through endothelial LDL receptors, specifically scavenger receptor B1 (SR-B1) interacting with the guanine nucleotide exchange factor dedicator for cytokinesis (DOCK4), with expression of both being elevated in atherosclerotic arteries compared to normal arteries (Borén *et al.*, 2020). The LDL particles in the sub-endothelial space are prone to oxidation through enzymatic and non-enzymatic mechanisms, leading to the formation of oxidised LDL (oxLDL) (Lillis *et al.*, 2015; Borén *et al.*, 2020).

1.1.4.1 Endothelial dysfunction

The endothelial cells are the primary component of the intimal layer and are involved in maintaining vascular integrity through regulating both endogenous and exogenous stresses (Qiu *et al.*, 2020), through the modulation of vasomotion, haemostasis, angiogenesis and vascular growth, as well as the trafficking of circulating cells through up-regulation of adhesion molecule expression. These adhesion molecules facilitate leukocyte migration into specific organs under typical physiological conditions and accelerating migration to sites of inflammation (Desideri and Ferri, 2005). Endothelial activation has no distinct definition but, can refer to the repeated exposure of the endothelium to elements such as reactive oxygen species (ROS), LDL and oxLDL, that are harmful or toxic to the endothelium, with prolonged exposure leading to an imbalance between endothelial repair and injury. This eventually results in endothelial dysfunction, a key stage in the development if atherosclerosis (Mannarino and Pirro, 2008; Qiu *et al.*, 2020) A dysfunctional endothelium is characterised by the retention of plasma lipoproteins, induction of immune cell infiltration, overproduction of chemokines and an increase in endothelial cell death, creating an inflammatory microenvironment (Varghese, Patel and Yadav, 2017; Qiu *et al.*, 2020). Another contributor to endothelial dysfunction is oxidative stress, which is defined as an imbalance between the synthesis of ROS and their elimination by the antioxidant defence system (Costa *et al.*, 2016). ROS originate from Nicotinamide adenine dinucleotide phosphate (NADPH) oxidase, uncoupled endothelial nitric oxide synthase (eNOS), mitochondrial enzymes, lipoxygenases and myeloperoxidases (Kattoor *et al.*, 2017). ROS are involved in various processes, such as the oxidation of LDL and apoptosis, that affect cardiac structure and function, contributing to the onset

and progression of heart failure (Costa *et al.*, 2016; Kattoor *et al.*, 2017). Endothelial dysfunction causes endothelial cells to produce adhesion molecules such as Intercellular adhesion molecule-1 and 2 (ICAM-1 and ICAM-2)), Vascular cell adhesion protein-1 (VCAM-1), and platelet endothelial cell adhesion molecule-1 (PECAM-1) (Michael A. and Guillermo, 2016). These molecules belong to a family of immunoglobulin-like molecules and they engage with leukocyte counter-receptors to mediate firm adhesion and/or trans-endothelial migration. ICAM-1 and VCAM-1 respond to cytokine or endotoxin challenge with a time- and dose-dependent increase in EC expression that is transcription-dependent, while ICAM-2 and PECAM-1 are constitutively expressed and are not up-regulated in response to cytokine challenge (Granger and Senchenkova, 2010; Golia *et al.*, 2014).

Other adhesion molecules include members of the selectin family i.e., E- and P-selectin. P-selectin is normally stored as a preformed reservoir in EC granules, also known as Weibel–Palade bodies, from which it can be rapidly mobilized to the cell surface by histamine, ROS, and leukotrienes (Granger and Senchenkova, 2010). A slower, more prolonged and transcription-dependent expression of P-selectin can be demonstrated within 4 hours after exposure to cytokines such as tumour necrosis factor-alpha (TNF-α). E-selectin is entirely under transcriptional regulation and requires up to 3 hours to achieve peak expression (Granger and Senchenkova, 2010; Barbier *et al.*, 2020). The expression of adhesion molecules, together with the secretion of chemoattractant mediators such as complement factors, interleukin (IL)-8, and monocyte chemoattractant protein-1 (MCP-1), leads to mononuclear cell recruitment into the vascular wall. Monocytes differentiate into macrophages (Bentzon *et al.*, 2014; Silva, Videira and Sackstein, 2018), which become foam cells via oxidised LDL uptake, and then release a variety of pro-inflammatory cytokines such as soluble CD40 ligand, IL-1, IL-3, IL-8, and IL-18, and TNF-α (Golia *et al.*, 2014; Silva, Videira and Sackstein, 2018). A summary detailing the factors involved with endothelial dysfunction is shown in figure 1-2.

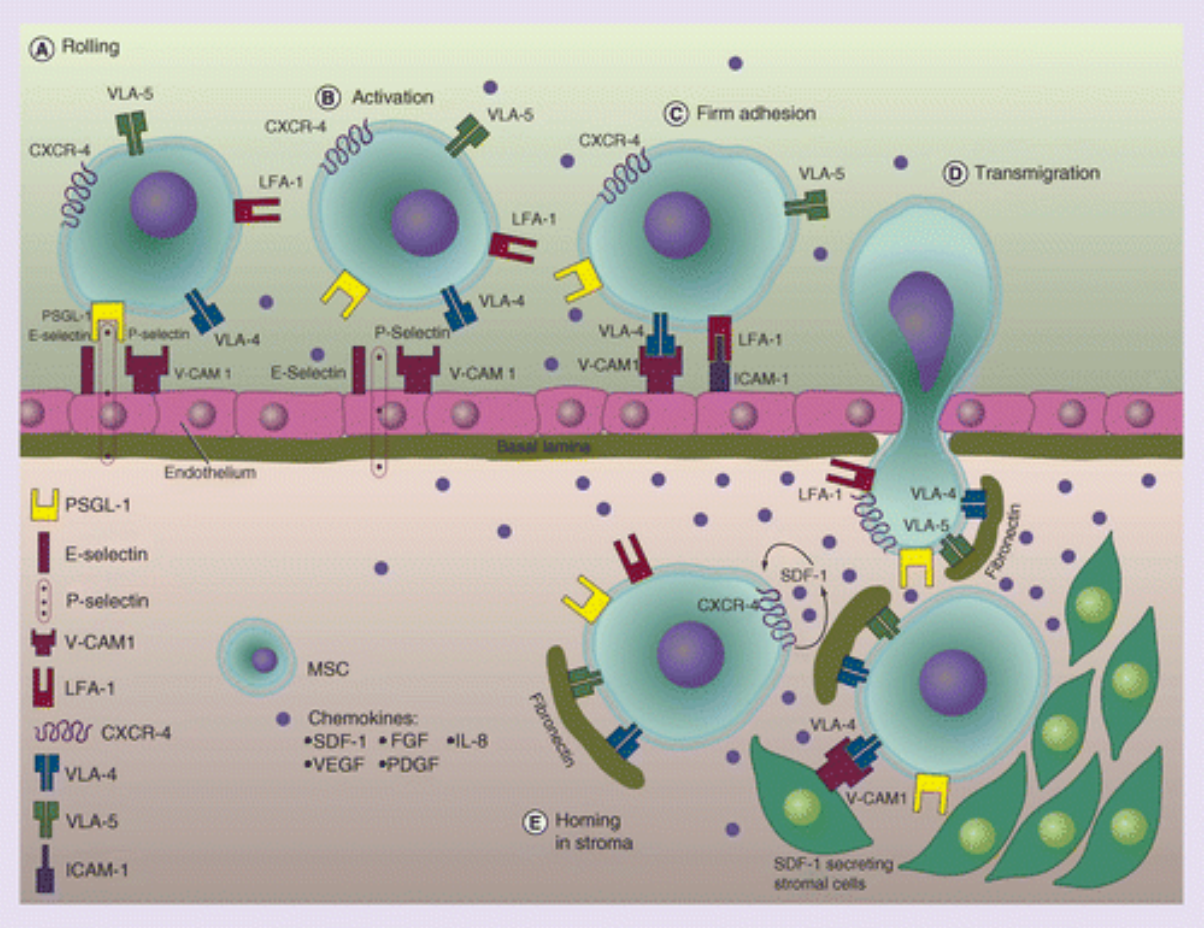

Figure 1-2: Adhesion molecules and chemokines associated with endothelial dysfunction (Khan, Adil and Olson, 2017). This image details the homing of MSCs to activated endothelium denoting the adhesion molecules that would aid in the recruitment, attachment and migration of cells into the sub-endothelial space.

1.1.4.2 Macrophages and foam cells in atherosclerosis

Because of their capacity to take up oxLDL, and LDL to a lesser extent, macrophages have a key role to play in the pathogenesis of atherosclerosis (Lillis *et al.*, 2015). This oxidised form of LDL is more readily taken up by macrophages than the native form, with macrophages possessing receptors that are specific for oxLDL such as scavenger receptor A1/II (SR-A1/II), SR-B1, and CD36, which have also been identified on smooth muscle (Li and Mehta, 2005; Lillis *et al.*, 2015). Macrophages that have taken up oxLDL are referred to as foam cells due to the formation of lipid droplets as a result of excessive lipid accumulation that exceeds the haemostatic capacity of macrophages (Guerrini and Gennaro, 2019). Once in the sub-endothelial space, monocytes differentiate into macrophage and dendritic cell like phenotypes (H. Xu *et al.*, 2019). Those resident in vascular tissue are involved in the early stages of

plaque formation, actively ingesting excess cholesterol present in the subendothelial space and becoming foam cells (H. Xu *et al.*, 2019). The oxLDL also activates scavenger receptor/toll like receptor (TLR) cooperative signalling pathways that contribute to the induction of pro-inflammatory downstream signalling cascades (Lara-Guzmán *et al.*, 2018). These pro-inflammatory signals contribute to endothelial dysfunction, which in turn promotes the expression of adhesion molecules that aid in the trapping and infiltration of circulating monocytes, perpetuating the cycle of inflammation and contributing to plaque progression (Guerrini and Gennaro, 2019). Macrophages that have accumulated in the atherosclerotic plaque also display a reduced capacity to migrate, adding to their failure to resolve inflammation and contributing to plaque progression (Guerrini and Gennaro, 2019).

One of the key pro-inflammatory mediators is interferon-gamma (IFN-γ), which is involved in the initiation and modulation of numerous pro-atherogenic processes, one of which is promotion of foam cell formation (Voloshyna, Littlefield and Reiss, 2014). This cytokine plays a key role in endothelium mediated recruitment of monocytes and T-cells to the atherosclerotic plaque. Macrophage derived foam cells that have accumulated in the sub-endothelial space secrete a variety of factors such as platelet derived growth factor (PDGF) and matrix metalloproteases (MMPs) which contribute to the migration and proliferation of SMCs (Voloshyna, Littlefield and Reiss, 2014; Biros, Reznik and Moran, 2021). Figure 1-3 details the process of macrophage infiltration into the sub-endothelial space where they become foam cells upon exposure to LDL and its variants.

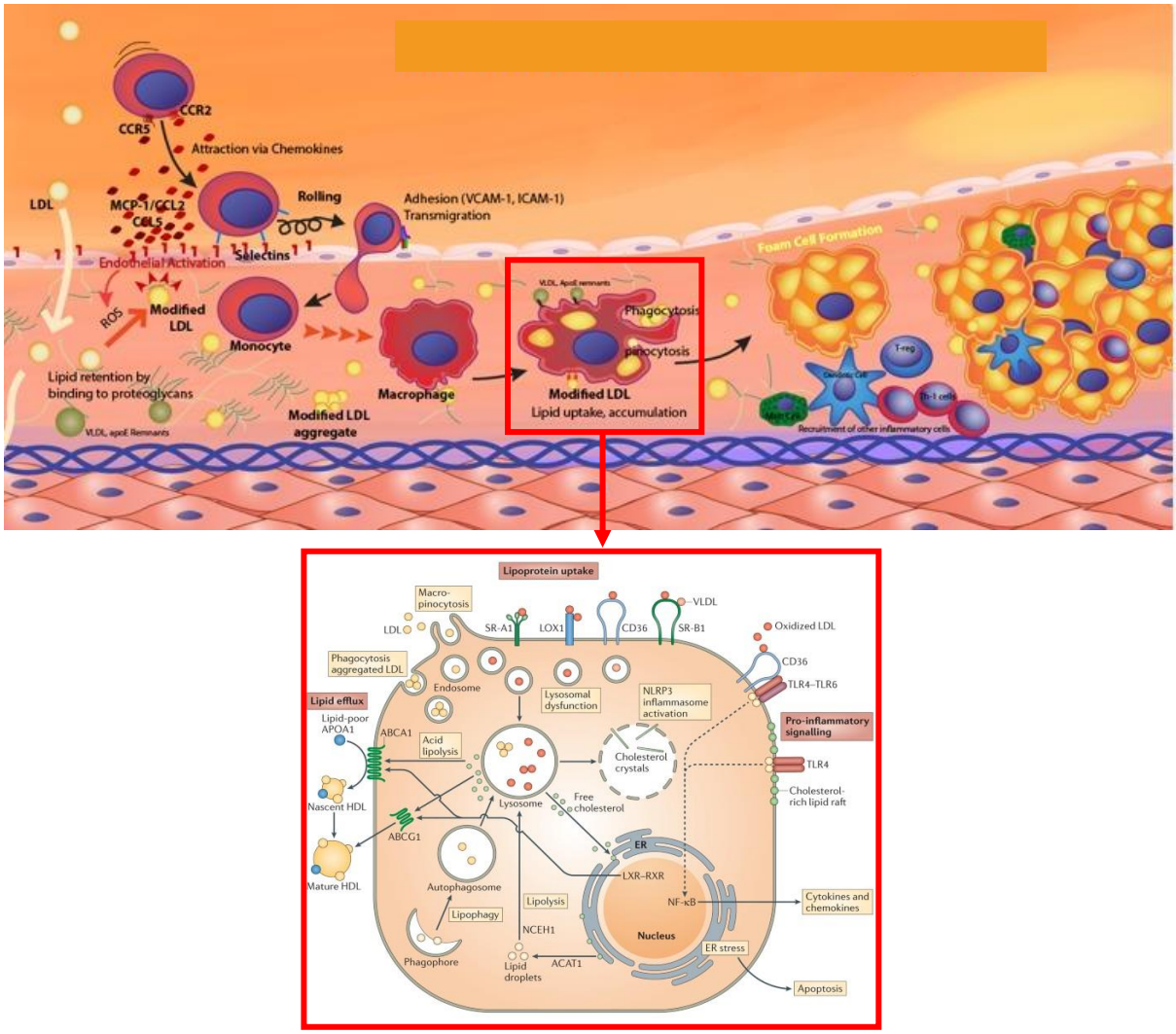

Figure 1-3: Mechanisms of foam cell formation (Moore, Sheedy and Fisher, 2013; Linton *et al.*, 2019). These images detail the process of monocyte recruitment, differentiation into macrophages and the process of foam cell formation within the macrophage. The activated endothelium promotes the adhesion and transmigration of circulating lymphocytes where they then ingest available lipid through scavenger receptors, becoming foam cells.

SMCs which are resident in the media, migrate to the intima where they proliferate and produce extracellular matrix. Smooth muscle cells are also prompted to take up oxLDL, thus becoming foam cells (Kattoor *et al.*, 2017). Certain constituents of the extracellular matrix, especially proteoglycans, bind lipoproteins, thus prolonging their residence in the intima, and render them more susceptible to oxidative modification and glycation (Di Pietro, Formoso and Pandolfi, 2016; Kattoor *et al.*, 2017). As the lesion progresses, calcification may then occur, and in addition to proliferation, cell death (including apoptosis) commonly occurs in the established atherosclerotic lesion. The extracellular lipid that accumulates in the intima can coalesce and form the classic, lipid-rich “necrotic” core of the

atherosclerotic plaque (Libby and Theroux, 2005; Geovanini and Libby, 2018).

1.1.5 Role of Shear Stress

Hemodynamic shear stress refers to the force that acts on the endothelial cell surface as a result of blood flow, and plays a vital role in determining endothelial cell phenotype and function as well as embryonic cardiovascular development (Malek, Alper and Izumo, 1999). Normal stretch of the vessel due to the effects of blood pressure are transferred to all vessel wall layers. In contrast, the effects of shear stress are principally applied only to the vascular endothelium (Cunningham and Gotlieb, 2005). The endothelium responds to shear stress through various physiological and pathological mechanisms depending on the kind and the magnitude of shear stresses (Lehoux and Jones, 2016). More specifically, the exposure of vascular endothelium to typical arterial shear forces stimulates endothelial cells to release agents with antithrombotic properties, such as prostacyclin, nitric oxide (NO), and thrombomodulin. Therefore, normal shear stresses act to maintain an endothelial phenotype that inhibits atherogenesis, thrombosis, adhesion of leukocytes, smooth muscle proliferation and endothelial apoptosis (Papaioannou and Stefanadis, 2005; Davies, 2009).

A disruption of the biomechanical forces, such as shear stress, that maintain endothelial cell integrity can also result in the activation of the endothelium, which then results in initiation of the inflammation response. Changes in the magnitude of shear stress can activate cellular proliferation mechanisms as well as initiating vascular remodelling processes (Davies, 2009). A high grade of shear stress increases wall thickness and expands the vessel's diameter so that shear stress values return to their normal values. Contrastingly, lower shear stresses result in a reduction of vessel diameter which can then lead to intima-media hyperplasia. Low shear stress that displays varying direction (oscillating shear stress) has been associated with the development of atherosclerotic impairment in (Papaioannou and Stefanadis, 2005; Lehoux and Jones, 2016).

In arterial circulation, shear stress has an important role in determining where most vascular pathology originates and it is also implicated in the development of endothelial phenotypic changes that are associated with increased atherosclerosis susceptibility, initiation and development (Davies, 2009).

Regions of the arterial tree with uniform geometry are exposed to a unidirectional and constant flow, which aids in generating physiologic shear stress, while vessel arches and bifurcations are exposed to an oscillatory and disturbed flow, which determines a low shear stress. Atherosclerotic lesions develop mainly in areas of low shear stress, while those exposed to a physiologic shear stress are protected (Cecchi *et al.*, 2011; Nigro, Abe and Berk, 2011). A developing atherosclerotic lesion can alter the shear stress profile on the endothelium. A narrowed lumen that results from an atherosclerotic plaque can create flow separation in the region immediately downstream and the altered flow has similar properties to plaque free regions that are susceptible to shear induced changes, indicating that lesion induced changes to blood flow may facilitate the growth of the lesion over time. Studies on endothelial cells show that the altered flow pattern promotes pro-inflammatory gene and protein expression that is conductive to atherosclerosis susceptibility, plaque growth and instability and an increased risk of thrombus (Davies, 2009).

1.4 Therapies for Cardiovascular Disease (CVD)

In a number of instances, the treatment or management options for atherosclerosis, and cardiovascular disease in general, involves a change in lifestyle (e.g., lowering dietary cholesterol and exercise) (Toulassi *et al.*, 2021) but in more serious cases, drugs are prescribed which can either slow or completely stop the progression of atherosclerosis. Some of these include statins and fibrates that are used to reduce circulating levels of LDL (Solanki, Bhatt and Johnston, 2018).

1.1.6 Surgical Interventions

In more severe cases, surgical avenues are used to alleviate the symptoms. Procedures include angioplasty which is the widening of narrowed arteries using a balloon, endarterectomy which involves the removal of fatty deposits in the vessel to improve circulation and thrombolytic therapy that is to remove clots at the site of formation and bypass surgery (Leong *et al.*, 2017). The most common type of heart surgery is coronary artery bypass grafting and this involves the grafting of a healthy artery or vein from the body, which then bypasses the obstructed portion of the coronary artery, creating a new path for oxygen-rich blood to flow to the heart muscle (Leong *et al.*, 2017). Recent years have seen

advancements in percutaneous coronary intervention, which involves the widening of occluded vessels with stents. One example of stents used is the drug eluting stent (DES) which has come to replace the use of bare metal stents (BMS) (Leong *et al.*, 2017; Park *et al.*, 2020). DES work by releasing one or more bioactive agents that act on tissues adjacent to the stent. The bioactive component can be either linked to the stent surface or embedded and released from within polymer materials, or surrounded by and released by a carrier (Fattori and Piva, 2003; Lee and Hernandez, 2018). Compared to bare metal stents, DES have fewer incidences of in-stent chronic total occlusion as a result of increased thrombus formation (Fattori and Piva, 2003; Bangalore *et al.*, 2018). These surgical interventions serve to cater for more severe presentations of CVD and patients will still need pharmaceutical intervention of some kind to aid with inflammation reducing irregularities in lipid metabolism, which are the key drivers of atherosclerosis.

1.1.7 Drug Therapies

There is a broad variety of alternative therapies available for the treatment and management of cardiovascular disease but, as a number of them have no proven benefits to the patient's health, drug therapies and scientifically tested alternatives remain the best option to effectively curb the progression of cardiovascular disease.

1.1.7.1 Cholesterol Regulation

For atherosclerosis in particular which involves excessive inflammation that is propagated by lipid modifications, drugs that regulate cholesterol levels are the go-to therapy currently in use. Statins fall under this category and are recommended for most patients because they are the only cholesterol-lowering drug class that has been directly associated with reducing the risk of a heart attack or stroke. There are other cholesterol lowering drugs available, such as (1) bile acid binders, which are also referred to as resins, (2) Nicotinic acid and (3) Fibric acids (Pahan, 2006; Kuo, Huang and Hsieh, 2020). Bile acids are synthesised in the liver from cholesterol and facilitate the absorption of fatty acids and lipid soluble vitamins. Bile acid binders, or resins, function by binding bile acids in the intestines preventing reabsorption by increasing faecal excretion which is an important pathway for cholesterol

clearance. Increased faecal excretion of bile acids results in increased bile acid synthesis which leads to increased expression of LDL receptors in the liver and subsequent reduction in circulating levels of LDL (Hansen, Sonne and Knop, 2014; Ross *et al.*, 2015).

Nicotinic acid, or niacin, has benefits primarily in increasing high density lipoprotein cholesterol (HDL-C), and has also been shown to decrease concentrations of LDL. The mechanisms of action of this drug have not been fully elucidated, as such it's use in the treatment of cardiovascular disease remains limited, although its use in conjunction with statins results in reduced morbidity and mortality and promoting regression of coronary atherosclerosis (Shah *et al.*, 2013; Zeman *et al.*, 2015).

Fibric acid or fibrins do not directly affect cholesterol biosynthesis but rather lower plasma levels of fatty acid and triacylglycerol and can also increase HDL levels and educe LDL particle size (Pahan, 2006; Boden, Sidhu and Toth, 2014). These drugs, however, are not in common use due to evidence linking some variants, such as clofibrate and ciprofibrate cause peroxisome proliferation which causes hepatomegaly and tumour formation in rodent livers (Pahan, 2006).

Statins have proven to be the most effective, and with fewer deleterious effects, at lowering cholesterol and remain then primary drug of choice for patients with cardiovascular disease.

1.1.7.2 Statins: Pharmacology and Systemic Effects

Statins are categorically classified as HMG CoA reductase inhibitors and their purpose is to prevent the formation of cholesterol and are most effective at lowering LDL cholesterol. They do this by interfering with the conversion of HMG-CoA to the cholesterol precursor mevalonate. They also help lower triglycerides and raise HDL cholesterol (Pahan, 2006; Pinal-Fernandez, Casal-Dominguez and Mammen, 2018). HMG CoA reductase is the rate-limiting enzyme for cholesterol synthesis. Normally in mammalian cells this enzyme is suppressed by cholesterol derived from the internalization and degradation of LDL via the LDL receptor. Competitive inhibitors of the reductase induce the expression of LDL receptors in the liver, which in turn increases the catabolism of plasma LDL and lowers the plasma concentration of cholesterol, an important determinant of atherosclerosis (Stancu and Sima, 2001; Sirtori, 2014). They are the most efficient agents for reducing plasma cholesterol, being also

appreciated for their good tolerance. Angiographic studies have demonstrated that these compounds reduce the progression and may induce the regression of atherosclerosis. There are a variety of statins available for clinical use such as atorvastatin, fluvastatin, lovastatin, mevastatin, pitavastatin, pravastatin, rosuvastatin and simvastatin (Davies *et al.*, 2016). Atorvastatin and rosuvastatin have been shown to have the greatest potency and they also have the longest half-lives (20 h) versus about 12 h for simvastatin. All the others have a context half-life of 4 hours (Sirtori, 2014; Chiang *et al.*, 2015). The statins are commonly grouped in two types. Type 1 compounds are natural or fungal-derived statins (lovastatin, simvastatin, pravastatin). Type 2 statins are synthetic statins and are known to form more interactions with HMG-CoA reductase because of their structural characteristics. Lovastatin, simvastatin, atorvastatin, and fluvastatin are lipophilic, whereas pravastatin and rosuvastatin are more hydrophilic (Davies *et al.*, 2016). The lipophilic properties of the statins are accompanied, except for pitavastatin, by low systemic bioavailability because of an extensive first-pass metabolism by the liver. The functional difference between natural and synthetic statins relies on their ability to interact and inhibit the HMG-CoA reductase and on their lipophilicity (Gazzerro *et al.*, 2012; Davies *et al.*, 2016).

Angiographic studies have demonstrated that these compounds reduce the progression and may induce the regression of atherosclerosis (Stancu and Sima, 2001). Statins have been shown to have pleiotropic effects as the products of the inhibited enzyme are necessary for a variety of physiological processes. Statins modulate a series of processes leading to reduction of the accumulation of esterified cholesterol into macrophages, increase of endothelial NO synthase, reduction of the inflammatory process, increased stability of the atherosclerotic plaques, restoration of platelets activity and of the coagulation process as well as the inhibition of tumour cell growth and enhancement of rises in cytosolic Ca^{2+} concentration (Stancu and Sima, 2001; Sandhu, Mamas and Butler, 2017). This elevation of cytosolic Ca^{2+} concentration has been demonstrated for human umbilical vein endothelial cells (HUVECs) upon Incubation of the cells with cerivastatin or fluvastatin. Heinke et. al., (2004) demonstrated that a 24hour incubation of HUVECs with either cerivastatin or fluvastatin significantly increased the resting Ca^{2+} concentration. This effect manifested at a concentration of 1 μM with

Cerivastatin. This increase of resting Ca^{2+} concentration in the presence of cerivastatin also occurred when the nitric oxide synthase was inhibited (Heinke *et al.*, 2004). The elevation of Ca^{2+} concentrations has also been observed after introduction of high concentrations of simvastatin to rat L6 myoblasts, and a similar effect was observed in cardiomyocytes (Baker and Tarnopolsky, 2001; Heinke *et al.*, 2004; Pinal-Fernandez, Casal-Dominguez and Mammen, 2018).

Statins can also reduce the expression and function of molecules on the leukocytes surface. Atorvastatin reduces the number of intimal macrophages, monocyte-chemoattractant protein-1 (MCP-1) and the activation of nuclear factor NFkB in hypercholesteraemic rabbits. The effect this has is to limit the inflammation process which is a key physiological marker of atherosclerosis. They have also demonstrated the ability to inhibit trans-endothelial migration and chemotaxis of neutrophils, which possibly explains the anti-inflammatory effect of these compounds. Another anti-inflammatory effect of statins on monocytes and macrophages is the decrease of the expression of intercellular adhesion molecule -1 and the secretion of interleukin-6 (IL-6), induced by lipopolysaccharides (Stancu and Sima, 2001; Gazzerro *et al.*, 2012). Additionally, all statins, except for pravastatin, reduce aortic smooth muscle cell (SMC) proliferation. Preclinical observations and in vitro studies suggest that apoptosis can modulate the arterial wall in restenotic or proliferative lesions, where SMCs are dominant. It was reported that statins can induce apoptosis of vascular SMCs in culture. This was demonstrated by examining lesioned carotid arteries from rabbits that received fluvastatin or atorvastatin, 5 days prior to lesion induction. The rabbits presented an increased number of apoptotic SMCs (Stancu and Sima, 2001).

Statins have been shown to have positive effects regarding preventing the progression of atherosclerosis and have been prescribed to those at risk of developing coronary artery disease to lower the likelihood of this happening. Given the pleiotropic effects induced by statins, there is potentially a broader selection of molecular and cellular effects that have yet to be determined. Figure 1-4 details the known/suspected pleiotropic effects of statins.

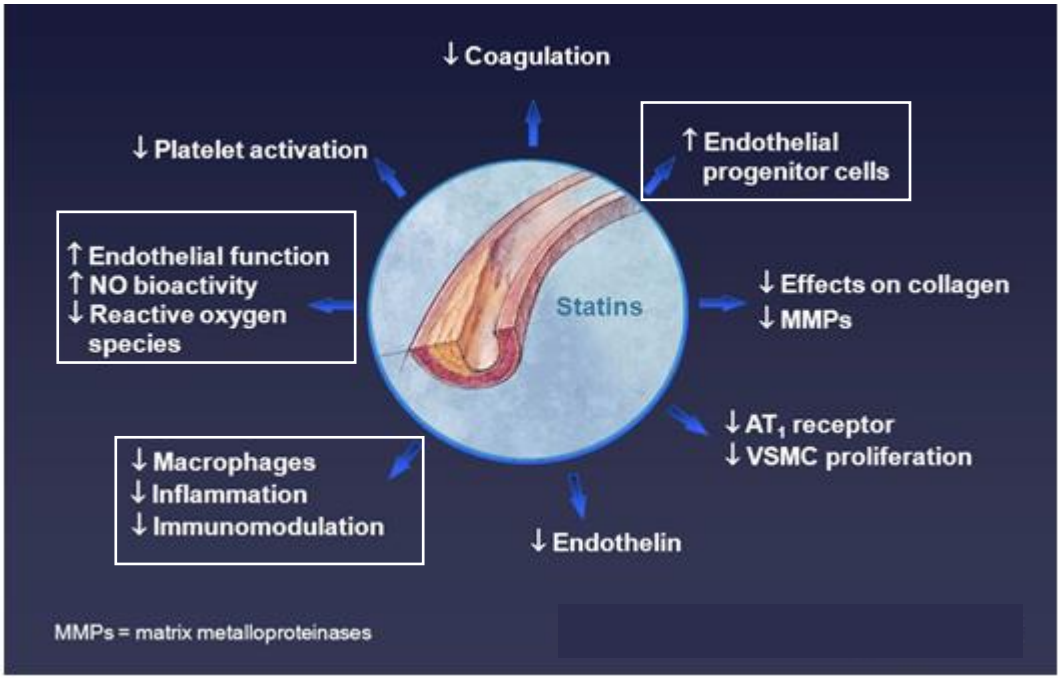

Figure 1-4: Pleiotropic effects of statins. *(Gupta et al., 2018)* This figure denoted the suspected pleiotropic effects of statins in cardiovascular disease, separate from their cholesterol lowering function. Text contained in white boxes indicates areas of interest for this thesis.

1.1.8 Alternative Therapies

There are also a variety of alternative therapies that rely on natural products/extracts to counteract the processes initiated by the risk factors that cause the development of cardiovascular disease. A number of these therapies have unsubstantiated cardiovascular effects and most research on these products is either inconclusive, conflicting, or shows no benefit for their use (Rabito and Kaye, 2013). Some of these include; (1) Marine-derived omega-3 polyunsaturated fatty acids which are used to prevent the adverse consequences of cardiovascular disease. Reportedly, these function by lowering triglyceride levels, preventing arrhythmias, decreasing platelet aggregation, or lowering blood pressure (Rabito and Kaye, 2013). (2) Garlic, which is used mainly as a dietary supplement for treatment of hyperlipidaemia, heart disease, and hypertension but there is no conclusive evidence verifies these beneficial effects. (3) Ginseng has also been used as a treatment for cardiovascular disease with the purported effects being cardio-protection, antihypertensive effects, and attenuation of myocardial hypertrophy and heart failure. (4) Antioxidants, which include anthocyanins, beta-carotene, catechins, coenzyme Q10, flavonoids, lipoic acid, lutein, lycopene, selenium, and vitamins C and E, have shown

promising results in laboratory and observational studies. Unfortunately, systematic reviews of the literature and large, randomized, controlled trials have overall found no advantageous effects of antioxidant supplements for primary or secondary prevention and, it has been found that vitamin A, beta-carotene, and vitamin E may actually increase mortality (Rabito and Kaye, 2013).

1.1.9 Cell Therapy

Another technique that shows promise for the treatment of cardiovascular disease is regenerative medicine. This technique is used in a number of situations where a vessel needs to be replaced or where there is damage to the muscles of the heart. This process involves the conditioning of cells into becoming a desired tissue type with the same or similar physical properties as the native tissue. These can then be transplanted into the patient with a reduced likelihood of tissue rejection as well as eliminating the need of a donor or the derivation of autologous donor tissue.

Cell therapies have gained popularity over the years and have been effectively used to repair damaged organs and tissues. In the case of cardiovascular disease, transplanted adult bone marrow has been shown to improve left ventricle ejection fraction, reduce infarct size and ameliorates remodelling in patients with ischaemic heart disease (Afzal *et al.*, 2015; Fisher *et al.*, 2016). Other studies have demonstrated scar tissue reduction and cardio-protection after mesenchymal stem cell (MSC) transplantation. MSCs are broadly distributed throughout the body outside bone marrow and reside in adipose tissue, gut, lung, liver, placenta, amniotic fluid, dental pulp, periodontal ligament and in the heart. The cells most commonly used in clinical trials to date originate from bone marrow i.e., MSCs and mesenchymal precursor cells (MPCs), adipose tissue, and umbilical cord. There are also cells that bear the same characteristics of MSCs found in peripheral blood (Karantalis and Hare, 2015). The main mechanisms of action that are responsible for the observed cardio-protective effect of MSCs are (1) reduction of fibrosis, (2) stimulation of angiogenesis, and (3) restoration of contractile function through engraftment, differentiation, and stimulation of endogenous cardiac stem cells to proliferate and differentiate. These effects occur in concert and together lead to the replacement of scarred or dysfunctional myocardial tissue with contractile and perfused tissue (Karantalis and Hare, 2015;

Liesveld, Sharma and Aljitawi, 2020).

Numerous efforts to further enhance the therapeutic potential of MSCs by genetically modifying or pre-treating MSCs with various drugs and cytokines are being undertaken. One attempt involved combining MSCs and simvastatin. It did not affect the reduction in perfusion defect, scar size, or end-diastolic volume, it did, however, potentiate increases in ejection fraction and systolic wall thickening, as well as improved MSC retention and survival (Karantalis and Hare, 2015; Bagno *et al.*, 2018).

The discovery and categorisation of endothelial progenitor cells as a circulating precursor to vascular endothelial cells has led to the consideration of using these cells in the treatment of cardiovascular diseases in terms of improving the repair of damaged vasculature (Urbich and Dimmeler, 2004).

1.5 Endothelial Progenitor Cells

1.1.10 Characterisation and Behaviour

The progenitor cells that are able to differentiate into functional endothelial cells and sustain vasculogenesis are broadly called endothelial progenitor cells. Human endothelial progenitor cells (EPCs) have been defined as circulating cells that express a variety of cell surface markers similar to those expressed by vascular endothelial cells, adhere to endothelium at sites of hypoxia/ischemia, and participate in neovascularisation. The first reported existence of a bone marrow– derived circulating progenitor for the endothelial lineage called the endothelial progenitor cell (EPC) in 1997 by Ashara et. al initiated a robust area of investigation in experimental animals and human subjects (Yoder, 2012; Marchetti, 2015).

Three different populations of putative human EPCs, with a variety of names in the literature i.e. EPC, Colony-forming Unit Epithelial cell (CFU-EC), Circulating angiogenic cell (CAC), Circulating endothelial precursors (CEP), Endothelial colony forming cell (ECFC), Low proliferative potential-ECFC (LPP-ECFC), High proliferative potential-ECFC (HPP-ECFC), Early Outgrowth EPC (CFU-EC, CFU-Hill, CAC), Late Outgrowth EPC (ECFC), have been defined using four cell culture and cell sorting protocols;

(1) *Circulating Angiogenic Cells (CACs)*: These are obtained from the low-density mononuclear cell (MNC) fraction of human peripheral blood or cord blood. These cells are cultured on fibronectin coated

plates and incubated with a mixture of cytokines. After 4-7 days in culture, the non-adherent cells are removed and the remaining cells are examined for their ability to take up acetylated low-density lipoprotein (AcLDL) and to bind to Ulex europaeus agglutinin1 (lectin), both considered to be hallmarks of EC function. CACs are further characterized by their morphology, adhesion to fibronectin, and cell surface protein expression. The isolated cells display pro-angiogenic activity *in vitro*, by secretion of angiogenic cytokines, and also *in vivo*, but lack the capacity to inosculate into a new blood vessel (Medina *et al.*, 2010; Marchetti, 2015)

(2) *Colony-Forming Unit-Hill (CFU-Hill) and CFU-Endothelial Cells (CFU-EC)*: CFU-Hill are also obtained from the MNC fraction of peripheral blood. MNCs are cultured in the same way as CACs for two days, after which the cells of interest, located in the non-adherent cell population, are removed and re-plated once more on fibronectin-coated plates. After three days, positive colonies are identified as having a central core of "round" cells, with more elongated "sprouting" cells at the periphery (Marchetti, 2015). Immuno-histochemical staining will confirm whether cells generated in this assay express the endothelial markers von Willebrand factor, Vascular endothelial growth factor receptor-2 (VEGFR2) and CD31. The isolated cells, however, lack the capability to form new vessels in vivo (Marchetti, 2015; Ravishankar, Zeballos and Balachandran, 2017).

(3) *Late outgrowth endothelial cells (OECs) or endothelial colony forming cells (ECFCs)*: These cells are obtained by plating human peripheral blood or cord blood-derived MNC on dishes coated with rat collagen type I and in media containing endothelial growth factors. Non-adherent cells are discarded daily and fresh medium is added. Within one to three weeks, cells possessing clonal ability appear with endothelial cobblestone morphology and varying proliferative potentials. Among the ECFC population it is possible to identify a distinctive population of high proliferative potential endothelial colony forming cells (HPP-ECFCs), which give rise to low proliferative potential endothelial colony-forming cells (LPP-ECFCs), generating endothelial clusters and finally mature non-dividing endothelial cells (Kachamakova-Trojanowska *et al.*, 2015; Marchetti, 2015).

(4) *HPP-ECFC* can be re-plated in secondary and tertiary colonies and retain high telomerase activity.

These cells have the ability to form colonies after 100 population doublings and are found in cord blood. The colonies contain cells that can differentiate into endothelial capillary-like tubes in vitro. Adult peripheral blood contains LPP-ECFCs with the ability to proliferate for 20 - 30 population doublings. ECFC-derived cells express many EC antigens, including CD31, CD105, CD144, CD146, Von Willebrand factor (VWF), VEGFR-2, and Ulex Europaeus Agglutinin I (UEA-1) (Zhang, Malik and Rehman, 2014a; Marchetti, 2015).

As yet, there is still no uniformity in terms of the nomenclature used to define EPC subtypes, for example early outgrowth EPCs can also be, and frequently are, referred to as CACs (Medina *et al.*, 2017). Consequently, identification, and classification is based on expression of these surface antigens. For general purposes, cells can be defined as EPCs if they are positive for VE-Cadherin, CD31/PECAM-1, CD34, CD45, CD45.1, CD45.2, CD117/c-kit, CD133, CXCR4, ETV2/ER71, MCAM/CD146, Tie-2, VEGF R2/KDR/Flk-1 and VEGF R3/Flt-4. These markers are, however, shared amongst a number of hematopoietic and vascular endothelial subsets. The EPCs be discriminated by an extensive gene expression analysis or use of a variety of functional assays that are not often applied (Yoder, 2012; Medina *et al.*, 2017; Chopra *et al.*, 2018a).

EPCs can be isolated from circulating mononuclear cells, bone marrow, and cord blood. When these cells are injected into animal models with ischemia, they are rapidly incorporated into sites of neovascularization. Given that atherosclerosis involves damage and dysfunction of endothelial cells, the existence of EPCs has led to the hypothesis that circulating endothelial progenitor cells might contribute to ongoing endothelial repair which may reduce the rise of occurrence of acute cardiovascular events (Hill *et al.*, 2003). Asahara et. al initially identified and isolated a supposed EPC in adult human peripheral blood. Since then, distinctly different cell populations have been isolated and called EPCs. These cell populations have subsequently been shown to improve vascular function through two principal mechanisms (1) direct incorporation into injured endothelium with formation of a functional blood vessel and/or (2) local secretion of pro-angiogenic factors with a paracrine effect to trigger existing endothelial cells to form the new vessel (Hill *et al.*, 2003; Marchetti, 2015). These cells

have also been identified as biomarkers for cardiovascular disease and have been proposed as a potent cell-based therapy for their capacity to stimulate vascular repair in physiological and pathological conditions (Fadini, Losordo and Dimmeler, 2012; Chopra *et al.*, 2018b).

1.1.11 Role in Vascular Neogenesis

Asahara et. al established, in their 1997 publication, that purified $CD34^{+}$ hematopoietic progenitor cells from adults can differentiate *ex vivo* to an endothelial phenotype. These EPCs showed expression of various endothelial markers and are incorporated into neo-vessels at sites of ischemia (Lee *et al.*, 2014; Peters, 2018). Since the initial discovery of EPCs and their association with vascular repair, numerous studies have been carried out and have demonstrate that EPCs were indeed pro-angiogenic in a variety of ischemia models. In models of myocardial infarctions an arterial injury EPCs have been shown to localize preferentially to sites of vascular lesions, after which they divide, proliferate and become incorporated into the endothelial layer of existing vessels, and promote the outgrowth of new vascular networks. These cells also have an effect on surrounding cells by producing angiogenic growth factors (Kunz *et al.*, 2006; Zhang, Malik and Rehman, 2014b).

The two types of EPC that have garnered the most attention, in regards to vascular repair, are Early (CFU-EC, CFU-Hill, CAC) and Late (ECFC)-Outgrowth Endothelial Progenitor Cells. Currently EPCs are defined as either early or late outgrowth based on their biological properties and their time of appearance during *in vitro* culture (Cheng *et al.*, 2013). The early outgrowth cells are short lived, with a life span of less than two weeks, and do not differentiate into endothelial cells *in vivo*. They can, however, restore endothelial function and enhance angiogenesis after ischaemia through paracrine effects. The late outgrowth EPCs have a high proliferative potential, are able to differentiate into vascular endothelial cells and form networks *in vivo* and *in vitro* (Cheng *et al.*, 2013). The angiogenic function and morphology is maintained in patients with cardiovascular disease risk factors and patients at end stage renal failure. It has also been demonstrated that their proliferation and tube forming ability are increased with laminar shear stress which suggests a role in autologous vascular repair (Zhao *et al.*, 2016). The presence of circulating early outgrowth endothelial progenitor cells, categorised as

colony forming units (CFU-EC), can be used to determine the severity of cardiovascular disease. The number of these cells in circulation is inversely related to an individual's cardiovascular risk profile (Kunz *et al.*, 2006).

The extent and type of vascular intima repair or regeneration seems to be dependent on the extent and type of injury and the age of the host (Kachamakova-Trojanowska *et al.*, 2015). EPCs can mediate vascular repair and attenuate atherosclerosis progression even in the continued presence of vascular injury. Although the mechanisms involved are still not clear, EPCs seem to contribute to the restoration of the endothelial monolayer. In addition, autologous EPCs that overexpress endothelial nitric oxide synthase (eNOS) improve endothelial integrity when transplanted into mice after carotid artery balloon injury. Increased NO bioavailability significantly strengthens the vasoprotective properties of the reconstituted endothelium, leading to inhibition of neo-intimal hyperplasia (Renna *et al.*, 2017).

1.1.11.1 EPC Homing

For EPCs to contribute to vascular repair, they must first be mobilised to the injury site where they can differentiate into mature endothelial cells. The homing of EPCs to neovascular area requires a coordinated sequence of multistep events that conclude with differentiation into endothelial cells. The homing of leukocytes to denuded endothelium is well documented and the homing of EPCs has been shown to share some commonalities. Both involve a multistep cascade of adhesive and signalling events including chemotaxis, selectin-mediated tethering and rolling, and integrin-mediated firm adhesion and diapedesis (Li *et al.*, 2015; Williams and Silva, 2015). These processes are mediated mainly via growth factors which include, but are not limited to, stromal-derived factor (SDF-1), VEGF, granulocyte-colony-stimulating factor (G-CSF), stem cell factor, soluble intercellular adhesion molecule, granulocyte-monocyte-colony-stimulating factor, hepatocyte growth factor, interleukin-6 (IL-6), IL-10, oestrogen, and eNOS (Maeng *et al.*, 2009; Li *et al.*, 2015).

SDF-1, a member of the chemokine CXC subfamily, was identified as an important factor for the trafficking of EPCs to ischemic tissues; it has also been recognized as a prominent target for increasing the engraftment of progenitor cells (Maeng *et al.*, 2009; Ramji and Davies, 2015). β2-integrin expressed

in EPCs, as well as platelets, have also been shown to mediate augmentation of the homing and neovascularization capacity of EPCs *in vitro* and *in vivo*, while CXCR2 also increased the homing of circulating EPCs to the sites of artery injury, possibly by enhancing adhesion of EPCs to extracellular matrix co-immobilized with chemokines. Maeng et. al demonstrated that insulin-like growth factor-2 (IGF2) strongly stimulates the events required for EPC homing. IGF2 expressed under hypoxic conditions promoted both the recruitment and incorporation of EPCs specifically through an IGF2R-dependent signalling pathway, but had no significant effects on the expression of known molecules related to EPC recruitment such as CXCR4/CXCR2, VEGFR2, integrins, and their ligands. Vascular smooth muscle cells (VSMCs) exposed to the blood flow might also secrete arrest chemokines, thus facilitating the capture of circulating progenitor cells (Hristov *et al.*, 2007; Maeng *et al.*, 2009).

The homing of circulating EPCs to sites of arterial injury is a complex process primarily directed by signalling via key CC- and CXC-chemokines and their respective receptors (e.g., CCR2, CCR5, CXCR2 and CXCR4) as well as via β-integrins and P-selectin. It has been revealed that blocking CXCR4 significantly reduced the adhesion of EPCs after arterial wire-injury *in vivo*. Additionally, SDF-1 mediated migration of isolated EPCs, enhanced their matrix arrest when acting as a soluble chemokine, and was further secreted by activated platelets and SMCs after arterial wire-injury (Hristov *et al.*, 2007; Mayorga *et al.*, 2018). The SDF-1 (CXCL12)/CXCR4 axis is of interest as it is vital for angiogenesis, vasculogenesis as well as vascular repair (Ratajczak *et al.*, 2006; Mayorga *et al.*, 2018), and studies have highlighted it's importance in recruiting stem cells to sites of vascular injury (Sainz and Sata, 2007; Xu *et al.*, 2017; Liesveld, Sharma and Aljitawi, 2020).

Adhesion molecules of the selectin and integrin family are also essential for EPC arrest to endothelial cells or extracellular matrix compounds both *in vitro* and *in vivo*. EPCs have also been found to exhibit surface expression of the P-selectin glycoprotein ligand-1 (PSGL-1) and were recruited on activated endothelial cells in a P- and E-selectin-dependent manner. Chemokines such as CCL2 have also been shown to trigger integrin activation to mediate arrest of rolling leukocytes (Liu *et al.*, 2016; Barbier *et al.*, 2020).

Platelets have also been shown to have some influence in regards to guiding EPC homing. In the pathogenesis of atherosclerosis, activated platelets play a crucial role in terms of propagating the inflammatory response. Soon after endothelial denudation, platelets interact with the extracellular matrix and become activated. Activated platelets produce SDF-1 and the CXCL7 precursor β-thromboglobulin, and also induce secretion of diverse chemokines, such as CCL2 and CXCL8. Thus, the platelet-coated extracellular matrix represents an attractive adhesive surface promoting arrest of circulating $CD34^+$ progenitor cells *in vitro* as well as *in vivo* (Hristov *et al.*, 2007).

1.1.12 Effect of Statins on EPC Activities

Beyond their effects on lowering cholesterol, statins have additional pleiotropic effects that are still under investigation. Some of these reported effects include modulation of immune responses, enhancement of anti-inflammatory processes, and their alterations of signalling pathways that involve cholesterol intermediates. There are a multitude of diseases in which statins induce a clinical benefit attributed to these pleiotropic effects. These include multiple sclerosis (MS), inflammatory bowel diseases (IBDs), rheumatoid arthritis (RA), systemic lupus erythematosus (SLE), chronic obstructive pulmonary disease (COPD), cancer, strokes, Parkinson's and Alzheimer's diseases, bacterial and HIV infections (Ramji and Davies, 2015; Gorabi *et al.*, 2020).

In relation to EPC behaviour, statins have been shown to have a role in enhancing revascularisation after ischaemic events. According to Chiang *et al.,* (2015), administration of the most potent statins, atorvastatin and rosuvastatin, had the effect of promoting EPC-mediated small vessel formation which enhanced the recovery of capillary density in ischaemic hind limb mice (Chiang *et al.*, 2015). Following statin administration, several genes are activated that stimulate ischaemic neovasculogenesis by promoting the homing of EPCs to the ischaemic site. According to Kunz et. al (2006), EPC levels have been found to be lower in older patients and patients undergoing haemodialysis but increase with statin therapy (Kunz *et al.*, 2006).

The effect of statins on circulating EPC numbers in patients with ischaemic heart failure was

demonstrated by Oikonomou et. al (2015) who evaluated the effect of varying doses of atorvastatin. The doses used were 10mg/day and 40mg/day and they demonstrated that there was a marked increase in numbers of EPC after drug administration, with the 40mg/day dosage showing higher numbers of EPCs compared to the baseline and the 10mg/day dosage (Oikonomou *et al.*, 2015).

The current data available on the interactions between statins and EPCs has repeatedly shown that statins can increase the numbers of EPCs in circulation and this in turn contributes positively to endothelial repair and neovascularisation in patients with cardiovascular disease (Chiang *et al.*, 2015; Gorabi *et al.*, 2020). A likely mechanism behind enhanced recruitment of EPCs could lie in the homing signals of the SDF-1/CXCR4 axis, which have been shown to have significance for angiogenesis and vascular repair (Mayorga *et al.*, 2018), expecially given that statins have been associated with having an effect on this axis (Gao, Yu and Tang, 2019; Yu and Feng, 2008). Figure 1-5 details the mechanisms associated with EPC migration and differentiation.

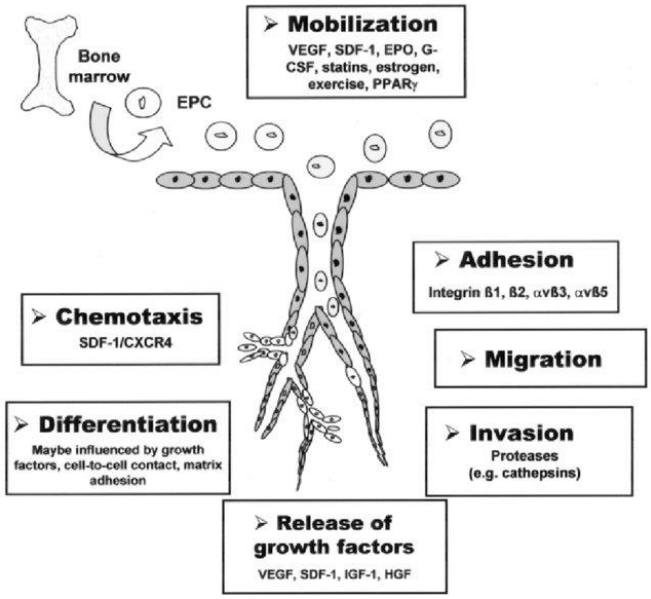

Figure 1-5: Mechanisms associated with EPC recruitment and differentiation (Meiliana and Wijaya, 2009). This image details the factors known to affect EPC behaviour, with statins included as promoters of mobilisation of this cell type and SDF-1/CXCR4 being mediators of chemotaxis.

Given the vast amount of interest in the role of EPCs and the established correlation of statins and these cells, there is value to be gained in determining the exact mechanisms in play between them and the effect they have on vascular repair. The primary mode of assessment of this interaction have been

the use of animal models (Zhang *et al.*, 2014; Mayorga *et al.*, 2018) or the use of clinical studies to evaluate these interactions (Shimoni *et al.*, 2016; Hennekens, Schuttenberg and Pfeffer, 2019; Wiśniewski *et al.*, 2020), which highlights a need for alternative methods of evaluating statin-EPC interactions that are easy to access and allow control of variables.

1.6 Development of a 3D Tissue Engineered Blood Vessel (TEBV)

1.1.13 Tissue Engineering Concepts and Components

Tissue engineering involves the development of tissue and organ substitutes by controlling biological, biophysical and/or biomechanical parameters in the laboratory. This allows for accurate and real-time studies on a variety of tissues and organs and related diseases without the need to use human volunteers or relying on animal models that do not provide the full picture in terms of understanding human structures and processes in health and disease states (Castells-sala *et al.*, 2015). A key component of tissue engineering is using nature as a model for the development of extracellular matrix analogues (scaffolds), either from natural or synthetic origin as well as bioreactors and bio-devices to mimic natural physiological conditions of particular tissues (P. Zhao *et al.*, 2018). These scaffolds embed cells in a three-dimensional environment that display signals critical for the determination of cellular fate, in terms of proliferation, differentiation and migration, among others. The type of cell to be used is also of great importance as this can determine the efficacy of the engineered tissue in terms of replicating native conditions and can also determine usability of the engineered tissue un clinical settings (Castells-sala *et al.*, 2015; P. Zhao *et al.*, 2018). Figure 1-3 shows the inter relation and combinations of the factors to be considered for tissue engineering.

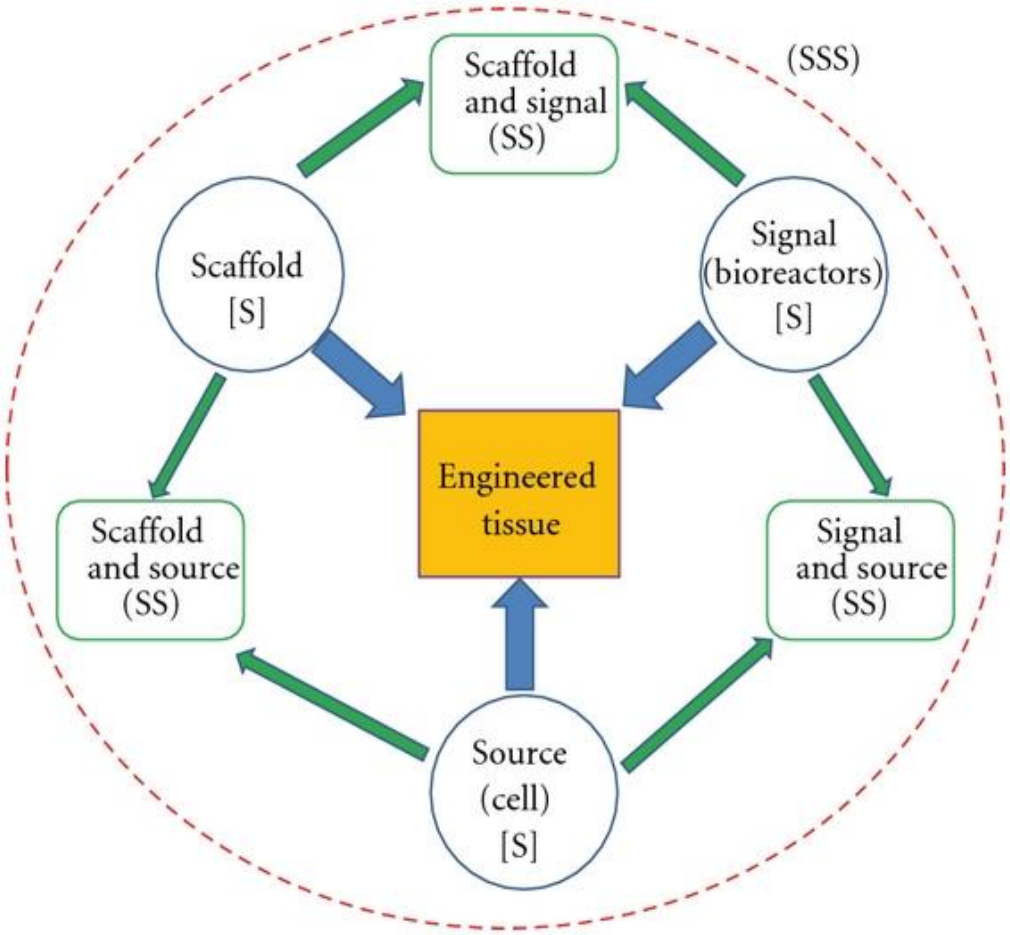

Figure 1-6: Combinations of cell source, scaffold material and signals for generating engineered tissues (Nemeno-Guanzon *et al.*, 2012). Tissue engineering triad of cells or source, signals (provided chemically by growth factors/cytokines or physically by a bioreactor), and the scaffold which acts as a template for tissue formation allowing the cells to migrate, adhere, and produce tissue. These components make up the Triple S (Source, Scaffold, and Signal) of tissue engineering. Any combination of these triad components has been considered in various studies in cell therapy which accounts for SS (Scaffold/Signal, Scaffold/Source, and Signal/Source). Finally, these three components (Source, Scaffold, and Signal or SSS) have also been considered altogether in some research projects.

Ideally, engineered tissues would be three dimensional (3D) representations of physiological and pathophysiological systems that would show the interactions between cell-cell and cell-ECM and can determine whether a given cell undergoes proliferation, differentiation, apoptosis or invasion. However, studies on cellular biology have commonly been performed on two dimensional (2D) cultures, where cells are grown under non-physiological conditions. Specifically, they are unnaturally polarized having one side attached to a rigid and flat substrate and the other one exposed to culture media, which reduces cell-cell and cell-ECM interactions (Castells-sala *et al.*, 2015). The generation of a 3D tissue engineered model would offer a closer representation of native tissues and facilitate a more

detailed understanding of the functioning of the studied system.

1.1.13.1 Cell Source

This is a crucial step in the tissue engineering process and becomes especially vital when intended for clinical applications. The cells selected should fulfil a specific requirement, namely the cells should be able to integrate successfully into the specific tissue and secrete various growth factors and cytokines that activate the endogenous tissue regeneration program. The first approach in cell-based techniques is the use of native progenitor cells (Castells-sala *et al.*, 2015). For the evaluation of cardiovascular disease, the cells needed to replicate vascular tissue will be primary Human Cardiac Artery Smooth Muscle Cells (HCASMCs) for the medial layer and Human Umbilical Vein Endothelial Cells (HUVECs) for the intimal layer. These cells have been used successfully by Musa *et al*., (2016) to establish a protocol to determine the pro and anti-aggregatory properties of the intimal layer of blood vessels using real-time measurements of cytosolic Ca^{2+} signalling to assess platelet activation (Musa, Harper and Yang, 2016). Other works that are aimed at generating functional TEBVs focus on usability for engraftment. An example of this is the work done by L'Heureux et. al., (2006) who used fibroblasts extracted from skin biopsies from patients with advanced cardiovascular disease. While not using cells natively found in a blood vessel, they were able to demonstrate that the TEBV created was anti-thrombogenic and mechanically stable for 8 months *in vivo*. Histological analysis showed complete tissue integration and formation of vasa vasorum (L'Heureux *et al.*, 2006). More recent approaches for vascular tissue engineering utilise embryonic stem cells which can be differentiated into endothelial and smooth muscle cells (Hielscher *et al.*, 2018), as well as induced pluripotent stem cells (iPSCs) which are somatic cells reprogrammed into a stem cells (Hielscher *et al.*, 2018; Song *et al.*, 2018). For example, Nakagami et al., (2006), utilised murine embryonic stem cell–derived embryoid bodies on matrigel and found that differentiated embryonic stem cells (ESCs) seeded on matrigel additionally secreted the growth factors VEGF, basic fibroblast growth factor (bFGF), hepatocyte growth factor (HGF), transforming growth factor (TGF-β) and angiopoietin (Ang-1) (Nakagami *et al.*, 2006; Babczyk *et al.*, 2014). These studies demonstrate that the type of cells used define the type of application they can be used for.

Based on the cell type, the engineered product can be used to determine ideal conditions for generating a specific tissue or can be used directly *in vivo* to replace damaged tissue or can be used to evaluate the various mechanisms that are involved in various disease states.

1.1.13.2 Scaffold Materials

The main role of scaffolds is to provide an appropriate backbone on which cells can be successfully cultured and eventually develop into the desired tissue types. The scaffolds utilised for tissue engineering need to mimic the cellular micro-environment which is mainly generated by the extracellular matrix. Scaffolds, therefore, should incorporate the appropriate biophysical, biomechanical and biochemical cues that guide cell proliferation, differentiation, maintenance and function (P. Zhao *et al.*, 2018). An ideal biomaterial to be used as a scaffold designed for clinical applications should fulfil a set of requirements. First of all, biocompatibility and biodegradability are required. The material needs to allow scaffold replacement by proteins synthesized and secreted by native or implanted cells. Additionally, the material must be clinically compliant to minimize inflammatory and immunological response (Castells-sala *et al.*, 2015). Scaffolds can either be natural or synthetic. The biggest advantage of natural scaffolds is that they are readily accessible and provide a wide range of cues that participate in the process of morphogenesis and function acquisition of different cell types. However, its composition strongly depends on the specific animal origin and the isolation and purification procedures, compromising assay reproducibility. On the other hand, synthetic scaffolds can be custom tailored to mimic specific ECM properties, providing controllable cellular environments (Castells-sala *et al.*, 2015).

Some examples of scaffold used in tissue engineering include Bio-ceramic scaffolds, mainly hydroxyapatite (HA) which have been used to re-create bone tissue. This material shares many of the mineral components of native bone and its biocompatibility and bioactivity successfully promotes new bone formation *in vivo* (Castells-sala *et al.*, 2015). For cartilage repair, a number of natural scaffolds have been utilised i.e., collagen, fibrin, hyaluronan, agarose, alginate or gelatin. In addition to natural scaffolds, synthetic scaffolds are regarded with a variety of advantages, the most relevant being their

reproducibility. For instance, polyurethane, Poly- (Ethylene Glycol) (PEG), elastin-based polymers and self-assembling peptides, such as KLD-12 and RAD16-I are being widely used (Castells-sala *et al.*, 2015). For cardiovascular repair, the preferred natural materials that can be used as scaffolds include gelatines, collagens, laminin, silk, vitronectin and fibrin. Another is chitosan which has been widely used as soft and injectable material and it has been proved that its application in ischemic myocardium could improve myocardial infarction microenvironment (Castells-sala *et al.*, 2015; Lee and Kim, 2018). Acellular tissue matrices have also been used for the regeneration of skin and genitourinary tissues, including urethra and bladder, with no evidence of immunogenic rejection (Sobti *et al.*, 2018). They are fabricated by removing cellular components from tissues by mechanical and chemical manipulation to produce collagen-rich matrices which supports the cell growth. These acellular matrices are considered an ideal scaffolding system due to their structural and mechanical similarity to native tissues (Babita Mahanta, 2014; Li and Cui, 2014; Song *et al.*, 2018).

1.1.13.3 Static and Dynamic Culture Conditions

Traditionally, cell cultures used for tissue engineering have been grown on a 2D surface under static conditions where the cells are incubated with supplemented culture media and nutrients are transferred through simple diffusion which is sufficient to maintain cell viability. The obvious limitation with this is that tissues are not two-dimensional structures and involve the interplay of a variety of factors. For a tissue engineered model to be effective, it must bear as close a resemblance as possible to the native tissue in question. This aim has been greatly aided by the development and use of bioreactors. A bioreactor is a device that reproduces the physiological environment, including biochemical and mechanical functions, that are specific to the tissue that is to be regenerated. Bioreactors can also be used to apply mechanical strength during maturation of the tissue and for studying and understanding the mechanical factors influencing tissue regeneration (Polak, 2010). They have been successfully used for supplying nutrients, oxygen, removing catabolites, monitoring pH and applying mechanical stresses to stimulate the formation of extracellular matrix (Polak, 2010; Selden and Fuller, 2018). For vascular tissue engineering, the key stimuli needed are shear stress and pressure

and in the context of vascular grafts, axial stretching or torsion loads are of importance in generating tissues that are able to withstand physiological stresses (Selden and Fuller, 2018; Stefani *et al.*, 2018). Examples of vascular tissue engineering approaches incorporating dynamic flow and shear stress have been increasing over the years. An example of this is the creation of porous tubular scaffolds by Tresoldi et. al., where they used a gel comprised of alginate and gelatin, functionalised with fibronectin, delivered onto a porous scaffold to create a tubular structure in a modified bioreactor that was able to provide longitudinal rotation and ensure full coverage of then porous scaffold with the functionalised gel (Tresoldi *et al.*, 2019), with the aim of optimising endothelial seeding into a tubular structure capable of withstanding physiological shear.

1.1.14 Comparison of Animal Models vs. Tissue Engineered Models

Animal models have proven useful over the course of decades of scientific research. A number of different animal models have been developed to support preclinical and clinical research (Oppi, Lüscher and Stein, 2019). However, many of the conventional animal models are not suitable models for studying human disease as the disease pathologies are likely to be different as will the specific cellular responses. The limitations are more pronounced when it comes predicting the effectiveness of treatment strategies in human beings (Rahbari *et al.*, 2017). With the increasing importance of evidence-based interventions in clinical practise, reliable and accurately representative models of human tissues and systems need to take precedence over the traditional animal model. An example of this is observations on the effect of ketamine, a common anaesthetic used in animal studies. It was found that ketamine inhibited platelet aggregation through suppression of IP_3 formation and inhibiting the activity of thromboxane synthase (Nakagawa *et al.*, 2002; Lisek, Zylinska and Boczek, 2020). Ketamine has also been found to interfere with endothelial nitric oxide production and smooth muscle Ca^{2+} signalling (Akata, Izumi and Nakashima, 2001; Kurebayashi and Ogawa, 2001). Using *in vitro* culture models eliminates some but not all of the problems associated with clinical research using human subjects and animal models of disease. In many cases, culture models help to overcome barriers and allow researchers to gain a better understanding of disease pathogenesis, characteristics

and responses to treatments (Mobasheri and Lewis, 2013).

1.1.15 Applications and Relevance of TEBV

The development of a tissue engineered blood vessel (TEBV) that incorporates a medial and intimal layer will provide an ideal and unique opportunity to study a variety of factors that are involved in maintaining vascular homeostasis as well factors that contribute to pathogenesis and vascular repair processes. The use of cells and components that are part of the native tissue would provide a detailed representation of the cell-cell interactions, changes in surface receptor expression in various physiological states and allows for the controlled introduction of other factors such as drugs, platelets and other cell types. With the incorporation of a perfusion system, flow conditions and their effects can also be assessed under various physiological states.

1.7 Development of a Perfusion System

As mentioned previously, shear stress is a necessary element in the maintenance of vascular homeostasis and variations from normal physiological values contributes to pathological processes, in this case vascular remodelling due to cardiovascular disease.

1.1.16 Shear Stress and its Effects

As mentioned in earlier, under normal conditions, shear stresses maintain their direction and their magnitude within a range of values that impedes atherogenesis, thrombosis, adhesion of leukocytes, smooth muscle proliferation and endothelial apoptosis (Papaioannou and Stefanadis, 2005). The haemodynamic conditions inside blood vessels lead to the development of superficial stresses near the vessel walls, which can be divided into two categories: (1) circumferential stress due to pulse pressure variation inside the vessel; (2) shear stress which is applied on the vessel walls by the flow of blood. Shear-induced mechanotransduction, which refers to the conversion of mechanical stresses to biochemical responses, is particularly important in arteries, in which blood flow regulates vascular tone and structure. This regulation occurs via mechanically stimulated release of potent, shear-responsive, endothelial-derived factors such as nitro-vasodilators, prostaglandins, lipoxygenases, hyperpolarizing factors, growth factors and other related molecules (Papaioannou and Stefanadis, 2005; Davies, 2009).

Normal arterial shear stress is usually greater than 15 dyne/cm^2 and induces endothelial quiescence and an atheroprotective gene expression profile whereas shear stresses lower than 4 dyne/cm^2 stimulates an atherogenic phenotype (Malek, Alper and Izumo, 1999).

1.1.17 Benefits and Limitations of Perfusion System

The biggest advantage of using a perfusion system is that it allows for the generation of the necessary biomechanical forces that are reflective of physiological and pathological conditions. As has been already mentioned, shear stress is vital in maintaining vascular tone and conditioning cells to have the expected native morphology. It will be possible to visualise in real time the interactions between the TEBV and the cells and substances that will be perfused over it. The main limitation with this system is maintenance of sterile conditions and conserving cell culture conditions as they would be in an incubator.

1.1.18 Types of Perfusion

Perfusion, overall, refers to the delivery of blood or other fluid to tissues and organs. In the field of tissue engineering, the ability to maintain suitable oxygen tensions and nutrient diffusion throughout the scaffold is critical for cell viability and function. One of the ways that this has been addressed is through the use of channelled scaffolds (Lovett *et al.*, 2009). Channelled scaffolds have been formed by incorporating phosphate-based glass fibres into collagen scaffolds or by using a laser cutting system to bore holes into a scaffold. Another technique that can be used to enhance vascularisation is directing scaffold vascularization through micro-patterning or molecular gradients. This offers scaffold cues that can effectively dictate the migration and alignment of cells within the construct (Lovett *et al.*, 2009). Work with scaffold patterning has included the formation of grooved, porous poly-caprolactone scaffolds. These scaffolds were produced by mixing the poly-caprolactone (PCL) with Poly D, L-lactic-co-glycolic acid (PLGA) micro/nanoparticles and casting the polymer onto a grooved surface before leaching out the micro/Nano spheres. This process produces surfaces that are conducive for vascular cell alignment and also increase medium diffusion. By stacking these layers, it may be possible to build up 3D tissues with cellular organization for blood vessel formation, an outcome that may also be

directed by forming gradients within the scaffold (Lovett *et al.*, 2009).

Aside from modifications to the scaffold to facilitate diffusion of oxygen, carbon dioxide and nutrients, bioreactor systems are often used to perfuse culture medium through a porous scaffold to try to maintain cell viability in the middle and homogeneity throughout the construct. One way this can be achieved is through the use of rotating bioreactors. The horizontally rotating bioreactors, or slow-turning lateral vessels, were designed as a rotating cylinder of culture medium, with a gas-permeable membrane for oxygen and carbon dioxide exchange, and fittings for sampling or medium exchange. The speed of the rotation could be controlled to match the settling velocity of the tissue constructs, keeping them suspended within the vessel. This approach has been used for engineering of bone, cartilage, and cardiac tissue (Lovett *et al.*, 2009).

Microfabrication techniques have gained popularity as they offer fine control over the formation of a microvascular network. Through the fabrication of a negative mould, a complex capillary pattern may be formed and serve as a template for moulding materials. These capillary networks may be perfused and incorporate an endothelial layer, providing a mimic of natural vasculature as well as oxygen and nutrient delivery and waste removal. Standard techniques use plasma etching or lithographic techniques to produce desired features with micron-scale precision, with replica moulds of polydimethylsiloxane (PDMS) cast from the negative feature moulds. These moulds may then be bonded with one another before seeding with endothelial cells to form cylindrical capillary channels. Direct-write assembly has been used to form 3D microfluidic devices for vascular tissue engineering (Lovett *et al.*, 2009).

Microfluidic channels are especially attractive since they can be easily multiplexed with integrated fluid handling operations for efficient and high throughput cellular analysis, imaged for in situ monitoring of cellular events, and can recapitulate a physiological cellular microenvironment with controllable distribution of biochemical molecules and shear stresses at the cellular resolution (Toh *et al.*, 2007). The main limitation with these systems is they are commonly used in 2D settings, with the cells being perfused being cultured on glass or plastic surfaces, which is not representative of native tissue arrangements. Cells grown in a 3D

model have proven to be more physiologically relevant and showed improvements in several studies of biological mechanisms like: cell number monitoring, viability, morphology, proliferation, differentiation, response to stimuli, migration and invasion of tumour cells into surrounding tissues, angiogenesis stimulation and immune system evasion, drug metabolism, gene expression and protein synthesis, general cell function and *in vivo* relevance (Anton *et al.*, 2015).

In addition to perfusion, the exertion of shear stress and laminar flow, especially in vascular tissue engineering, is an important aspect in generating the necessary stimuli for cell function. Anisi et. al., (2014) utilised computational fluid dynamics to optimise conditions in their bioreactor/flow chamber. They utilised endothelial cells cultured on a collagen matrix and exposed to unidirectional pulsatile flow, generated by a peristaltic pump. They managed to attain endothelial elongation and alignment along the direction of flow with minimal detachment of cells (Anisi *et al.*, 2014). Parallel plate flow chambers, microfluidic chambers and cone-plate chambers are other common means of generating shear stress (Wang *et al.*, 2016). Under steady, pulsatile laminar flow wall shear stress, endothelial cells elongate and align parallel to the flow direction through cytoskeletal remodelling, while under oscillatory flow, these cells are randomly oriented, adopt a polygonal shape and behave in a manner that is typical of endothelial dysfunction (Wang *et al.*, 2016; Kouzbari *et al.*, 2019). This demonstrates the importance of flow type and directionality in improving endothelial function and generating stimuli that are reflective of physiological as well as pathological conditions.

1.8 Project Rationale

There is an increasing need for the development and use of more biomimetic models, that can replicate structural and environmental cues, to study disease pathology and associated/potential therapies, and which can alleviate the reliance on animal models. As pertains to cardiovascular disease, lipid irregularities in atherosclerosis have long been known to be a driving force towards disease progression. Statins have been the primary prescription to lower levels of cholesterol, thus halting or reversing disease progression. Their association with improving patient health following ischaemic cardiac events, possibly through their effects on EPCs, and concurrent interest in EPC role

in vascular healing, have led to investigations aimed at defining a new role for statins in managing atherosclerosis and related cardiovascular diseases. Tissue engineering provides a unique opportunity to create vascular models, which would alleviate the need for animal models, provide physiological relevance - as tissues would be made using human cells and be subjected to various stimuli in a controlled manner- and can be used to more accurately study human biological processes.

1.9 Project Aims

The primary aim of this thesis was to evaluate the pleiotropic effects of statins using 3D blood vessel models, with a special focus on EPC homing under shear stress. As such, the following objectives were developed and implemented per experimental chapter:

- Chapter 3 - To isolate and characterize endothelial progenitor cells (EPCs) and evaluate their responses to atorvastatin individually and in co-culture with endothelial cells (HUVECs). To do this, EPCs were obtained from commercial sources and healthy volunteers. EPC were characterized based on morphological factors such as colony formation and tube formation, as well expression of key surface markers.
- Chapter 4 - following optimization of isolation and characterization protocols for EPCs, their migratory responses to varying concentrations of atorvastatin were evaluated using a scratch wound model. Responses were compared to MSCs from different species.
- Chapter 5 - To evaluate EPC responses to tissue engineered constructs;
    - Create tissue engineered intimal and medial layers and a composite blood vessel model enabling the study of individual cell types, their contribution and sensitivity to a lesion and atorvastatin.
    - Adapt a commercially available parallel plate flow chamber to accommodate 3D tissues; compare shear stress with that of oscillating rocker
    - Evaluate effect of atorvastatin incubation time on homing
    - Determine atorvastatin’s effect on SDF-1/CXCR4 axis.

- Chapter 6 - Develop a foam cell model to evaluate atorvastatin’s effect on foam cell formation.

Chapter 2:
Materials and Methods

2.1 Materials

APPLICATION	MATERIALS	SUPPLIER
Cell culture: Items used for Cell maintenance and differentiation	DMEM	Scientific Lab Supplies
	Medium 200	GIBCO, Life Technologies
	Medium 231	GIBCO, Life Technologies
	Low serum growth supplement (LSGS)	GIBCO, Life Technologies
	Smooth muscle growth supplement (SMGS)	GIBCO, Life Technologies
	Penicillin/Streptomycin (AA)	Scientific Lab Supplies
	L-glutamine (LG)	Scientific Lab Supplies
	Trypsin	Scientific Lab Supplies
	Foetal bovine serum (FBS)	Scientific Lab Supplies
	Human cardiac artery smooth muscle cells (HCASMC)	GIBCO, Life Technologies
	Human umbilical vein endothelial cells (HUVEC)	GIBCO, Life Technologies
	Rat bone marrow stem cells (rMSC)	Freshly isolated
	Human bone marrow stem cells (hMSC)	Isolated from bone marrow mononuclear cells, Lonza
	Endothelial progenitor cells	Biochain (Amsbio) and isolated from Healthy volunteers
	RAW 264.7 (RAW264)	ATCC
	Cell scrapers	Scientific Lab Supplies
	Atorvastatin Calcium Trihydrate (5g)	Active Pharma Supplies Ltd.
	Cell counting kit-8 (CCK-8) Cell proliferation	Dojindo Molecular

	assay and cytotoxicity assay	Technologies Inc
	LDL (100mg)	2bscientific
	IFN-γ	Peprotech
	Lipopolysaccharide (LPS)	Sigma (Merck)
	Ascorbic acid	Sigma (Merck)
	Beta glycerophosphide	Sigma (Merck)
	Dexamethasone	Sigma (Merck)
	Non-essential amino acids (NEAA)	Sigma (Merck)
	Insulin-transferrin-selenium (ITS)	GIBCO, Life Technologies
	L-proline	Sigma (Merck)
	Sodium pyruvate	Sigma (Merck)
	TGF-β3	GIBCO, Life Technologies
	3-Isobutyl-1-methylxanthine (IBMX)	Sigma (Merck)
	Insulin	GIBCO, Life Technologies
	Indomethacin	Sigma (Merck)
EPC isolation	Ficoll-paque	Sigma (Merck)
	Luer lock syringes (60ml)	Scientific Lab Supplies
	Acid citrate dextrose (ACD) (85 mM sodium citrate, 78 mM citric acid and 111 mM d-glucose)	All from Sigma (Merck)
Imaging	Olympus Confocal microscope (Fluoview FV1200)	Olympus
	Leica inverted fluorescence microscope (MSV269)	Leica
	Olympus brightfield microscope (CKX41)	Olympus

	EVOS brightfield microscope	EVOS
Perfusion	Watson-Marlow 505 series peristaltic pump	Watson-Marlow
	PDMS	Scientific lab supplies
	Parallel plate flow chamber (ProFlow Chamber)	Warner Instruments, USA
	Fluorescein isothiocyanate isomer I	Sigma
	Silicon grease	RS
3D Models	Rat tail collagen I	Scientific Lab Supplies (Corning)
	Whatman filter paper	Scientific Lab Supplies
	Scalpel blades	Scientific Lab Supplies
	Polytetrafluoroethylene (PTFE)	Scientific Lab Supplies
	Fibronectin from bovine plasma	Sigma (Merck)
Cell staining	5-(and-6) carboxyfluorescein diacetate, succinimidyl ester, mixed isomers (CFSE)	GIBCO, Life Technologies
	Mouse anti-human PECAM-1 (CD31),	Santa Cruz Biotechnology
	goat anti-mouse IgG FITC	Santa Cruz Biotechnology
	Alexafluor-568 Goat anti-mouse IgG	Gibco Life Technologies.
	Hoechst-33258	ThermoFisher Scientific
	E-selectin Alexa fluor 488-conjugated primary antibody	R&D Systems
	Nile Red	Sigma (Merck)
	Oil Red-O	Sigma (Merck)
	Anti-mouse CD36 antibody	abcam
	Anti-mouse CD146 antibody	abcam

	Flk-1-NL463 conjugated antibody	Santa Cruz
	Mouse anti-human CD45 antibody	Santa Cruz
	Mouse anti-human CD34 antibody	Santa Cruz
	Rabbit anti-human CXCR4 antibody	Abcam
	Donkey anti-rabbit IgG	R&D Systems
	Poly-L, D-lactic acid (96% l/4% d) (PLA)	Purac BV (Gorinchem, the Netherlands).
Electrospinning	Chloroform	Sigma (Merck)
	N-N-dimethyl formamide (DMF)	Sigma (Merck)
	Acetate sheets	Ryman's
	3M spray on adhesive	Amazon/Ryman's
	ABTS	Sigma
Cytokine profiling	SDF-1 mini ABTS ELISA kit	Peprotech
	Tween-20	Sigma (Merck)
	Copper sulphate ($CuSO_4.5H_2o$)	Scientific Lab Supplies
Miscellaneous	EDTA	Sigma (Merck)
	Isopropanol (isopropyl alcohol/propan-2-ol)	Sigma (Merck)
	Bovine serum albumin (BSA)	Sigma (Merck)
	Phosphate buffered saline (PBS)	Scientific Lab Supplies
	UV cabinet	BioRad
	Slide-a-lyzer dialysis cassettes	ThermoFisher Scientific
	dialysis cassette floats	ThermoFisher Scientific
	99.9% Ethanol	Scientific Lab Supplies
	Plate reader	Biotec
	Silicon glue	RS

	Phosphoric acid	Sigma (Merck)
	Sulphonamide	Sigma (Merck)
	Naphthalene-diamine-hydrochloride	Sigma (Merck)
	Sodium nitrile	Sigma (Merck)
	Iron III chloride ($FeCl_3$)	Sigma (Merck)
	See-saw rocker	Cole-Parmer
	Hydrochloric acid (HCL)	Thermo-fisher

2.2 Methods

2.1.1 Cell culture

2.1.1.1 HCASMC

Human cardiac artery smooth muscle cells (HCASMCs) were used in the assembly of the tissue engineered blood vessel (TEBV). These cells were cultured in medium 231 and supplemented with smooth muscle growth supplement (SMGS) as per the supplier specifications. The cells used in the assembly of the TEBV were between P3 and P5.

2.1.1.2 HUVEC

Human Umbilical Vein Endothelial Cells (HUVECs) were cultured in medium 200 supplemented with low serum growth supplement (LSGS) as per the supplier recommendations. The cells used were between P2 and P5.

2.1.1.3 RAW 264

RAW 264 cells were cultured in DMEM supplemented with 10%FBS, 1%LG and 1% AA. Cells were sued between P3 and P14.

2.1.1.4 rMSC

Rat mesenchymal stem cells (rMSC) were derived from rat bone marrow by Hamza A. Owida (Owida *et al.*, 2017), and were cultured using Alpha MEM (without L-glutamine) and supplemented with FBS, L-glutamine and AA. The supplements were mixed as follows based on total media volume; 10% FBS, 1% L-glutamine and 1% AA. Cells used were between passage 3 and 6 (P3 and P6).

2.1.1.5 hMSC

Cell were obtained from Anthony Deegan and were previously differentiated into monocytes (Deegan, 2013). Cells were cultured in DMEM (4.5g/L glucose) supplemented with 10% FBS, 1% AA and 1% LG. Cells used were between passage 3 and 6 (P3 and P6).

2.1.1.5.1 Tri-lineage differentiation

This was carried out for rMSCs and hMSCs. Cells were seeded at 1 x 10^4 cells per well in a 12 well plate

and cultured for 21 days. Cells were differentiated along osteogenic, chondrogenic and Adipogenic lineages (Chong *et al.*, 2012; Heidari *et al.*, 2013). Osteogenic media was comprised of ascorbic acid (5µM), beta glycerophosphide (10mM), dexamethasone (0.1µM), FBS (10%), NEAA (1%) and L-glutamine (1%); Chondrogenic media was comprised of insulin-transferrin-selenium (ITS) (1%), dexamethasone (0.1µM), ascorbic acid (50µM), L-proline (40µg/ml), sodium pyruvate (1%), TGF-β3 (10ng/ml), FBS (1%), NEAA (1%) and L-glutamine (1%). Adipogenic media was comprised of dexamethasone (0.5µM), 3-Isobutyl-1-methylxanthine (IBMX) (0.5mM), Insulin (10µg/ml), indomethacin (100µM), FBS (10%), NEAA (1%) and L-glutamine (1%). Control samples were fed with the standard media composition described previously. All media was changed every 2 days. After 21 days, samples were fixed with 4% PFA for 20 minutes then stored in PBS. To assess differentiation, samples were stained with alizarin red, alcian blue and oil red-O for osteogenic, chondrogenic and Adipogenic differentiation respectively.

2.1.1.5.1.1 Histological staining

2.1.1.5.1.1.1 Alizarin red

To identify mineral/calcium deposits, a 2% alizarin red solution, prepared in distilled water, was added to fixed cells for 15 minutes at room temperature. The stain was then removed and the cells washed twice with dH_2O. Following this, cells were imaged with EVOS microscope.

2.1.1.5.1.1.2 Alcian Blue

To identify glycosaminoglycans secreted by chondrocytes, a 0.1% solution of alcian blue was prepared by filtering 1% (v/v) alcian blue mixed with 0.1M HCl. Cells were stained for 15 minutes, followed by two dH_2O washes. Cells were imaged using EVOS microscope.

2.1.1.5.1.1.3 Oil Red-O

To identify cellular lipid content, a 0.5% solution of oil red-O in isopropanol was diluted 3:2 with deionised dH_2O and added to fixed cells for 15 minutes. The stain was removed and cells washed twice with dH_2O. Cells were imaged using EVOS microscope.

2.1.1.6 Commercially sourced EPCs

Purchased cell were revived and cultured according to supplier protocol. Frozen cells were first thawed in a 37°C water bath, followed by transfer inti a 15 ml falcon tube. The vial containing the cells was rinsed with 1 ml of fresh growth medium, which was also added to the falcon tube. Cells were centrifuged for 6 minutes at 400g. Supernatant was removed and the resultant cell pellet was transferred to a T-25 flask topped up with 8 ml of EPC medium.

2.1.1.7 EPC isolation from whole blood and culture

EPCs were isolated by collecting 60mL of whole blood from healthy volunteers. To prevent coagulation, the blood was split into 2 falcon tubes with 5mL of ACD (85 mM sodium citrate, 78 mM citric acid and 111 mM d-glucose) in each. The blood-anticoagulant mix is then split into 15ml falcon tubes and centrifuged at 2800 rpm for 8 minutes. After Centrifugation, the sequence of layers occurs as follows (seen from top to bottom) (figure 2-1): Plasma, enriched cell fraction (interphase consisting of lymphocytes / Peripheral bone marrow cells (PBMCs)), Erythrocytes and granulocytes. The plasma fraction is carefully discarded, to avoid agitating the layers, leaving approximately 0.5-1mL above the interface.

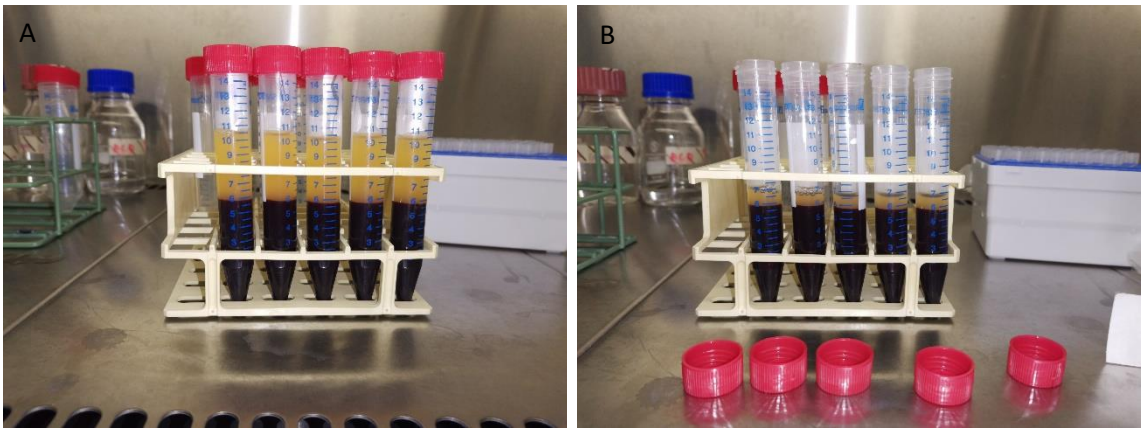

Figure 2-1: Blood separation. Here we see the expected separation of blood components (A). The plasma fraction is discarded leaving the enriched fraction above the layer of RBCs and granulocytes (B).

The enriched cell fraction is pooled into one tube and diluted 1:1 with PBS. To further separate the cell i.e., eliminate residual plasma and RBCs, the pooled fraction is carefully layered over 8mL of Ficoll-paque, ensuring no mixing of the layers, and centrifuged again for 20 minutes at 400g. After

centrifugation, any residual red blood cells are below the separation medium and the enriched cell fraction should be immediately above it with diluted plasma and platelets above this. Discard the plasma layer and leave about 0.5mL above the enriched cell fraction. The cell rich fraction was again diluted with PBS (topped up to 10mL), then centrifuged again at 400g for 10 minutes. After centrifugation, supernatant is discarded, and the resultant pellet is resuspended in 2mL of complete EPC media, comprised of Medium 200, 10% FBS and 1% AA. The cell suspension is then split into 2 wells of a 12 well plate that has been coated with fibronectin (at a concentration 0f 2.5 µg/cm^2). Some cells were cultured on collagen (2mg/ml) coated plates as a comparative substrate. After seeding, the well-plate is transferred to an incubator (37°C; 5% CO_2). The cells are now at culture day zero (D0). On the following day (D1), the contents of the wells are agitated and transferred to new wells (figure 2-2).

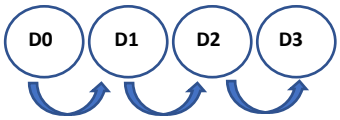

Figure 2-2: Sequence of cell transfer. To ensure trapping as many adherent cells as possible, after initial seeding in the first well, the next day, media is removed and sedimented cells are mixed with fresh media, which is agitated to gather all non-adhered cells, and transferred to another well. This was repeated daily for 3 days at which point the majority of adherent cells had been collected.

This agitation and transfer of non-adherent cells to new wells was carried out for another 3 days to ensure maximum collection of non-adhered cells. Media is changed daily for the first 7 days then every 2-3 days for the duration of culture.

2.1.1.8 RAW 264

Isolated from mice, RAW264.7 cells were cultured in DMEM supplemented with 10%FBS, 1%LG and 1% AA. Cells were used between P3 and P14.

2.1.1.9 Cell fixation

To preserve cells/tissue samples, they were fixed with 4% PFA; 20 minutes for monolayer culture and 1 hour for TE constructs. This was followed by removal of the fixative and addition of PBS for storage at 4°C.

2.1.1.10 EPC characterisation

2.1.1.10.1 Morphology

Isolated EPCs were cultured in Medium 200 supplemented with 1%AA and 10% FBS. Cells were cultured for up to 20 days as they are not proliferative and attain senescence after this time frame. Cells used for experimentation were aged between 8 and 20 days. Images were taken every 3 days for duration of culture and sued to evaluate morphology changes, colony and tube formation.

2.1.1.10.2 Key biomarker expression

Immunostaining was carried out to identify specific markers of EPC identification. Antibodies used were CD31, CD34, CD45, Flk-1 and CXCR4. Samples were first incubated with 5% BSA for 1 hour, followed by addition of the primary antibodies, used at a concentration of 1:200. Samples were incubated for 2 hours at 37°C, 5% CO_2. Following this, samples were washed twice with 0.05% Tween 20, then twice with PBS before the addition of secondary antibody at 1:400 dilution. Secondary antibody was incubated for 1 hour at 37°C, 5% CO_2. This was followed by 2 washes with 0.05% Tween 20, and another 2 washes with PBS. DAPI was used at a concentration of 10 ng/ml. Negative controls were done by adding the secondary antibody to PBS only wells. Images were taken using the confocal microscope.

2.1.1.11 Statin dose

The statin used was Atorvastatin Calcium Trihydrate (Active Pharma Supplies). The drug was weighed and dissolved in methanol to make a 20mg/ml stock solution. A fresh stock solution was made per day of experimentation. The working concentrations used across all experiments were 0.6µg/ml, 1.2µg/ml, 3µg/ml, 6µg/ml, 10 µg/ml, 30 µg/ml, 60 µg/ml, 80 µg/ml, 100 µg/ml, 120 µg/ml, 140 µg/ml, 160 µg/ml, 180 µg/ml, 200 µg/ml, 400 µg/ml and 800 µg/ml. Dilutions were made by adding stock solution to supplemented culture media.

2.1.1.12 Cell viability assays

To evaluate if there was any effect on cell proliferation with the addition of atorvastatin, CCK-8 was used to measure cell metabolism before and after addition of atorvastatin. Cells were seeded into a

well plate and incubated overnight. This was followed by taking a baseline reading by adding 10 µl of CCK-8 to 100 µl of fresh media and incubating the samples for 3 hours at 37°C/5% CO_2. The media with the reagent was collected and read using a plate reader (Biotec). After determining the baseline, atorvastatin was used at 0.6, 1.2, 3, 6, 30, 60, 80, 100, 120 and 140 µg/ml. The cells were then incubated with the drug for 24 hours. The dosed media was then removed and replaced with fresh media containing CCK-8 diluted 1:10 with media. Samples were then incubated for 3 hours at 37°C/5% CO_2, followed by reading with the plate reader at 450nm. Absorbance values were used to plot comparative graphs to gauge the effect of atorvastatin on cell metabolism.

2.1.1.13 Electrospinning

Aligned PLA nanofibers were prepared through previously established protocol (Yang, Wimpenny and Ahearne, 2011), with some modification, to generate the scaffold. 2% PLA solution was prepared by dissolving PLA in a mixture of chloroform and DMF (in a 7:3 ratio) to generate nanofibers through electrospinning. 250µl (0.250ml) of the solution was delivered at a rate of 0.025 ml/min from a syringe pump through an 18-gauge (18G) needle which was attached to the positive electrode. The generated fibres were deposited on the collector which was connected to the negative electrode. The distance between the needle tip and the collector was set at 15cm. The electrodes were supplied with a power supply charged at ±6 kV (Spellman HV, Pulborough, 26 United Kingdom). Once the desired volume of polymer was deposited on the collector, the fibres were gathered using a 16cm^2 acetate frame coated with adhesive. The frame facilitates easier collection of the aligned fibres, maintaining fibre orientation and providing stability. Prior to use in cell culture, the fibres were sterilised under UV light for 90 seconds three times. The fibres are then incubated with fibronectin, at a concentration of 10mg/ml, for one hour before cell seeding.

2.1.2 Scratch wound migration assay

To evaluate effect of atorvastatin on wound closure, a scratch wound was created with a 1-10µl pipette tip scraped over the centre of the confluent HUVEC layer from the top to the bottom of the well. After generation of the lesions, the cells were washed with PBS and topped up with fresh supplemented

media. Atorvastatin doses used were 0µg/ml, 30µg/ml, 60 µg/ml, 80 µg/ml, 100 µg/ml, 120 µg/ml and 140 µg/ml. After creation of the scratch, the rMSCs, hMSCs and EPCs, labelled with CFSE, were added at a density of $5x10^3$ cells per well. Samples were incubated at 37°C, 5% CO_2. Images were taken at 1 hour and 24 hours for comparison. Scratches were placed on the bottom of the culture wells to ensure imaging of the same location at both time points. Dyes used for cell identification/tracking are detailed below.

2.1.2.1 Live-cell tracking

2.1.2.1.1 Hoechst-33258

This nuclear stain was used at a concentration of 2 µl in 10 ml of PBS, diluted from the 10 mg/ml stock solution. The diluted solution was then added to the HUVECs seeded in a well plate and incubated at 37°C for 15 minutes. After this, the cells were washed with PBS and topped up with fresh supplemented media. For HUVECs in suspension, following the dye incubation period, cells were centrifuged and supernatant replaced with fresh media and the pellet resuspended.

2.1.2.1.2 CFSE

This membrane stain was used at a concentration of 5µM. The cells to be stained (rMSCs, hMSCs and EPCs) were passaged and counted and re-suspended in 1m of fresh supplemented media. The stain was then added and the cells incubated for 15 minutes at 37°C. The cell suspension was centrifuged for 3 minutes at 1200rpm and the pellet re-suspended in 5ml of fresh supplemented media.

2.1.3 3D vascular models

2.1.3.1 Collagen gel formation

2.1.3.1.1 Low concentration

The collagen gel was prepared at a concentration of 3 mg/ml. The other reagents used to make the hydrogel were 10x DMEM, 1M sodium hydroxide (NaOH) and sterile filtered deionised water (dH_2O). Depending on the desired final volume, the reagents are added one by one and to prevent premature gelation, the reagents were mixed in an ice bath with the collagen added last. Sample calculation is detailed below. Once the collagen is added, the solution is mixed by pipetting up and down several times until homogenous. Care is taken in the mixing to prevent formation of bubbles in the solution.

(**a**) **Collagen vol.** = $(\text{Desired concentration} \div \text{stock concentration})$ x total volume.

(**b**) **DMEM vol.** = Final volume ÷ 10

(**c**) **NaOH vol.** = Volume of collagen x 0.023

dH_2O/cell suspension vol. = total volume – (a + b + c)

2.1.3.1.2 Plastic compression

To increase collagen concentration and stiffness, the collagen gels underwent plastic compression following a procedure modified from Brown et al., (2005). 1500µL of collagen solution, made as previously described, was poured into customised metal moulds placed in 9.6 cm² petri dishes under sterile conditions. A sterile cover slip (24 x 24mm) was placed at the bottom of the mould to create a sealed space and to prevent the gel from leaking into the petri dish. Two filter paper frames were placed within the mould to provide structural support for the gel. The frames were sized at 0.9 x 0.9cm. To solidify the gels, they were then placed in an incubator at 37°C, 5% CO_2 for 2 hours. This process is detailed further in figure 2-3. These gels were made specifically for use in the atherosclerosis plaque model and RAW cells were seeded on top of the gel before solidification so that they were partially immersed in the gel and only located on the upper surface versus within the whole gel.

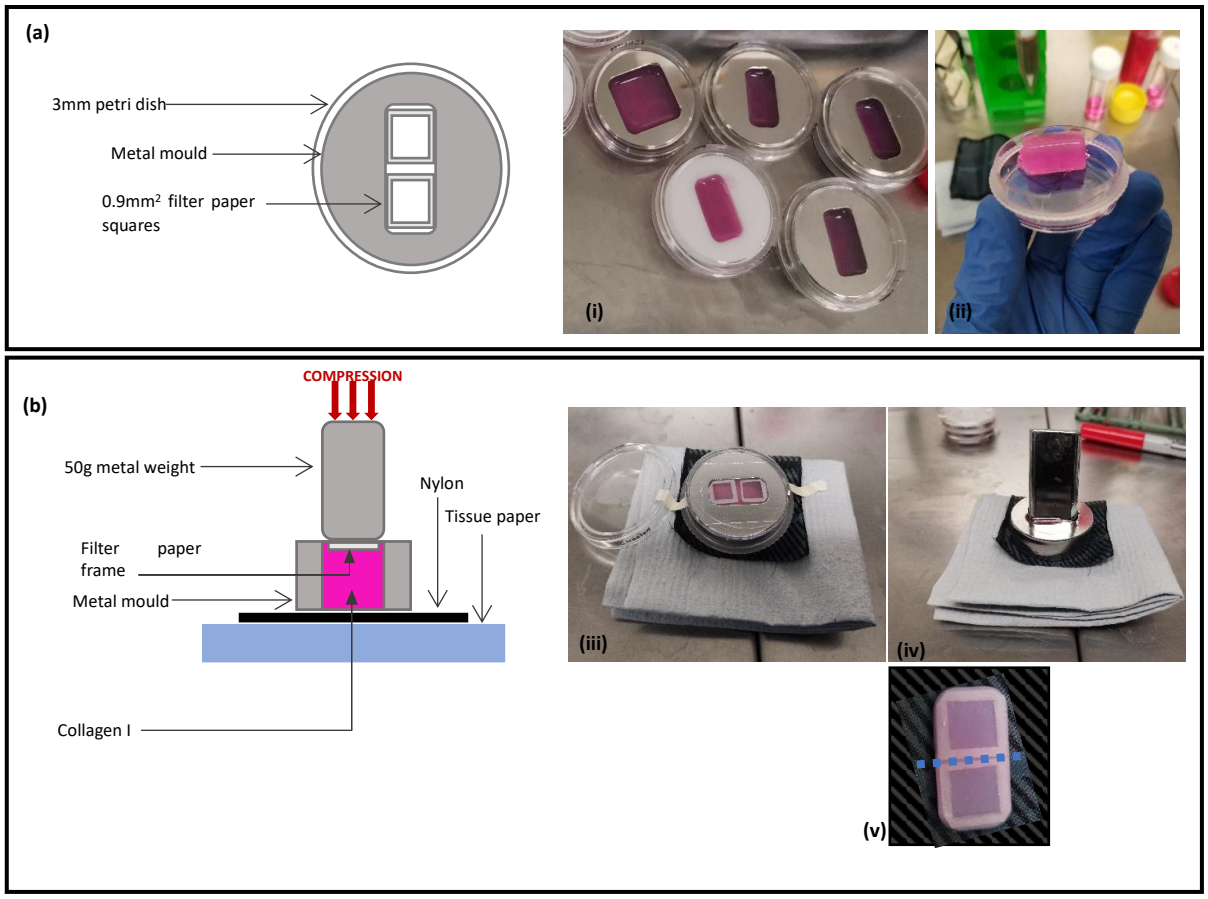

Figure 2-3: Collagen gel compression. Panel (a) shows the preparation of the moulds before collagen addition. (i) shows the solidified collagen in the moulds and (ii) the gel removed from the mould. To compress and extract the gels (b), the mould was turned upside down on a piece of nylon placed on layered sterilised tissue (iii). Once inverted, the glass cover slip is carefully removed to avoid breakage, after which the weight, designed to fit into the mould, is placed on the gel (iv). The weight is left on the gel for 5 minutes until the majority of the water content is removed. The filter paper frames are separated using a scalpel (v), then transferred to a 24 well plate for culture.

2.1.3.2 Electrospinning PLA nanofibers

Aligned PLA nanofibers were used in the assembly of the TE constructs used here. Fibers were made by first dissolving Poly-L, D-lactic acid (96% L/4% D, inherent viscosity of 5.21 dL/g) (PLA) in chloroform for at least 8 hours, followed by addition of DMF for a further 8 hours of mixing to make a 2% PLA solution. Chloroform and DMF were mixed in a 7:3 ratio respectively. The operational parameters of nanofiber fabrication followed a previously established protocol (Yang, Wimpenny and Ahearne, 2011; Njoroge *et al.*, 2021). Briefly, the 2% PLA solution was deposited on detachable metal collectors, consisting of two partially insulated steel blades (30 cm × 10 cm). The steel blades were connected to a permanent copper plate with a steel wire, and had a 5 cm gap between for fiber deposition. Fiber deposition involved connecting the permanent copper plate to a negative electrode, and a syringe

containing the 2% PLA solution was connected to a positive electrode. The PLA was extruded through an 18G needle and delivered at a rate of 0.025 mL/min. The electrodes were electrified with a power supply charged at ±6 kV (Spellman HV, Pulborough, 26 United Kingdom). Nanofibers were collected and attached onto pre-cut acetate frames. Before use in cell culture, aligned nanofibers were sterilized by UV irradiation thrice per side.

2.1.3.3 TEML

Representing the medial layer of a blood vessel, the tissue engineered medial layer (TEML) is made of HCASMCs embedded in a collagen type I hydrogel. The HCASMCs were seeded into the collagen gel at a density of 1 x 10^5 cells per hydrogel. 200µl of the cellular gel solution was pipetted into a hollow rectangle made of filter paper measuring 0.5cm x 2.4cm on the outside and 0.2cm x 2cm on the inside (figure 2-4). The dimensions of the filter paper were guided by the dimensions of the flow chamber and the gasket. The filter paper was placed on a piece of polytetrafluoroethylene (PTFE) to allow ease of transfer into a 6 well plate after gelation.

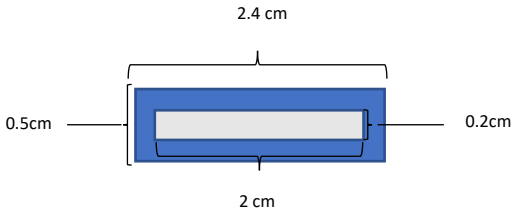

Figure 2-4: Filter paper frame. 200µl of collagen gel containing HCASMCs at a density of 1x105 cells was deposited into the hollow portion of the frame to create the medial layer of a blood vessel. After 10 days, the intimal layer is created on top of the medial layer of a blood vessel. After 10 days, the intimal layer is created on top of the medial layer, with a nanofiber mesh separating the two layers.

The TEML was then placed in a humidified incubator set at 37°C and 5% CO_2 for 30 minutes to permit it to set. After transfer to a 6 well plate, the TEML is cultured for at least 3-4 days in 3ml of smooth muscle supplemented media to allow the cells to elongate and proliferate. Media was changed every 2 days.

2.1.3.4 TEIL

Representing the intimal layer, the tissue engineered intimal layer (TEIL) was fabricated by first making a collagen gel using the protocol and dimensions previously described in section 2.1.7.1. After the collagen gel has set, aligned PLA nanofibers coated in fibronectin were placed on the surface of the gel then the HUVECs are seeded on top to create a representation of the intimal layer. The HUVECs are seeded on the gel surface at a density of $4x10^4$ cells per gel. The cells are allowed to attach onto the nanofibers for at least 40 minutes. This is followed by sealing the fibres and cells onto the construct using acellular collagen. The collagen is carefully pipetted onto the edges of the construct and allowed to set in an incubator set at 37°C and 5%CO_2. The excess nanofibers are then cut off of the construct using a sterile blade. As with the TEML, the sample was then cultured in HUVEC media for at least 3-4 days to allow attainment of normal cell morphology and surface area coverage.

2.1.3.5 TEBV

This model is a combination of the TEML and TEIL to make a tissue engineered blood vessel TEBV). Assembly was carried out as follows; after the HCASMCs have attained the desired spindle shaped morphology, HUVECs are seeded onto the fibronectin coated PLA nanofibers as described above. The fully assembled TEBV was then placed back into a new 6 well plate and topped up with both HCASMC and HUVEC supplemented media in a ratio of 7:3 respectively. The complete TEBV schematic is shown in figure 2-5.

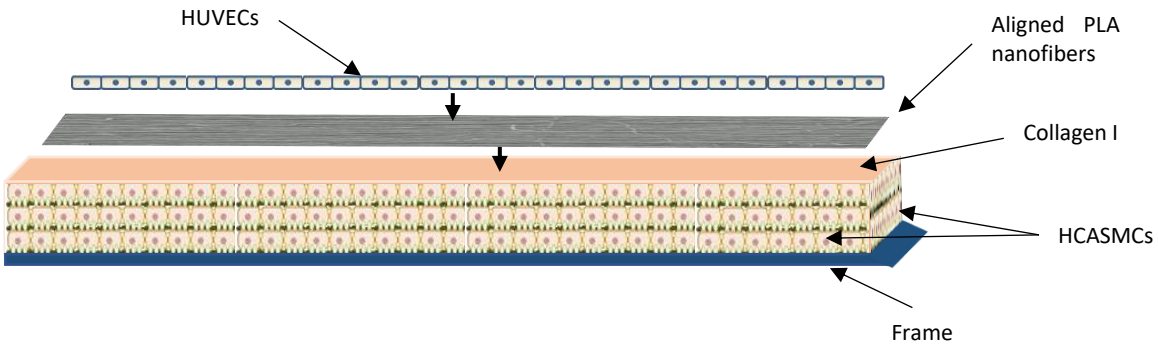

Figure 2-5: Schematic of TEBV. This schema highlights the placement of cells and nanofibers in the assembly of the TEBV. Exclusion of the HUVECs and nanofibers or HCASMCs creates either TEML or TEIL respectively.

To ensure full coverage of the TE constructs, specifically the TEIL and TEBV, with endothelial cells, HUVECs were initially stained with Hoechst, seeded onto the TEML or acellular collagen gel, and imaged to confirm seeding was successful. Representative images can be seen in figure 2-6.

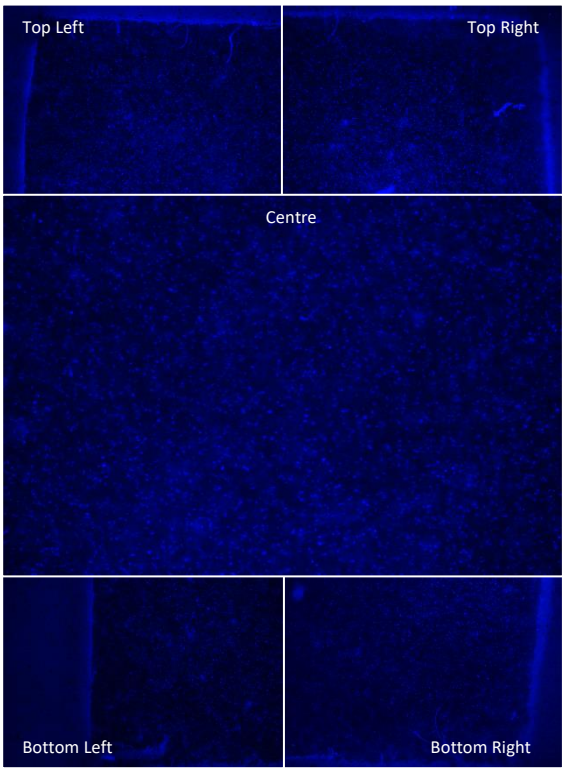

Figure 2-6: Endothelial coverage post seeding on TE constructs. Hoechst-stained cells are visible as blue dots on the surface of the constructs represented here. This was done to verify success of endothelial seeding onto TEIL and TEBV.

2.1.3.6 3D Lesion Models

2.1.3.6.1 $FeCl_3$

To mimic vascular injury, a $FeCl_3$ lesion was created by dipping a $1mm^2$ ($0.1cm^2$) square of filter paper in 10% $FeCl_3$ and placing this onto the upper surface of the constructs for 1 minute. After this, the constructs were washed with PBS to eliminate excess $FeCl_3$, then topped up with fresh media.

2.1.3.6.2 Mechanical injury

A $1mm^2$ piece of filter paper was placed on the surface of the tissue engineered (TE) constructs for 1 minute then carefully peeled off the surface.

2.1.4 Perfusion system

2.1.4.1 Perfusion chamber

To generate peristaltic flow and a range of shear stress values, a peristaltic pump (Watson-Marlow 505 series, Fluid technology, UK) was used along with a commercially sourced parallel plate flow chamber (ProFlow Chamber, Warner Instruments, USA). The chamber was originally designed for 2D perfusion but was modified for our purposes. Details of the modifications are explained later in this section. The perfusate was contained in a 7ml reservoir connected to the pump and flow chamber using polyethylene (PE-90) tubing. The flow chamber inlet was connected to the reservoir and the outlet to the pump. The set-up of this system can be seen in figure 2-7.

2.1.4.2 Perfusion gaskets

To facilitate the perfusion of our 3D vascular models, specialised gaskets were created. The dimensions of the space within the gasket used were length 25mm (2.5cm), depth (thickness) 3mm (0.3cm), width 5mm (0.5cm). The gasket was synthesised using PDMS. The PDMS was prepared by mixing Quantum Silicone (Qsil) polymer and cross-linker in a 10:1 ratio. 3ml of the solution is prepared in a small cell culture dish and left to set at room temperature overnight. Once the solution has set and the PDMS is firm to touch, acetate templates are used to cut out the gasket. First a circular ring with a diameter of

30mm (3cm) is cut then a rectangular opening in the centre of the circle bearing the measurements described in figure 2-7 (PDMS gasket).

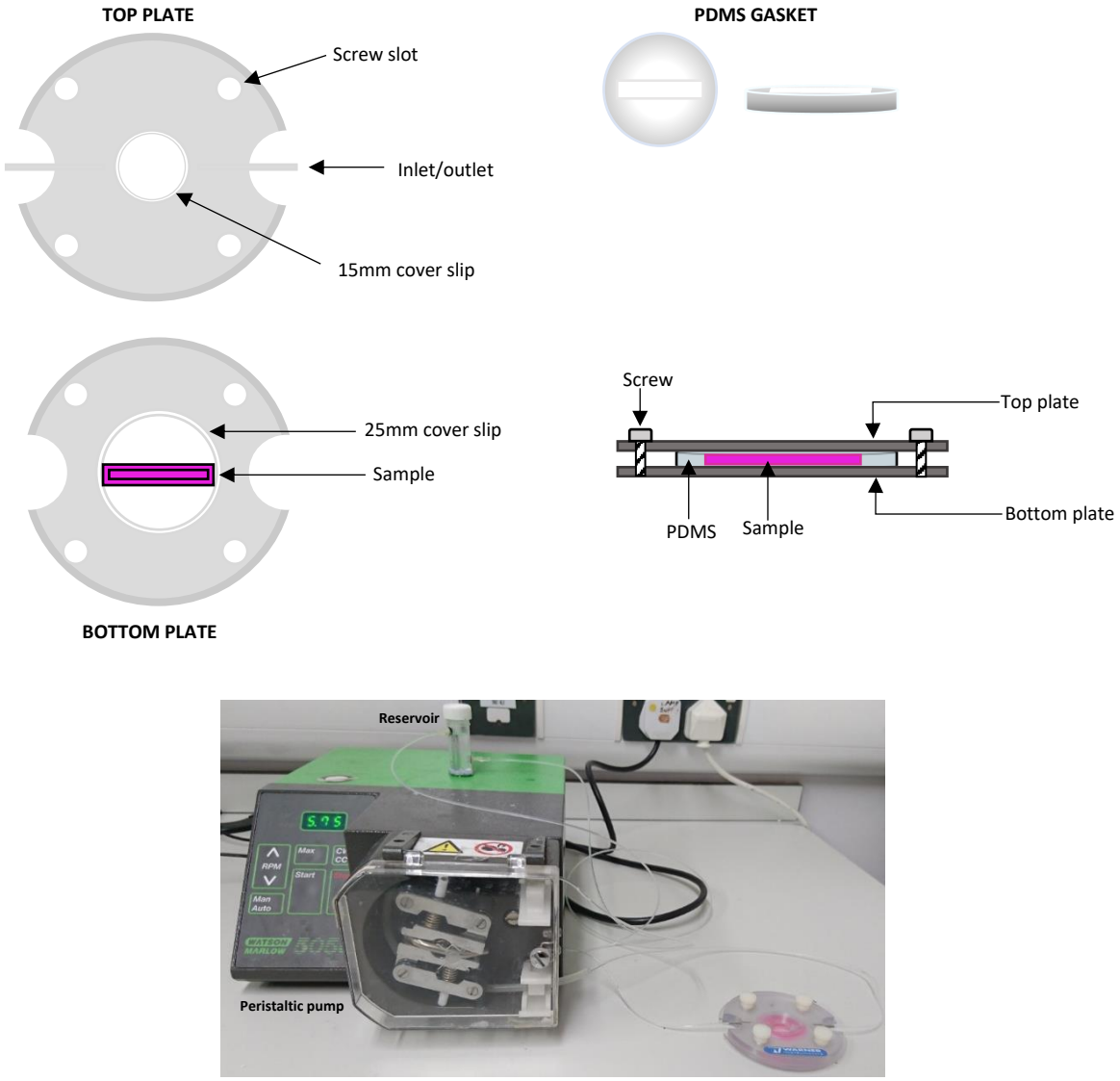

Figure 2-7: Perfusion chamber assembly. The sample is aligned along the flow path between the inlet and outlet on the bottom plate. The outlet, affixed with silicone grease to the top plate, is aligned in the same way and placed over the sample. The assembled chamber is connected to a reservoir and a peristaltic flow pump.

Assembly was accomplished by first installing the cover slips into the designated view slots using silicone grease. Once in place, the sample was placed on the bottom plate and aligned with the inlet and outlet. The custom PDMS gasket was affixed to the top plate with silicone grease after ensuring alignment with the inlet and outlet. The two halves of the chamber, with the gasket and sample in

place, were put together ensuring the sample was positioned entirely within the gasket. Once this was accomplished, the screws are inserted and tightened to ensure the system was sealed and water-tight. The inlet and outlet were then connected to the tubing, that was in turn connected to the pump and reservoir.

2.1.4.3 Shear stress

The assembled flow chamber was used to generate laminar flow as well as exerting shear stress on the intimal surface of the vascular models. The dimensions of the gasket used, which comprises and determines the dimensions of the flow chamber, were length: 25mm (2.5cm), width: 5mm (0.5cm) and depth/height: 3mm (0.3cm) when empty and 2.5mm (0.25cm) with TE constructs. The key dimensions that affect the shear stress profile are the depth and width of the chamber. The equation used to determine the shear stress generated on the endothelial/upper surface of the TE constructs was:

$$\tau = \frac{6uQ}{bh^2}$$

(Wong *et al.*, 2016)

This equation derived from Wong et. al., 2016, is intended for use in a parallel stationary-plate flow chamber, with τ being the shear experienced on the upper surface of the construct. With this equation, shear stress between stationary parallel plates is described as a function of volumetric fluid flow (Q) (Wong *et al.*, 2016). The values required for the equation are the viscosity of the fluid being perfused (u), the flow rate (Q), the gasket width (b) and the gasket height with TE construct placed within (h). The flow rate used for the perfusion of the constructs was 0.07cm^2/s. This value, using a viscosity value of 1.5 Cp (Jeevasankar *et al.*, 2008), is used to determine that the shear stress exerted on the construct surfaces is 20.16 dyne/cm^2. Aside from generating a useful range of shear stress values that range from 1.44 dyne/cm^2 to 172.8 dyne/cm^2, the chamber was also able to consistently generate a laminar flow profile with the modified gasket design.

2.1.4.4 See-saw Rocker

The TE constructs were placed in a 48 well plate and topped up with 600µL of perfusate, then placed

on a standard see saw rocker set at 70 rpm for 1 hour at 7θ.

2.1.4.5 Flow pattern characterisation

To determine the nature of the flow pattern within the perfusion chamber, fluorescein was used in conjunction with PBS to visualise the flow pattern. The chamber and pump were assembled as in figure 2-6. The reservoir was first filled with PBS, which was then pumped through the chamber. After this, the contents of the reservoir were removed and replaced with the fluorescent solution. As the solution flowed into the chamber, it was possible to visualise fluid movement as the two liquids mixed. Video footage was recorded and still images isolated.

2.1.4.6 Perfusate cell labelling

Cells were stained with CFSE, a live cell tracker. This membrane stain was used at a concentration of 2µl in 1ml of cell suspension. The cells to be stained were passaged and counted and re-suspended in 1m of fresh supplemented media. The stain was then added and the cells incubated for 15 minutes at 37°C. The cell suspension was centrifuged for 3 minutes at 1200rpm and the pellet re-suspended in 5ml of fresh supplemented media. The cell suspension was left to sit for the final esterification step for 30 minutes at 37°C before use. Imaging was done using Leica inverted fluorescence microscope and a confocal microscope.

2.1.5 Cytokine characterisation and quantification

2.1.5.1 SDF-1

The reagents for the mini ABTS ELISA kit were reconstituted according to manufacturer's protocol. 100µl of the capture antibody, diluted in PBS to a concentration of 2µg/ml, was added to the requisite number of wells, sealed and incubated overnight at room temperature. The wells were the aspirated and washed 4 times with 300µl of wash buffer per well. The wash buffer is comprised of 0.05% Tween 20 in PBS. Next, 300µl of 1% BSA in PBS (block buffer) was added to the wells and incubated for at least 1 hour at room temperature. The block buffer was then aspirated and the plate washed 4 times with the wash buffer. 100µl of sample solution (or standard) was added to each well and incubated at room temperature for at least 2 hours. The plate is then aspirated and washed 4 times. Next, the

detection antibody, diluted in diluent (0.05% Tween 20 + 0.1% BSA) to a concentration of 0.5µg/ml. The plate was then incubated for at least 2 hours at room temperature. After this, the plate was again aspirated and washed 4 times. A 1:2000 dilution of Avidin-HRP conjugate was then added to the wells (100µl/well) and incubated for 30 minutes at room temperature. This was then followed by another 4 washes, after which 100µl of ABTS liquid substrate was added per well. This was incubated at room temperature - with observation every 5 minutes for up to 1 hour - until colour development was observed. Once this was achieved, the plate was read using a plate reader set at 405nm.

2.1.6 Atherosclerotic plaque model

2.1.6.1 OxLDL synthesis

200µl of LDL solution was mixed with 4ml PBS and 10µM $CuSO_4.5H_2O$ to make a final solution of 5mg/ml oxLDL. This solution was incubated for 24 hours at 37°C, 5% CO_2. After oxidation, solution turns cloudy. To remove $CuSO_4$ from the oxidised solution, thus preventing further oxidation, the solution was then transferred to a slide-a-lyzer dialysis cassette and dialysed in 550ml of 10µM EDTA in PBS for 24 hours. Dialysis solution was changed every two hours for 8 hours then left to continue dialysis for the remainder of the duration. The dialysis solution was kept in motion using a magnetic stir bar. After dialysis was complete, solution was removed from the cassette, aliquoted and stored at -80°C. All procedures were carried out under sterile conditions.

2.1.6.2 Foam cell formation

To promote foam cell formation in RAW 264, cells were incubated with either oxLDL, oxLDL and LPS, oxLDL and IFN-γ or LPS, IFN-γ and oxLDL. LPS and IFN-γ were both used at a concentration of 100ng/ml, oxLDL at 100µg/ml. IFN-γ and oxLDL Incubation was done overnight. Cells were first incubated with IFN-γ, IFN-γ + LPS, or LPS overnight, after which the media was removed and replaced with LDL/oxLDL loaded media for a further overnight incubation. After incubation, media was replaced with normal cell media either with or without atorvastatin. For samples loaded with oxLDL, concentrations of oxLDL were maintained in the media used for experimentation.

2.1.6.3 Co-culture with HUVEC: Nanofiber well inserts

RAW 264 cells were cultured in conjunction with HUVECs. The two cell layers were separated using a customised nanofiber insert with the HUVEC layer seeded on the nanofibers and above the RAW cells. Assembly of this system is shown in figure 2-8. Aligned nanofibers were collected on acetate frames and were affixed to the customised rings using silicone glue. The fibres were allowed to dry onto the ring for 2 hours in an oven set at 50°C. To facilitate media flow, a split rubber ring was affixed to the bottom of the assembled insert. Before use in cell culture, the inserts were sterilised by first incubating them in 70% IMS for 2 hours followed by three 90s exposures to UV light.

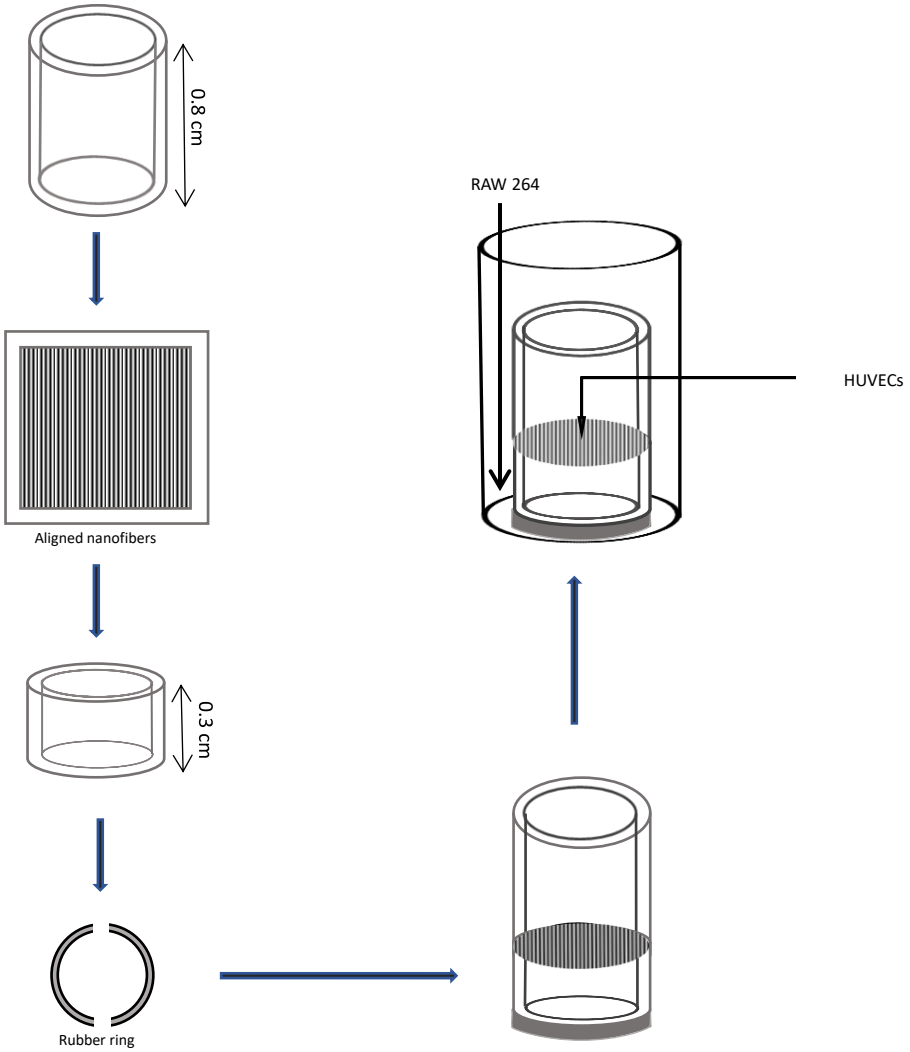

Figure 2-8: Nanofiber well insert assembly. The customised rings were fused together with the aligned nanofibers between. A split rubber ring was affixed to the bottom portion of the insert. After sterilisation, HUVECs are seeded onto the fibronectin coated nanofibers. The completed insert is placed inside a 24 well plate well seeded with RAW 264.

2.1.6.4 Immunostaining

The sample was first incubated with 5% BSA for 1 hour at room temperature. Then the primary antibody was added at a 1:200 dilution and incubated for 2 hours at 37°C/5% CO_2. The primary antibody is removed and the sample washed 2x with 0.05% Tween20 then 2x with PBS. The secondary antibody was then added and incubated with the sample for 1 hour at 37°C/5% CO_2. After the incubation, the secondary antibody is removed and the sample washed again with 0.05% Tween20 (2x) then PBS (2x). After the washes, the sample is incubated with DAPI at 1µg/ml for 10 minutes after which the stain is removed and the sample washed with PBS before imaging. Negative control for secondary antibody was carried out by adding secondary antibody to PBS only wells. Specific antibodies used are detailed in the respective chapters.

2.1.6.5 Nile Red Staining

Nile red was obtained as a powder which was reconstituted by dissolving in isopropanol to make a 1mg/ml stock solution that was diluted to 1µg/ml for active use. Staining was done on fixed samples. Samples were first washed twice with PBS, then 500µl Nile red working solution (1µl Nile red stock in 1ml PBS) was added to samples. Samples were incubated with the dye for 20 minutes at room temperature, after which they were washed again with PBS. DAPI (10ng/ml) was added to samples for 10 minutes for nuclear staining. DAPI was then removed and sample washed again with PBS, followed by imaging.

2.1.6.6 Oil Red-O quantification

Staining was done on fixed cells. Filtered oil red-o working solution was added to sample wells (500µl for 24 well plate) for 20 minutes at room temperature. After this, wells were gently washed with dH_2O. This was followed by the addition of 500µl isopropanol per well. The well plate was then placed on an orbital shaker for 25 minutes. After this, 100µl of solution was collected in a 96 well plate and sample absorbance was read at 540nm. This would allow reverse determination of ox-LDL uptake.

2.1.6.7 NO quantification

This assay was used to track nitric oxide production in the atherosclerosis plaque model. Samples were

mixed 1:1 (50µl:50µl) with gries buffer comprised of 1% sulphonamide, 2.5% phosphoric acid and 0.1% Naphthalene-diamine-hydrochloride. The mixture was read using a plate reader at 546nm. Quantification was done based on a standard curve created using a sodium nitrile dilution series.

2.1.7 Statistics

Statistical analysis was carried out where applicable with primary testing being one-way ANOVA, two-way ANOVA and one sample T and Wilcoxon tests carried out. All analysis was carried out using GraphPad Prism 8 and specific details regarding tests carried out per data set are detailed further in upcoming chapters. All tests used a minimum of 3 repeats per group and the data is expressed as mean ± SEM. Statistical significance was expressed a $P<0.05$.

Chapter 3:

Endothelial Progenitor Cell (EPC) Characterization

3.1 Introduction

Endothelial Progenitor cells (EPCs) is a broad reference to cells possessing the capability to differentiate into endothelial cells. These cells have been defined as circulating cells that express a variety of cell surface markers similar to those expressed by vascular endothelial cells, adhere to endothelium at sites of hypoxia/ischemia, and participate in neovascularisation (Luo *et al.*, 2018); Yoder, 2012). Early work in the isolation and characterisation of this cell type identified that purified $CD34^+$ hematopoietic progenitor cells from adults can differentiate *ex vivo* to an endothelial phenotype. (Poay Sian Sabrina Lee and Kian Keong, 2014) demonstrated that these EPCs showed expression of various endothelial markers and are incorporated into neo-vessels at sites of ischemia. Earlier studies suggested EPCs exhibited a $CD34^+/CD133^+/VEGFR2^+$ phenotype. Later studies also considered the expression of *CD45, CD105, CD106, CD117, CD144,* acetylated low-density lipoprotein uptake, and aldehyde dehydrogenase activity (Chong, Ng and Chan, 2016). Other characteristics that can be used to define the EPC type are the capacity for tube formation and the formation of colonies.

Tube formation in EPCs is commonly carried out by seeding cells in Matrigel and supplementing with angiogenic factors such as VEGF. This results in the formation of tube-like structures (Huang *et al.*, 2012; Zhao *et al.*, 2018), an observation also seen for cells cultured in collagen gels and has mainly been linked to colony forming EPCs (Peters, 2018).

Colony formation, feature was first described by Asahara et., al. 1997, and was observed on plated $CD34^+$ cells after 5 days of culture (Yoder, 2012b; Asahara *et al.*, 1997). This was achieved by replating non-adherent cells after isolation from human? blood then quantifying the appearance of EPC derived colonies (Yoder, 2012b; Hill *et al.*, 2003). Numerous follow-up studies have identified colony formation as a marker of an EPC phenotype, with colonies described as clusters of rounded cells surrounded by cells possessing an elongated spindle shape (Abou-Saleh *et al.*, 2009).

In this study, we intended to obtain EPC from commercial sources and to isolate this cell type from whole blood from healthy volunteers. This would be flowed by an evaluation of their capacity for colony formation, tube formation and the expression of CD34, CD45, CD31, Flk-1 and CXCR4, which

would identify the cells as endothelial progenitors for subsequent chapter studies. Staining was done on cells that were between 14 and 20 days old.

3.2 Materials and methods

Materials used for this chapter are listed in chapter 2, section 2.1 under cell culture, EPC isolation and cell staining sections of table 1. EPCs were obtained from whole blood collected from healthy, drug free volunteers.

3.1.1 EPC culture

Following the established isolation and culture protocols, EPC cultures were maintained by culturing cells as described in section 2.1.1.8. Briefly, following isolation using differential centrifugation, cells were cultured on either collagen or fibronectin coated plates and fed with medium 200 supplemented with 10% FBS and 1% AA. After separation from whole blood, cells were first plated in 2 wells of a 12 well plate for the first day, followed by a transfer of unattached cells to a new well daily for 4 days, which allowed maximum trapping of unattached cells. Media was changed daily for the first 7 days then changed every 2 days for the duration of culture.

3.1.2 EPC characterisation

To aid in the identification of isolated cells, colony formation, surface marker expression and tube formation evaluations were done as described in section 2.1.2, and will be discussed further in this chapter.

3.1.3 Immunostaining

The expression of Flk-1 (KDR/VEGFR-2), CD45, CD31 (PECAM-1), CXCR4 and CD34 were used to characterise this cell type. Protocol for staining is as described in section 2.1.2.2. Primary (1°) antibodies were used at a dilution of 1:200 with PBS while secondary antibodies were used at a dilution of 1:400 with PBS.

3.3 Results

3.1.4 Commercially available EPCs

Initially, cells were sourced commercially from Biochain (amsbio), and were revived according to the supplier's protocol. Unfortunately, there were unidentified particulates observed within the culture vessel that covered the base of the flask and prevented attachment of the EPCs. The number of EPCs observed in the flask were also very minimal, preventing attempts at proliferating these cells and establishing a cell line. The status of the cells after culture can be seen in figure 3-1.

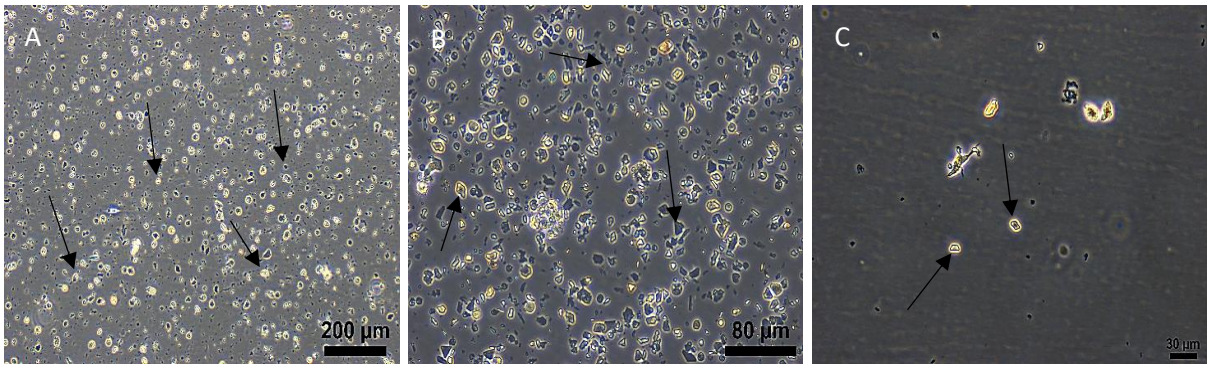

Figure 3-1: EPC morphology. These images are of P0 EPCs taken at 10x **(A)** and 20x **(B, C)**. Image C is of one of the structures identifiable as a cell within the flask and was taken after a media change. Image A and B Show the contents of the flask 1 hour after seeding. The arrows in the images identify the unknown elements within the flask.

The bulk of the contents within the flask had irregular geometric shapes and appeared to be crystalline in nature. An assessment of the supplemented media ruled it out as the source of these structures. It is likely the anomalous structures observed in the culture vessel were crystals derived from the freezing medium. It was not possible to eliminate these structures which affected cell attachment and therefore proliferation as a result, alternative methods were employed to isolate and characterise EPCs. EPCs used for later experiments were isolated from whole blood, derived from healthy, drug free volunteers, as detailed in section 2.1.1.6.

3.1.5 Morphology evaluation

To determine the ideal substrate that will allow effective culture of peripheral blood EPCs, a comparative between collagen and fibronectin was made. Following isolation from whole blood, cells were seeded in two wells of a 12 well plate, on the first day. From day 2 till day 4, during the daily media change, old media was discarded and fresh media agitated and transferred to a new well to collect as many non-adhered adherent cells as possible. Representative images are shown in figure 3-2.

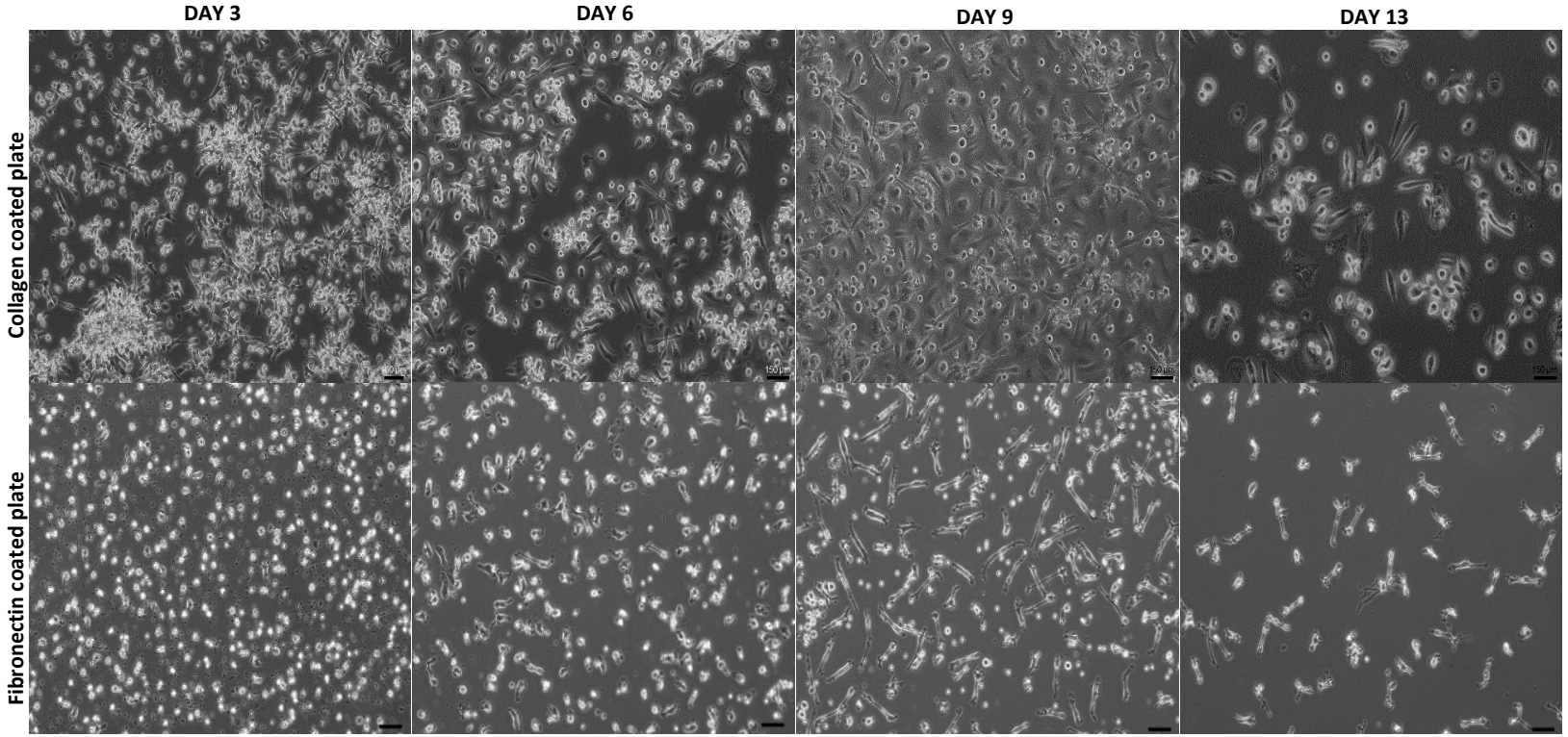

Figure 3-2*:* **Endothelial progenitor cell culture on collagen vs. fibronectin coated plates.** Representative images showing cell morphology over time on different culture plates. Images taken at 10X. Scale bar = 150 µm

The key difference between the different types of coating was that the cells grown on the collagen coated plates displayed mixed morphologies, with this heterogenicity being maintained throughout the culture process and managed to survive for slightly longer before cell density began to diminish around D10. Cells on the fibronectin coated plates were more homogenous in appearance, gradually adopting the spindle like shape of early EPCs, which was maintained for the duration of culture. Proliferation was not observed with the cultured cells but rather a gradual decline in cell population after 10 days of culture. Depending on volunteer, the average total density of isolated cells ranged between 2 x 10^5 and 4 x 10^5 cells. The density of cells within the wells started decreasing as can be seen between day 9 and 13 (Figure 3-2). At the end of culture, cell population was fully homogenous in appearance, following the well-to-well transfer in the first **4 days of culture.**

3.1.6 Colony formation

Certain subsets of EPCs are characterised by their ability to form colonies *in vitro*. representative images showing colony formation are shown in figure 3-3. Colonies were observed on cells cultured on either fibronectin or collagen.

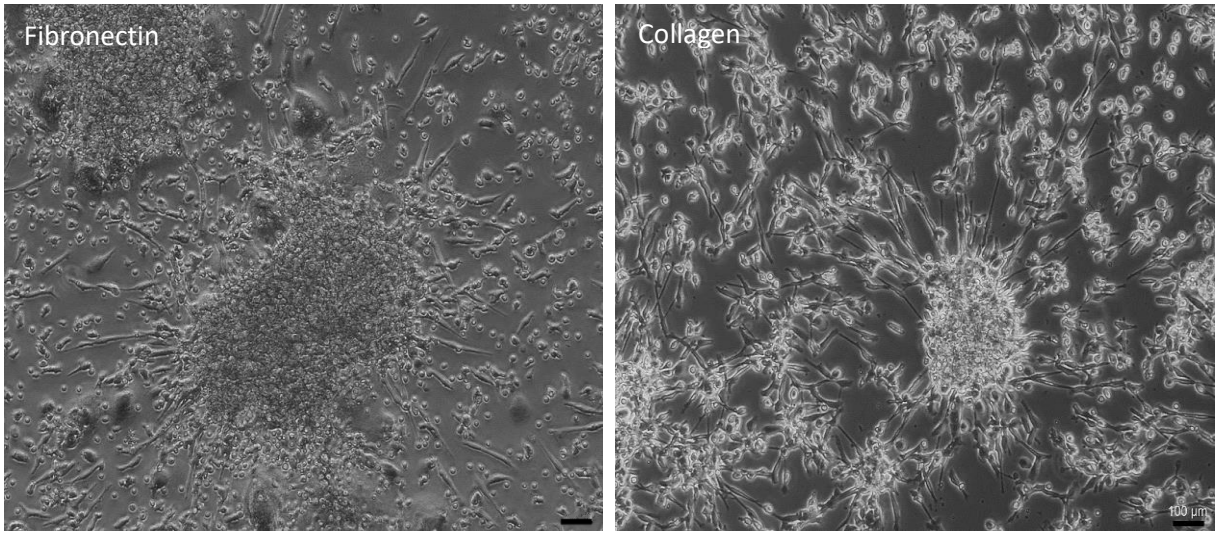

Figure 3-3: Colony formation collagen vs. fibronectin coating. Representative images showing colony growth in isolated cells on both collagen and fibronectin coated plates. Images taken at 10X. Scale bar = 100 µm

Colonies were observed fairly early in culture (between day 2 to day 6). For both types of coating, spindle like projections can be seen on the edges of the colony. These colonies gradually dissipated to

be replaced with exclusively spindle like cells on the fibronectin coated plates, as seen in figure 3-2, or a mix of rounded and elongated cells on the collagen coated plates, also represented in figure 3-2.

3.1.7 Tube formation

Another defining characteristic of EPCs is their ability to form tube-like structures. During culture, appearance of tube-like structures was seen in some of the wells, the collagen coated plates showed these structures after 20 days of culture while the fibronectin coated plates developed them after 13 days. These structures appeared after 10 days in culture. As can be seen in figure 3-4, these tube-like structures appear to be formed from a number of cells linked end to end to form the tube.

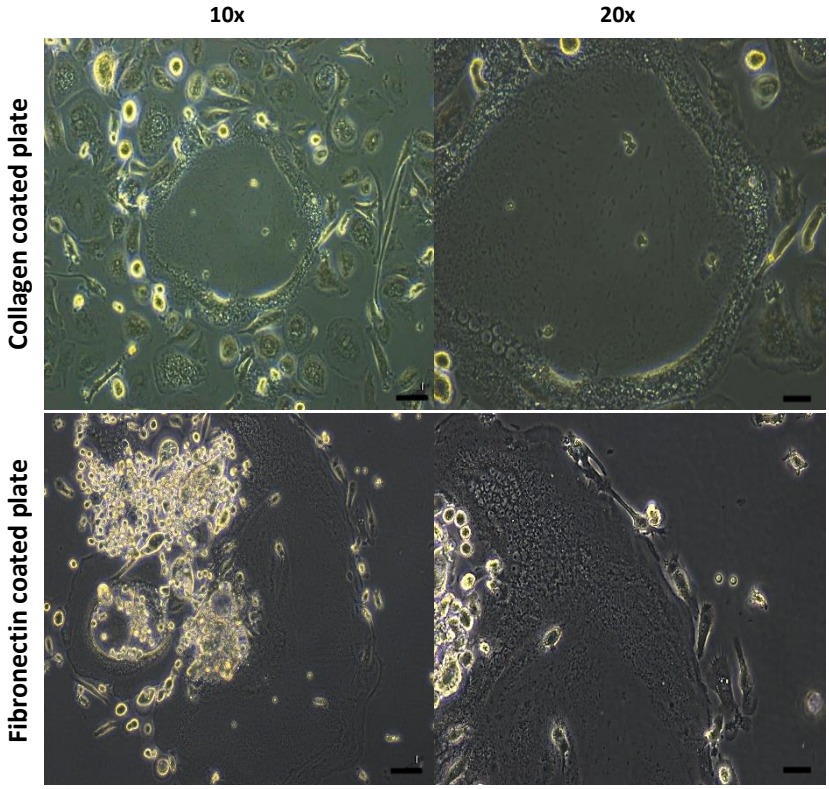

Figure 3-4: Tube formation. Representative images showing tube formation in EPC culture. Images taken at 10 and 20x, with scale bar representing 100 µm and 30 µm respectively.

After about 10 days of culture some wells showed signs of tube formation, with approximately 2-3 tubes appearing per well. On the fibronectin coated plates, the tubes appear to be cells aligning themselves in this orientation end to end forming a tube while the tube-like structures appearing on

the collagen coated plates appear to be a continuous membrane, with no individual cells being obviously distinguishable as they are on the fibronectin coated plates.

3.1.8 Immunostaining

Immunostaining was done to determine the expression profile of the isolated cells. All staining was done on cells cultured on fibronectin. Cells used were between 14 and 20 days old. Staining was done by adding 1° antibody diluted 1:200 in PBS and 2° antibody diluted 1:400 in PBS. Secondary antibody negative controls were done at the same dilution in the absence of the 1° antibody, representative images are in figure 3-6. Staining was done for CD34, CD45, CD31, Flk-1 and CXCR4, representative images are in figure 3-5.

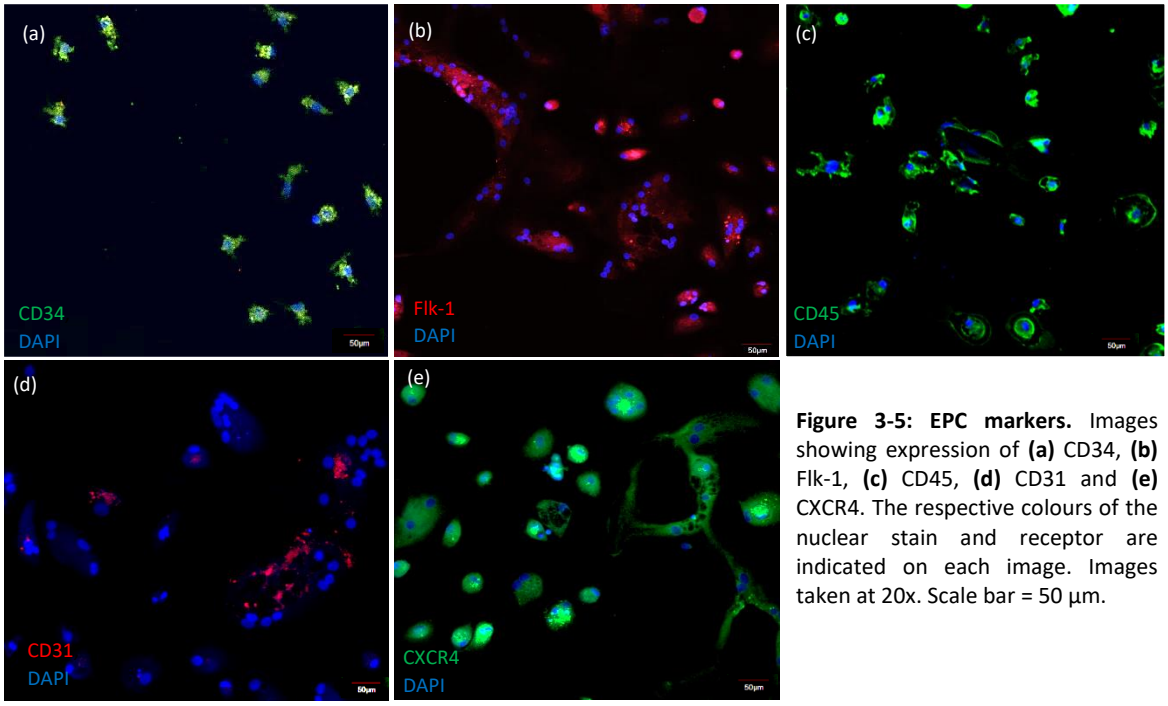

Figure 3-5: EPC markers. Images showing expression of **(a)** CD34, **(b)** Flk-1, **(c)** CD45, **(d)** CD31 and **(e)** CXCR4. The respective colours of the nuclear stain and receptor are indicated on each image. Images taken at 20x. Scale bar = 50 µm.

Figure 3-5 shows the results of the antibody staining, with cells showing positivity for all the selected markers i.e., CD34, Flk-1, CD45, CD31 and CXCR4, strongly suggesting that these cells fit under the descriptor for EPC. Extent of staining is mostly ubiquitous for all the markers examined here, with CD31 showing the smallest distribution, appearing fragmented and not fully surrounding the cell nuclei.

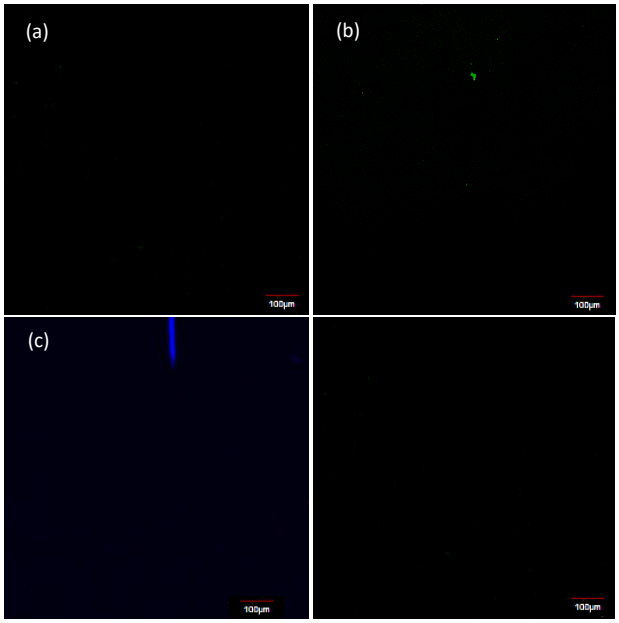

Figure 3-6: 2° Antibody negative controls. (a) Donkey anti-mouse IgG-FITC conjugated (CD34 and CD45). **(b)** Donkey anti-rabbit IgG NL493 conjugated (CXCR4). **(c)** mouse monoclonal IgG; Flk-1 Alexa Fluor® 594 conjugated. **(d)** Donkey anti-mouse IgG Rhodamine conjugated. Scale bar = 100 µm.

3.4 Discussion

The term endothelial progenitor cell was first used to define circulating cells that were able to display cell surface antigens similar to endothelial cells. As yet, there is no universal agreement on what specifications constitute an endothelial progenitor cell, primarily due to variations in isolation, culture and identification (Richardson and Yoder, 2011). In terms of what general characteristics are expected of the EPC, some agreement can be made on the expression of CD34, Flk-1 (VEGFR-2/KDR) and CD133 being strongly suggestive of the EPC phenotype. Further to this, the additional expression of CD45 would also support that these cells are of a haematopoietic lineage. Given the variety of identification characteristics, it becomes challenging to clearly identify isolated cells as EPCs. Recent works have attempted to narrow down the classification criteria for endothelial progenitors. As described by Huizer et. al., 2017, there are three categories of progenitor cells based on FACS sorting for specific surface markers. The three variants of progenitors are; haematopoietic progenitor cells (HPCs), circulating endothelial cells (CECs) and culture-generated outgrowth endothelial cells (OECs) (Huizer *et al.*, 2017). They were also able to sub-divide HPCs into 4 sub-groups based on CD34, CD133 and c-kit staining, namely $CD133^{neg}$c-kit^{high}, $CD133^{low}$c-kit^{high}, $CD133^{high}$c-kit^{high}, and $CD133^{high}$c-$kit^{neg/low}$. They identified that expression of CD34 and CD45 was positively linked with CD133, and that expression of other endothelial markers, such as Flk-1, CD146 and CD105, were indicative of small independent sub-populations (Huizer *et al.*, 2017). CECs were identified as expressors of CD34 and Flk-1 while negative for CD45, with additional expression of CD144 and CD146 (Huizer *et al.*, 2017). OECs were plated without sorting, developing the typical spindle shaped morphology of early EPCs. These developed further after 1-3 weeks of culturing into OECs, which displayed characteristic cobblestone morphology, expression of VWF and formation of tube-like structures. These cells were found to express high levels of CD31, CD144, CD146 and CD105, while not expressing CD45 and CD133 (Huizer *et al.*, 2017). From their findings, it is possible to extrapolate that the cells isolated here were at the very least of an endothelial progenitor phenotype.

An important mechanism for the homing of EPCs to sites of vascular injury is the SDF-1 (CXCL12)/CXCR4

axis. CXCR4 is conspicuously expressed on haematopoietic stem cells and has been demonstrated to be important in their recruitment and homing (Sainz and Sata, 2007). The cells imaged here demonstrate strong expression of CXCR4, further suggesting that they are of a haematopoietic lineage. In regard to the morphological appearance of the cells cultured here, there is consistency with reports on classification of this cell type. Abou-Saleh et al. 2009 characterise their cells based on the appearance of cultured colonies. As is described in sources dealing with EPCs, the colonies have an appearance matching those seen in figure 3-2, where a central core of rounded cells is possessed of elongated sprouting cells at the periphery (Abou-Saleh *et al.*, 2009). Here we have clear demonstration of this phenomenon which was observed fairly early in culture and later made way to homogenous cultures of the elongated cell phenotype. Further steps that could be taken to isolate a purer fraction of this cell type, or variants thereof, would be to conduct more functional assays such as acetylated LDL uptake as well as further characterisation of tube formation using standardised assays. This would also be done in conjunction with FACS analysis of a wider array of surface markers such as CD133. In regards to the intentions of this thesis, the characteristics described here were sufficient to allow subsequent experimentation with these cells.

3.5 Conclusion

Based on the key surface marker expression profiles demonstrated here, it is possible to say that the cells isolated can be defined as EPCs based on morphological and phenotypic characterisation. In the up-coming chapters, their responses to atorvastatin and interactions with endothelial cells and tissue engineered constructs will be determined and this will further allow functional confirmation of cell type.

Chapter 4:

Evaluating Atorvastatin's Effect on Stem Cell Homing Using a 2D Scratch Wound Model

4.1 Introduction

The maintenance of vascular integrity is vital to blood circulation and thus the health of organs and tissues in the body. There are a number of mechanisms in place to regulate the maintenance of vascular integrity. One of these is the recruitment of cells to sites of vascular injury. Cellular migration and integration is an essential aspect of numerous physiological processes, including neovascularization and angiogenesis, immunologic responses, wound healing, and organ repair (Dar, Kollet and Lapidot, 2006). A key player in ensuring vascular health is the endothelial cell. These cells are responsible for the regulation of vascular tone, vascular permeability, vessel wall inflammation, and thromboresistance (Hirase and Node, 2012). Endothelial cells respond to and produce vasoactive substances that are able to regulate vascular permeability, smooth muscle cell functionality and recruitment of immune cells (Hirase and Node, 2012). In regards to their own migration, three mechanisms are involved in this process; chemotaxis which refers to directional migration in response to chemoattractants (chemokines), haptotaxis, which is the directional migration toward a gradient of immobilized ligands and mechanotaxis, which refers to the directional migration generated by mechanical forces (Lamalice, Le Boeuf and Huot, 2007). Another mechanism involved in vascular repair is the recruitment of circulating progenitor cells. Endothelial progenitor cells have received considerable interest since their discovery by Asahara et. al. in 1997 and are believed to contribute to the process of vascular repair (Sandhu, Mamas and Butler, 2017). These cells are believed to originate from the bone marrow and are mobilized into peripheral blood to participate in vasculogenesis and angiogenesis through the secretion of cytokines (Chong, Ng and Chan, 2016). These cells are a viable candidate for therapy due to the ease of their isolation and potent vasculo-and angiogenic effects (Chong, Ng and Chan, 2016). Other types of stem cells types have also proven to be useful tools for therapy. Mesenchymal stem cells (MSCs) are defined as multipotent cells capable of self-renewal and with the capacity to differentiate into a variety of mesenchymal cell types (Karp and Leng Teo, 2009). Introduction of MSCs to diseased hearts has been shown to improve cardiac function through stimulation of endogenous repair mechanisms. Different types of MSCs exert varying effects on tissues

they are introduced to. For example, adipose derived stem cells can produce large amounts of extracellular matrix along with immunomodulatory effects while bone marrow derived stem cells have a stronger proangiogenic and immunomodulatory effect (Bagno *et al.*, 2018). As pertains to vascular repair, bone marrow MSCs have been shown to produce higher amounts of cell migration related chemokines, specifically stromal derived factor-1 (SDF-1) (Bagno *et al.*, 2018). Chemokines are known to bind multiple receptors, with the same receptor being able to bind more than one chemokine. An exception to this rule is SDF-1, which exclusively binds to CXCR4 only (Kucia *et al.*, 2005). For the homing of haematopoietic cells, the SDF-1/CXCR4 axis is crucial. Expression of SDF-1 is elevated in a majority of tissues following injury, and is vital in mobilization and migration of stem cells from the bone marrow to the site of tissue injury (Dimova *et al.*, 2019; Mayorga *et al.*, 2018). In studies utilising rodent systems, Mayorga et al., 2018, demonstrated that exogenous SDF-1, delivered through gene transfer or by infusion of MSCs, was enough to induce stem cell homing to injured myocardial tissue (Mayorga *et al.*, 2018). The exclusivity of this chemokine-receptor pair suggests that they have a uniquely important biological role. SDF-1 can be expressed by stromal and endothelial cells including bone marrow, heart, skeletal muscle, liver, brain and kidney, and genetic knockouts of SDF-1 and CXCR4 results in significant defects in the colonisation of embryonic and haematopoietic stem cells, as well as defects in the development of the heart, brain and large vessels (Ratajczak *et al.*, 2006).

The primary role of statins is to competitively inhibit HMG CoA, which induces the expression of LDL receptors in the liver, which in turn increases the catabolism of plasma LDL, resulting in the reduction of circulating LDL levels (Sandhu, Mamas and Butler, 2017). Atorvastatin has repeatedly been demonstrated as having effects outside of cholesterol lowering. These pleiotropic effects include actions such as attenuation of vascular inflammation, improved endothelial cell function, decreased vascular smooth muscle cell proliferation and migration, stabilization of atherosclerotic plaque, and inhibition of platelet aggregation (Sadowitz, Maier and Gahtan, 2010).

Here we attempted to determine the effect atorvastatin has on HUVEC migration and wound closure. This was achieved by carrying out a scratch wound assay with atorvastatin at different concentrations.

A scratch wound was selected due to the ease and speed of execution. We further assess the influence of HUVECs co-cultured with rMSCs, hMSCs and EPCs with atorvastatin to evaluate if stem cells from different species have varying effects and whether MSCs and EPCs have different effects on cell migration and wound closure. The extent of wound closure was examined after 24 hours.

4.2 Materials and methods

4.1.1 Human umbilical vein endothelial cell (HUVEC) culture

As described in section 2.1.1.2, HUVECS were cultured in medium 200 supplemented with 2% LSGS. Cells between P2 and P5 were used in the experiments detailed in this chapter.

4.1.2 Rat mesenchymal stem cell (rMSC) culture

As described in section 2.1.1.3 and 2.1.1.5, rMSCs were cultured in DMEM supplemented with 1% AA, 1% LG and 10% FBS. Cells between P3 and P6 were used in experiments detailed in this chapter.

4.1.3 Human mesenchymal stem cell (hMSC) culture

As described in section 2.1.1.4 and 2.1.1.5, hMSCs were cultured in DMEM supplemented with 1% AA, 1% LG, 1% NEAA and 10% FBS. Cells between P3 and P6 were used in experiments detailed in this chapter.

4.1.4 Trilineage differentiation

As described in section 2.1.1.6, a trilineage differentiation along osteogenic, chondrogenic and adipogenic lineages was carried out for rMSC and hMSCs to confirm their stemness. After differentiation, cells were stained with alizarin red and alcian blue for osteogenic and chondrogenic differentiation respectively, with oil red-O and Nile red staining done for the adipogenic lineage. Specific staining protocols are described in sections 2.1.1.6.1.1, 2.1.1.6.1.2, 2.1.1.6.1.3 and 2.1.14 respectively.

4.1.5 Atorvastatin dose effect

As described in section 2.1.3, atorvastatin was dissolved in methanol and diluted to the following concentrations; 30µg/ml, 60µg/ml, 80µg/ml, 100µg/ml, 120µg/ml and 140µg/ml. During dilution with culture media, care was taken to ensure that methanol amounted to less than 1% of total media volume per sample. The assay to assess cell viability was CCK8. The assay was carried out after a 24-hour incubation with or without atorvastatin, followed by the addition of the reagent as detailed in section 2.1.4.

4.1.6 Scratch wound

As described in section 2.1.6.2, a 10µl pipette tip was used to generate a scratch on a confluent layer of cells seeded in a 48 well plate. To aid in visualisation of cell migration and homing, HUVECs were stained with the nuclear dye Hoechst-33258, as described in section 2.1.6.1.1, while rMSCs, hMSCs and EPCs were stained with the membrane dye as described in section 2.1.6.1.2. Quantification of cells within the scratch wound was done using ImageJ.

4.1.7 Immunostaining

As described in section 2.1.13, samples were first incubated with 5% SA for 1 hour followed by addition of 1° antibody for 2 hours and 2° antibody for 1 hour. Antibodies were used at 1:100 and 1:200 respectively.

4.3 Results

4.1.8 Human umbilical vein endothelial cell (HUVEC) culture

The cells achieved the expected cobblestone morphology and were successfully utilised in the proceeding series of experiments. Cell proliferation rates were consistent and sufficient to provide the necessary number of cells for all subsequent experiments. Cells used for experimentation were between passage 2 (P2) and passage 5 (P5). Images of the cell morphology can be seen in figure 4-1.

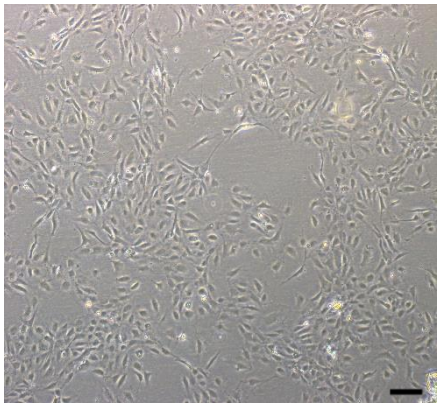

Figure 4-1: HUVEC morphology. Here we see typical HUVEC appearance in culture, with cobblestone morphology. HUVECs imaged are at P2. Scale bar = 100 µm

4.1.9 Rat mesenchymal stem cell (rMSC) culture

These cells adopted a flattened and spread-out morphology with spindle like projection as can be seen in figure 4-2. These also displayed rapid proliferation, doubling every 2 days. Cells used were not older than P6. To further evaluate the stemness of these cells, a tri-lineage differentiation was carried out as detailed in section 2.1.1.5. Images detailing progression of differentiation are shown in figure 4-3 and 4-4. Cells used for differentiation were at P4, n=3.

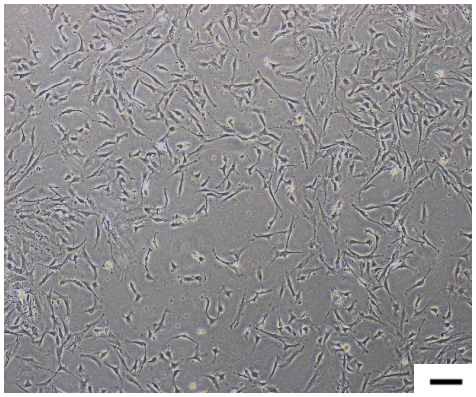

Figure 4-2: rMSC morphology. These images show the cell morphology observed in these cells during monolayer culture. Cells imaged here are at P4 and 4x magnification. Scale bar = 100 µm.

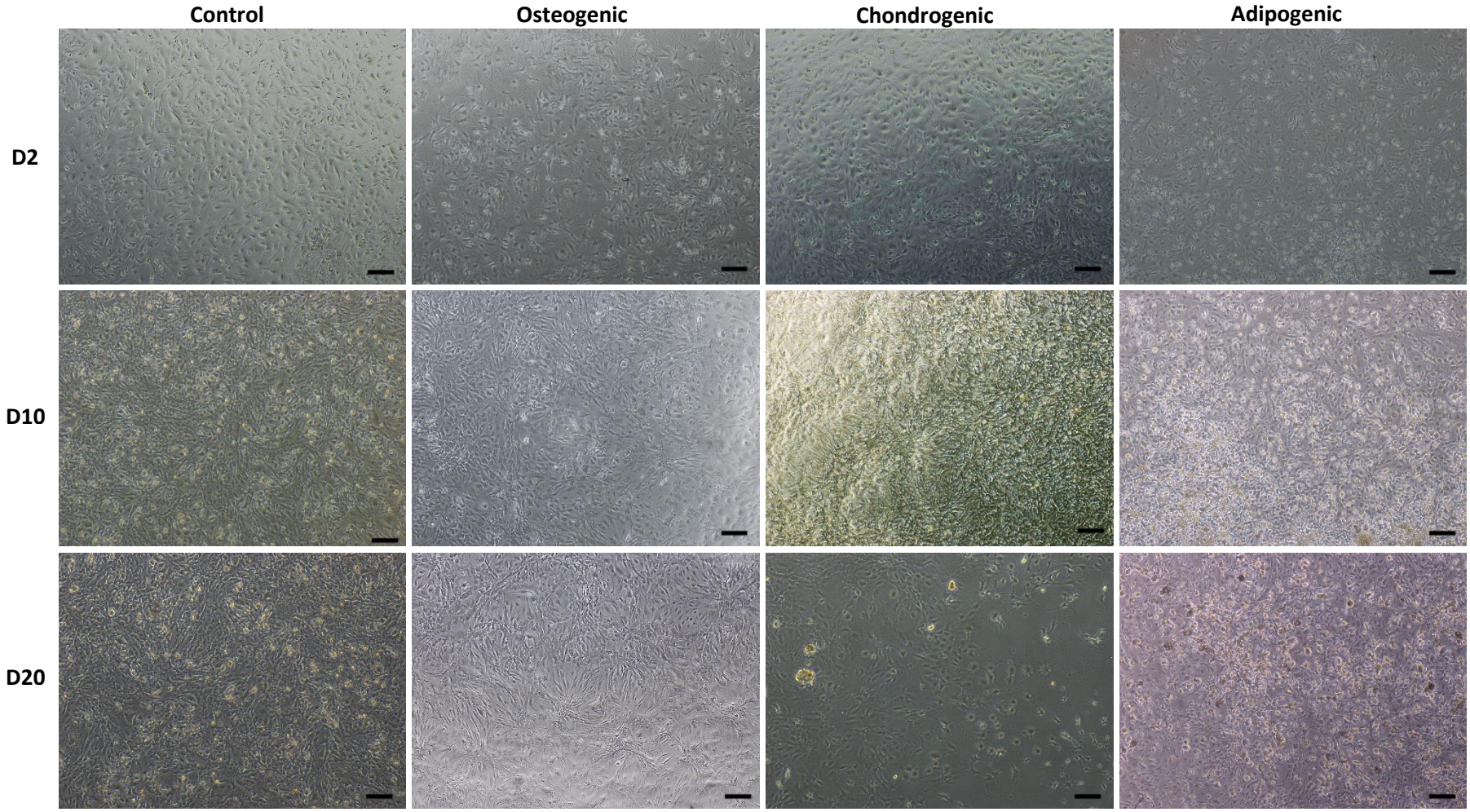

Figure 4-3: Trilineage differentiation timeline. This panel illustrates the morphological changes occurring over time during differentiation under osteogenic, chondrogenic and adipogenic stimulation. All images taken at 4x.

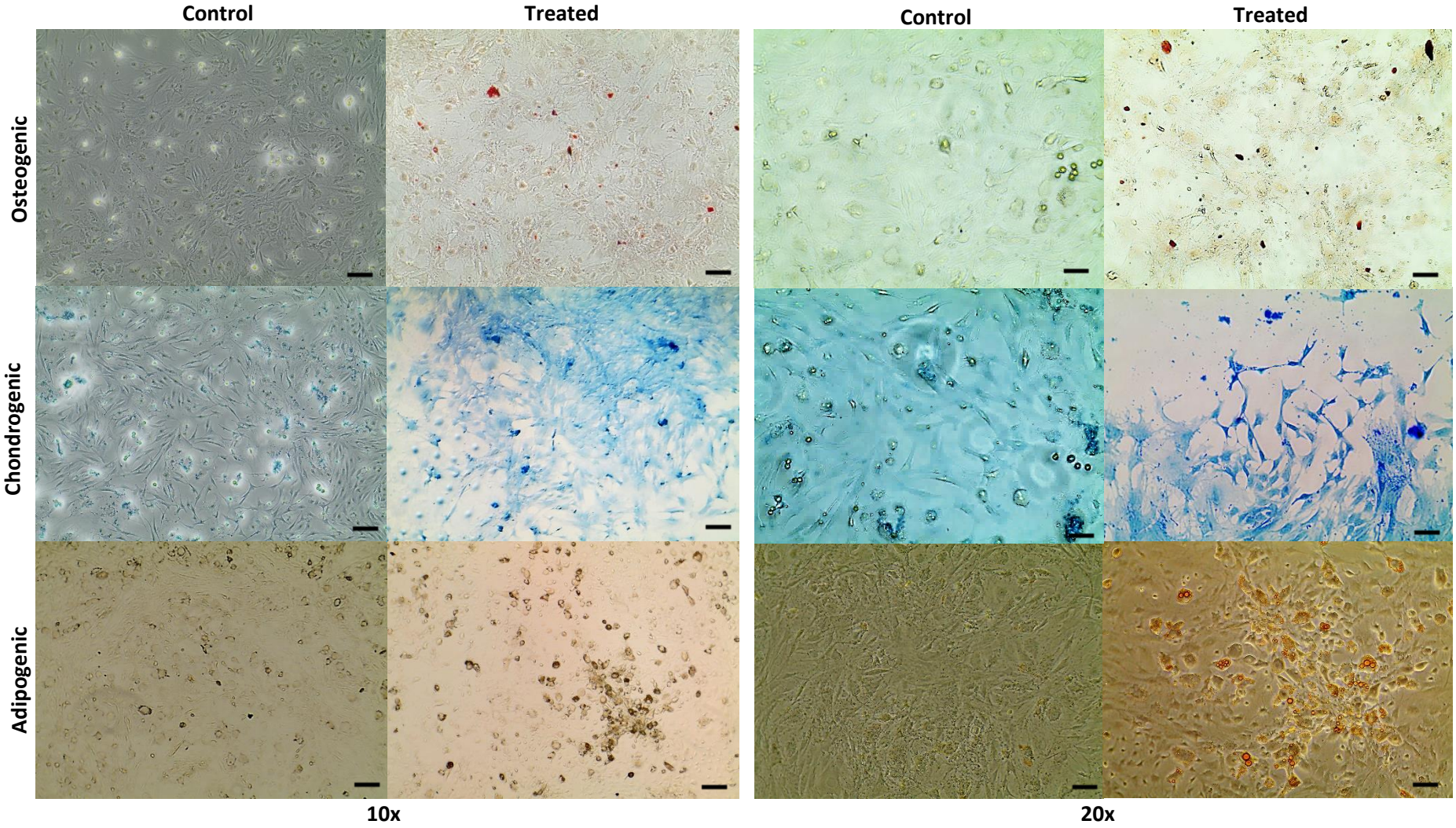

Figure 4-4: rMSC trilineage differentiation. Cultured cells were exposed to either osteogenic, chondrogenic or Adipogenic media for 21 days. Morphological changes were observed between the control and treated samples and staining with alizarin red, alcian blue and oil red-o demonstrates differentiation of rMSCs along the osteogenic, chondrogenic and adipogenic lineages respectively. Scale bar = 100 µm.

Looking at figure 4-3, the cells have a fairly similar phenotype at day 2, with the appearance of small lipid droplets visible in the adipogenic differentiation. These droplets get denser as the culture ages as seen at day 10 and eventually the droplets get larger as can be seen at day 20. Their completion of differentiation into adipocytes is confirmed in image 4-4 with distinct oil red-o (red) stained lipid droplets that are more easily distinguished at 20x. Osteogenically differentiated cells started to grow in clusters at day 10, with the clusters being more numerous at day 20. Staining with alizarin red is necessary to distinguish any further morphological and phenotypic changes to these cells. This is confirmed with the presence of mineral deposits stained red in figure 4-4. In figure 4-3, cells undergoing chondrogenic differentiation are extremely confluent at day 10 but density dramatically decreases at day 20. At day 20, typical chondrocyte morphology can be seen and their terminal differentiation is confirmed with the alcian blue staining seen in figure 4-4.

4.1.10 Human mesenchymal stem cell (hMSC) culture

These cells were successfully cultured and displayed an elongated phenotype as seen in figure 4-5. They were not highly proliferative cells, doubling approximately every 5 days. Cells used for experimentation were between P3 and P6.

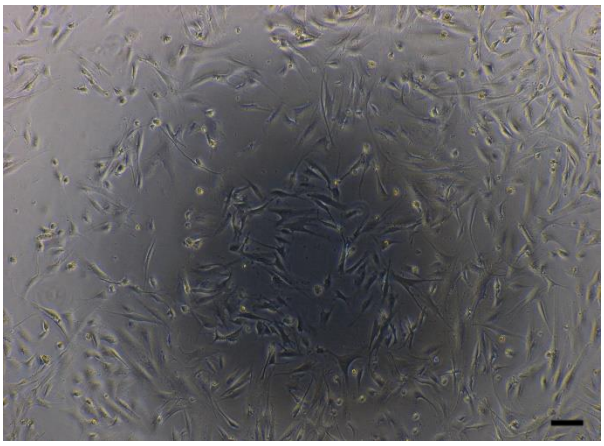

Figure 4-5: hMSC morphology. This representative image shows the hMSC morphology typically observed during culture. Cells were imaged at 4x and at P4. Scale bar = 100 µm

As with the rMSCs, tri-lineage differentiation was carried out to verify the stemness of these cells. Images detailing the differentiation are shown if figures 4-6 and 4-7. Cells used were at P4, n=3.

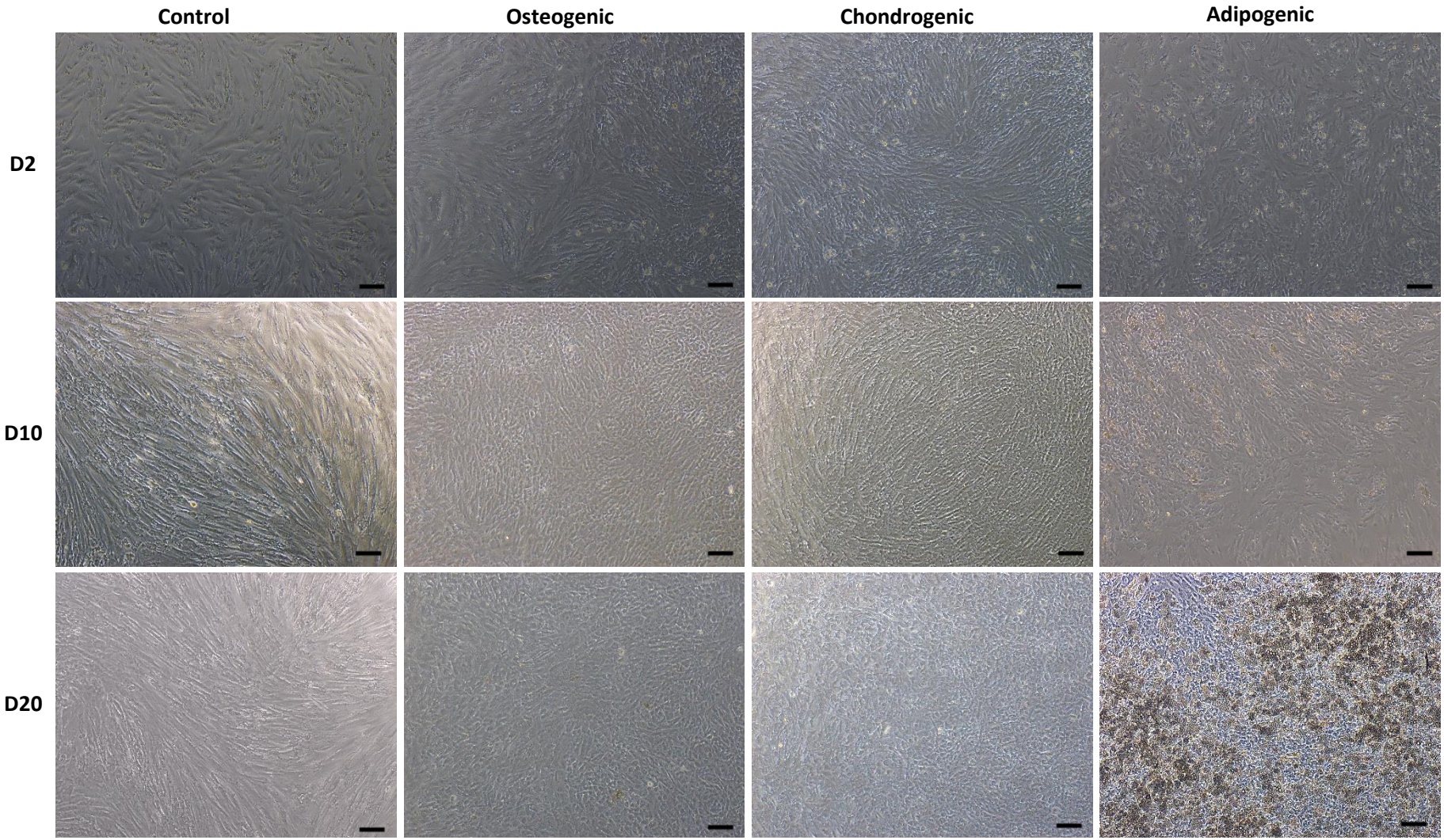

Figure 4-6: Trilineage differentiation morphological changes in hMSCs. This image details the morphological changes hMSCs underwent under osteogenic, chondrogenic and adipogenic stimulation. Images taken at 10x. Scale bar = 100µm

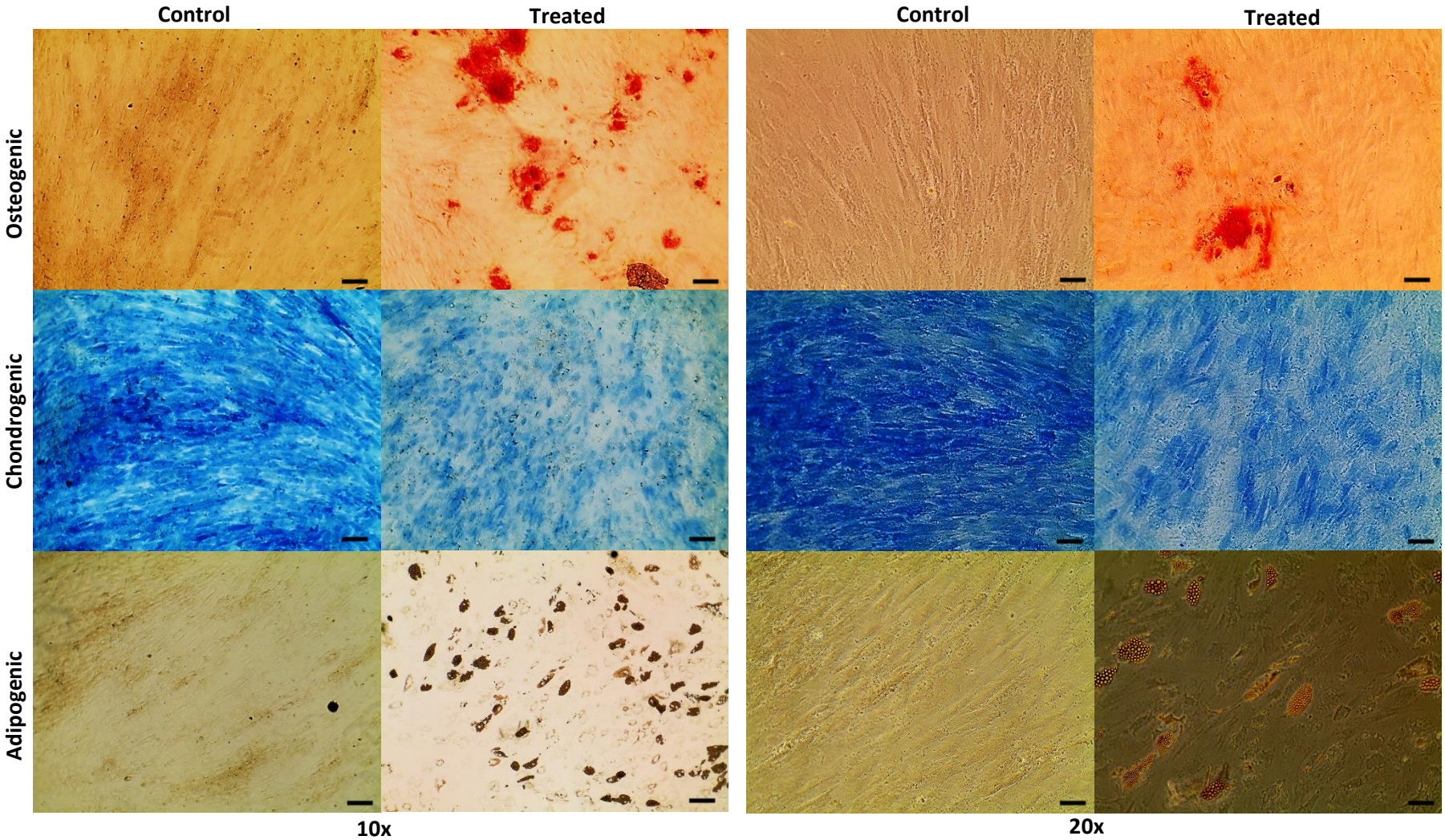

Figure 4-7: Trilineage histological staining. The staining demonstrates that it was possible to differentiate these cells along the desired lineages, with noticeable mineral deposits in the osteocytes, faint blue staining for the chondrocytes and red stained lipid vesicles for the adipocytes. Scale bar = 100 µm

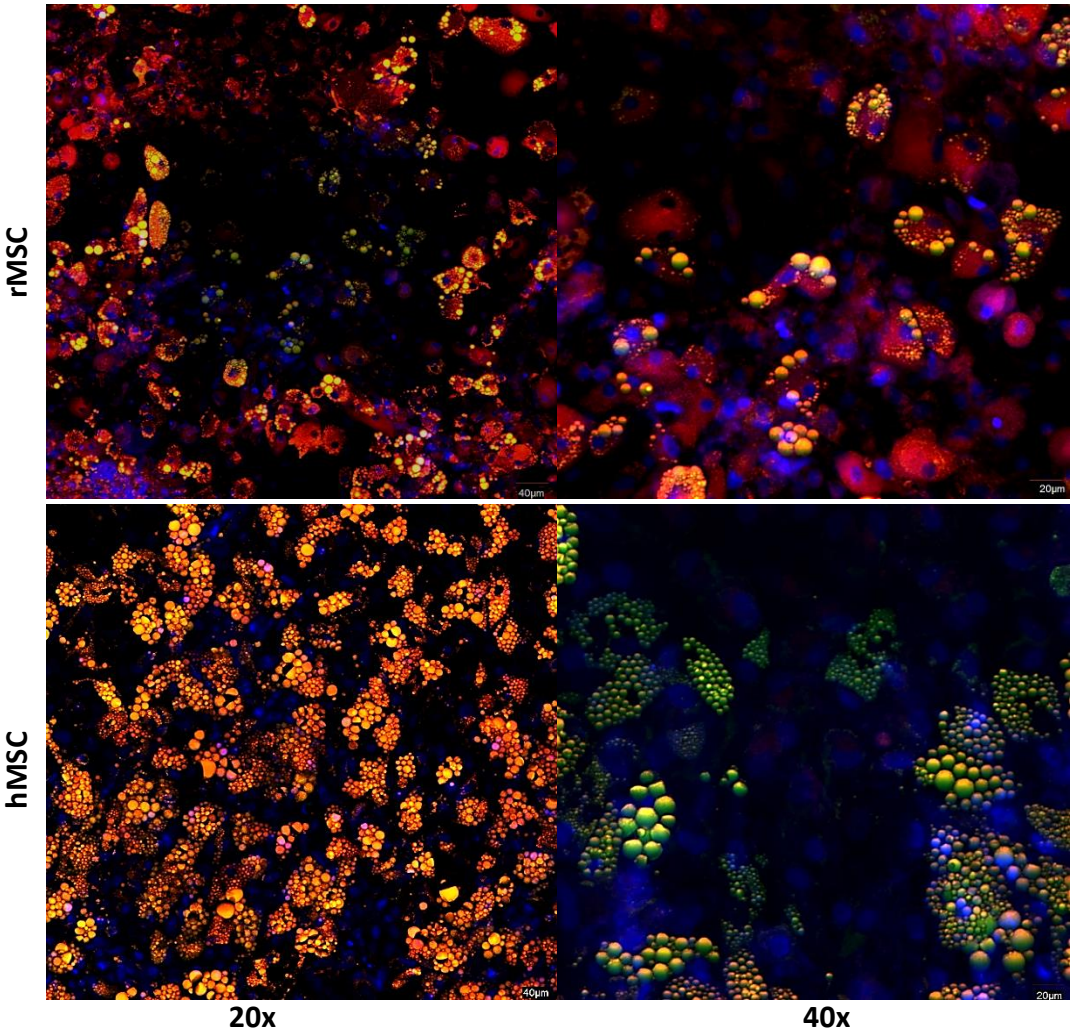

Figure 4-8: Nile red staining of adipogenic differentiation of rMSCs and hMSCs. Nile red staining was done using both FITC and Texas red emission to denote internalised lipid (gold) as well as the cell membrane (red). The gold colouration is a result of FITC and Texas red overlay. A larger density of lipid droplets is visible on the hMSCs compared to rMSCs. Blue staining is DAPI. Scale bar = 40 µm for 20x and 20 µm for 40x.

Across all lineages, as seen in figure 4-6, there are signs of differentiation as early as day 2, with cells starting to lose the elongated phenotype associated with hMSCs. At day 20, both osteogenic and chondrogenic lineages appear to have smaller cells than the control. Density of cells is also maintained in the chondrogenic lineage, unlike what is seen in the rMSCs between day 10 and 20. Histological staining (figure 4-7) for osteogenic and adipogenic differentiation of hMSCs shows clear mineral staining for the osteogenic and lipid staining for the adipogenic. The chondrogenic staining appears ambiguous with the control samples displaying stronger GAG staining, possibly due to the level of confluency of the cells here. As with the rMSCs, he adipocytic differentiation samples are beginning to

develop lipid droplets at day 2, which get denser and universally distributed by day 20 (figure 4-6). These droplets are larger and more ubiquitously distributed than those seen in the rMSCs, as seen in figure 4-8, which details adipogenic differentiated cells stained with Nile red. For both cell types, their multipotency was confirmed through successful differentiation into osteogenic, chondrogenic and adipogenic lineages.

4.1.11 The effect of atorvastatin dose on cells' metabolic activities

To determine if atorvastatin has any detrimental effect on cell metabolism, a CCK8 assay was done comparing a control sample with various doses of atorvastatin i.e., 30µg/ml, 60mg/ml, 80mg/ml, 100µg/ml, 120µg/ml and 140mg/ml. This assay functions by measuring metabolic activity through the conversion of tetrazolium salts (WTS-8) to formazan through NADPH. This evaluation was done for HUVECs, EPCs and rMSCs. CCK8 readings were taken after a 24-hour incubation with or without atorvastatin. HUVECs were seeded at a density of 2 x 10^4 cells per well of a 96 well plate, EPCs at 4 x 10^3 cells per well and rMSCs at 1 x 10^4 cells per well. CCK8 readings were taken as described in section 2.1.4. Effect of atorvastatin on proliferation of these cells is shown in figure 4-9. CCK8 control for the methanol used to deliver atorvastatin is shown in figure 4-10.

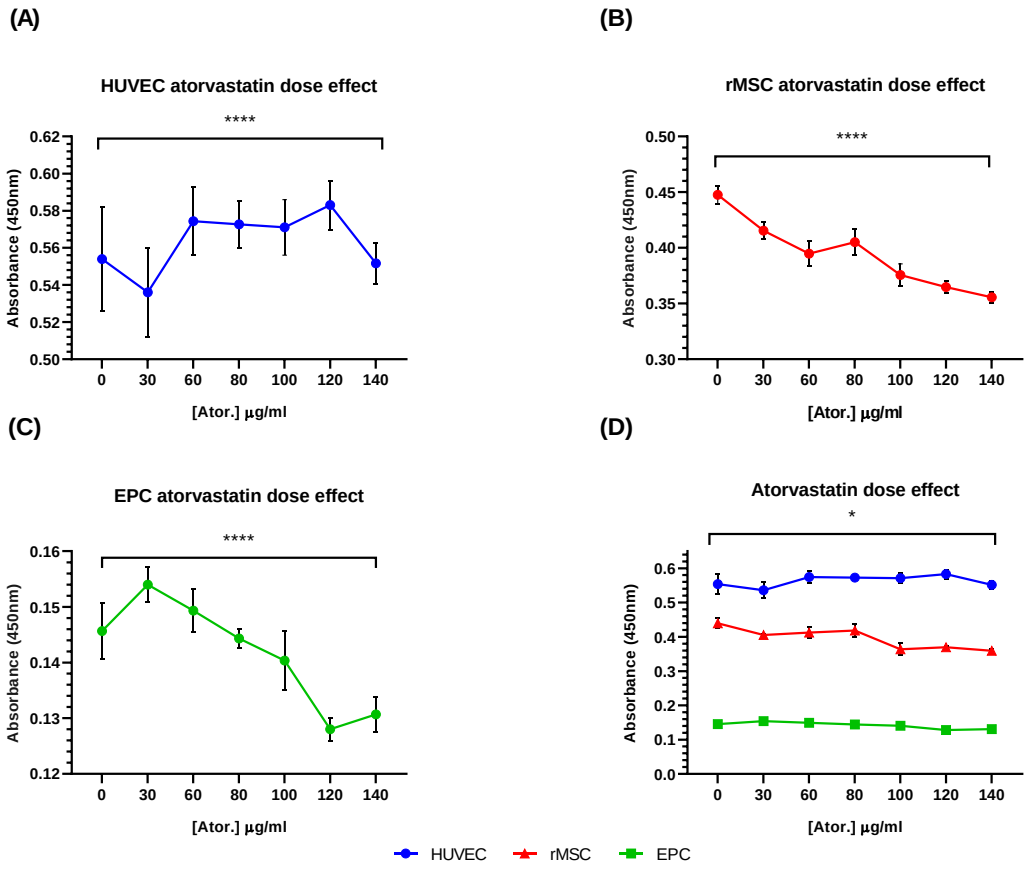

Figure 4-9: Atorvastatin effect on proliferation using CCK8. (A) atorvastatin effect on HUVEC proliferation. **(B)** atorvastatin effect on rMSC proliferation. **(C)** atorvastatin effect on EPC proliferation. **(D)** comparative of atorvastatin effect on cell proliferation for all cell types. From A to C, n= 3, 3 and 6 respectively. Statistical significance determined using one sample t- and Wilcoxon test for **(A-C)** p <0.0001****, and two-way ANOVA for **(D)** p = 0.0264*. Analysis indicated significance between concentrations of atorvastatin.

For the three cell types represented here, only the HUVECs appear to be positively impacted by higher concentrations of atorvastatin, with the highest reading being observed at 120µg/ml. EPCs demonstrate a rise in viability via metabolic markers only at 30µg/ml and 60µg/ml, while rMSCs are overall negatively affected by atorvastatin. The differences in OD readings between cell types is due to the different seeding densities used, as specified above. The data presented here suggests that atorvastatin's effect is not only dose dependent but also cell type dependent, with 60µg/ml being the ideal concentration for HUVECs, 30µg/ml for EPC and no atorvastatin has the best effect on rMSCs.

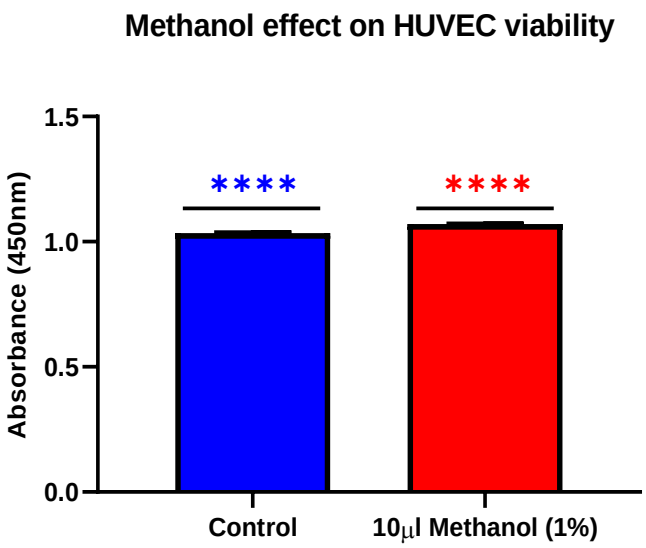

Figure 4-10: Methanol effect on cell viability. A CCK8 evaluation was done to determine the potential effect of methanol, the delivery vehicle selected for atorvastatin, on viability of HUVECs. $2x10^4$ HUVECs were seeded with plain media and the maximum usable volume of methanol (10µl/1%) was added, followed by a 24-hour incubation. N = 9. Statistical significance determined using two-way ANOVA, with significance identified between methanol and control ($p < 0.0001$****) and also within each variable ($p = 0.0443$ *).

The findings in figure 4-10 indicate that methanol does not have a negative effect on cell viability detected with CCK8, but rather appears to marginally promote metabolic activity compared to the control. Future experimentation involved the use of methanol at levels below 1% i.e., ≤ 5µl/ml of media used.

4.1.12 The effect of atorvastatin and MSCs on cell distribution in a scratch wound model

To assess the impact atorvastatin has on cell migration and wound closure, 4 x 10^4 HUVECs were seeded per well in a 48 well plate. Once confluent (figure 4-10 A), HUVECs were first stained with Hoechst as described in section 2.1.6.1.1. A scratch wound was then created using a 10µl pipette tip (figure 4-10 B). Denuded cells were aspirated and the well washed with PBS. This was followed by the addition of either rMSC, hMSCs or EPCs that had been stained with CFSE, as described in section 2.1.6.1.2, at a density of 5 x 10^3. Atorvastatin was also added to the wells at this time; concentrations used were 30mg/ml, 60µg/ml, 80µg/ml, 100µg/ml, 120µg/ml and 140µg/ml. Fluorescent images of the wells were taken at the 1 hour and 24-hour time points to track migration. Quantification of

migrated cells was done using ImageJ. Appearance of HUVECs before and after lesioning are shown in figure 4-11.

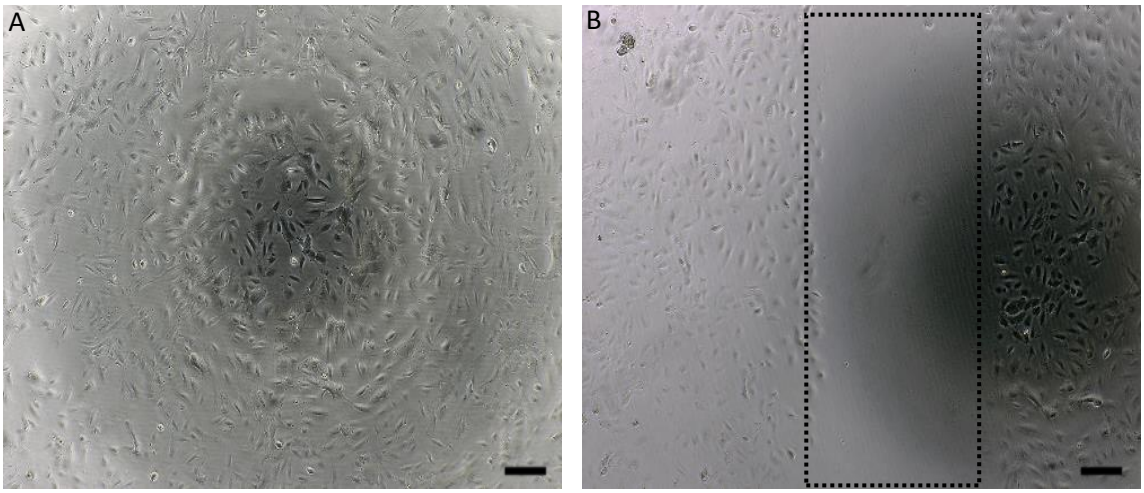

Figure 4-11: HUVECs pre- and post- scratch wound. (A) shows HUVECs at 100 percent confluence in a 48 well plate before creation of the scratch wound. (B) scratch wound on confluent HUVEC layer, denoted by black dotted line. Scale bar = 100 µm.

4.3.1.1 HUVECs and rMSCs

Representative images of wound closure with HUVEC and rMSC co-culture under different doses of atorvastatin are shown in figure 4-11. Quantification based on image analysis is shown in figure 4-12.

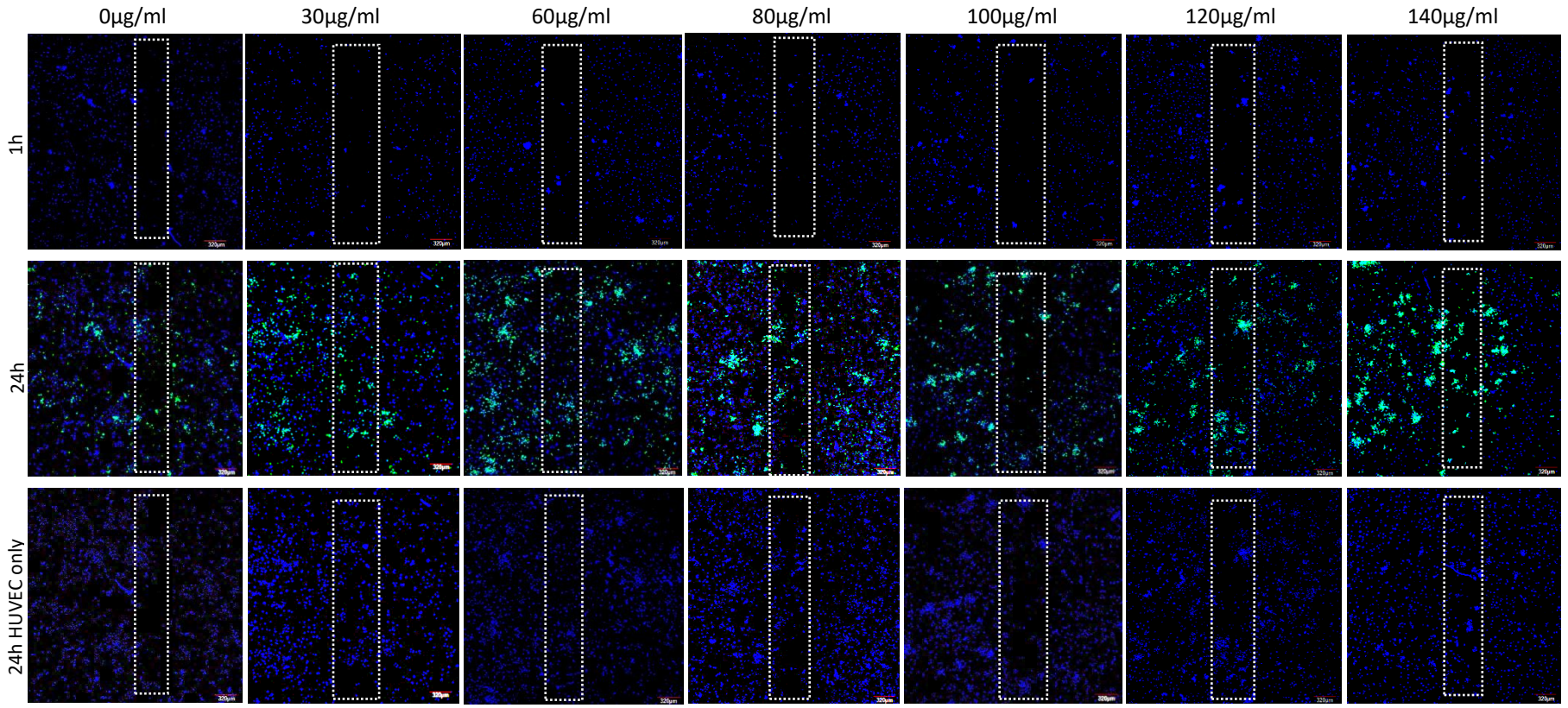

Figure 4-12: Atorvastatin effect on rMSC and HUVEC wound closure. Higher concentrations of atorvastatin appear to have a concentration of cells within the scratch wound after 24 hours. The rMSCs (green) are more clearly visible as clusters at 120mg/ml and more so at 140µg/ml. White dotted lines denote the denuded area. rMSC. HUVEC. Images taken at 4x. Scale bar = 100 µm.

The extent of the scratch wound has observably altered over 24 hours and there appears to be a correlation between drug dosage and distribution of cells within the lesion area. The cells present within the lesion area were counted and the comparative data is represented in figure 4-12.

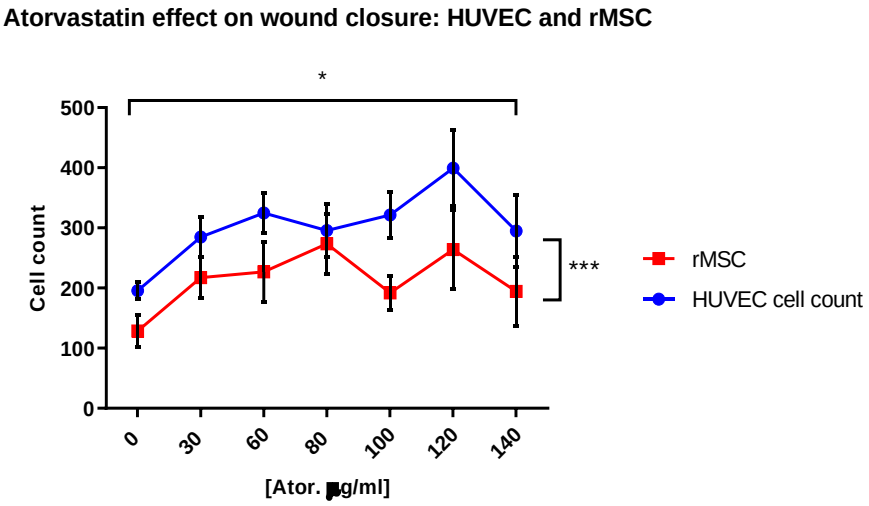

Figure 4-13: Distribution and number of HUVECs and rMSCs within scratch wound. Representation of cells located within the scratch wound created on confluent HUVECs, following **a** 24-hour incubation with rMSCs, and atorvastatin at different concentrations. Statistical significance between concentration of atorvastatin and number of cells present in scratch wound was determined using two-way ANOVA, p = 0.0218*. Significance was also found for differences in density of rMSC and HUVECs within the scratch wound, p = 0.0004 ***. N=9.

Upon an evaluation of cell distribution, the behaviour observed appears to be more in line with cell migration towards the lesion site resulting in closure of the lesion versus homing of suspended rMSCs. This behaviour also appears to be dose dependent with the highest number of cells present within the lesion after 24 hours being at 120µg/ml (Figure 4-12). A comparative with figure 4-11 shows that although there is a greater density of cells present at 120µg/ml, the cells appear smaller and are not evenly distributed throughout the scratch wounds but rather localised in the centre of the well. Across all the doses, HUVECs are more numerous than the rMSCs in denuded area. Two-way ANOVA was carried out, along with a one sample t and Wilcoxon test. Statistical significance was found between atorvastatin doses as well as between cell types.

4.3.1.1 HUVECs and hMSCs

Representative images of wound closure with HUVEC and hMSC co-culture under different doses of atorvastatin are shown in figure 4-13. Quantification based on image analysis is shown in figure 4-14.

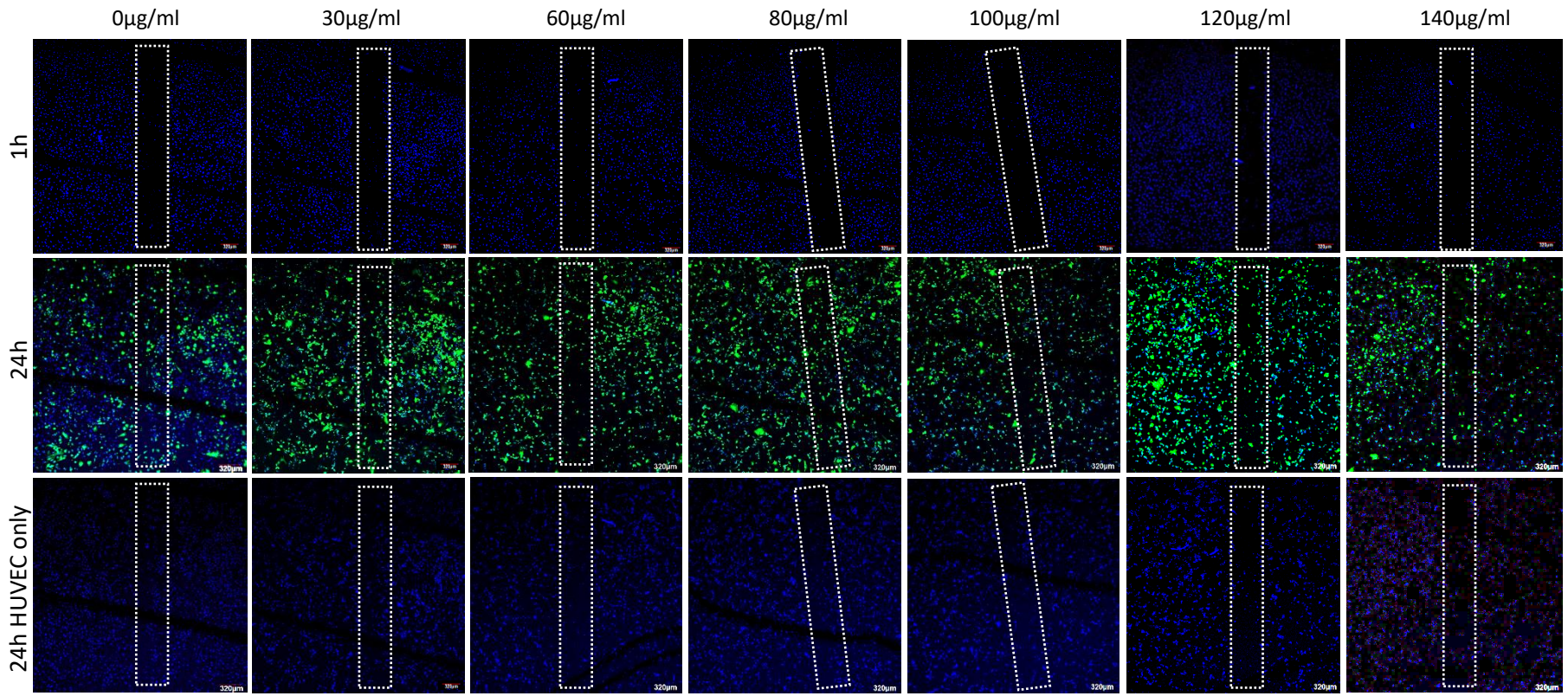

Figure 4-14: Atorvastatin effect on wound closure-HUVEC and hMSC co-culture. These representative images compare extent of infiltration into the scratch wound by HUVECs and hMSCs. Images show appearance of the scratch wound taken within 1-hour of endothelial layer disruption and after 24 hours in the presence of atorvastatin. hMSC. HUVEC. Images taken at 4x. Scale bar = 100 µm.

Across various doses of atorvastatin, the densest coverage of the scratch wound is observed at 60µg/ml and 80µg/ml. The closure seems to be predominantly as a result of hMSC (green) migration and distribution within the scratch area versus HUVECs (blue). Higher doses (100-140µg/ml) still have a clearly visible denuded area after 24 hours.

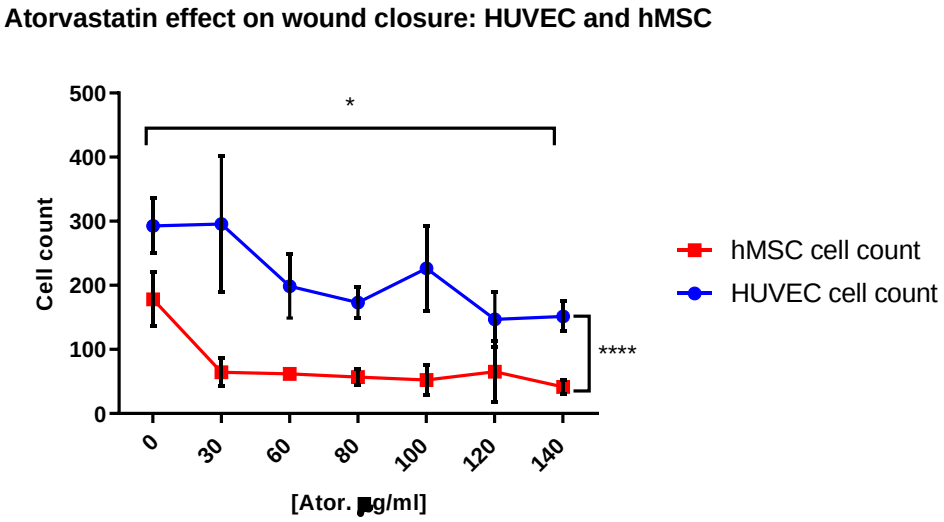

Figure 4-15: Distribution and number of HUVECs and hMSCs in scratch wound. Representation of cells located within the scratch wound created on confluent HUVECs, following **a** 24-hour incubation with hMSCs, and atorvastatin at different concentrations. Statistical significance between concentration of atorvastatin and number of cells present in scratch wound was determined using two-way ANOVA. Statistical significance denoted by P = 0.0382*. Significance was also found for differences in density of hMSC and HUVECs within the scratch wound, p < 0.0001. N=6.

Contrary to the observations with the rMSCs, more cells were present within the wound region after 24 hours at lower concentrations of atorvastatin (figure 4-13 and 4-14), specifically 30µg/ml, with HUVECs present in greater numbers than hMSCs across all the doses. Barring a small rise at 120µg/ml, the general trend reflects a negative effect of atorvastatin on wound closure. This data suggests there is some species variation in terms of responses to atorvastatin. Two-way AVOVA was carried out along with a one sample t and Wilcoxon test. Statistical significance was found between doses of atorvastatin as well as between cell types.

4.1.12.1 HUVECs and EPCs

Representative images of wound closure with HUVEC and hMSC co-culture under different doses of atorvastatin are shown in figure 4-15. Quantification based on image analysis is shown in figure 4-16.

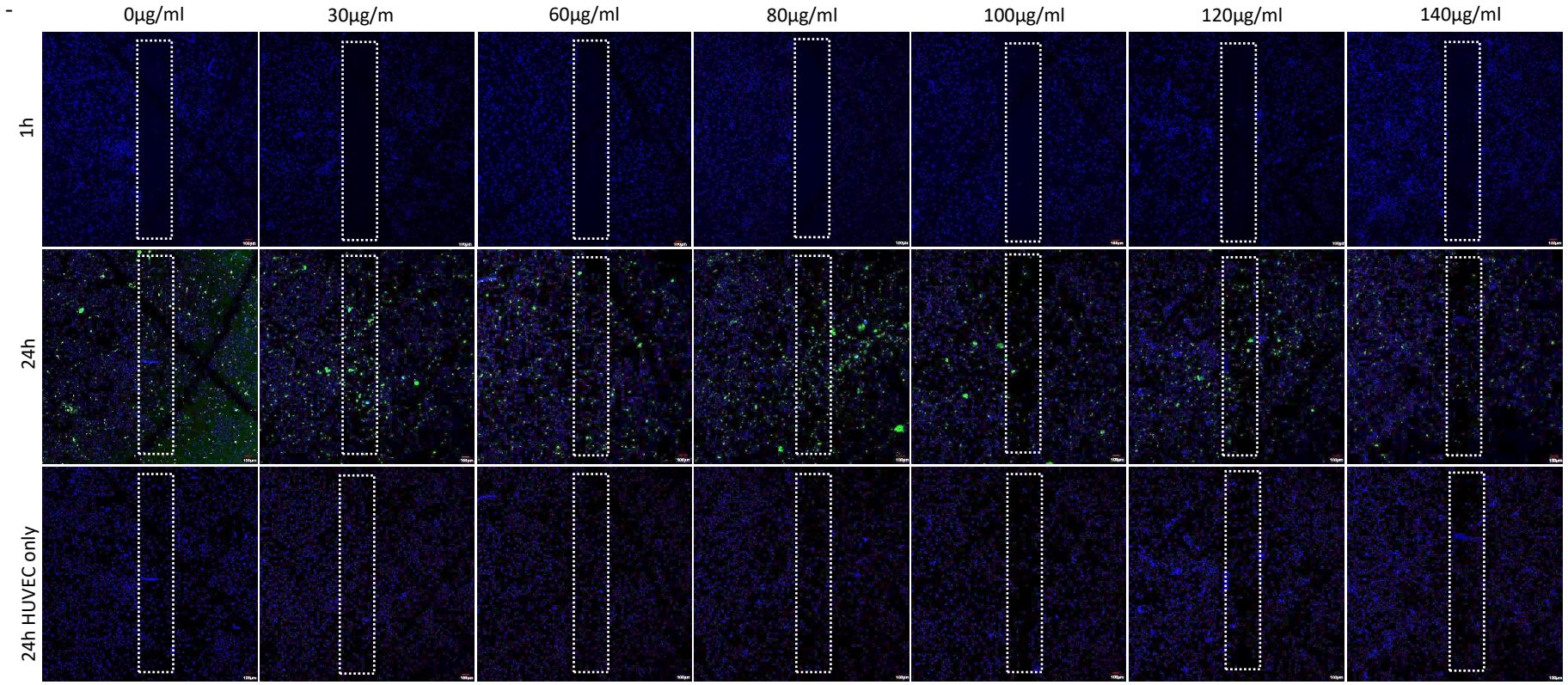

Figure 4-16: Atorvastatin effect on wound closure-HUVEC and EPC co-culture. These representative images compare extent of infiltration into the scratch wound by HUVECs and EPCs. Images show appearance of the scratch wound taken within 1-hour of endothelial layer disruption and after 24 hours in the presence of atorvastatin. EPC. HUVEC. Images taken at 4x. Scale bar = 100 µm.

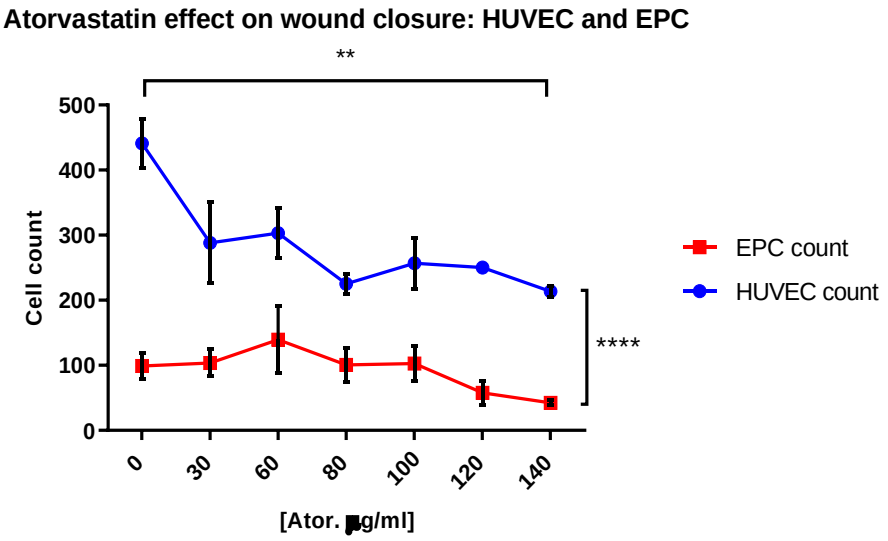

Figure 4-17: Distribution and number of HUVECs and EPCs in scratch wound. Representation of cells located within the scratch wound created on confluent HUVECs, following **a** 24-hour incubation with hMSCs, and atorvastatin at different concentrations. Statistical significance between concentration of atorvastatin and number of cells present in scratch wound was determined using two-way ANOVA. Statistical significance denoted by P = 0.0024**. Significance was also found for differences in density of EPCs and HUVECs within the scratch wound, p < 0.0001 ****. N=3.

The distribution profile of EPCs within the scratch wound at varying doses of atorvastatin follows that seen in HUVECs for this particular cell combination. EPCs seem to respond to atorvastatin better than the other human cell types, with peak attachment being achieved at 60µg/ml, versus 0µg/ml with the hMSCs, once again demonstrating that responses are dependent on cell type and combinations of cells. 60µg/ml also appears to be the ideal dose of atorvastatin for HUVECs when cultured with rMSCs and EPCs. Even though higher cell numbers are recorded at higher doses for the HUVEC-rMSC co-culture, an assessment of figure 4-11 indicates that the cells are more in clusters at doses above 100µg/ml, and there is incomplete closure of the scratch wound. It is believed the cluster of cells seen in figure 4-11 at 120µg/ml and 140µg/ml were not migratory but rather deposited by gravity in the centre of the well. Statistical significance was determined by carrying out a two-way ANOVA as well as a one sample t and Wilcoxon test. The two-way ANOVA showed significance in the interaction between atorvastatin dose and cell numbers within the scratch wound as well as significance between atorvastatin doses and extent of infiltration between cell types, suggesting that the dose and cell types present contribute to the observed result.

4.1.13 Immunostaining

4.1.13.1 CXCR4: hMSCs

To determine if atorvastatin or the scratch wound has any effect on CXCR4 expression on hMSCs, a key receptor for vascular homing, a scratch wound was created on a confluent layer of hMSCs followed by the addition of atorvastatin at 30, 60 and 120µg/ml. The same doses were added to intact cells as a comparative. Representative images are shown in figure 4-18.

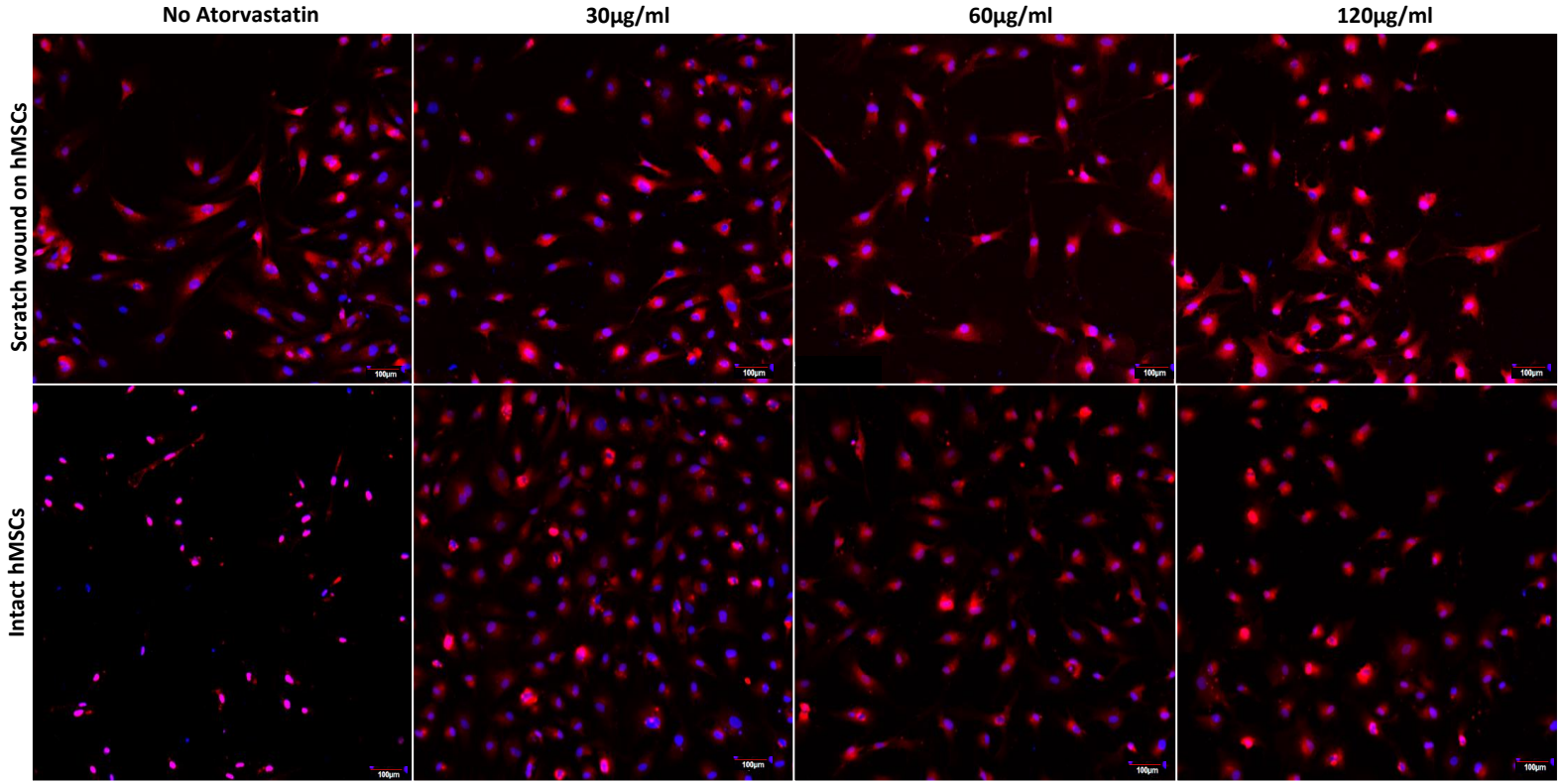

Figure 4-18: Atorvastatin effect on CXCR4 expression on hMSCs. These images show variations in CXCR4 expression between an intact and disrupted hMSC layer at different doses of atorvastatin. CXCR4. DAPI. Images taken at 10x. Scale bar = 100 µm.

From figure 4-18, it appears as though the absence of an injury and atorvastatin results in reduced expression of CXCR4 in hMSCs while the inclusion of atorvastatin appears to increase expression of this receptor, both with and without an injury, suggesting atorvastatin may stimulate expression of CXCR4, with the brightest staining, with large stained cytoplasm morphology, observed at 120µg/ml. Cells in the scratched wells appear to be more spread out while those in the intact wells appear smaller overall, possibly due to cell spreading as they migrate to cover the denuded area, resulting in staining that appears compacted around the nucleus. The doses selected reflect the concentrations where the densest accumulation of cells within the scratch wound were recorded.

4.1.13.2 CXCR4: HUVECs

To determine if atorvastatin or the scratch wound has any effect on CXCR4 expression on HUVECs, a scratch wound was created on a confluent layer of HUVECs followed by the addition of atorvastatin at 30, 60 and 120µg/ml. The same doses were added to intact cells as a comparative. Representative images are shown in figure 4-20.

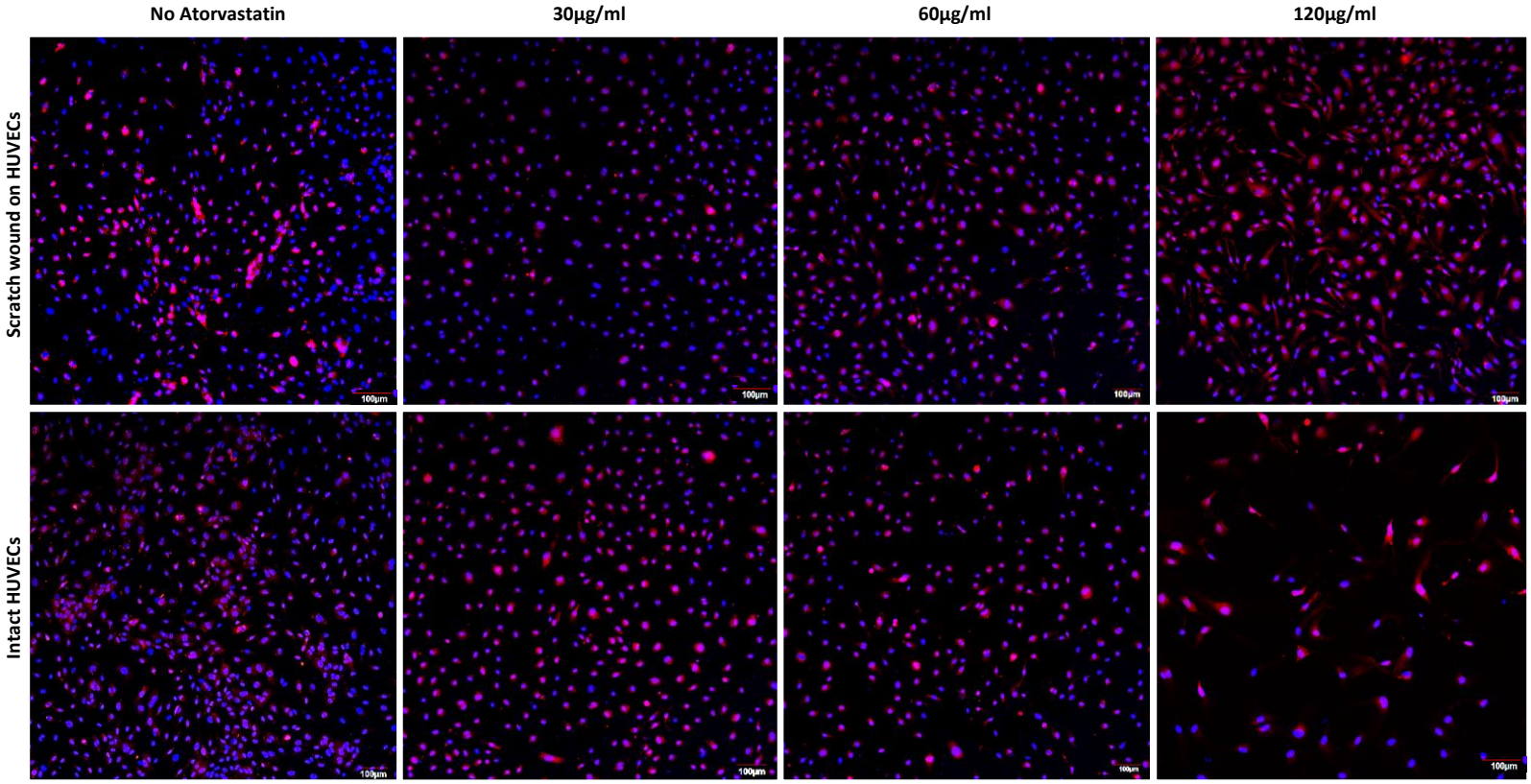

Figure 4-19: Atorvastatin effect on CXCR4 expression on HUVECs. These images show variations in CXCR4 expression between an intact and disrupted HUVEC layer at different doses of atorvastatin. CXCR4. DAPI. Images taken at 10x.

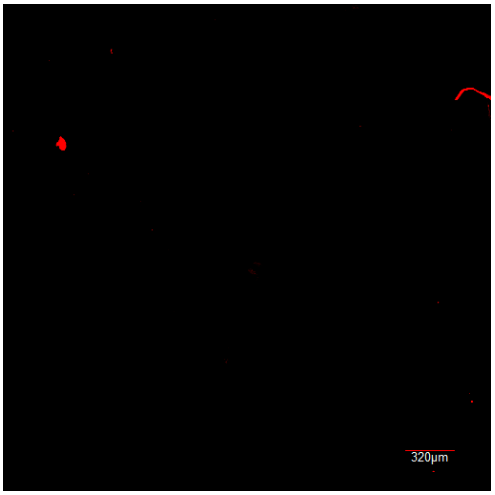

Figure 4-20: Secondary antibody negative control: Mouse anti-rabbit IgG-TR (Texas Red) Conjugated used as secondary antibody for CXCR4. Image taken at 4x, scale bar = 320 µm.

An examination of figure 4-19 shows that expression of CXCR4 appears less on HUVECs when compared to hMSCs. There appear to be basal expression of CXCR4 as suggested by the drug free samples, either with or without a scratch wound. While expression appears consistent across the samples represented here, 120µg/ml atorvastatin appears to influence increased expression of CXCR4 on HUVECs with a scratch wound, although cells here appear to have atypical morphology, adopting a "comma" like appearance compared to the mostly rounded appearance of cells at lower concentrations of atorvastatin. There also appears to be a moderate increase in expression at 60µg/ml on the scratched samples compared to the 30µg/ml and drug free samples. These images also suggest that atorvastatin has an effect on CXCR4 expression, but to a lesser extent in HUVECs than MSCs, highlighting this receptor's role in recruiting circulating cells versus impacting resident endothelial cells.

4.4 Discussion

4.1.14 Cell distribution/migration towards wound closure

The data here suggests that HUVEC migration is a larger contributor to wound closure compared to homing of either rMSCs, hMSCs and EPCs. The effect of atorvastatin has also been shown to be both dose dependent and cell type dependent with the murine cells responding better than the human cells (figure 4-12), and between human cells, the EPCs (figure 4-16) are more responsive to atorvastatin than the hMSCs (figure 4-14), demonstrating an increase in cells within the scratch wound in the presence of atorvastatin up to 60µg/ml. This suggests that the beneficial effects of atorvastatin, within the bounds of the experiments carried out here, are primarily on homing of EPCs to sites of vascular injury, an observation supported by findings which demonstrate that statins promote EPC mobilization and homing (Oikonomou *et al.*, 2015). The effects seen with rMSCs could be explained by the cross reactivity of human and murine SDF-1, the primary chemokine responsible for the migration and homing of bone marrow derived cells. There is remarkable conservation of the amino acid sequence for SDF-1 during evolution in different species, with murine and human SDF-1 being cross reactive, suggesting an important biologic role (Dar, Kollet and Lapidot, 2006). This biological importance is supported by the observation that knockouts of SDF-1 and its receptor CXCR4 are lethal (Ratajczak *et al.*, 2006).

It was also possible to demonstrate the effect atorvastatin has on the production of CXCR4 (figure 4-17 and 4-18). Findings from a murine model by Li et al., 2015 showed that atorvastatin increases the migration ability of MSCs and improves cardiac performance due to up-regulated expression of CXCR4 (Li et al., 2015), which supports the observations seen here on human MSCs. Liu et. al., also demonstrated that increased surface expression of CXCR4 in mesenchymal stem cells resulted in enhanced migration (Liu *et al.*, 2011), which is not what is seen here, suggesting that either the concentrations used here were not ideal for enhancing hMSC migration, some other conditions must be met to increase homing along with increasing CXCR4 expression, or that these observations do not apply for human cells as these studies are based primarily on observations in murine models (Zhang

et al., 2014; Bing *et al.*, 2016), which could be supported by the observations in figure 4-12 which show that the best response was seen in HUVECs co-cultured with murine cells. Further evidence to support the suggestion that other mechanisms might be in play can be derived from Rüster et. al., 2006, who propose that the interaction of MSCs with the endothelial layer is through shear, p-selectin and VCAM-1 (Rüster *et al.*, 2006). Additionally, the expression of CXCR4 in HUVECs was not greatly affected by the inclusion of atorvastatin, suggesting that some other mechanism may be involved in their migration into the scratch wound, or possibly the interplay between cell types could be a contributing factor.

4.1.15 Atorvastatin dose effect

The data represented here demonstrates that there is variation in viability due to atorvastatin based on cell type. Figure 4-9 (D) suggests that although there is an observable decrease in viability demonstrated by plots A-C, the compounded change when the plot are combines is not that large across the selected doses of atorvastatin. The assay used to determine cell viability relies on the activity of NADPH to convert tetrazolium salts to formazan, which gives the colour change used to quantify cell viability. Interference in the availability of NADPH would result in discrepancies in determining actual cell viability. Atorvastatin has been demonstrated to activate nitric oxide synthase (NOS), which mediated the survival of implanted MSCs in mini-swine (Song *et al.*, 2013a). NADPH is required for the functioning of NOS, which is involved in the production of nitric oxide (Förstermann and Sessa, 2012). This finding is consistent with other reports that statins suppress NADH/NADPH oxidase23 or that a metabolite of atorvastatin has an antioxidant property (Sugiyama *et al.*, 2005). These observations suggest that the availability of NADPH would be restricted in the presence of atorvastatin, which would in turn limit the conversion of the tetrazolium salts to the formazan end-product, thus giving the impression of reduced cell viability. This supposition explains what is seen with the rMSCs and EPCs but not the HUVECs, which demonstrate increased viability on this assay at 60-120µg/ml atorvastatin, as seen in figure 4-1 A.

4.5 Conclusion

The data collected and presented here shows that atorvastatin has a positive impact on scratch wound closure, specifically in the context of HUVEC migration in the scratch wound versus migration of suspended cells to the scratch wound, and primarily with rMSC and HUVEC co-culture. rMSCs, in conjunction with HUVECs, demonstrated increased migration with increased atorvastatin concentration, attaining maximum infiltration at 120µg/ml. Contrastingly, hMSCs cultured together with HUVECs did not respond positively to atorvastatin. This observation is in line with published work and highlights the issue with using murine models to correlate responses with human tissue. In regards to the human cells used, it was determined that EPCs respond better to atorvastatin than MSCs, and the best response was at 60µg/ml, which highlights the potential importance of EPCs in vascular repair, especially in the presence of atorvastatin. The data here also sheds light on the interplays that happen between cells types, further demonstrating the need of the creation of biomimetic systems to generate clinically relevant data, and also to clarify the roles of individual cells as well as cellular co-cultures. It is also important to consider a wider array of atorvastatin doses to accurately determine the ideal dose to obtain optimal results but this also needs to be done in a 3D context as the experimental set-up here is not an accurate representation of physiological conditions. The absence of shear, for example, could greatly alter the responses seen. The data here, however, manages to scratch the surface, demonstrating that atorvastatin stimulates expression of CXCR4 in hMSCs and it also promotes EPC infiltration into sites of endothelial damage in a dose dependent manner. It was also possible to show that different cell combinations give rise to varying responses to atorvastatin. The experiments conducted and conclusions drawn could be taken further to gain a better understanding of the mechanisms involved in cell homing and migration in the presence of atorvastatin.

Chapter 5:

Evaluating Atorvastatin's Effect on Stem Cell Homing Using a 3D Blood Vessel Model.

5.1 Introduction

Maintenance of vascular integrity is a vital process in ensuring vascular health. The endothelium plays a major role in repair mechanisms and maintaining homeostasis, primarily due to its location between circulating blood and the underlying tissue (Sima, Stancu and Simionescu, 2009). In the context of atherosclerosis, vascular inflammation promotes the development of atherosclerosis and the deterioration of atherosclerotic plaques (Peng *et al.*, 2018). This process takes place over several years and involves activation of the endothelium, recruitment of immune cells, migration and proliferation of smooth muscle cells among other processes (Ramji and Davies, 2015). Aside from endothelial activation, another key contributor is shear stress, specifically regions exposed to low (less than 15dyne/cm^2) oscillatory or turbulent shear, have been shown to be the most vulnerable to the development of atherosclerotic plaques (Bentzon *et al.*, 2014), while regions that are exposed to laminar flow with shear rates at or higher than 15dyne/cm^2 are protected (Cheng *et al.*, 2006). These regions of irregular shear stress can be found at arterial bifurcations or the inner curvature of the coronary artery (Cheng *et al.*, 2006). Endothelial cells are particularly sensitive to shear stress and it regulates numerous functions such as inflammation, proliferation, and migration. Low shear contributes to the development of atherosclerosis by inducing endothelial expression of inflammatory molecules that coordinate the migration of leukocytes from the blood to the vascular wall (Mahmoud *et al.*, 2016). Another contributor to endothelial dysfunction and activation is the accumulation of oxLDL in the intimal layer, which in turn leads to local inflammation where ROS are overproduced (Gao *et al.*, 2020).

Statins function as competitive inhibitors of 3-hydroxy-3-methylglutaryl coenzyme A reductase (HMG-CoA), the rate regulating step in cholesterol synthesis (Stancu and Sima, 2001; Peng *et al.*, 2018; L. Xu *et al.*, 2019). Aside from reducing levels of circulating LDL through inhibition of cholesterol synthesis, statins have been shown to possess a variety of pleiotropic effects. One proposed effect of statin treatment is enhancing the recruitment of haematopoietic cells to damaged endothelium to promote vascular repair. Statin-MSC therapies have been studied and been found to improve heart function as

well as reducing scar hypertrophy, and promote osteogenic differentiation of MSCs (Gorabi *et al.*, 2020). Of interest to this project is the effect that statins have on the recruitment of circulating/ bone marrow derived endothelial progenitor cells (EPCs). The characteristics of these cells have been discussed previously in chapter 3, but briefly, statins, specifically atorvastatin, have been shown to increase circulating levels of these cells as well as promote their mobilization, differentiation, and improve their survival (Walter, Dimmeler and Zeiher, 2004; Sandhu, Mamas and Butler, 2017). Concerning this effect on EPC mobilisation to sites of vascular injury, a proposed mechanism involves the stromal derived factor-1 (SDF-1/CXCL12)/CXCR4 axis. SDF-1 is the only ligand that CXCR4 interacts with, and their interactions have been the focus of a lot of research due to their importance in the mobilization of EPCs and other progenitor cells (Hristov *et al.*, 2007), and also the observation that knockouts of either the receptor or its ligand results in a significant defects of colonization of embryonic bone marrow by haematopoietic stem cells and in the development of the heart, brain and large blood vessels (Ratajczak *et al.*, 2006). The CXCR/SDF-1 axis has also been associated with numerous downstream molecules that are involved in the physiological and pathological changes in diseases such as vasculopathy, local inflammation, cell migration and proliferation, and increased levels have been associated with dyslipidaemia (Gao, Yu and Tang, 2019). High doses of HMG-CoA inhibitors have been associated with decreasing circulating SDF-1 levels under hyperlipidaemic conditions (Camnitz *et al.*, 2012; Gao, Yu and Tang, 2019). This trend, however, appears to be the opposite in the absence of elevated lipid levels, with low dose statin (10nM to 100nM) resulting in increased EPC mobilisation and angiogenesis when used in combination with SDF-1, or with increased local over expression of SDF-1 (Yu and Feng, 2008). It has also been suggested that vascular SDF-1/CXCR4 limits atherosclerosis through the maintenance of vascular integrity, preservation of endothelial barrier function, and normal contractile phenotype in smooth muscle cells (Döring *et al.*, 2017). Many of the studies that have identified these effects of statins are based on the use of animal models which bring about its own issues, such as relatability due to species variation and the requirement of anaesthetics which may cloud the accuracy of observations (Janssen *et al.*, 2004;

Sashindranath *et al.*, 2019). More recent approaches are attempting to use tissue engineering to create biomimetic vessels (Papaioannou *et al.*, 2019; Evans, Iruela-Arispe and Zhao, 2021) to study various aspects of cardiovascular disease, which eases the burden on the need for animal models as well as allowing for more flexibility of experimental design.

Using principles of tissue engineering, this chapter will focus on evaluating the role atorvastatin plays on the homing of human mesenchymal stem cells (hMSCs) and, primarily, EPCs to sites of vascular injury on three blood vessel modes, i.e., intimal layer only (TEIL), medial layer only (TEML) and a composite model incorporating both layers (TEBV). Specifically, this effect will be evaluated under dynamic flow in a customised parallel plate flow chamber as well as in a see-saw rocker. The effect of type of injury on the number of homing cells and the production of SDF-1 will also be evaluated for all these models. The proposed effect of atorvastatin is detailed in figure 5-1. The complementary expression of CXCR4 on the blood vessel models was also investigated through immune-histological staining.

5.2 Materials and methods

5.1.1 HCASMC culture

As described in section 2.1.1.1, Human cardiac artery smooth muscle cells (HCASMCs) were used in the assembly of the tissue engineered blood vessel (TEBV) and tissue engineered medial layer (TEML). These cells were cultured in medium 231 and supplemented with smooth muscle growth supplement (SMGS) as per the supplier specifications. The cells used were between P3 and P5.

5.1.2 HUVEC culture

As described in section 2.1.1.2, Human Umbilical Vein Endothelial Cells (HUVECs) were cultured in medium 200 supplemented with low serum growth supplement (LSGS) as per the supplier recommendations. The cells used were between P2 and P5 for the creation of TEBV and tissue engineered intimal layer (TEIL).

5.1.3 hMSC culture

As described in section 2.1.1.5, human mesenchymal stem cells (hMSC) were cultured in DMEM (4.5g/L glucose) supplemented with 10% FBS, 1% AA and 1% LG. Cells used were between passage 3 and 6 (P3 and P6).

5.1.4 EPC culture

Following the isolation protocol described in section 2.1.1.8, EPCs were cultured in medium 200 supplemented with 10% FBS and 1% AA on fibronectin (2.5µg/cm^2) coated plates. Cells used were cultured for up to 20 days after primary isolation.

5.1.5 Electrospinning PLA nanofibers

Aligned PLA nanofibers were used in the assembly of the TE constructs used here. Fibers were made by first dissolving Poly-L, D-lactic acid (96% L/4% D, inherent viscosity of 5.21 dL/g) (PLA) in chloroform for at least 8 hours, followed by addition of dimethylformamide (DMF) for a further 8 hours of mixing to make a 2% PLA solution. Chloroform and DMF were mixed in a 7:3 ratio respectively. The operational parameters of nanofiber fabrication followed a previously established protocol (Yang, Wimpenny and

Ahearne, 2011; Njoroge *et al.*, 2021). Briefly, the 2% PLA solution was deposited on detachable metal collectors, consisting of two partially insulated steel blades (30 cm × 10 cm). The steel blades were connected to a permanent copper plate with a steel wire, and had a 5 cm gap between for fiber deposition. Fiber deposition involved connecting the permanent copper plate to a negative electrode, and a syringe containing the 2% PLA solution was connected to a positive electrode. The PLA was extruded through an 18G needle and delivered at a rate of 0.025 mL/min. The electrodes were electrified with a power supply charged at ±6 kV (Spellman HV, Pulborough, 26 United Kingdom). Nanofibers were collected and attached onto pre-cut acetate frames. Before use in cell culture, aligned nanofibers were sterilized by UV irradiation thrice per side.

5.1.6 Dynamic flow TE constructs

5.1.6.1 TEML

As described in section 2.1.8.1, the TEML was made by embedding HCASMCs in a collagen type I hydrogel. The HCASMCs were seeded into the collagen gel at a density of 5 x 10^5 cells/ml. 200µl of the cellular gel solution was pipetted into a hollow rectangle made of filter paper measuring 0.5cm x 2.4cm on the outside and 0.2cm x 2cm on the inside (figure 5-1). The dimensions of the filter paper were determined by the dimensions of the flow chamber and the gasket. The filter paper was placed on a piece of polytetrafluoroethylene (PTFE) to allow ease of transfer into a 6 well plate after gelation.

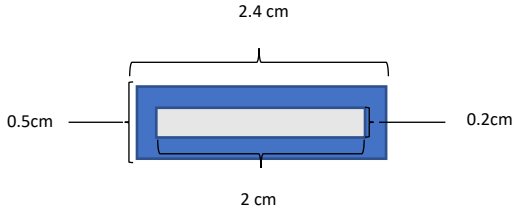

Figure 5-1: Filter paper frame. 200µl of collagen gel containing HCASMCs at a density of 5 x 10^5 cells/ml was deposited into the hollow portion of the frame to create the medial layer of a blood vessel. After 10 days, the intimal layer is created on top of the medial layer of a blood vessel, with a nanofiber mesh separating the two layers.

The TEML was then placed in a humidified incubator set at 37°C and 5% CO_2 for 30 minutes to permit it to set. After transfer to a 6 well plate, the TEML is cultured for at least 3-4 days in 3ml of smooth muscle supplemented media to allow the cells to elongate and proliferate. Media was changed every 2 days.

5.1.6.2 TEIL

As described in section 2.1.8.2, TEIL was fabricated by first making a collagen gel using the protocol and dimensions previously described in section 2.1.7.1. After the collagen gel set, aligned PLA nanofibers coated in fibronectin were placed on the surface of the gel, followed by HUVECs seeding ($2x10^5$ cells/ml) on top to create a representation of the intimal layer. The construct was then incubated for at least 40 minutes at 37°C/5% CO_2 to allow firm cell attachment. This was followed by sealing the fibres and cells onto the construct using acellular collagen. After gelation, the excess nanofibers were cut off from the construct using a sterile blade. TEIL was cultured in HUVEC media for at least 3-4 days to allow attainment of normal cell morphology and surface area coverage before use.

5.1.6.3 TEBV

As described in section 2.1.8.3, the TEBV is a composite of the TEML and TEIL. Assembly was carried out in stages; first was creation of TEML and culturing until cells adopt spindle shaped morphology, followed by nanofiber placement and HUVEC seeding. The complete TEBV was placed back into a new 6 well plate and topped up with both HCASMC and HUVEC whole media in a ratio of 7:3 respectively. The complete TEBV schematic is shown in figure -2.

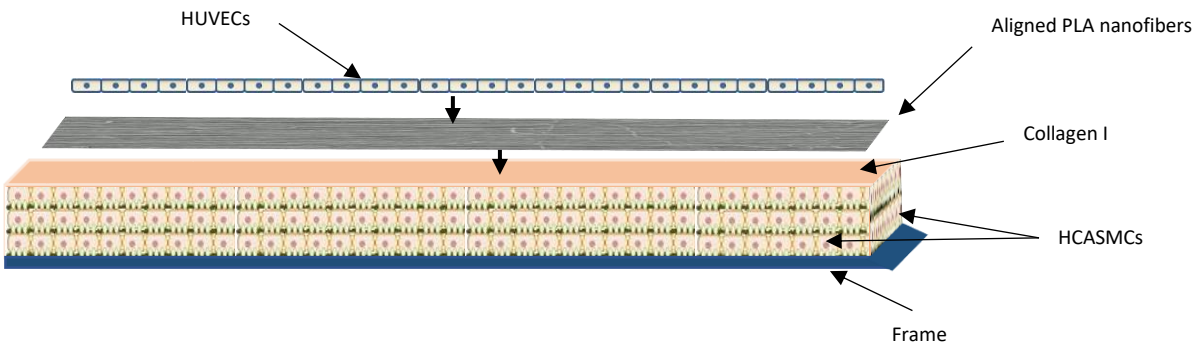

Figure 5-2: Schematic of TEBV. This schema highlights the placement of cells and nanofibers in the assembly of the TEBV. Exclusion of the HUVECs and nanofibers or HCASMCs creates either TEML or TEIL respectively.

5.1.7 TE constructs for see-saw rocker experiments

In regards to assembly of these constructs, the protocol followed was the same as that described in sections 5.2.5.1 to 5.2.5.3, the only change made was in the shape of the constructs i.e., from rectangular (figure 1) to square but with the same surface area, with the square gels measuring 1.09 cm^2 on the outer edge of the frame and 0.66 cm^2 on the inner edge. This change allowed the use of the constructs in a 24 well plate.

5.1.8 $FeCl_3$ injury of TE constructs

To mimic vascular injury, a $FeCl_3$ lesion was created by dipping a $1mm^2$ ($0.1cm^2$) square of filter paper in 10% $FeCl_3$ and placing this onto the upper surface of the constructs for 1 minute, generating a lesion approximately 1.5-2 mm in diameter. After this, the constructs were washed with PBS to eliminate excess $FeCl_3$, then topped up with fresh media.

5.1.9 Mechanical injury of TE constructs

A $1mm^2$ piece of filter paper was placed on the surface of the constructs for 1 minute then carefully peeled off the surface, generating a lesion with the same dimensions as the filter paper square. After removal of the filter paper square, constructs were washed once with PBS.

5.1.10 Experimental settings for shear stress generation on TE constructs

5.1.10.1 Parallel plate flow chamber

5.1.10.1.1 Perfusion chamber

To generate peristaltic flow and a range of shear stress values, a peristaltic pump (Watson-Marlow 505 series, Fluid technology, UK) was used along with a commercially sourced parallel plate flow chamber (ProFlow Chamber, Warner Instruments, USA) (figure 5-3). The system is comprised of a top and bottom plate with view slots included. The view slots were designed to accommodate coverslips; 15mm in top plate, 25mm in bottom plate. The top and bottom plate are combined to form a complete chamber using screws as detailed in figure 5-3. The chamber was originally designed for 2D perfusion but was modified for our purposes, allowing the incorporation of 3D TE models. Details of the modifications are explained later in this section. The perfusate was contained in a 7ml reservoir connected to the pump and flow chamber using polyethylene (PE-90) tubing. The flow chamber inlet was connected to the reservoir and the outlet to the pump. The set-up of this system can be seen in figure 5-3.

5.1.10.1.2 Perfusion gaskets

To facilitate the perfusion of our 3D vascular models, specialised gaskets were created. The dimensions of the space within the gasket used were length 25mm (2.5cm), depth (thickness) 3mm (0.3cm), width

5mm (0.5cm). The gasket was synthesised using PDMS, which was prepared by mixing Quantum Silicone (Qsil) polymer and cross-linker in a 10:1 ratio. 3ml of the solution is prepared in a small cell culture dish and left to set at room temperature overnight. Once the solution has set and the PDMS is firm to touch, acetate templates are used to cut out the gasket. First a circular ring with a diameter of 30mm (3cm) is cut then a rectangular opening in the centre of the circle bearing the measurements described in figure 5-3.

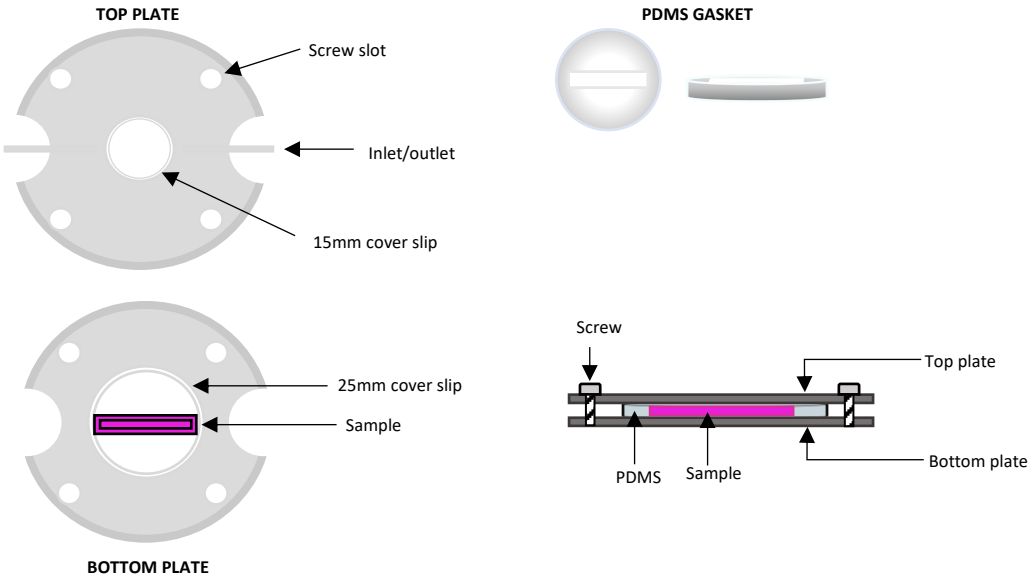

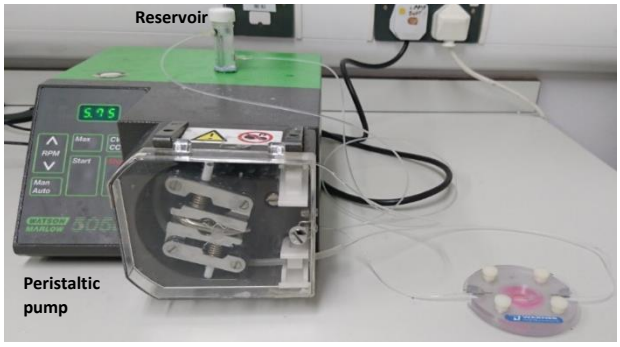

Positioning for viewing and imaging

Figure 5-3: Perfusion chamber assembly. The sample is aligned along the flow path between the inlet and outlet on the bottom plate. The outlet, affixed with silicone grease to the top plate, is aligned in the same way and placed over the sample. The assembled chamber is connected to a reservoir and a peristaltic flow pump. The chamber, reservoir and pump could then be moved for real time observation of cell attachment using an inverted fluorescence dissection microscope.

Assembly was accomplished by first installing the cover slips into the designated view slots using silicone grease. Once in place, the sample was placed on the bottom plate and aligned with the inlet and outlet. The custom PDMS gasket was affixed to the top plate with silicone grease after ensuring alignment with the inlet and outlet. The two halves of the chamber, with the gasket and sample in place, were put together ensuring the sample was positioned entirely within the gasket. Once this was accomplished, the screws are inserted and tightened to ensure the system was sealed and water-tight. The inlet and outlet were then connected to the tubing, that was in turn connected to the pump and reservoir. The complete and connected system was then positioned under the fluorescence dissection microscope for live imaging and flow is initiated.

5.1.10.1.3 Shear stress calculation

The assembled flow chamber was used to generate laminar flow as well as exerting shear stress on the intimal surface of the vascular models. The dimensions of the gasket used, which comprises and determines the dimensions of the flow chamber, were length: 25 mm (2.5 cm), width: 5 mm (0.5 cm) and depth/height: 3 mm (0.3 cm) when empty and 2.5 mm (0.25 cm) with a TE construct. The key dimensions that affect the shear stress profile are the depth and width of the chamber. The equation used to determine the shear stress generated on the endothelial surface of the TEBV was:

$$\tau = \frac{6uQ}{bh^2}$$

(Wong *et al.*, 2016)

The values required for the equation are; (1) the viscosity of the fluid being perfused (u), (2) the flow rate (Q), (3) the gasket width (b) and (4) height between the TE construct and the top plate of the chamber (h). The flow rate used for the perfusion of the constructs was 0.07 cm^2/s. This value, using a viscosity value of 1.5 Cp (Jeevasankar *et al.*, 2008), derived from estimations based on supplemented media perfused with suspended cells, is used to determine that the shear stress exerted on the construct surfaces is 20.16 $dyne/cm^2$. Aside from being capable of generating a useful range of shear stress values, ranging from 1.44 $dyne/cm^2$ to 172.8 $dyne/cm^2$, the chamber was also able to

consistently generate a laminar flow profile with the modified gasket design.

5.1.10.1.4 Flow pattern characterisation

To determine the nature of the flow pattern within the perfusion chamber, fluorescein isothiocyanate I to visualise the flow pattern. This solution was diluted 1:50 in PBS. The chamber and pump were assembled as in figure 5-3. The reservoir was first filled with PBS, which was then pumped through the chamber. After this, the contents of the reservoir were removed and replaced with fluorescein. As the solution flowed into the chamber, it was possible to visualise fluid movement as the two liquids mixed. Video footage was recorded and still images isolated.

5.1.10.2 See-saw rocker model

The TE constructs were placed in a 48 well plate and topped up with 600 µL of perfusate (CFSE labelled EPCs suspended in media), then placed on a standard see-saw rocker set at 70 rpm for 1 hour at 7θ, generating a maximum shear stress of 2.2 dyne/cm^2 (Zhou *et al.*, 2010).

5.1.10.3 Perfusate cell labelling

Cells were stained with CFSE, a live cell tracker. This membrane stain was used at a concentration of 5 µM. The cells to be stained were passaged and counted and re-suspended in 1m of fresh supplemented media. The stain was then added, and the cells incubated for 15 minutes at 37°C. The cell suspension was centrifuged for 3 minutes at 1200 rpm and the pellet re-suspended in 5 ml of fresh supplemented media. The cell suspension was left to sit for the final esterification step for 30 minutes at 37°C before use. Imaging was done using Leica inverted fluorescence microscope. Stained cells were used for both dynamic perfusion (perfusion chamber) as well as in the rocker perfused models. Staining aided with both visualisation and subsequent quantification with ImageJ by counting attached cells on whole construct surface.

5.1.11 Atorvastatin dose

Atorvastatin calcium trihydrate, as detailed in section 2.1.3, was dissolved in methanol to create a stock solution of 20 mg/ml. This was diluted further in media to a final concentration of 60 µg/ml. Atorvastatin was added to the TE constructs before perfusion with hMSCs or EPCs, and samples were

incubated for 1, 3, 5, 7, and 9 hours.

5.1.12 SDF-1 quantification

The reagents for the mini ABTS ELISA kit were reconstituted according to the manufacturer's protocol. 100µl of the capture antibody, diluted in PBS to a concentration of 2µg/ml, was added to the requisite number of wells, sealed, and incubated overnight at room temperature. The wells were then aspirated and washed 4 times with 300µl of wash buffer per well. The wash buffer is comprised of 0.05% Tween 20 in PBS. Next, 300µl of 1% BSA in PBS (block buffer) was added to the wells and incubated for at least 1 hour at room temperature. The block buffer was then aspirated, and the plate washed 4 times with the wash buffer. 100µl of sample solution (or standard) was added to each well and incubated at room temperature for at least 2 hours. The plate is then aspirated and washed 4 times. Next, the detection antibody, diluted in diluent (0.05% Tween 20 + 0.1% BSA) to a concentration of 0.5µg/ml. The plate was then incubated for at least 2 hours at room temperature. After this, the plate was again aspirated and washed 4 times. A 1:2000 dilution of Avidin-HRP conjugate was then added to the wells (100µl/well) and incubated for 30 minutes at room temperature. This was then followed by another 4 washes, after which 100µl of ABTS liquid substrate was added per well. This was incubated at room temperature - with observation every 5 minutes for up to 1 hour - until colour development was observed. Once this was achieved, the plate was read using a plate reader set at 405nm.

5.1.13 Immunostaining

Samples for immunostaining were first blocked with 5% BSA for 1 hour at room temperature then aspiration of BSA. This was followed by addition of 1° antibody diluted 1:200 with PBS. Samples were incubated with 1° antibody for 2 hours at 37°C/5% CO_2. After this incubation, samples were washed once with 0.05 Tween20 and 3 times with PBS. 2° antibody was diluted 1:400 with PBS, added to the sample and incubated for 1 hour at 37°C/5% CO_2. Following this incubation, samples were washed twice with 0.05% Tween20and twice with PBS. Samples were then incubated for 10 minutes with 10ng/ml DAPI, followed by a final three washes with PBS, followed by imaging. Secondary antibody negative control was carried out by incubating secondary antibody (at the described concentration)

with a sample without primary antibody incubation.

5.3 Results

5.1.14 Cell culture

5.1.14.1 HUVEC morphology

Cultured cells achieved expected cobblestone morphology and were successfully seeded onto the TE constructs. Cell morphology is detailed in figure 5-4.

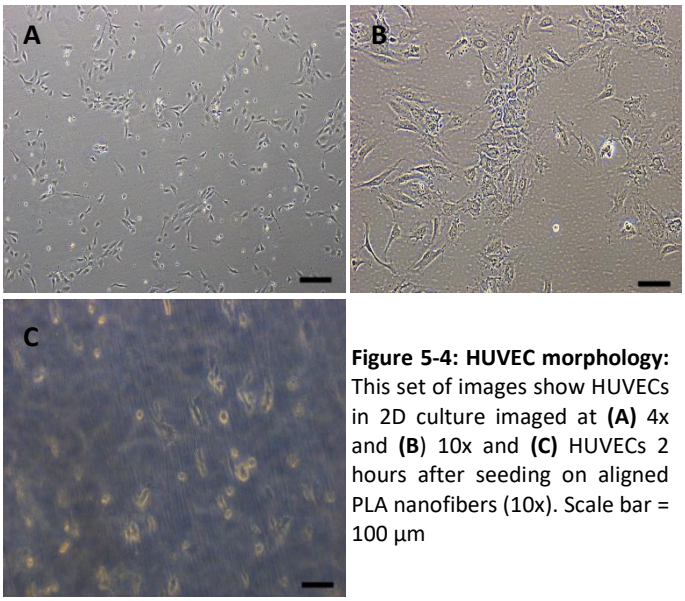

Figure 5-4: HUVEC morphology: This set of images show HUVECs in 2D culture imaged at **(A)** 4x and **(B**) 10x and **(C)** HUVECs 2 hours after seeding on aligned PLA nanofibers (10x). Scale bar = 100 µm

5.1.14.2 HCASMC morphology

Cultured cells attained expected spindle shaped morphology in both 2D and 3D culture. Cell morphology is detailed in figure 5-5.

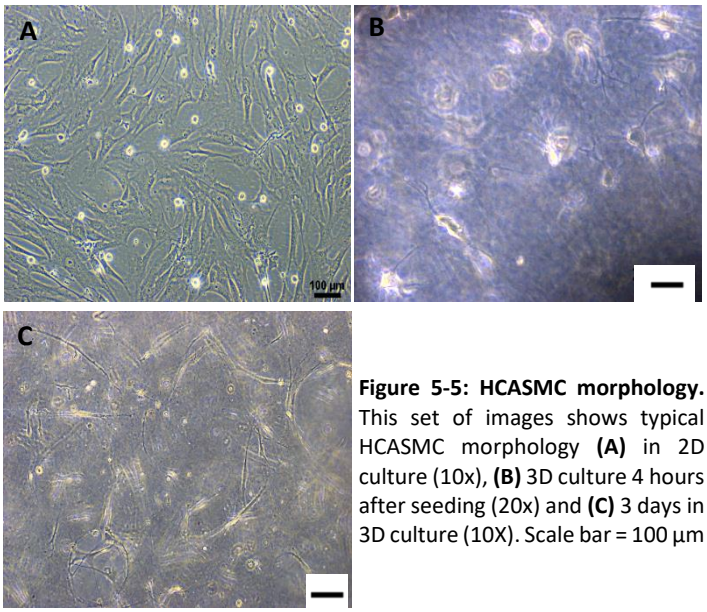

Figure 5-5: HCASMC morphology. This set of images shows typical HCASMC morphology **(A)** in 2D culture (10x), **(B)** 3D culture 4 hours after seeding (20x) and **(C)** 3 days in 3D culture (10X). Scale bar = 100 µm

5.1.15 Flow characterisation

To determine the nature of the liquid flow within the perfusion chamber, the set up defined in section 5.1.10.1.2 (figure 5-3), and the methodology described in section 5.1.10.1.4 were carried out to characterise the nature of the flow pattern through the parallel plate flow chamber. Representative images describing the flow pattern can be seen in figure 5-6.

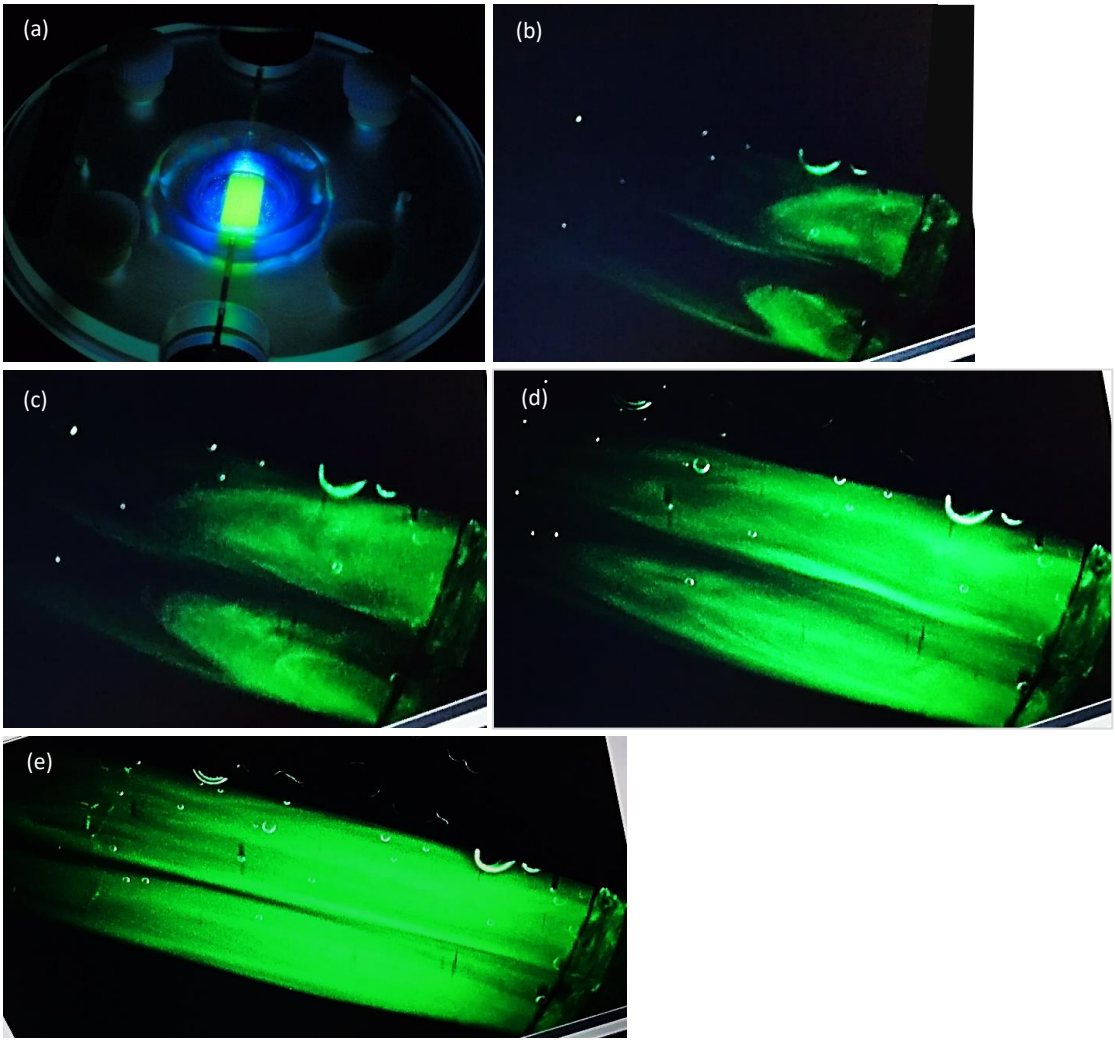

Figure 5-6: Flow pattern characterisation. Still images isolated from video footage showing **(a)** perfusion chamber with fluorescein. **(b, c)** inlet flow pattern at start. **(d, e)** flow pattern through centre of chamber.

The fluorescein solution gives a strong green glow seen in figure 5-6 (a). The initial turbulent flow seen in figure 5-6 (b) and (c) stabilised as the solution moved through the chamber, adopting a more laminar profile. Flow seems to fill at the edges of the chamber before the centre as seen between (b) and (e) as it adopts a more laminar flow profile.

5.1.16 Atorvastatin effect on cell homing: Dynamic flow with hMSCs

To evaluate the extent of attachment onto a lesioned TEBV, hMSCs were perfused over $FeCl_3$ lesioned TEBVs that were incubated either with or without 60µg/ml atorvastatin for 3 and 5 hours. $FeCl_3$ was applied onto the surface of the construct for 1 minute using a $1mm^2$ piece of sterilised filter paper. CFSE labelled hMSCs were perfused at a density of 6 x 10^3 cells/ml, and subjected to a shear stress of 20.16 dyne/cm^2 for 45 minutes, followed by a 10-minute PBS wash to remove any cells not fully adhered to the surface of the construct. Images were taken at the end of perfusion; representative images are in figure 5-7. Attached cells were quantified and this is represented in figure 5-8.

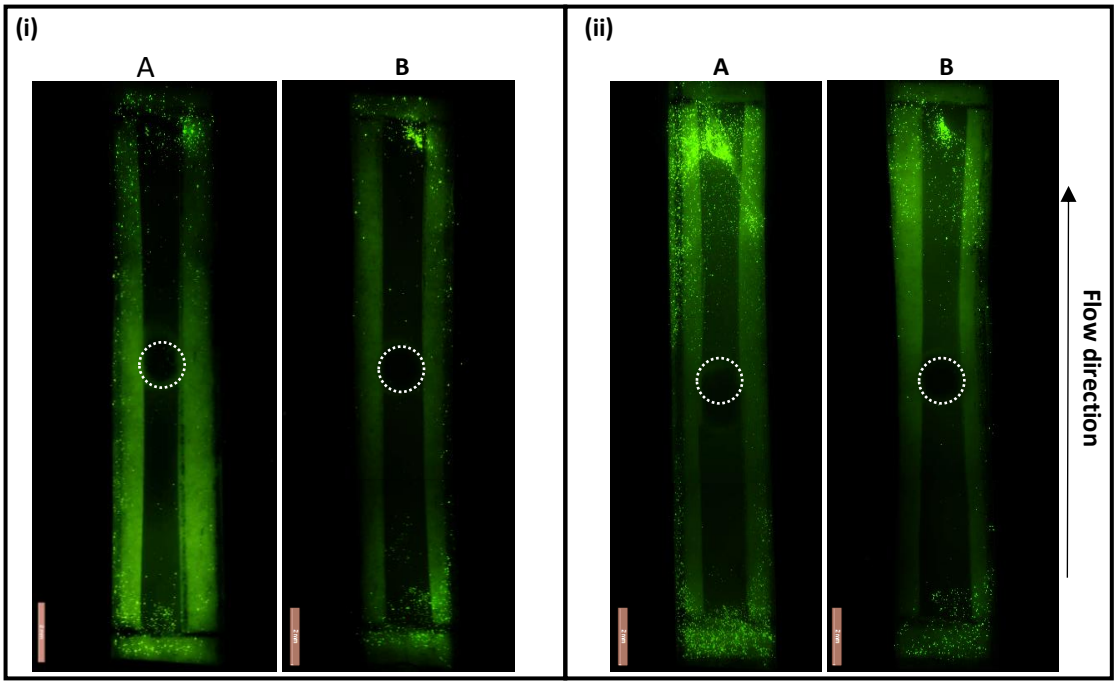

Figure 5-7: hMSC perfusion over $FeCl_3$ lesioned TEBV. Panel (**i**) denotes a 3-hour comparative (**A**) with atorvastatin and (**B**) without atorvastatin. Panel (**ii**) is a 5-hour comparative with (**A**) TEBV with atorvastatin and (**B**) without atorvastatin. Green dots are CFSE labelled cells. Circle denotes lesion area. Images taken at 0.8X. Scale bar = 2mm

As can be seen in figure 5-7, the cell attachment is densest at the inlet and outlet ends of the constructs. This pattern follows the flow pattern observed in figure 5-6, where we can see more turbulent flow at the inlet and outlet ends of the flow chamber, with a more laminar flow profile in the centre of the chamber, where the lesion was placed. Closer examination of the 5 hours with atorvastatin sample shows attachment in the central regions of the construct, but majority of attachment in this region is localised to the edges of the construct and primarily at the inlet and outlet

ends. Even though there is turbulent flow at the inlet and outlet end, density of attached cells is still varied between samples, with those treated with atorvastatin showing denser cell attachment at both the inlet and outlet at both 3 and 5 hours, and those treated for 5 hours having a denser accumulation of cells than those incubated for 3 hours.

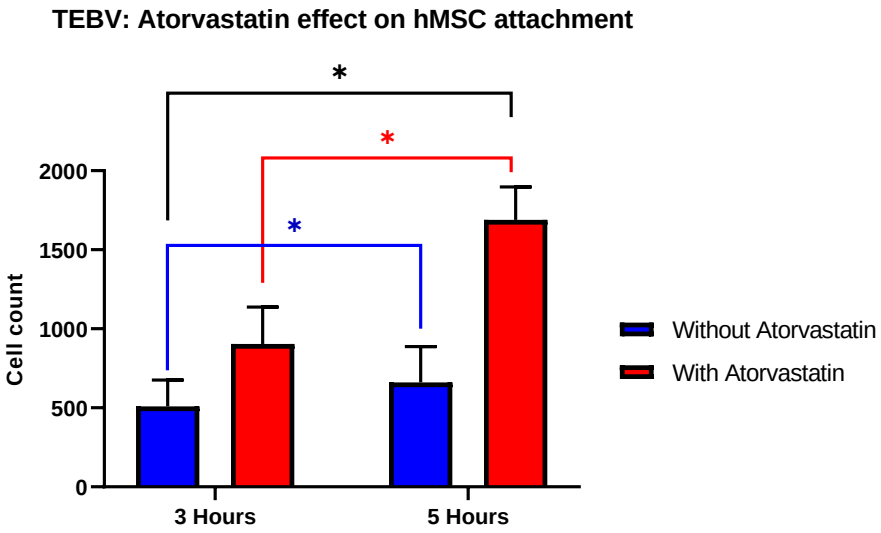

Figure 5-8: hMSC attachment on $FeCl_3$ lesioned TEBV. Plot denotes cell attachment following a 45-minute perfusion with hMSCs, at 20.16 dyne/cm^2, over $FeCl_3$ lesioned TEBV, incubated for 3 and 5-hours with and without atorvastatin. Statistical analysis was done using two-way ANOVA and significance was identified between time points, p= 0.0163 *, * and also between groups i.e., with and without atorvastatin, p = 0.0344 *. N=4.

The presence of atorvastatin has a positive impact on the recruitment of cells onto the surface of a lesioned TEBV as shown in figure 5-8. Longer incubation periods also result in higher numbers of cells attached to the endothelial surface of the TEBV.

5.1.17 Atorvastatin effect on cell homing: Dynamic flow with EPCs

To determine the effect of the individual layers of the blood vessel model, the TEIL, TEML and TEBV were assembled as detailed in section 5.2.5.1 to 5.2.5.3. Constructs were lesioned with $FeCl_3$ and incubated with 60µg/ml atorvastatin for 3 and 5 hours. The extent of cell attachment on each model, with and without atorvastatin and after 3 and 5-hour incubations, was evaluated under pulsatile flow at 20.16 dyne/cm^2. As with the hMSCs in the previous heading, EPCs at a density of 6 x 10^3 cells/ml-

were labelled with CFSE then perfused over the constructs for 45 minutes, followed by a 10-minute PBS wash. The constructs were then removed from the perfusion chamber and imaged. Extent of cell attachment is detailed below per TE model.

5.1.17.1 TEIL

This model is comprised solely of endothelial cells seeded atop aligned PLA nanofibers. Representative images showing cell attachment are shown in figure 5-9 and image quantification is shown in figure 5-10.

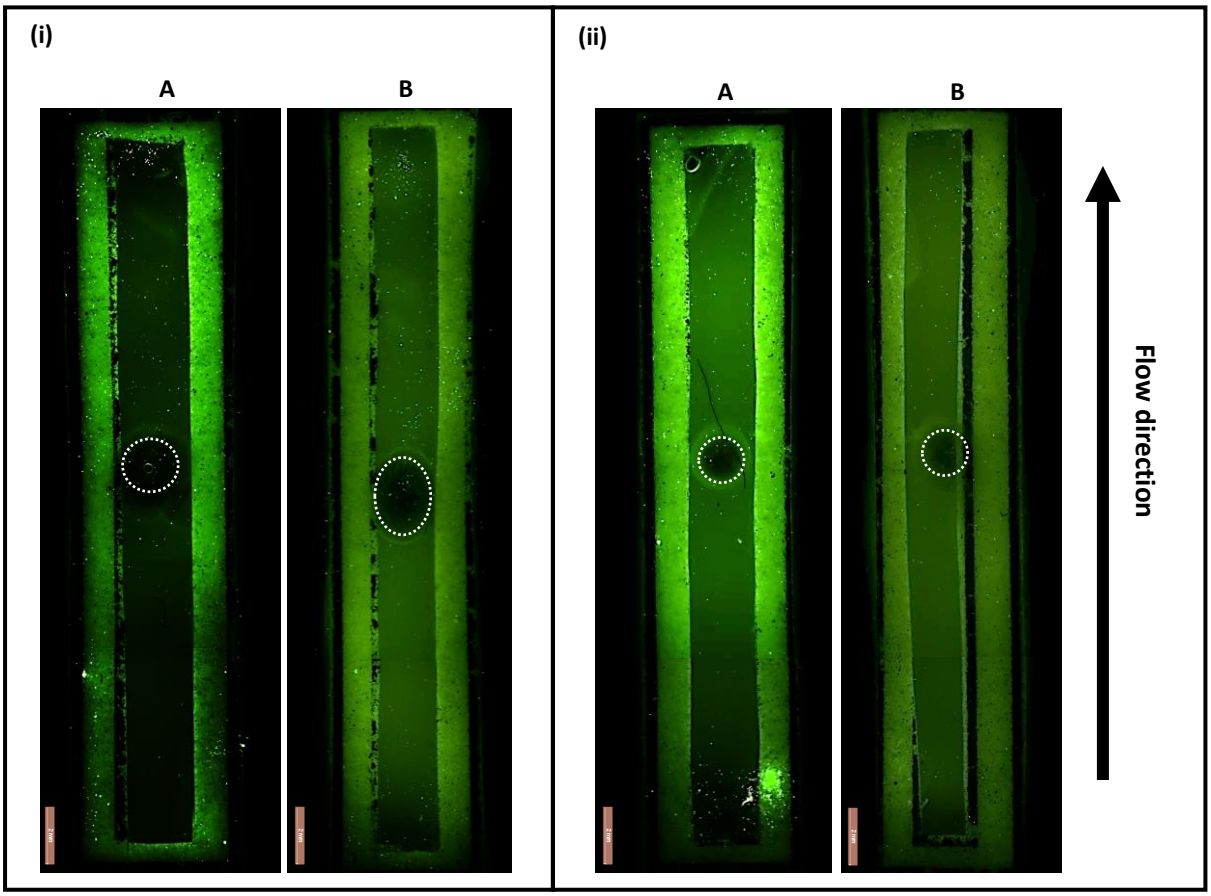

Figure 5-9: EPC attachment on $FeCl_3$ lesioned TEIL. Panel **(i)** shows the 3-hour comparative with **(A)** being with atorvastatin and **(B)** without. Panel **(ii)** shows the 5- hour comparative with **(A)** with atorvastatin and **(B)** without. Green dots are attached EPCs. Circle denotes lesion area. Images taken at 0.8X

The density of cells adhered to the lesioned surface is not as dramatic as that seen with the hMSCs, primarily as EPCs are smaller in size than the hMSCs. Distribution does appear denser on the 3 hours with atorvastatin sample, with cells distributed across the majority of the construct from the inlet to the outlet end, with some cells also present within the lesion site. For the 5-hour incubation samples,

cell attachment appears denser for the atorvastatin treated samples which follows the expected trend observed with hMSC perfusion over lesioned TEBVs.

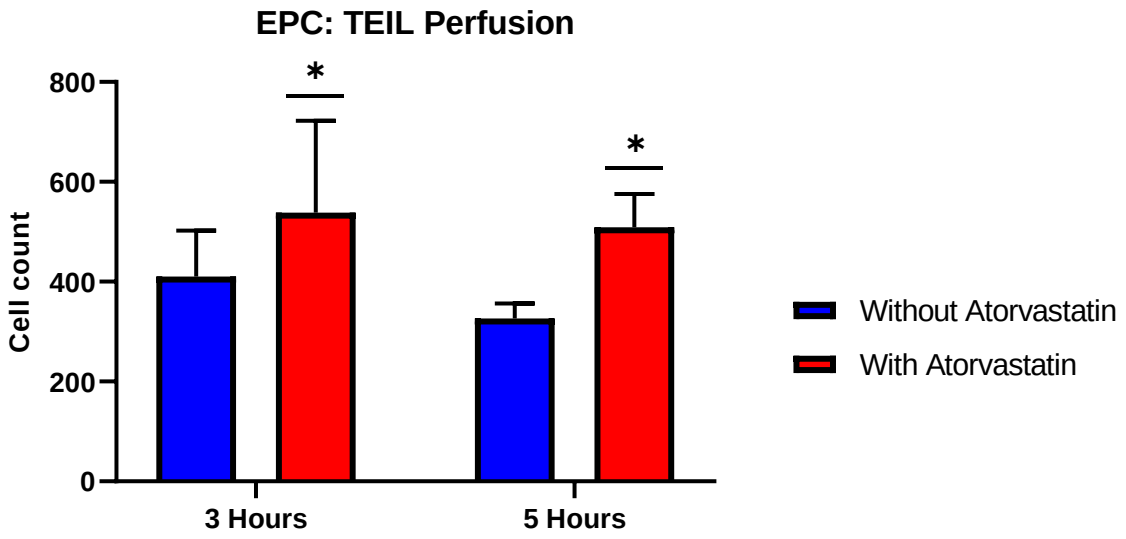

Figure 5-10: EPC attachment on $FeCl_3$ lesioned TEIL. This plot details the differences in cell attachment, following a 45-minute perfusion with EPCs at 20.16 dyne/cm^2, on a $FeCl_3$ lesioned TEIL after 3 and 5-hour incubations with and without 60µg/ml atorvastatin. One sample t-and-Wilcoxon test was carried out with significance identified for samples treated with atorvastatin, p= 0.0178 *. N=3.

As with the hMSC attachment on a lesioned TEBV, atorvastatin appears to positively influence numbers of attached cells for this model as well, with higher cell counts recorded for both the 3 and 5-hour time points. Unlike the hMSC perfusion over the TEBV, it appears that maximum attachment here is attained after 3 hours, with lower cell counts observed at 5 hours both with and without atorvastatin, implying a supporting role for the smooth muscle cell layer in enhancing cell recruitment signals.

5.1.17.2 TEML

As detailed previously, this model is comprised solely of smooth muscle cells (HCASMCs) embedded in a collagen gel. Constructs were also lesioned with $FeCl_3$ prior to perfusion with CFSE labelled EPCs (also at 6 x 10^3 cells/ml). Representative images are shown in figure 5-11 and image quantification is shown in figure 5-12.

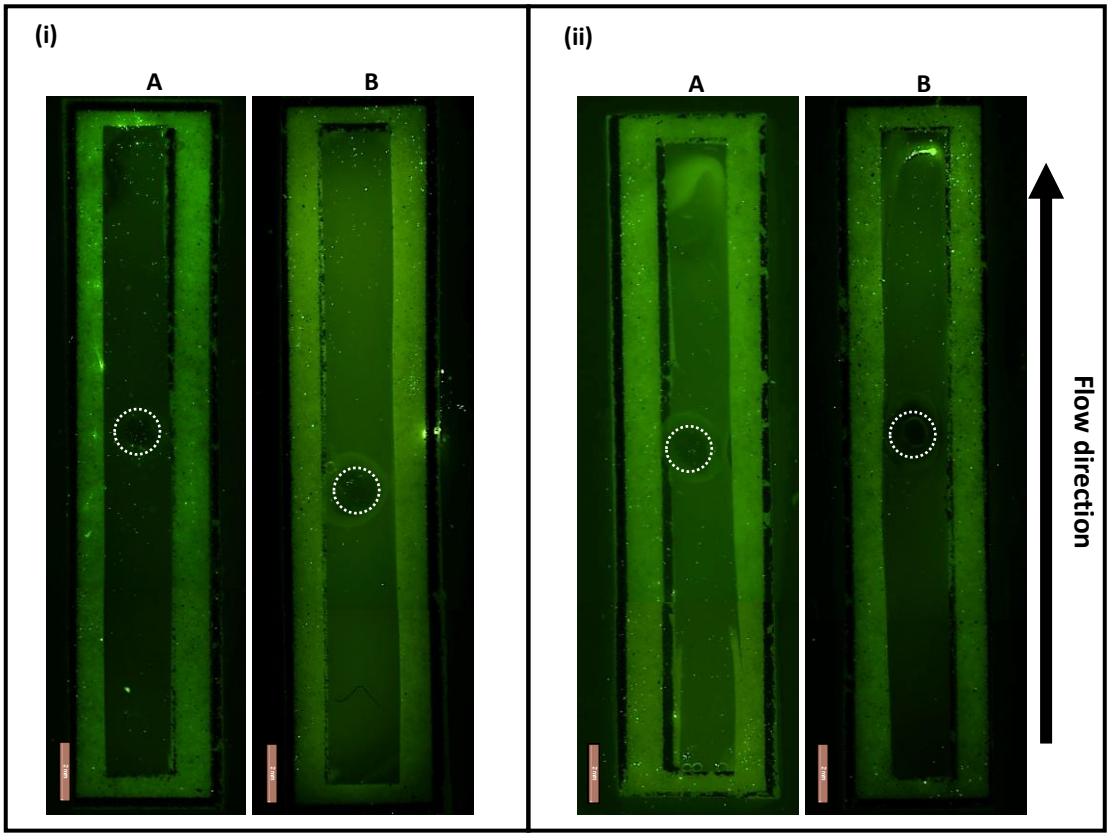

Figure 5-11: EPC attachment on $FeCl_3$ lesioned TEML. Panel **(i)** is a 3-hour comparative; **(A)** with atorvastatin and (B) without atorvastatin. Panel **(ii)** shows the 5-hour comparative **(A)** with atorvastatin and **(B)** without atorvastatin. Circle denotes lesion area. Images taken at 0.8X

Images represented in figure 5-11 show cell attachment on the surface of lesioned constructs with and without atorvastatin. Samples treated with atorvastatin appear to have denser accumulation of attached cells, especially after 3 hours. Quantitation is required to clearly distinguish differences in cell attachment.

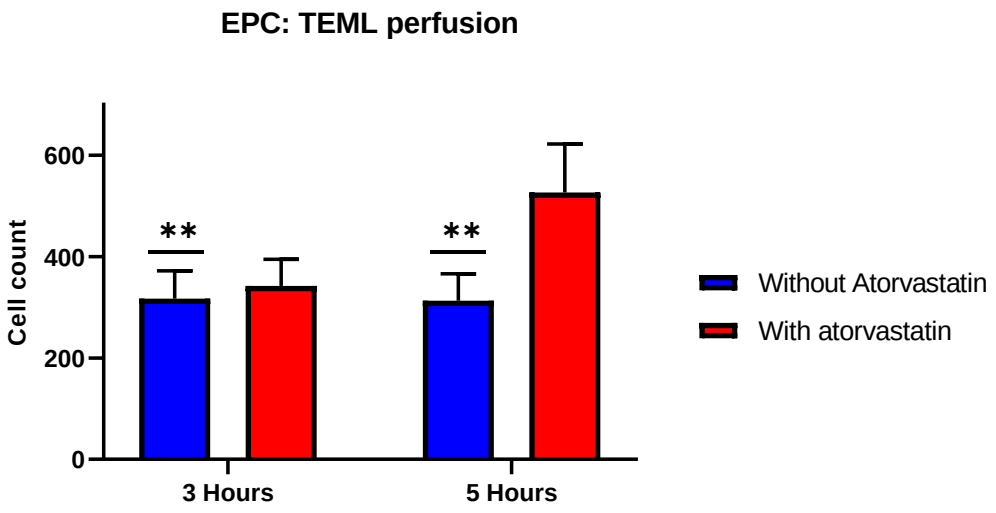

Figure 5-12: EPC attachment on $FeCl_3$ lesioned TEML. This plot compares extent of EPC attachment, following a 45-minute perfusion at 20.16 dyne/cm^2, on a $FeCl_3$ lesioned TEML incubated for 3 and 5-hours both with and without atorvastatin. Statistical analysis was done using one sample t-and Wilcoxon test, and significance was identified for samples without atorvastatin, p = 0.0044 **. N=3.

Once again it appears that atorvastatin has an impact on extent of cell attachment on lesioned blood vessel models. A comparative of figure 5-12 and figure 5-8 shows there is a similar trend in that time affects extent of cell attachment i.e., longer incubations result in more cells attaching to the surface of the construct. Interestingly for the TEML (figure 5-12), the significance determined between time points without atorvastatin, suggests that time has no notable impact on cells attaching on the surface of the TEML, while the inclusion of atorvastatin results in more cells attaching at both the 3 and 5-hour time points, with a marked increase after 5 hours.

5.1.17.3 TEBV

This model is a composite of smooth muscle cells seeded in a collagen gel with endothelial cells seeded above on aligned PLA nanofibers. As with the previous two models, CFSE labelled EPCs were perfused at a density of 6x 10^3 cells/ml for 45 minutes, followed by a 10-minute PBS wash. Representative perfusion images are shown in figure 5-13 with image quantification shown in figure 5-14.

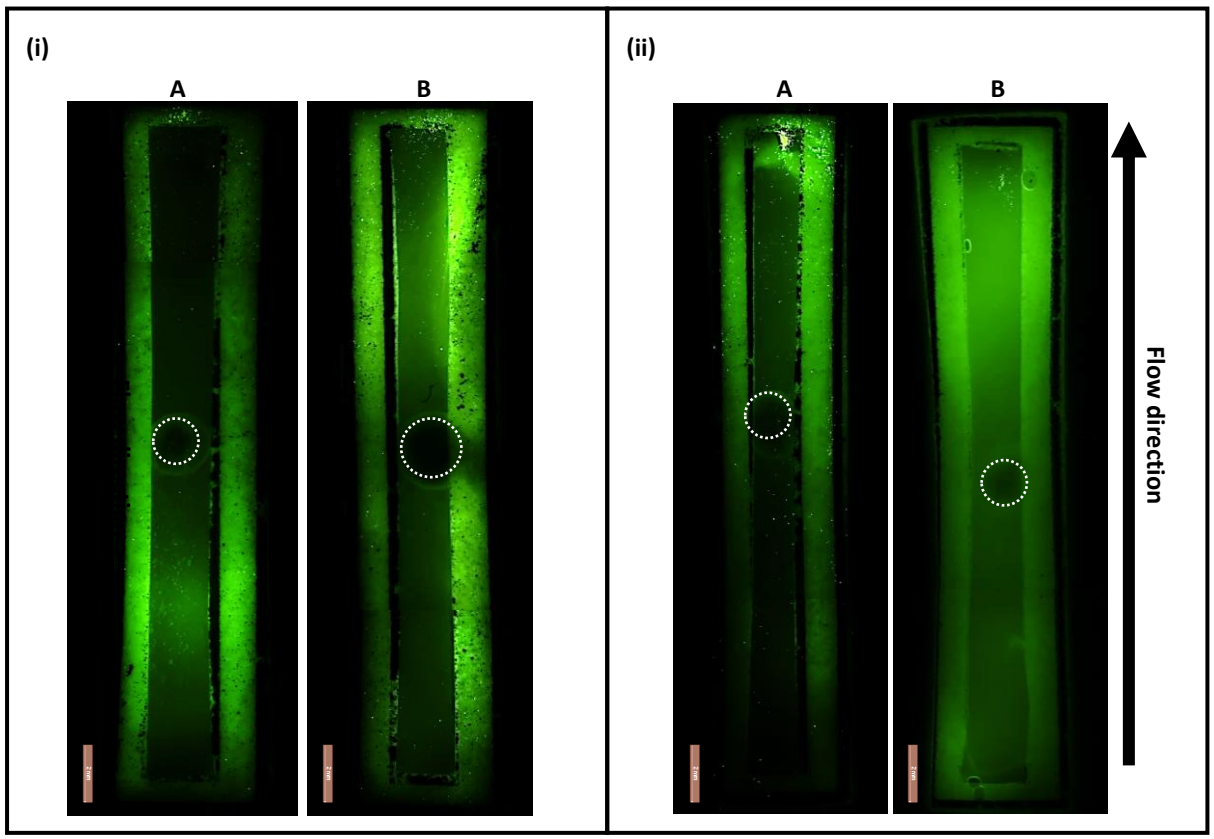

Figure 5-13: EPC attachment on $FeCl_3$ lesioned TEBV. Panel (i) compares the 3-hour time points, with **(A)** being the atorvastatin treated construct while **(B)** is untreated. Panel **(ii)** compares the 5-hour time point **(A)** with atorvastatin and **(B)** without atorvastatin. Circle denotes lesion area. Images taken at 0.8X

The attachment pattern here appears localised from the middle of the construct towards the outlet end. The density of cells at the 5-hour timepoint without atorvastatin appears to be the lowest of the set, with a faintly appearing cluster of cells near the outlet end. Quantification of attachment differences is found in figure 5-14.

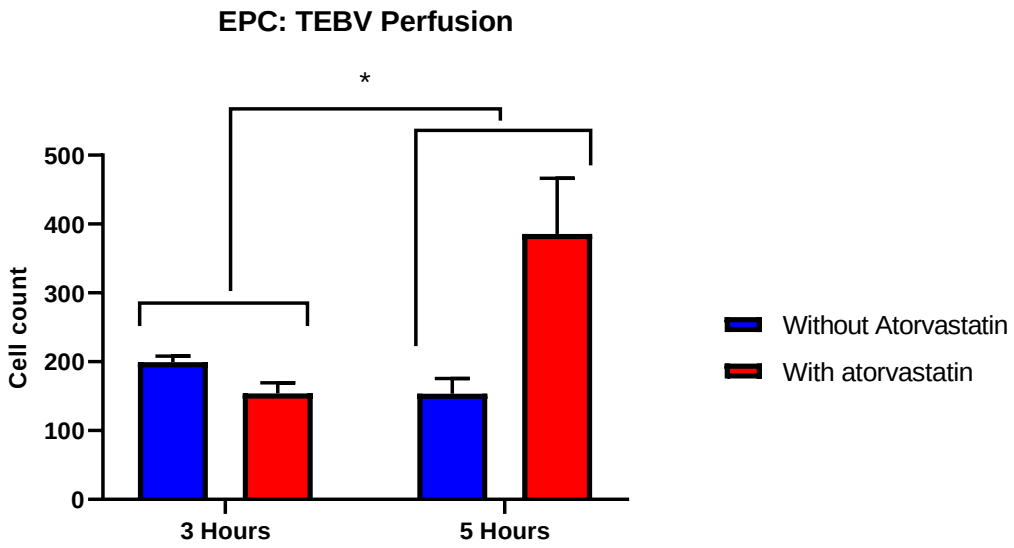

Figure 5-14: EPC attachment on $FeCl_3$ lesioned TEBV. This plot shows variations in cell attachment after 3 and 5-hour incubations with and without atorvastatin followed, by perfusion of EPCs at 20.16 dyne/cm^2. Statistical analysis used was two-way ANOVA and statistical significance was identified for the interaction between time, i.e., 3 and 5-hours, and the presence or absence of atorvastatin, p = 0.0432 *. N=3.

At the 3-hour time point, atorvastatin does not increase cell attachment compared to the control whereas the numbers are much higher at the 5-hour time point with atorvastatin than without. Interestingly, the number of attached cells is lower at 5 hours than 3 hours without atorvastatin which reflects the trend observed with the TEIL. This suggests that atorvastatin has more of an effect on the medial layer than the intimal layer as the $FeCl_3$ lesion burns through both layers of the model, exposing the smooth muscle cells. The trend observed here appears to be a blend of that seen in Figure 5-10 and Figure 5-12 in that without atorvastatin, there is a reduction in attached cells between 3 and 5 hours while there is an increase between 3 and 5 hours when atorvastatin is included, suggesting a synergistic effect between endothelial (HUVEC) and smooth muscle cells (HCASMC). Two-way ANOVA was used to analyse this data set.

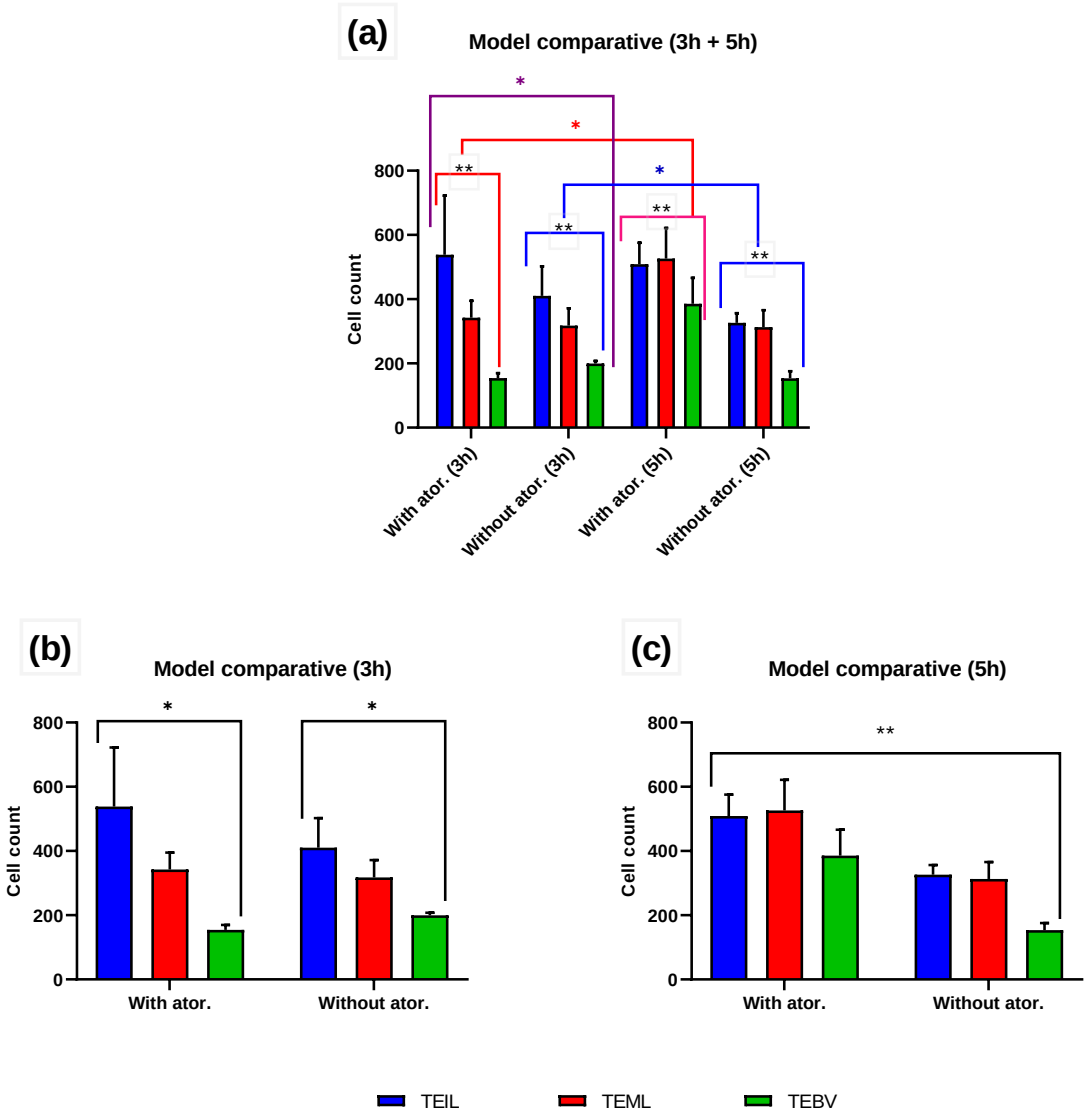

Figure 5-15: Comparative between models. Plots comparing differences in cell attachment on $FeCl_3$ lesioned TEIL, TEML and TEBV, following 45-minute perfusions with EPCs at 20.16 dyne/cm^2, and after 3 and 5-hour incubations either with or without atorvastatin. Two-way ANOVA was used for statistical analysis. **(a)** statistical significance was identified between time points (p = 0.0189 *, *, *), and between groups i.e., between TEBV, TEIL and TEML (p = 0.0016 **), and also between incubations with and without atorvastatin (p = 0.0189 *). **(b)** Statistical significance was identified between models i.e., TEIL, TEBV and TEML, p = 0.0204 *. **(c)** Statistical significance was identified between atorvastatin treated and drug free samples, p = 0.0017 **. For all plots, n=3.

Across all the models, atorvastatin has a positive impact on increasing numbers of attached EPCs on the lesioned models. In general, the longer the samples are incubated with atorvastatin, the higher the number of attached cells. The TEBVs record the lowest cells counts between the models both with and without atorvastatin, suggesting some modulatory effect when both medial and intimal layers are

present. Without atorvastatin, the numbers of attached cells on the TEML have very little variation between time points while the TEILs demonstrate the highest attachment at 3 hours with a decrease in attachment after 5 hours both with and without atorvastatin suggesting that the medial layer is involved in increasing/sustaining cell attachment in the presence of atorvastatin with longer incubations. The trend denoting atorvastatin's impact on cell attachment is more stable/consistent across models at the 5-hour time point, further suggesting that duration of incubation is a contributor to increasing factors responsible for either, or both, cell attachment and recruitment. The statistical analysis showed differences between TE models as well as with and without atorvastatin, suggesting an impact of cell type and atorvastatin on the responses seen.

5.1.18 Atorvastatin effect on cell homing using two injury models: Rocker flow with EPCs

Following the experiments carried out with the perfusion chamber, in an effort to increase data throughput, the mode of perfusion was changed from the use of a flow chamber to a rocker. For the rocker experimentation, factors kept consistent were cell density as well as mode of quantification of cell attachment. Aside from the reduction in shear forces exerted on the constructs, the duration of perfusion was also altered, from 45 minutes to 1 hour at 37°C/5% CO_2. Oscillating/ see-saw motion rocker are designed to generate low shear stresses i.e., up to 2.2 dyne/cm^2 (Tucker *et al.*, 2014). Two modes of injury creation were also employed i.e., $FeCl_3$ and mechanical injury detailed in section 5.2.7 and 5.2.8 respectively. With this perfusion model, it was also possible to evaluate cell attachment over a wider range of atorvastatin incubation time points i.e., 1, 3, 5, 7 and 9 hours. The same cell density used under dynamic flow was used for the models detailed below.

5.1.18.1 TEIL

Quantitative measurements of cell attachment for the TEIL after mechanical and $FeCl_3$ injury represented in figure 5-16.

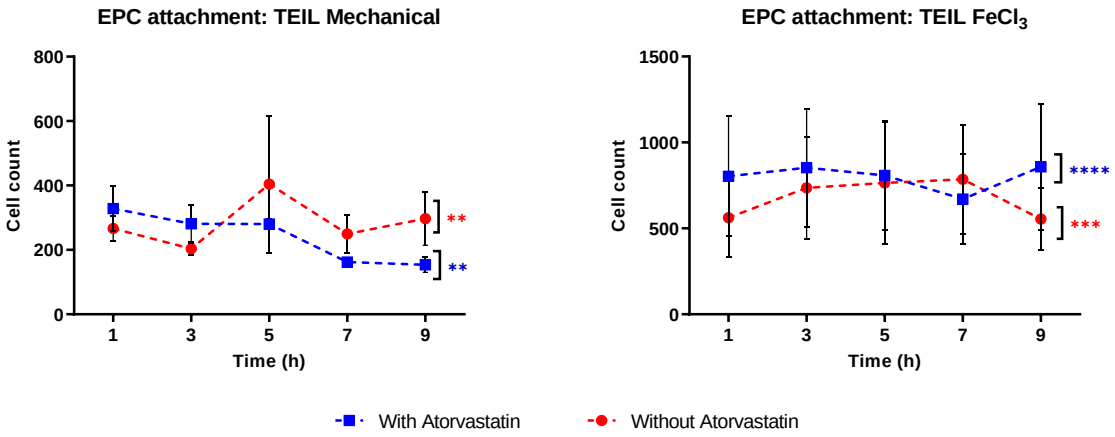

Figure 5-16: EPC attachment on TEIL with different injuries. These plots display cell attachment over various time points, for $FeCl_3$ or mechanically injured TEIL, incubated both with and without atorvastatin, and perfused with EPCs for 1 hour under a shear stress of 2.2 dyne/cm^2. One sample t-and-Wilcoxon test was carried out on the data sets, with significance identified between atorvastatin dosed and drug free samples for both mechanical ($p = 0.0023$ ** and 0.0011 ** for with and without atorvastatin respectively) and $FeCl_3$ injury ($p < 0.0001$ **** and 0.0002 *** for with and without atorvastatin respectively). N=3.

Figure 5-16 suggests the type of injury impacts the trend of cell attachment both with and without atorvastatin. With a mechanical injury, cell attachment with atorvastatin peaks sooner than without atorvastatin after which a decline is observed over time. Without atorvastatin, the peak is reached at 5 hours versus 1 hour with. The number of attached cells, however, drops after this time point as is observed with atorvastatin. A comparative with the same model in figure 5-9 shows the same trend at the 3 and 5-hour time points i.e., a decrease in attached cells at 5 hours both with and without atorvastatin. The mode of injury appears to impact density of attached cells as well with $FeCl_3$ injury having more cells counted on the construct surface than mechanical injury. This mode of injury also appears to trigger increasing cell attachment for a longer time frame before a decline is observed. With this mode of perfusion, a similar trend is observed to that seen in figure 5-9, in that the presence

of atorvastatin results in more cells attaching. For the mechanical injury, cell attachment peaks earlier (at the 1h time point), followed by a steady decline over time with atorvastatin, while the trend appears to be an interchange of increasing and decreasing cell attachment without atorvastatin, with peak attachment being observed after 5 hours. No statistical significance was found for these data.

5.1.18.2 TEML

Quantitative measurements of cell attachment for the TEML are represented in figure 5-17.

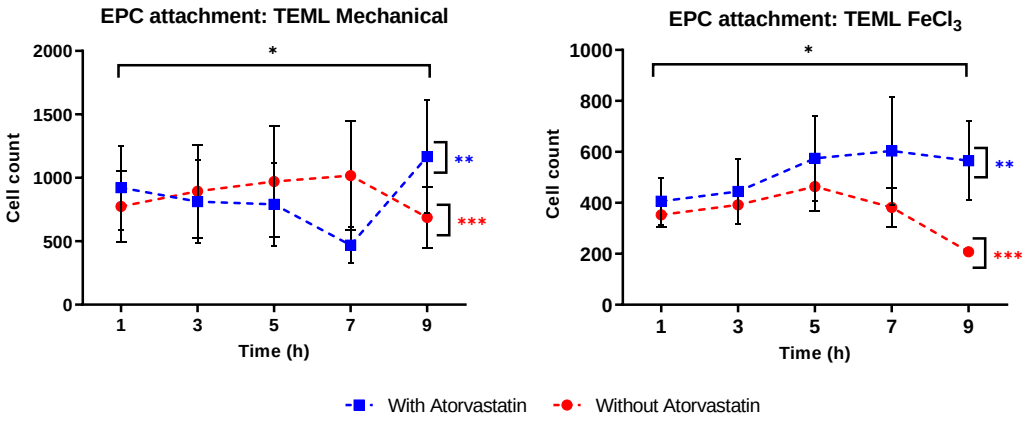

Figure 5-17: EPC attachment on TEML with different injuries. These plots display cell attachment over various time points, for $FeCl_3$ or mechanically injured TEML, incubated both with and without atorvastatin, and perfused with EPCs for 1 hour under a shear stress of 2.2 dyne/cm^2. One sample t-and-Wilcoxon test was carried out on the data sets, with significance identified between atorvastatin dosed and drug free samples for both mechanical ($p = 0.0018$ ** and 0.0001 ***, for with and without atorvastatin respectively) and $FeCl_3$ injury ($p = 0.0010$ ** and 0.0002 ***, for with and without atorvastatin respectively). Two-way ANOVA was also carried out and significance was identified for the interaction of time, and presence or absence of atorvastatin for both the mechanically ($p = 0.0106$ *) and $FeCl_3$ injured samples ($p = 0.0354$ *). N=3

Here, the type of injury appears to have a significant effect on cell attachment with and without atorvastatin. With a mechanical injury, atorvastatin treated samples show higher cell attachment at the earliest time point with a steady decline until the 7-hour time point while untreated samples show a gradual rise to the same time point, followed by a drop in the number of attached cells. With $FeCl_3$, both treated and untreated samples show the same trend i.e., a rise in attachment followed by a decline with the treated samples having higher cell counts. Inversely, the more severe injury ($FeCl_3$) shows fewer cells attached overall than the mechanically injured one, an observation opposite to the TEIL. A comparative with figure 5-11 shows that, with the $FeCl_3$ injury, atorvastatin dosing causes an

increase in cell attachment between 3 and 5 hours, a similar trend to the atorvastatin free samples, whereas in the perfused samples, there was little difference between 3 and 5 hours for the drug free controls. This “steady state” between 3 and 5 hours is observed for the atorvastatin treated samples with a mechanical injury. As with previous data, the presence of atorvastatin, overall, has a positive impact on increasing numbers of attached cells. Two-way ANOVA was used for this data set with significance determined for the interaction of evaluated variables.

5.1.18.3 TEBV

Quantitative measurements of cell attachment for the TEML are represented in figure 5-18.

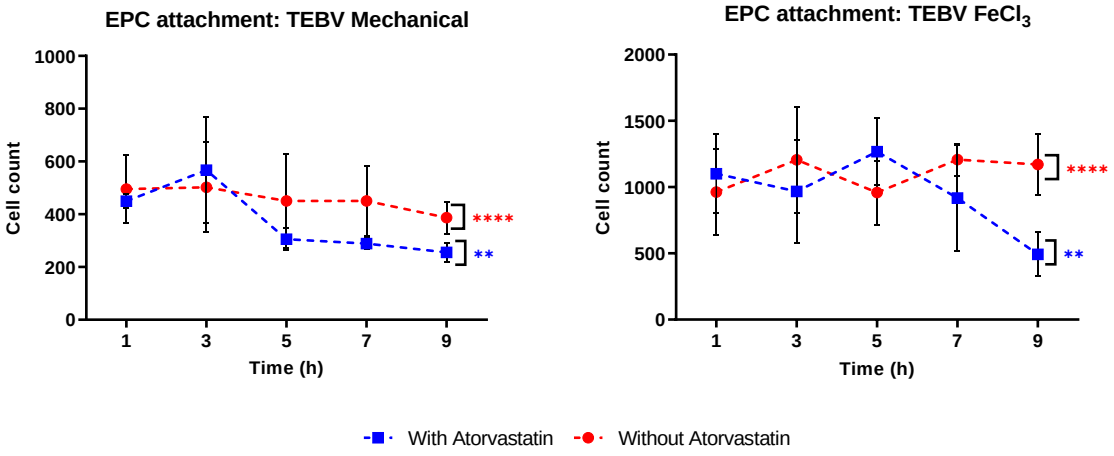

Figure 5-18: EPC attachment on TEBV with different injuries. These plots display cell attachment over various time points, for $FeCl_3$ or mechanically injured TEBV, incubated both with and without atorvastatin, and perfused with EPCs for 1 hour under a shear stress of 2.2 dyne/cm^2. One sample t-and-Wilcoxon test was carried out on the data sets, with significance identified between atorvastatin dosed and drug free samples for both mechanical ($p = 0.0032$ ** and < 0.0001 ****, for with and without atorvastatin respectively) and $FeCl_3$ injury ($p = 0.0018$ ** and < 0.0001 ****, for with and without atorvastatin respectively). N=3.

With the mechanical injury, the atorvastatin treated samples show peak cell attachment after 3 hours, after which there is a decline while the untreated samples appear to reach peak attachment after 1 hour followed by a steady decline but overall, with higher numbers of attached cells than the atorvastatin treated samples from 5 to 9 hours. With the $FeCl_3$ injury, the trend with atorvastatin treatment matches that observed for this model under dynamic flow i.e., peak attachment is reached after 5 hours. The untreated samples also show this similarity with perfused samples, with a higher

cell count at 3 hours and a decline at 5 hours with atorvastatin and a higher count at 3 hours than 5 hours without atorvastatin. However, at 7 hours, another rise is noted in the atorvastatin free samples, and appears to be maintained to the 9-hour time point whereas a sharp decline is observed at the same time points with the inclusion of atorvastatin. Regarding injury type, the trend here of overall cell attachment is the same as with the TEIL, in that the more aggressive injury ($FeCl_3$) results in a higher density of attached cells.

5.1.18.4 Comparative of rocker experimental conditions on cell homing

To evaluate if there were significant or observable differences between injury types, a comparative was done to evaluate extent of EPC homing between TE construct types across time points, both with and without atorvastatin, and within injury models. Data is represented in figure 5-19.

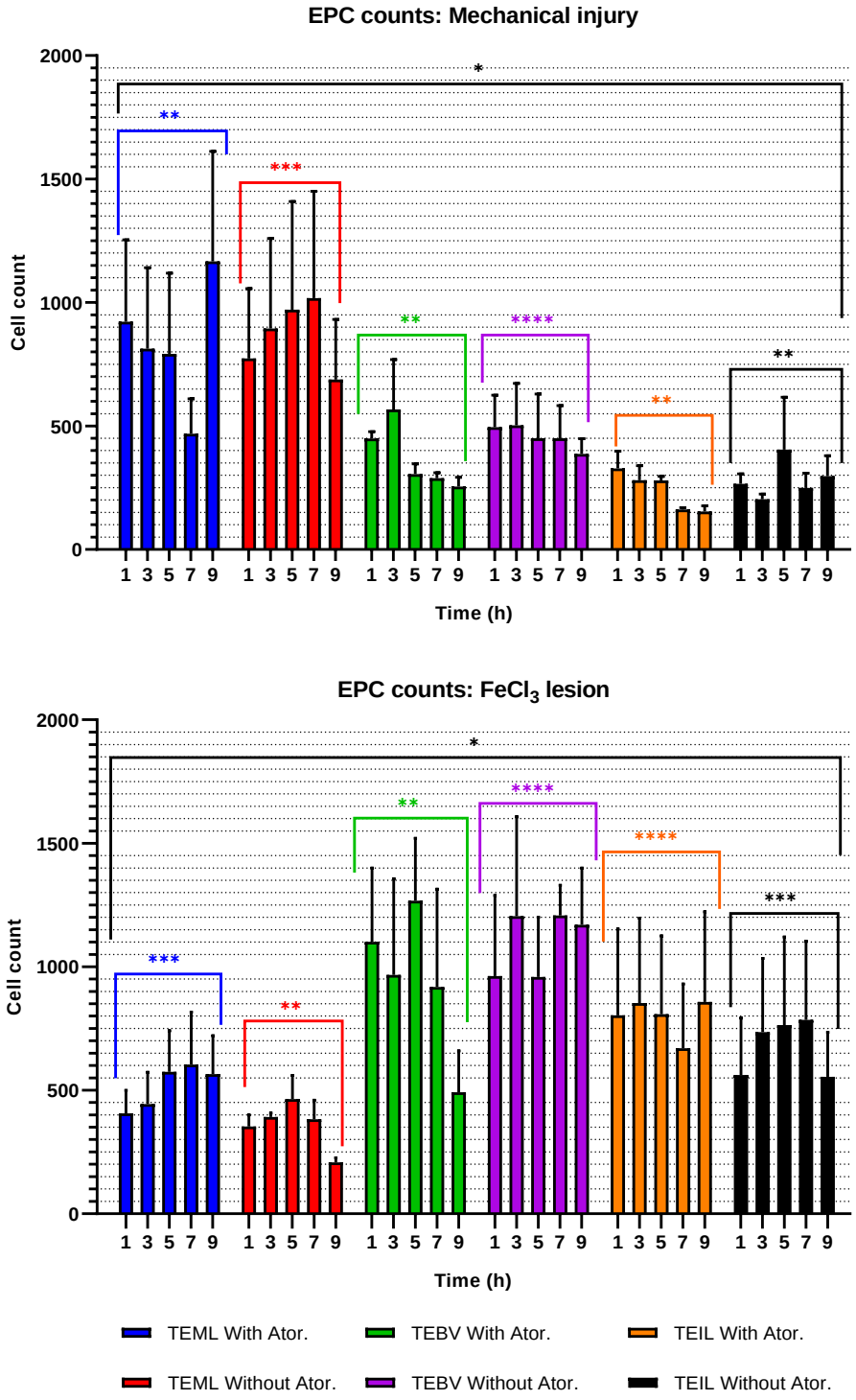

Figure 5-19: Model comparative. These plots compare EPC attachment on TEML, TEBV and TEIL, as well as comparing effect of atorvastatin on cell attachment, both compared across time points. These plots display cell attachment over various time points, for $FeCl_3$ or mechanically injured TEML, TEBV and TEIL, incubated both with and without atorvastatin, and perfused with EPCs for 1 hour under a shear stress of 2.2 dyne/cm^2. One sample t-and-Wilcoxon test was carried out on the data sets, with significance identified for each model, for both mechanical (p = 0.0018 **, 0.0001 ***, 0.0032 **, <0.0001 ****, 0.0023 **, and 0.011 **) and $FeCl_3$ injury (p = 0.0002 ***, 0.0010 **, 0.0018 **, <0.0001 ****, <0.0001 **, and 0.0002 **. Two-way ANOVA was also carried out for these data sets, with significance found for the interaction between time and the presence or absence of atorvastatin across all models, for both mechanical (p =0.0156 *) and $FeCl_3$ (p = 0.0416 *) injury types N=3.

Across the 3 different models, the biggest effect atorvastatin has on cell attachment appears to be regarding time taken to attain peak attachment. Samples treated with atorvastatin mainly attain peak attachment faster than untreated ones. A bigger effect is the type of injury on cellular responses. More aggressive injuries appear to affect the intimal layer response more than the medial layer where a stronger response was observed with the less aggressive injury. With both the $FeCl_3$ and mechanical injuries, the TEBV data appears to be a compounding of the TEML and TEIL responses, appearing as almost an average response between the two "half" models. With the $FeCl_3$ injury, cell attachment appears to follow TEBV > TEIL > TEML, suggesting that endothelial cells are more sensitive to $FeCl_3$ than the smooth muscle cells. On the other hand, a mechanical injury seems to favour attachment on the TEML, and very similar attachment profiles for the TEIL and TEBV, following the trend TEML > TEBV ≥ TEIL. The data shown in figure 5-19 also suggests that with a moderate injury, the *absence* of atorvastatin generally appears to generate a better homing response, whereas the more aggressive, oxidation based $FeCl_3$ injury appears to favour the inclusion of atorvastatin to increase/improve cell homing. It also appears that the optimal time frame to achieve maximum cell attachment is between 3 and 5 hours for both mechanical and $FeCl_3$ injuries. Two-way ANOVA was used to analyse the data sets presented in figure 5-19, denoting significance in attachment between the TE models.

5.1.18.5 Comparison of dynamic versus rocker flow on EPC homing

To determine if there were significant differences between mode of perfusion, the common time points between dynamic perfusion and rocker perfusion, with $FeCl_3$ injury, were compared. Results are presented in figure 5-20.

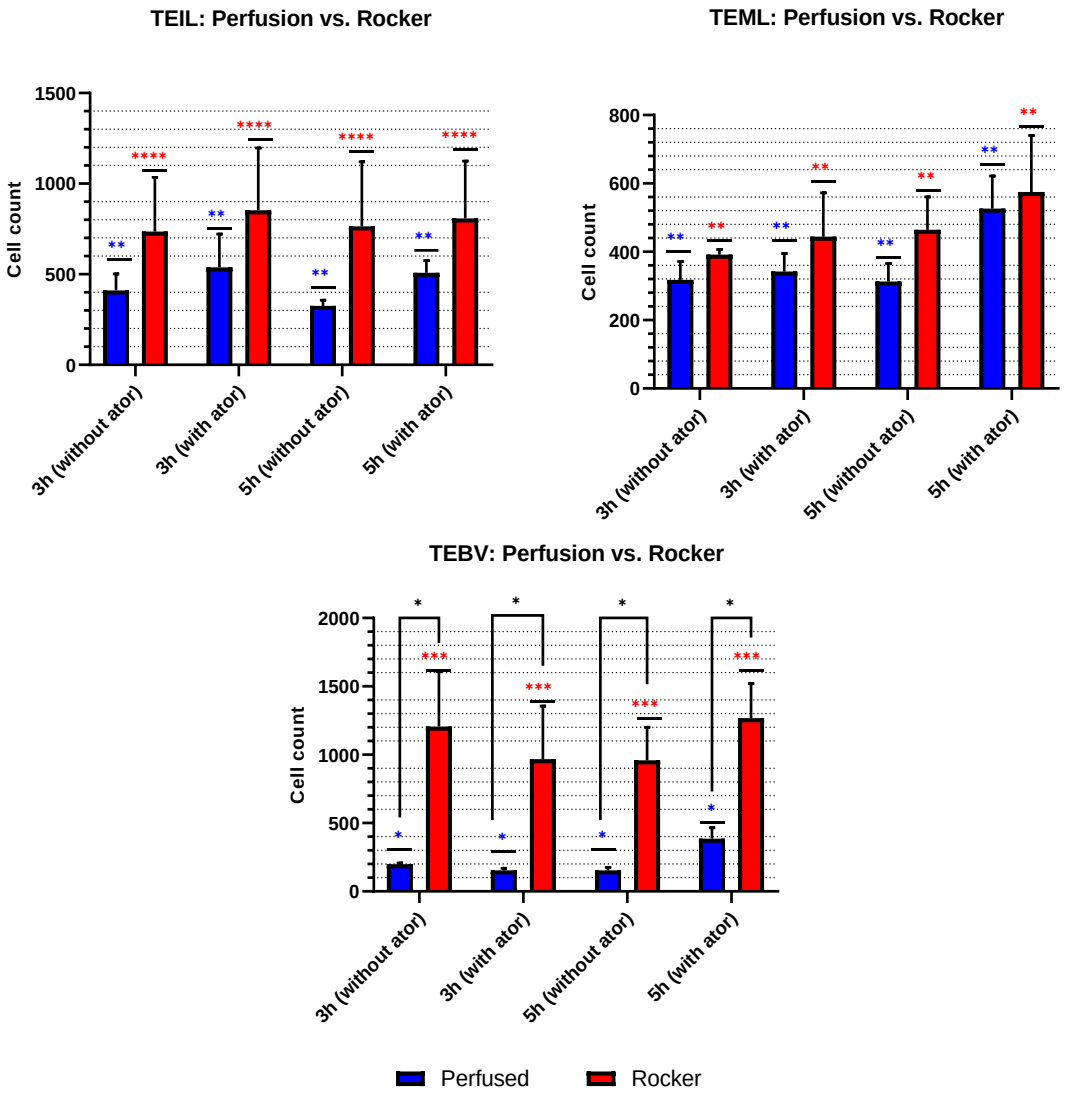

Figure 5-20: Comparative of 3 and 5-hour time points with $FeCl_3$ injury under perfused or see-saw rocker flow. These plots display cell attachment at 3 and 5-hours, following perfusion of EPC using either a parallel plate flow chamber, with shear stress of 20.16 dyne/cm^2, or see-saw rocker with shear stress of 2.2 dyne/cm^2 for 45-minutes and 1-hour respectively. Both types of perfusion were done over $FeCl_3$ injured TEBV, incubated both with and without atorvastatin. One sample t-and-Wilcoxon test was carried out on the data sets, with significance identified for each mode of perfusion (parallel plate versus see-saw rocker) per model, i.e., 20.16 dyne/cm^2 ($p = 0.0027$ ** (TEIL), 0.0052 ** (TEML) and 0.0273 * (TEBV)) and 2.2 dyne/cm^2 ($p < 0.0001$ **** (TEIL), = 0.0012 ** (TEML), and = 0.0008 *** (TEBV)). Additional significance was identified using two-way ANOVA for the TEBV comparative plot, with significance identified between time points, both with and without atorvastatin ($p = 0.0310$). N = 3.

The plots in figure 5-20 show that the observed trend i.e., cell attachment is increased with longer incubation and in the presence of atorvastatin, is not altered with different modes of perfusion. At the common time points i.e., 3 and 5 hours, samples perfused in the parallel plate flow chamber and those perfused using the see-saw rocker show the same trend. The only variation between the groups is that

the rocker flow samples generally have more cells attached on the construct surfaces than those under dynamic flow, with the largest variation in cell attachment observed in the TEBV samples where the rocker samples have significantly higher attachment. The data represented here suggests that 1) for the TEIL, the stronger contributor to cell attachment is the presence of atorvastatin, 2) for the TEML, incubation time and presence of atorvastatin both affect cell attachment and 3) for the TEBV, atorvastatin has a stronger effect with longer incubation, once again suggesting a synergistic interplay between the medial and intimal layers. No statistical significance was found between dynamic and rocker flow for any of the models.

5.1.19 Atorvastatin effect on SDF-1 production

To determine atorvastatin's effect on the primary cytokine that's associated with recruitment of cells to sites of vascular injuries, an evaluation of the production of SDF-1 was carried out. This was carried out for each of the models i.e., TEIL, TEML and TEBV and graphs are represented in figure 5-21 to figure 5-23. Readings were taken for media collected at the following time points 10 minutes, 1 hour, 3 hours, 5 hours, 7 hours, and 9 hours. Samples evaluated were lesioned with $FeCl_3$ or mechanically, and with and without atorvastatin.

5.1.19.1 TEIL

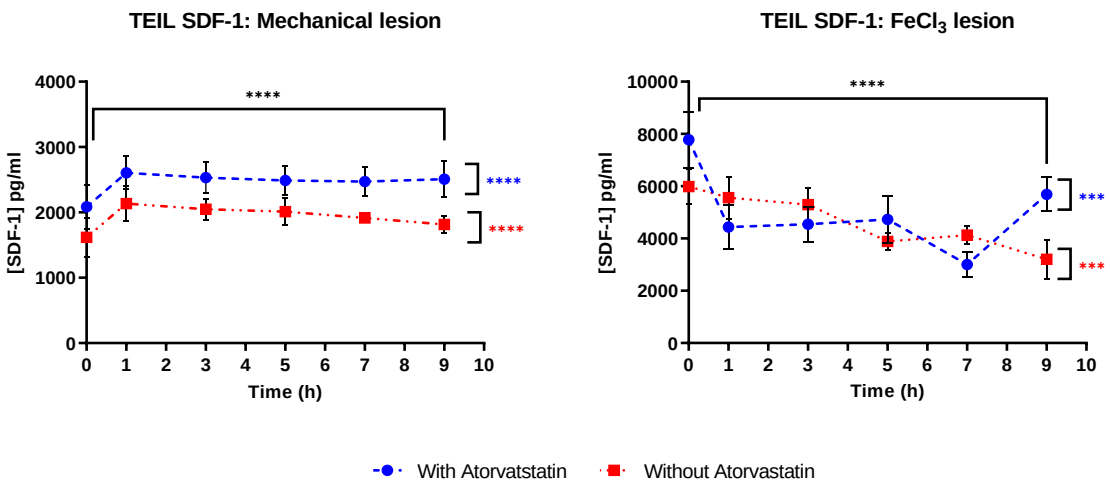

Figure 5-21: Effect of injury type and atorvastatin on SDF-1 production on TEIL. These plots display SDF-1 production over time on TEILs lesioned either mechanically or with $FeCl_3$, and then incubated with or without atorvastatin for the stipulated time points. One sample t-and-Wilcoxon test was carried out on the data sets, with significance identified for samples with or without atorvastatin, for both injury types i.e., mechanical ($p < 0.0001$ **** (With atorvastatin), and <0.0001 **** (without atorvastatin) and $FeCl_3$ lesion ($p = 0.0006$ *** (with atorvastatin), and 0.0001 *** (without atorvastatin). Additional significance was identified using two-way ANOVA, with significance identified between time points, both with and without atorvastatin for Mechanical ($p < 0.0001$ ****) and $FeCl_3$ injury ($p < 0.0001$****). N = 9.

The most observable effect of injury type on SDF-1 production is the stability/consistency of its production, with the mechanical injury showing a more stable trend than the $FeCl_3$ injury. Another difference is in the amounts of SDF-1 produced where the $FeCl_3$ injury samples show much higher concentrations of SDF-1 across all time points. With both treated and untreated samples with $FeCl_3$ injury, initial peak production is followed by a gradual decline over time, with atorvastatin treated samples showing higher production. With mechanical lesion, the trend is the same for both treated and untreated samples but with higher concentrations observed with atorvastatin.

5.1.19.2 TEML

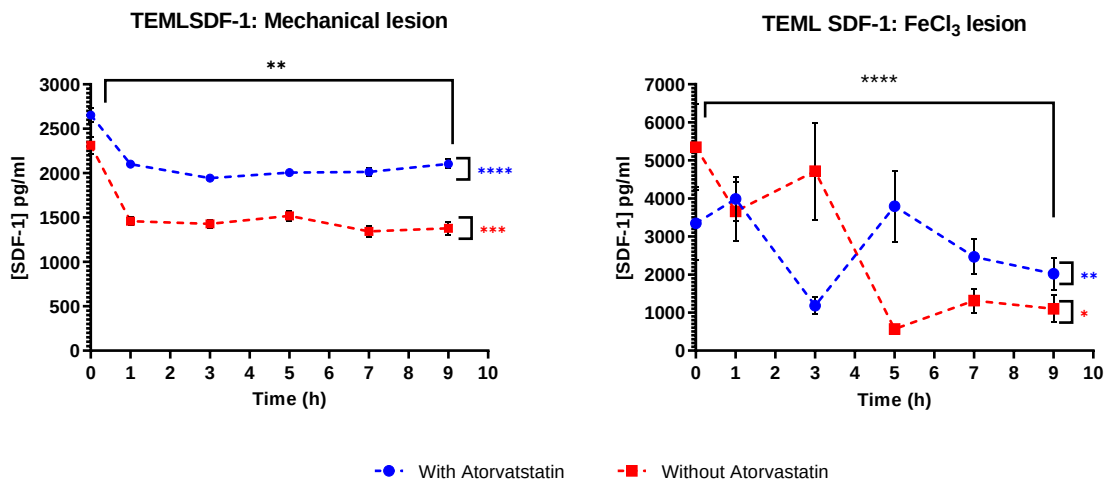

Figure 5-22: Effect of injury and atorvastatin on SDF-1 production on TEML. These plots display SDF-1 production over time on TEMLs lesioned either mechanically or with $FeCl_3$, and then incubated with or without atorvastatin for the stipulated time points. One sample t-and-Wilcoxon test was carried out on the data sets, with significance identified for samples with or without atorvastatin, for both injury types i.e., mechanical ($p < 0.0001$ **** (With atorvastatin), and = 0.0001 *** (without atorvastatin) and $FeCl_3$ lesion ($p = 0.0015$ ** (with atorvastatin), and 0.0208 * (without atorvastatin). Additional significance was identified using two-way ANOVA, with significance identified between time points, both with and without atorvastatin for Mechanical ($p = 0.0087$ **) and $FeCl_3$ injury ($p < 0.0001$ ****). N = 9.

As with the TEIL, $FeCl_3$ injury elicits an erratic response with fluctuations in production over time both with and without atorvastatin, and higher SDF-1 production over time. Samples without atorvastatin showed peak production after 10 minutes, generating the highest reading overall for $FeCl_3$ injury, with another rise at 3 hours followed by a decline, while treated samples peaked at 1 hour with another rise at 5 hours. With the mechanical injury, the trend is, again, similar to that of the TEIL in its consistency, but varies in that after initial peak production, levels of SDF-1 dropped after an hour followed by semi stable/consistent production over time. Again, as with the TEIL, treated samples showed higher levels of SDF-1 across all time points.

5.1.19.3 TEBV

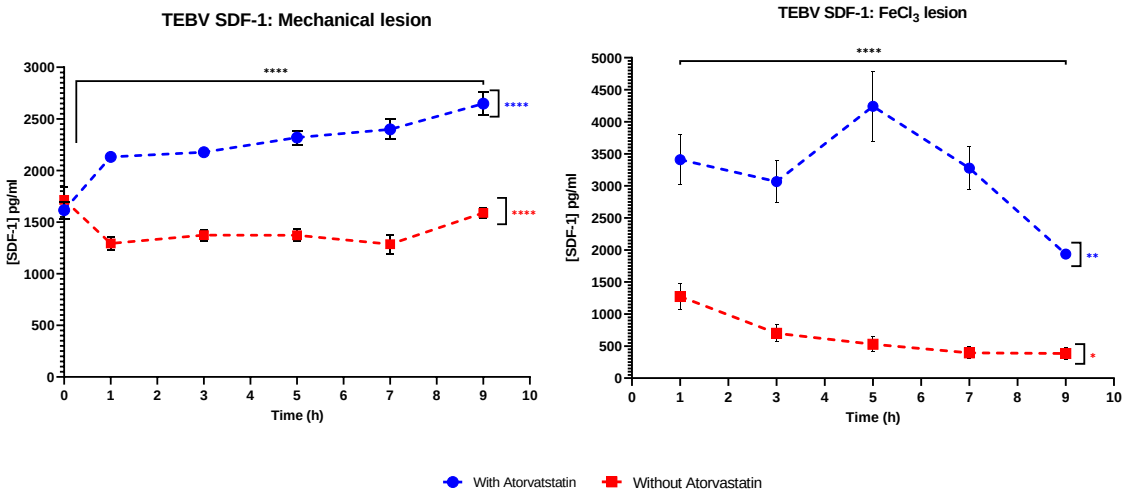

Figure 5-23: Effect of injury and atorvastatin on SDF-1 production on TEBV. These plots display SDF-1 production over time on TEBVs lesioned either mechanically or with $FeCl_3$, and then incubated with or without atorvastatin for the stipulated time points. One sample t-and-Wilcoxon test was carried out on the data sets, with significance identified for samples with or without atorvastatin, for both injury types i.e., mechanical ($p < 0.0001$ **** (With atorvastatin), and <0.0001 **** (without atorvastatin) and $FeCl_3$ lesion ($p = 0.0010$ ** (with atorvastatin), and 0.0163 * (without atorvastatin). Additional significance was identified using two-way ANOVA, with significance identified between time points, both with and without atorvastatin for Mechanical ($p < 0.0001$ ****) and $FeCl_3$ injury ($p < 0.0001$ ****). N = 9.

For this model, the biggest effect of injury type is seen in atorvastatin free samples with $FeCl_3$ injury. The highest production is seen after an hour followed by a sharp decline over time. The atorvastatin treated samples have peak production at the 5-hour time point, followed by a steep decline. As with the other models, the $FeCl_3$ lesioned samples show higher production of SDF-1 compared to the mechanically injured samples. For this model, the trend observed with the $FeCl_3$ lesion is consistent compared to the TEIL and TEML which showed peaks and drops across the time points. As with the other models, the presence of atorvastatin has a strong effect on the production of SDF-1, with consistently higher readings across most time points. Across all models, the mechanical injury triggers production of a roughly similar range of amounts of SDF-1, which are collectively lower than those with $FeCl_3$ injury. The consistency of the trend with both mechanical and $FeCl_3$ injury suggests that maintenance of SDF-1 is a concert effort between the medial and intimal layers, and that atorvastatin enhances its production.

5.1.20 Immunostaining

To determine if the primary receptor for SDF-1 is also affected by atorvastatin, immunostaining was done for CXCR4. 1° antibody was used at 1:200 dilution and 2° antibody at 1:400. Staining was done for TEBV, TEIL and TEML respectively, and representative images are shown in figure 5-24 to 5-26. E-selectin expression was also evaluated for TEIL, TEBV and TEML lesioned with $FeCl_3$. Images shown in figure 5-27. All images taken were only of the rocker perfused samples. Secondary antibody negative controls are seen in figure 5-28.

5.1.20.1 CXCR4: TEBV

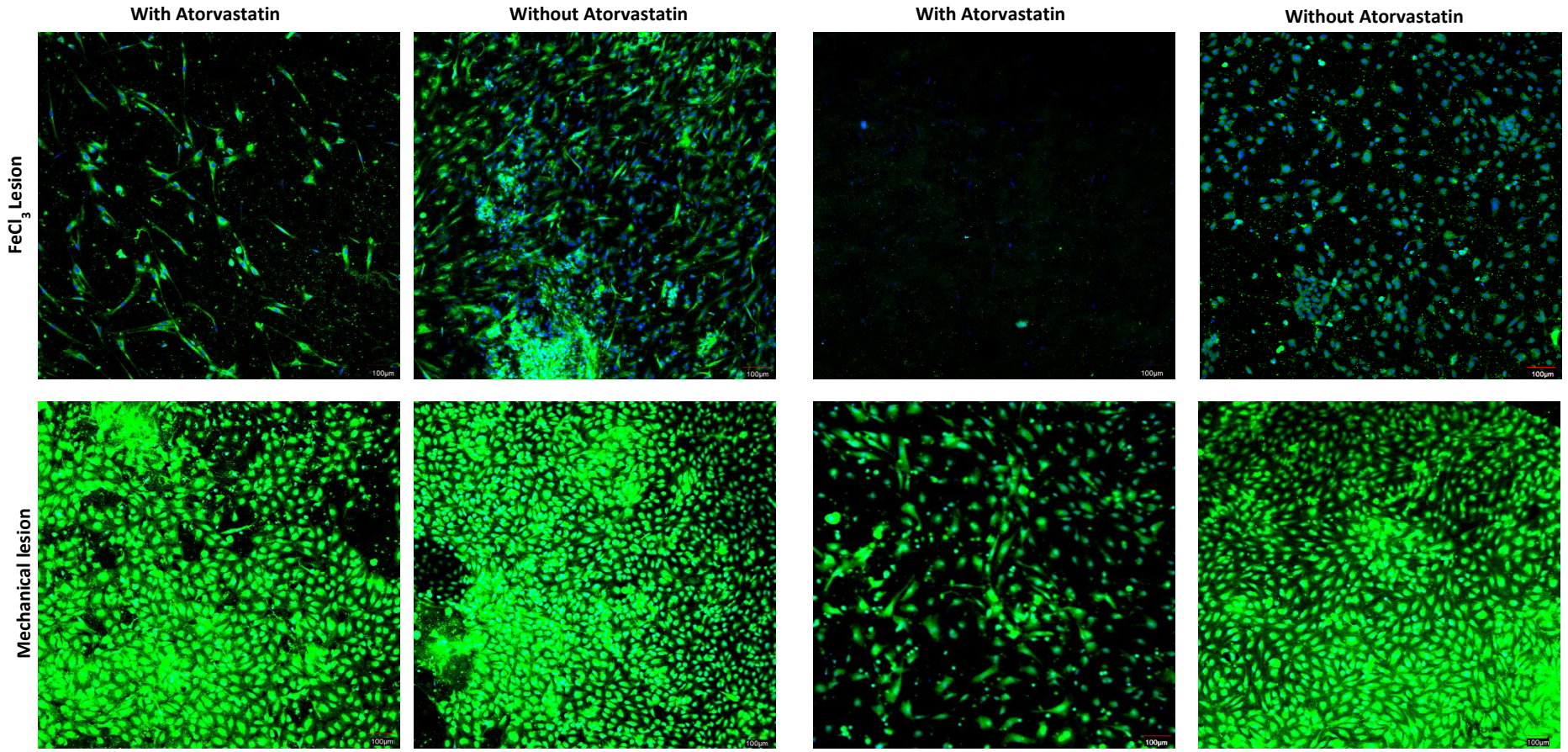

Figure 5-24: TEBV CXCR4 staining. Images were taken for the 1 and 9-hour time points comparing different lesions and the presence of atorvastatin on the expression of CXCR4. Images taken at 10x. CXCR4, DAPI.

The images shown in figure 5-24 suggest that atorvastatin reduces expression of CXCR4 with $FeCl_3$ injury. A comparative of time points for this injury type shows a general reduction in expression over time both with and without atorvastatin, with even low expression observed after 9 hours with atorvastatin. Expression with mechanical injury appears to be the same at the 1-hour time point both with and without atorvastatin, however, at 9 hours the atorvastatin treated sample displays lower levels of CXCR4 expression.

5.1.20.2 CXCR4: TEIL

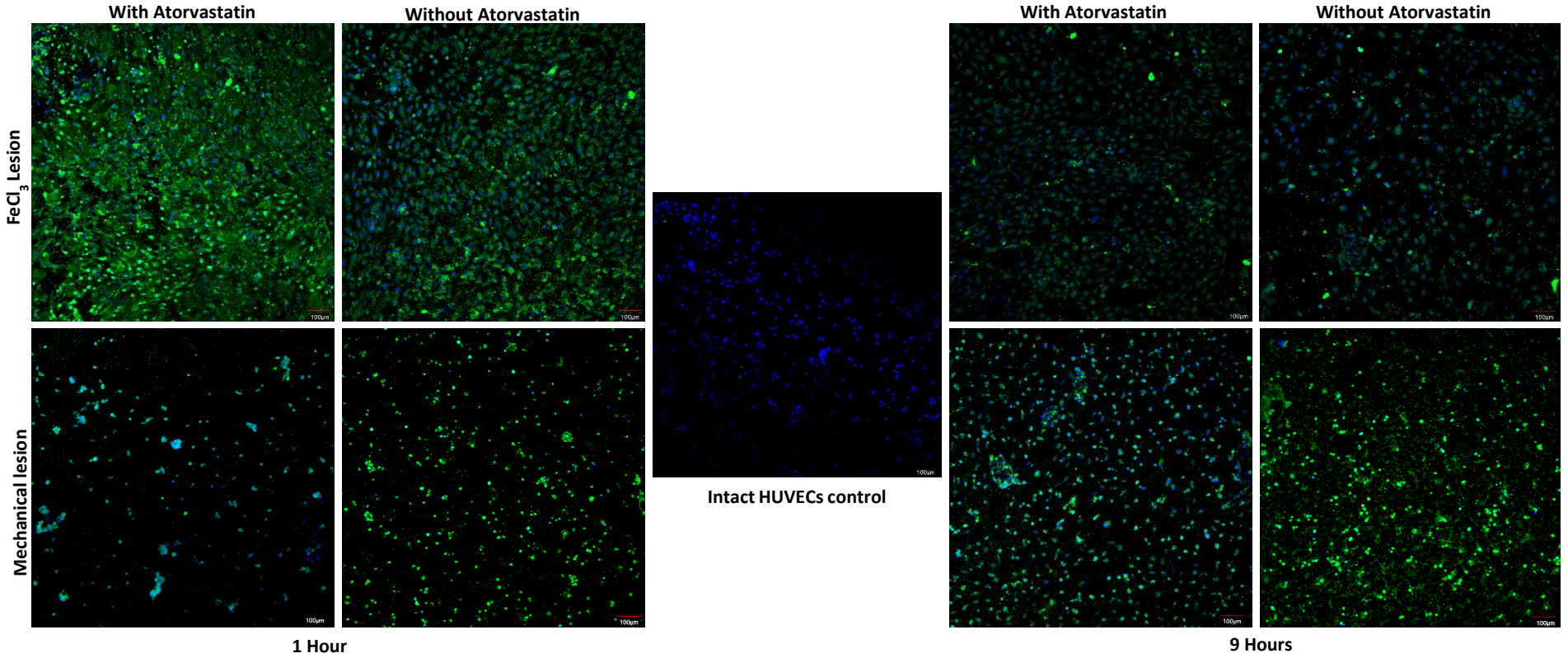

Figure 5-25*:* TEIL CXCR4 staining. Images were taken for the 1 and 9-hour time points comparing different lesions and the presence of atorvastatin on the expression of CXCR4. Images taken at 10x. CXCR4, DAPI.

Figure 5-25 suggests that atorvastatin inclusion, with $FeCl_3$ lesion, results in more CXCR4 expression at both the 1 and 9-hour time points and as with the TEBV, expression appears to reduce at the 9-hour time point both with and without atorvastatin. For the mechanically lesioned samples, the trend is similar to that observed with the TEBV in that there is less expression of CXCR4 with atorvastatin at both time points.

5.1.20.3 CXCR4: TEML

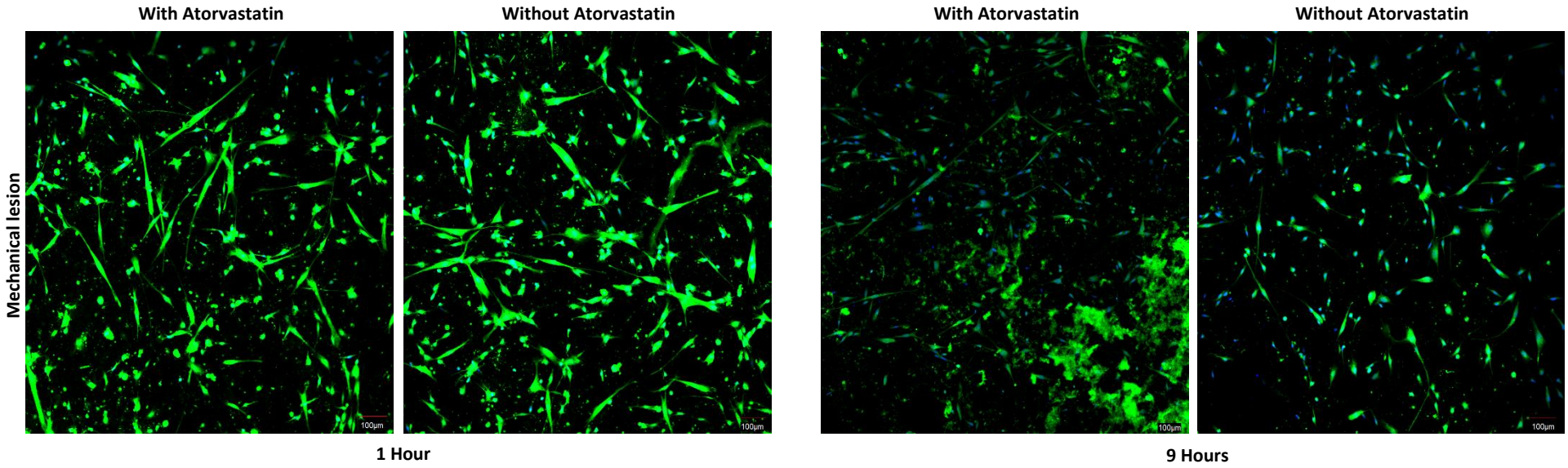

Figure 5-26: TEML CXCR4 staining. Images were taken for the 1 and 9-hour time points comparing the effect of the presence of atorvastatin on the expression of CXCR4. Images taken at 10x. CXCR4, DAPI.

For the TEML, expression of CXCR4 appears similar to both with and without atorvastatin at the 1-hour time point in that there does not seem significant difference between the two groups. There does appear to be a reduction after 9 hours with the atorvastatin treated samples appearing to have slightly lower expression than the atorvastatin free sample.

5.1.20.4 E-Selectin

Expression of this receptor was evaluated only for $FeCl_3$ lesioned samples treated with atorvastatin. Representative images are shown in figure 5-27.

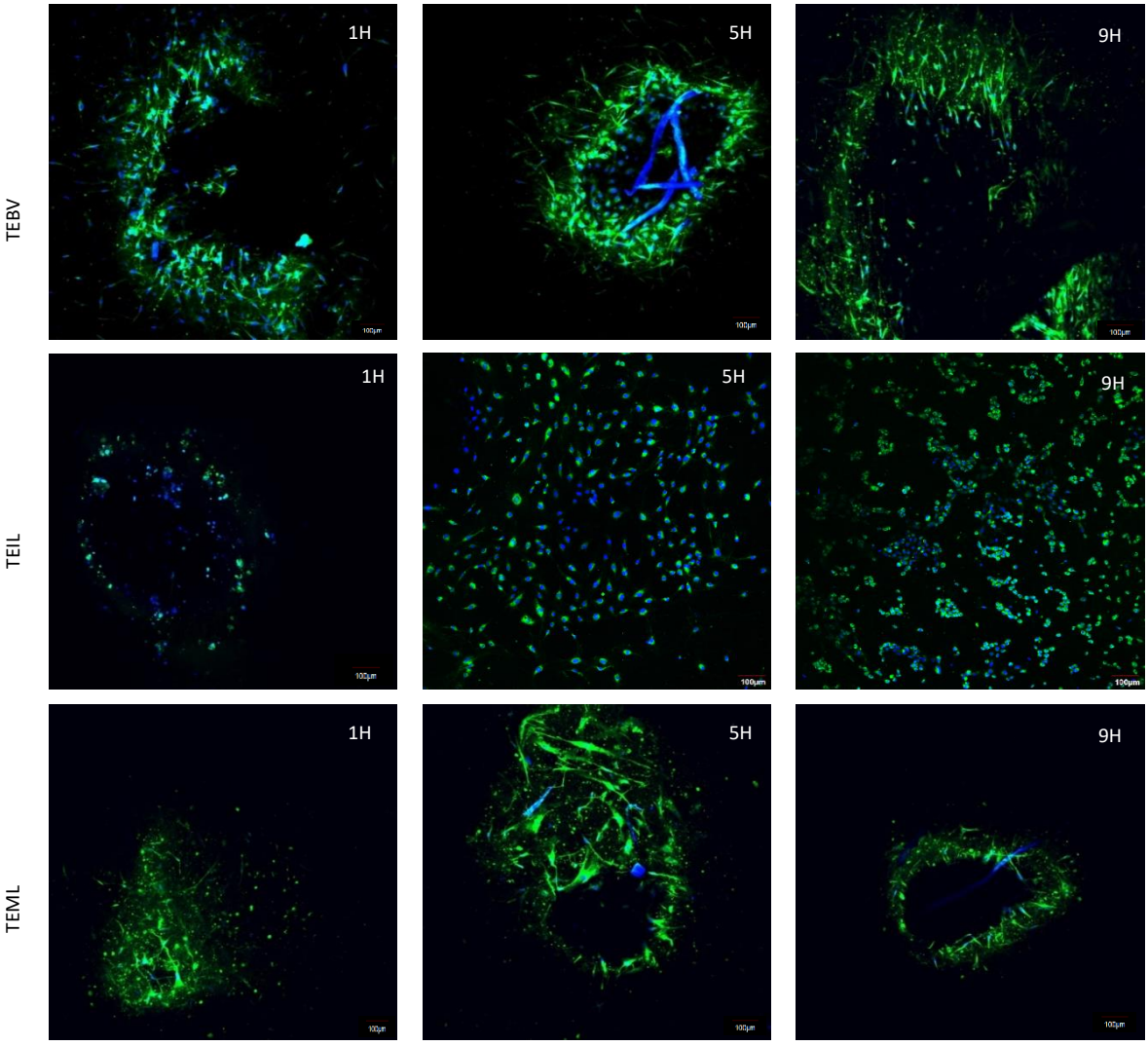

Figure 5-27: E-selectin expression in atorvastatin treated $FeCl_3$ lesioned TEBV, TEIL and TEML. Images are taken at the lesion site at 10x magnification. Expression was tracked at 1, 5 and 9-hour time points. Scale bar = 100 µm.

The images shown here confirm the expression of E-selectin across the models, with fairly consistent expression across all time points imaged, and may contribute to the attachment of cells onto the TE surfaces.

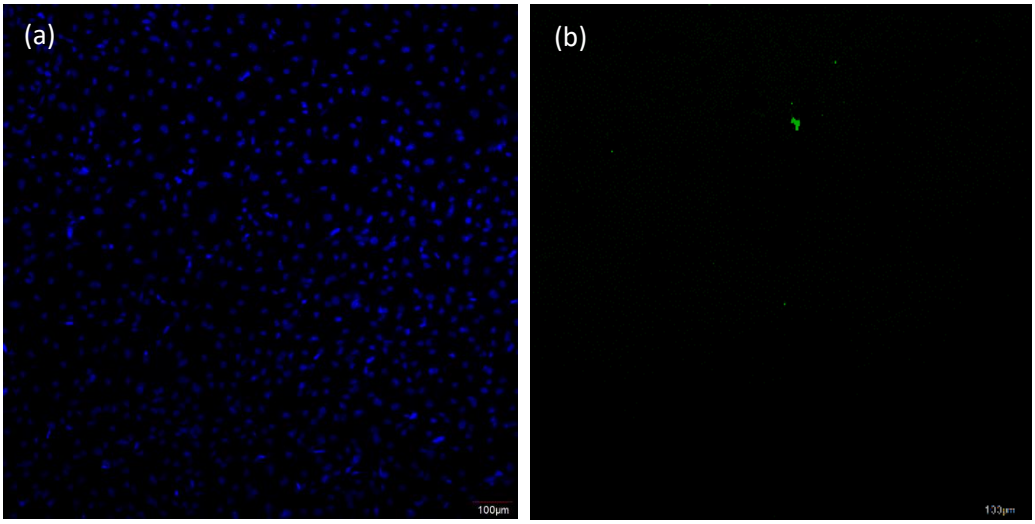

Figure 5-28: secondary antibody negative control. (**a**) E-selectin Alexa Fluor® 488-conjugated negative control (**b**) Donkey anti-rabbit IgG NL493 conjugated (CXCR4). DAPI. Images taken at 10x, scale bar = 100 µm

Figure 5-28 shows the negative antibody controls for the 1° antibodies used here. For E-selectin, as it is a fluorophore conjugated antibody, the antibody was added to cells that were known not to express E-selectin i.e., un-lesioned TEBVs not used for experimentation.

5.4 Discussion

Maintenance of vascular integrity is a vital process in maintaining vascular health. When an injury occurs on the endothelial layer, either by mechanical removal of the endothelium or inflammatory activation of the endothelium, it induces a cascade of proinflammatory events which result in the infiltration of monocytic cells and the proliferation of smooth muscle cells (Dimmeler and Zeiher, 2004). The proinflammatory events can lead to the development of atherosclerotic lesions, plaque rupture and cardiac infarctions. To reduce the likelihood of occurrence of these deleterious events, there are both endogenous i.e., resident endothelial cell based and exogenous i.e., circulating stem/progenitor cell based reparative mechanisms, which come together to reverse vascular damage and reinstate endothelial barrier function. They achieve this through regeneration of a functional endothelium and re-engagement of endothelial junctions (Evans, Iruela-Arispe and Zhao, 2021). Regarding the recruitment of circulating progenitor cells to sites of injury, the data presented here demonstrates that upon injury, the introduction of progenitor cells i.e., MSCs and EPCs, under physiologically relevant shear stress (20.16 dyne/cm^2), results in their attachment onto the lesioned surface of the vessel constructs evaluated. Beginning with perfusion of human MSCs (hMSCs), this effect appears to be both time dependent as well as affected by atorvastatin. The hMSCs used here (figure 5-7 and 5-8), can be defined as such due to the demonstration of their capacity to differentiate into other cell types i.e., adipocytes, osteocytes, and chondrocytes, represented in the previous chapter (figure 4-7 to 4-9). Homing of MSCs is defined as the arrest of MSCs within the vasculature of a tissue followed by the transmigration across the endothelium (Karp and Leng Teo, 2009) or as the ability of stem cells, either in circulation or exogenously introduced, to locate and enter an environmental niche (Liesveld, Sharma and Aljitawi, 2020). Here, it was possible to specifically demonstrate arrest and localisation of hMSCs to vascular injury. It was also possible to demonstrate an increase in the number of attached cells in the presence of atorvastatin. A number of studies have demonstrated the positive effect atorvastatin has on increasing survival of MSCs after transplantation into post-infarct hearts, thus improving cardiac function (Song *et al.*, 2013b; Cai *et al.*, 2014; Zhang

et al., 2014). Simvastatin has also been shown to have a beneficial effect on MSC and $CD133^+/CD34^+$ endothelial precursor chemoattraction and migration to injured areas, specifically lung and spinal injury, suggesting its effectiveness in attracting cells from the bone marrow to injured areas. The increased migratory capacity was also demonstrated in trans-well and Matrigel based migration assays (Gorabi *et al.*, 2020). It is also interesting to note that the effect of shear is that samples subjected to higher shear values showed lower cell attachment than those exposed to low shear stress (figure 5-20), an observation supported by previously published works (Truskey and Pirone, 1990; Maan, Menon and Pullarkat, 2017; Jötten *et al.*, 2019). The expression of E-selectin shown on the constructs used here (figure 5-27), shows that the TE constructs created were able to produce a receptor that aids in arrest of circulating lymphocytes and progenitor cells (Milstone *et al.*, 2000; Liu *et al.*, 2016). It was also possible to demonstrate E-selectin expression in smooth muscle cells, which has primarily only been reported in endothelial cells (Chen *et al.*, 1997), suggesting atorvastatin may have an effect on smooth muscle E-selectin expression.

The observation of increased attachment of hMSCs on the TEBV was also noted for EPCs and was consistent for all models in that, generally, more cells were counted with atorvastatin and with increased culture time. This same trend was noted when a different mode of perfusion was applied i.e., rocker motion (figure 5-16 to 5-20). For this set of figures, the other contributing factor is the type of injury used on the different models. The mechanical injury was less aggressive in that it involved the localised removal of a layer of cells, similar to the type of injury created by percutaneous transluminal coronary angioplasty (PTCA/balloon injury). $FeCl_3$ is widely used in vascular thrombosis models to trigger platelet activation and aggregation, and it works by creating reactive oxygen species (ROS) that trigger endothelial damage (Li, Nieman and Sen Gupta, 2016). The data presented here (figure 5-19) suggests that the $FeCl_3$ induced injury has more of an effect on the endothelial layer than the medial layer as the models that include an endothelial layer i.e., TEIL and TEBV, show higher density of attached cells with this mode of injury compared to mechanical injury. This figure also demonstrates a synergistic relationship between the intimal and medial layers, as the TEBV

attachment profiles consistently appear to be a merge of the observations on the TEML and TEIL, and additionally implies that oxidative damage has more of an effect on endothelial cells than smooth muscle cells. Additionally, the production of SDF-1 is significantly increased following $FeCl_3$ injury (figure 5-21 to 5-23) compared to mechanical injury. Oxidative stress is a key contributor to the development of cardiovascular disease (Sugiyama *et al.*, 2005), and has been defined as the imbalance between the synthesis of ROS and their elimination by antioxidant defence systems (Costa *et al.*, 2016). $FeCl_3$ induced oxidation can be a result of the Fenton reaction, which leads to the generation of hydroxyl radicals and lipid peroxidation (Woollard *et al.*, 2009). It can also oxidatively modify LDL, leading to vascular injury, and it can also form ferric oxide aggregates on the surface of the vascular lumen (Woollard *et al.*, 2009). Given its mode of action, $FeCl_3$ injury is more representative of the state of vasculature in atherosclerosis. A number of studies have highlighted the importance of ROS production in cellular signalling, e.g., in angiogenesis, in response to growth factors and other signals (Pi *et al.*, 2014; Prieto-Bermejo *et al.*, 2018). Low levels of ROS have been associated with contributing to maintaining pluripotency of adult stem cells while higher levels would commit them to a restricted lineage, a mechanism linked to the SDF-1/CXCR4 axis (Prieto-Bermejo *et al.*, 2018). Wollard et. al., (2009) demonstrated that extent of oxidative damage with $FeCl_3$ is reduced in the absence of blood (Woollard *et al.*, 2009), which would support the theory that the extent of oxidative damage done on the vascular models here generated sufficient oxidation to promote SDF-1 production, as was observed in figure 5-21 to 5-23, which was consistently and significantly higher in the $FeCl_3$ lesioned samples compared to the mechanical injury samples. This increase in SDF-1 could also potentially explain the higher attachment numbers observed with $FeCl_3$ injured models. Atorvastatin has also been shown to positively impact the migration of adipocyte derived stem cells and this has been linked to increased SDF-1 production (Cai *et al.*, 2013). Atorvastatin has also been associated with increasing mitochondrial ROS (Bouitbir *et al.*, 2016), which would also contribute to this observation of increased SDF-1 production.

Moving to the expression profiles observed for CXCR4, the primary receptor for SDF-1 (Ratajczak *et al.*, 2006; Sainz and Sata, 2007; Dimova *et al.*, 2019), its expression also appears to be affected by the mode of injury used, most notably with the TEBV (figure 5-24), in that the mechanically lesioned samples appear to have stronger expression of CXCR4 compared to the $FeCl_3$ lesioned samples at the selected time points. The expression of this receptor is also affected by atorvastatin and it also appears to be time dependent as expression appears lower in the 9-hour samples compared to the 1-hour samples, an observation that is reflected across all models (figure 5-24 to 5-26). This may not actively contribute to the homing of perfused EPCs as this was localised on the lesioned TE constructs, whereas CXCR4 on circulating EPCs would be more significant in recruiting them to the injured tissues (Ratajczak *et al.*, 2006; Hristov *et al.*, 2007; Dimova *et al.*, 2019). The expression of E-selectin has also been reported to be affected by SDF-1 (Liu *et al.*, 2016), so it is possible that the arrest of cells is due to this but further characterization is required to draw this conclusion. Because this receptor ligand pair are also associated with angiogenesis, it is possible that the expression on tissue locked cells serves to maintain vascular integrity, as noted by Döring et al. 2017, following injury and its expression reduces over time as cells are recruited to the lesioned surface of the constructs. Specifically, for the TEBV and TEIL, the less severe injury also displayed generally fewer cells attaching onto the surface, which might require more involvement of resident cells for repair function. Döring et al. 2017 also observed that endothelial CXCR4 deficiency resulted in arterial leakage and inflammatory leukocyte recruitment during atherogenesis (Döring *et al.*, 2017). The restricted expression observed with $FeCl_3$ could be associated with the levels of SDF-1 at the imaged time points in that higher levels of SDF-1 restrict expression of CXCR4 (Molino *et al.*, 2000), possibly through triggering internalisation of CXCR4 as SDF-1 binding to CXCR4 results in internalisation of CXCR4 (Förster *et al.*, 1998; Hattermann *et al.*, 2014), and possibly because expression of CXCR4 is heterogenous, with some endothelial cells expressing it and others not (Molino *et al.*, 2000). The expression variation between time points supports this observation, and suggests that the initial expression of CXCR4 is occuring at the same time as SDF-1 expression, until SDF-1 concentration

reached an ideal that ends up binding all available CXCR4, resulting in reduced expression over time duue to maximum internalisation. Estimating from the graphs detailing SDF-1 production over time, the prime concentration might be between 3000 and 4500 pg/ml.

5.5 Conclusion

Through the experiments carried out in this chapter, it was possible to demonstrate that atorvastatin has a positive effect on homing of circulating EPCs and hMSCs. It was interesting to note that this effect is both time and injury dependent, with generally higher numbers of attached cells recorded with longer incubations with atorvastatin, specifically more than 3 hours, and with the more aggressive $FeCl_3$ injury. The possibility of generating partial and composite blood vessel models allowed the demonstration of a synergistic effect between the intimal and medial layers of the vasculature, with mode of injury, specifically $FeCl_3$ induced oxidative damage, having a stronger effect on endothelial cells. This injury model also suggests that cellular responses to atorvastatin are improved in the context of oxidative damage. By adjusting the sizes of the TE constructs used, it was possible to increase throughput, and evaluate the effect of shear stress on cell homing to sites of vascular injury. With the two types of perfusion, it was possible to demonstrate the trends observed in terms of cell attachment between 3 and 5-hour incubations with the lesion were maintained, with the primary difference being the number of cells attached due to the variation in shear. The models used here not only allowed real time visualisation of cell rolling and attachment, but they also allowed relative quantification of this phenomenon on a time-point basis. It was also possible to further analyse the perfusate to categorise key cytokine production and track production over time. The production of SDF-1 and expression of CXCR4 were also shown to be affected by atorvastatin, incubation duration, and the mode of injury. These two factors complement each other, and this is more observable in the TEBV group. The $FeCl_3$ injured group shows high SDF-1 production compared to the mechanical injury one, and both produce greater amounts of SDF-1 in the presence of atorvastatin than the drug free group (figure 5-23). Whilst CXCR4 expression is lower in $FeCl_3$ lesioned group with atorvastatin, and with nearly zero expression at the 9-hour time point (Figure 5-24), this indicates that the CXCR4 receptors on the cells of TEBV are neutralized or internalized by the high concentrations of SDF-1 in their immediate surroundings, and with longer culture time, the more CXCR4 receptors are lost/neutralized.

It should be possible to quantify a wider array of cytokines and thus characterise the biochemical interplay involved in the process of cell homing and vascular repair, and the impact of atorvastatin on these parameters. These models have also shown to be more versatile than the classic animal model, allowing the comparison and quantification of an array of variables. They have also shown their usefulness as a potential drug screening tool, with the possibility of evaluating a selection of doses as well as drug combinations.

Chapter 6:

Atorvastatin's Effect on Atherosclerotic Plaque Model

6.1 Introduction

One of the main drivers of atherosclerosis is lipoprotein irregularities that result in plaque formation at vulnerable sites in the arterial tree. Plaque formation involves a variety of processes such as lipoprotein retention, inflammatory cell recruitment, foam cell formation, apoptosis, necrosis, SMC proliferation and matrix synthesis, calcification, angiogenesis, arterial remodelling and thrombosis (Bentzon *et al.*, 2014). One of the key cellular drivers of this process is the macrophage. In response to a steady accumulation of lipids and other inducers such as dysfunctional endothelial cells secreting cytokines and expressing adhesion molecules, monocytes are recruited from circulation and surrounding tissue (Bentzon *et al.*, 2014). The recruited monocytes infiltrate the sub-endothelial space, differentiating into macrophages and dendritic cell like phenotypes (H. Xu *et al.*, 2019). One of the receptors that facilitate macrophage infiltration into the sub-endothelial space is CD146. Expression of CD146 is found on a wide variety of cells within the vascular tree such as endothelial and smooth muscle cells, and recent findings have identified CD146 transcripts and proteins in atherosclerotic plaque biopsies (Blin *et al.*, 2019; Leroyer *et al.*, 2019). Increased expression of this receptor has been associated with several inflammatory diseases associated with endothelial lesion, and it has also been associated with the early stages of lymphocyte rolling on the endothelium (Blin *et al.*, 2019), as well as controlling the formation of foam cells (Luo *et al.*, 2017). The presence of oxidised LDL (oxLDL) has been demonstrated to increase expression of CD146 and it has been suggested that CD146 traps/ encourages retention of macrophages within the arterial wall (Leroyer *et al.*, 2019; Luo *et al.*, 2017).

Once the macrophages are exposed to atherogenic lipoproteins, they become foam cells. The primary contributing factor in foam cell formation is the excessive influx of modified LDL, such as oxLDL, and the accumulation of cholesterol esters within the macrophages. The foam cells then aggregate and proliferate leading to plaque progression by inducing a cascade of inflammatory responses that enhance lipoprotein retention, extracellular matrix modification and sustained chronic inflammation. The core of the plaque is comprised of these foam cells, that then become necrotic, as well as lipids,

cholesterol crystals and cell debris (Xu *et al.*, 2019; Collot-Teixeira *et al.*, 2007; Bobryshev, 2006). Cellular studies carried out to evaluate foam cell formation and behaviour will typically use stimulants to push macrophages to an inflammatory phenotype. Briefly, macrophages can have one of two defined phenotypes, namely M1 or pro-inflammatory and M2 or ani-inflammatory. Within this general definition, factors that affect their phenotype are dependent on recruiting signals and the macrophage location, resulting in a spectrum of activation between M1 and M2 (Murray *et al.*, 2014; Bashir *et al.*, 2016). Foam cells tend to fall under M1 macrophages as they both respond to and produce inflammatory cytokines such as IFN-γ, TNF-α and interleukin-6, 8 and 10 (Il-6, Il-8 and Il-10). Additional stimulants include bacterial fragments that interact with pattern recognition receptors (PRRs) and toll like receptors (TLRs), which would trigger a stronger inflammatory response, stimulating the production of more inflammatory cytokines as well as nitric oxide (NO) for pathogen destruction. Bacterial lipopolysaccharide (LPS) is the most common agent for this purpose, used primarily in conjunction with IFN-γ (Bashir *et al.*, 2016; Smith *et al.*, 2018; Elyasi *et al.*, 2020). The main animal models used are apolipoprotein deficient ($apoE^{-/-}$) and LDL receptor deficient ($Ldlr^{-/-}$) mice fed a "western" diet resulting in the development of atherosclerotic plaques in a manner similar to human pathology (von Scheidt *et al.*, 2017). Of these cytokines listed here, IFN-γ is of particular interest as it has been found to induce the production of other cytokines, in addition to having multiple effects on all stages of atherogenesis (Elyasi *et al.*, 2020). IFN-γ has been shown to activate a number of signalling pathways, including those that induce oxidative stress, promote foam cell formation and accumulation and smooth muscle proliferation and migration into the arterial intima (Elyasi *et al.*, 2020). As pertains to cholesterol transport/homoeostasis, IFN-γ changes the expression of the forward and reverse cholesterol transport proteins in a manner that enhances foam cell transformation, and exposure of mature macrophages and smooth muscle cells to IFN-γ has been shown to increase expression of scavenger receptors, leading to increased uptake of cholesterol (Elyasi *et al.*, 2020). Further to this, cholesterol metabolism has been identified as an important pathway in plaque progression. Unregulated oxLDL uptake and the release of excessive esterified

cholesterol lead to an accumulation of cholesterol ester, which in turn is stored as lipid droplets in the cytoplasm, triggering the formation of foam cells (Li *et al.*, 2017). Scavenger receptors have been associated with this lipid uptake process, specifically type A scavenger receptors and CD36, a type B scavenger receptor (a.k.a. SR-B1). These have been identified as the primary markers for lesional macrophages that become foam cells (H. Xu *et al.*, 2019). Macrophages are also able to remove intracellular free cholesterol via reverse cholesterol transport. This elimination, or efflux, of internalised lipid involves several membrane proteins, including ATP-binding cassette transporters A1 (ABCA1) and G1 (ABCG1) and type B scavenger receptors (Lin *et al.*, 2016). Cholesterol efflux is dependent on extracellular lipid acceptors such as HDL and lipid poor apoproteins. Blocking or inhibition of scavenger receptor A and CD36 results in the blocking of foam cell formation in both human and murine models (Rahaman *et al.*, 2006). CD36 has been identified as the most relevant HDL receptor and facilitates the selective uptake of cholesteryl ester from HDL into hepatocytes for disposal, and has been associated with the initiation of reverse cholesterol transport (RCT)/cholesterol efflux, with its overexpression resulting in enhanced cholesterol catabolism and excretion and slowing atherosclerosis progression (Kartz *et al.*, 2014).

The most commonly used drugs, for both the treatment and prevention of atherosclerosis, are statins. They function by lowering circulating LDL levels through inhibition of HMG-CoA (Cheng *et al.*, 2009). In addition to reducing circulating levels of LDL, statins have a number of pleiotropic effects that are still under investigation. In regards to foam cell formation, there is still some debate as to the effect statins, in this case atorvastatin, has on initiating cholesterol efflux/reverse cholesterol transport. Some studies report an inhibition of cholesterol efflux mechanisms (Qiu and Hill, 2008; Wang *et al.*, 2013) while more recent studies suggest the opposite effect i.e. atorvastatin promoted cholesterol efflux and reduced cholesterol content in a dose dependent manner (Zheng *et al.*, 2020; Peng *et al.*, 2018).

For this chapter, an investigation was carried out to determine if RAW264 cells, highly proliferative monocyte/macrophage like cells, could be induced to increase cholesterol uptake under the influence

of either, IFN-γ, LPS or both in order to generate foam cells. These lipid-loaded foam cells would then be cultured with different doses of atorvastatin to examine the influence of atorvastatin on oxLDL uptake, retention and cholesterol efflux. The experiences in Chapter 4 and 5 have been used to co-culture a foam cell model with intact and lesioned human umbilical vein endothelial cells (HUVECs). The co-culture mimicked the cellular environment of atherosclerotic plaques, and associated cytokine secretion through a new experimental setting. Again, atorvastatin was included with these models, with the aim of observing cellular cross-talk, and the responses characterised through quantification of oxLDL uptake/retention. Uniquely, it was possible to evaluate nitric oxide (NO) production in both HUVECs and foam cells cultured together. Attempts were also made to culture RAW264 with human cardiac artery smooth muscle cells (HCASMCs). Formation of 3D atherosclerotic plaque through culturing foam cell within dense collagen gel, achieved through a plastic compression technique, has been undertaken. There were unexpected difficulties and underlying mechanisms which have been confronted and explored.

6.2 Materials and methods

6.1.1 RAW 264 Culture

RAW264 cells were cultured in DMEM supplemented with 10%FBS, 1%LG and 1% AA. Cells were used between P3 and P14.

6.1.2 HUVEC Culture

HUVECs were cultured using Medium 200. P2-P5 cells were used for experimentation.

6.1.3 OxLDL Synthesis

OxLDL stock solution was prepared by sterile oxidation of LDL with copper sulphate ($CuSO_4$), followed by dialysis in 10µM EDTA. Stock solution obtained was 5mg/ml in concentration. Differentiation between LDL and oxLDL was done by comparing absorbance values of 5mg/ml LDL and oxLDL at 350, 400, 450, 500, 550 and 600nm. Absorbances were read using a plate reader. The characterisation protocol was adopted from Levitt, Chung and Suhling (2015) (Levitt, Chung and Suhling, 2015).

6.1.4 Foam Cell Formation

RAW264 cells were incubated with either LDL/oxLDL alone or LDL/oxLDL in combination with either LPS or IFN-γ. This was done in order to induce polarization of these cells into an M1 phenotype that would increase uptake of LDL/oxLDL and accelerate foam cell formation. LPS and IFN-γ were both used at a concentration of 100ng/ml, oxLDL and LDL at 100µg/ml.

6.1.5 Statin dose

Atorvastatin calcium trihydrate was dissolved in methanol to create stock solution of 20mg/ml. This was diluted in media to the following concentrations; 0.6µg/ml, 1.2µg/ml, 3µg/ml, 6µg/ml and 60µg/ml. These concentrations were used to evaluate their effect on LDL/oxLDL uptake and identify the best concentration to observe this effect.

6.1.6 Nile Red Staining

Nile red working solution (1µg/ml) was added to cell containing wells, and incubated for 20 minutes at room temperature. Nile red is a hydrophobic and metachromatic dye with poor solubility and

fluorescence in water, with colour emission varying from deep red to strong yellow gold in hydrophobic environments (Rumin *et al.*, 2015). Samples were washed twice with PBS them imaged using a confocal microscope. Imaging was done using either or both red and yellow-gold (red/green overlay) fluorescence. The red fluorescence (515-560nm excitation; >590 emission) primarily stains intracellular lipids while the yellow-gold (450-500nm excitation; >528 <590nm emission) can be used to view cytoplasmic lipid. Imaging is carried out with coupled wavelengths 488/565 to 585 (Rumin *et al.*, 2015; Greenspan and Fowler, 1985).

6.1.7 Oil Red-O Quantification

A 0.5% solution of oil red-O in isopropanol was diluted 3:2 with deionised dH_2O. Working solution was added to fixed cells and incubated for 20 minutes at room temperature. This was followed by a wash with dH_2O, then the addition of isopropanol to elute the internalised stain. 100µl of this solution was then quantified using a plate reader set at 540nm.

6.1.8 NO Quantification

Media samples were collected and mixed with Griess buffer (1% sulphonamide, 2.5% phosphoric acid and 0.1% Naphthalene-diamine-hydrochloride) followed by quantification with a plate reader set at 546nm. 50µl of media was added to 50µl of Griess buffer for quantification. Standard curve was created by measuring absorbance for a sodium nitrile dilution series.

6.1.9 Co-culture model

Co-culture was done with both HUVECs and HCASMCs together with RAW264. 4 x 10^4 HUVECs were seeded atop fibronectin coated nanofibers affixed to customised well inserts. The inserts were placed in wells seeded with 2.5 x 10^5 RAW264 cells. HUVECs used in co-culture model were aged between P2 and P4. HUVECs were either left intact lesioned with $FeCl_3$. $FeCl_3$ lesioning was done by dipping a 1mm^2 (0.1cm^2) square of filter paper in 10% $FeCl_3$ and placing this onto the upper surface of the constructs for 1 minute, followed by a PBS wash. The design of the insert i.e., the nanofiber sheet, allowed the separation of media used in this model. Co-culture with HCASMCs was done by seeding

2 x 10^5 cells in collagen gel, along with RAW264 following the high-density collagen (plastic compression) protocol detailed below.

6.1.10 3D Plaque Model

6.1.10.1 Collagen gel solution

Collagen gel was prepared at a concentration of 3 mg/ml. Following manufacturer's protocol, stock collagen solution was mixed with 10x DMEM, 1M NaOH and sterile filtered dH_2O. Depending on the desired final volume, the reagents are added one by one and to prevent premature gelation, the reagents were mixed in an ice bath with the collagen added last. Once the collagen is added, the solution is mixed by pipetting up and down several times until homogenous. Care is taken in the mixing to prevent formation of bubbles in the solution.

6.1.10.2 Plastic compression

6.1.10.2.1 RAW264 only

RAW264 cells were seeded into a collagen gel, followed by plastic compression to increase collagen concentration and stiffness. The plastic compression carried out was based on a procedure modified from Brown et al., (2005). 1500µL of collagen solution, made as previously described, was poured into customised metal moulds placed in 9.6 cm^2 petri dishes under sterile conditions. A sterile cover slip (24 x 24mm) was placed at the bottom of the mould to create a sealed space and to prevent the gel from leaking into the petri dish. Two filter paper frames were placed within the mould to provide structural support for the gel. The frames were sized at 0.9 x 0.9cm. To solidify the gels, they were then placed in an incubator at 37°C, 5% CO_2 for 2 hours. For cells seeded within the gel, cells were mixed with the collagen gel solution, which was then transferred to the compression moulds allowed to set and compressed for 5 minutes. Each mould was able to provide 2 compressed gels with approximately 2.5 x 10^5 cells.

6.1.10.2.2 RAW264-HCASMC co-culture

For the HCASMC co-culture model, 1000µl HCASMC-containing collagen gel was first dispensed into the moulds, followed by careful distribution of 500µl RAW264-containing collagen gel. This ensured the RAW cells were only located on the upper surface of the gel, versus dispersed throughout the bulk. The collagen was allowed to set for 2 hours in an incubator at 37°C and 5% CO_2, followed by the compression protocol.

6.3 Results

6.1.11 Foam cell formation model

To study atherosclerotic plaque model, foam cells formation is an essential step. Foam cells are lipid-laden macrophages, and typical in vitro practice involves culturing macrophage cell lines with low density lipoproteins. In this study, RAW264 murine macrophage cell line was used.

6.1.11.1 RAW264 culture

Cultured cells were highly proliferative, doubling population daily. They adopted a generally rounded morphology, with occasional fibroblast like cells appearing. Cells were semi-adherent and were able to grow in a sheet in 2D culture. How these cells appeared in culture is detailed in figure 6-1.

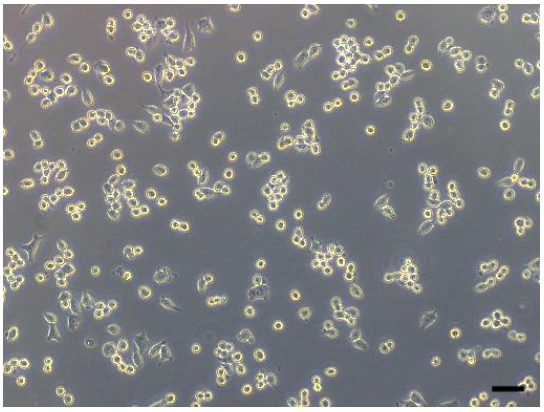

Figure 6-1: RAW264 in 2D culture. RAW264 in 2D culture having primarily rounded morphology. Image taken at 10x. Scale bar = 100 µm

6.1.11.2 Oxidation of LDL

Following the oxidation process detailed in section 6.2.3, characterisation of LDL and oxidized LDL (oxLDL) were carried out to verify if oxidation was successful. Briefly, the absorbances at different wavelengths were recorded for the stock LDL solution and the oxidised LDL. Concentrations of both were 5mg/ml. The wavelengths used were 350, 400, 450, 500, 550 and 600nm. These readings are represented in figure 6-2. Further to this, effect on cell viability was evaluated to determine if there are functional differences between oxidised and native LDL. Data is represented in figure 6-3.

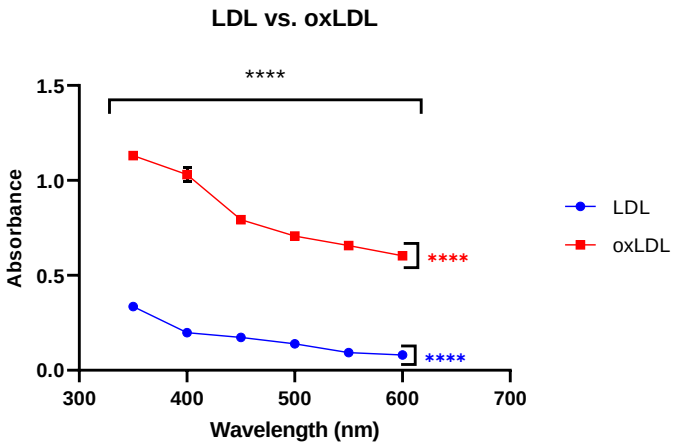

Figure 6-2: Absorbance comparative between LDL and oxLDL. Absorbance readings at different wavelengths, evaluating spectral differences between stock LDL and oxLDL, both at 5mg/ml. Two-way ANOVA and one sample t-and Wilcoxon test were carried out to determine significance, significance was identified between wavelengths and between LDL and oxLDL (P<0.0001 ****, ****, ****. N=3.

At the selected wavelengths, there is a difference in absorption intensity between LDL and oxLDL which suggests that there are structural, and thus spectral, differences between native LDL and the oxidised version-with oxLDL having a consistently higher absorption than LDL at all evaluated wavelengths-, showing that the oxidation protocol followed here was successful at generating an LDL variant. Two-way ANOVA was carried out and showed significance between LDL and oxLDL absorbance values. The data in figure 6-3 suggests there is also a functional difference between LDL and oxLDL, as LDL lowers cell viability compared to oxLDL.

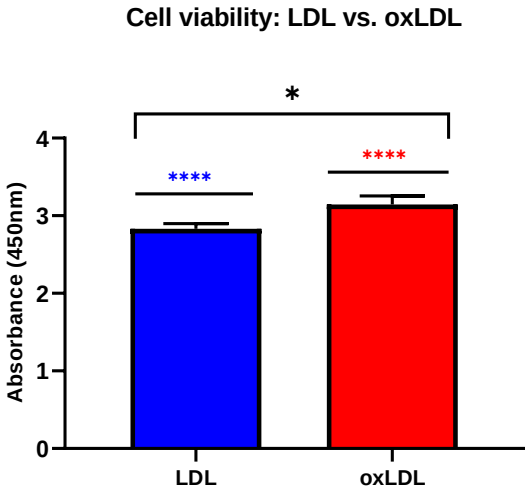

Figure 6-3: Effect of LDL oxidation on cell viability. Cells were cultured for 24 hours with 100µg/ml LDL or oxLDL, after which viability was assessed using CCK8. Statistical analysis was done with one way t-and Wilcoxon test, and unpaired t-test. Significance was identified for LDL and oxLDL absorbance values ($p < 0.0001$ ****, ****), as well as between absorbance values for LDL and oxLDL ($p = 0.0324$ *). N=6.

6.1.11.3 Effect of seeding density and oxLDL concentration on lipid uptake

To determine the ideal or maximum lipid uptake in RAW264, two experiments were carried out. The first evaluated effect of cell seeding density. RAW264 cells were seeded at 125 x10^3, 250 x 10^3, 375 x 10^3 and 500 x 10^3 cells in a 24 well plate, then incubated with a fixed concentration of oxLDL (100µg/ml) for 24 hours. The second experiment was evaluating the effect of oxLDL concentration on total uptake with a fixed cell number. 250 x 10^3 RAW264 cells were seeded and incubated with 50µg/ml, 100µg/ml, 150µg/ml, 200µg/ml and 250µg/ml oxLDL. For both experiments, quantity of internalised oxLDL was determined using oil red-O. The results are represented in figure 6-4 and 6-5 respectively. One-way Anova analysis was done, significance was considered for p vales lower than 0.05.

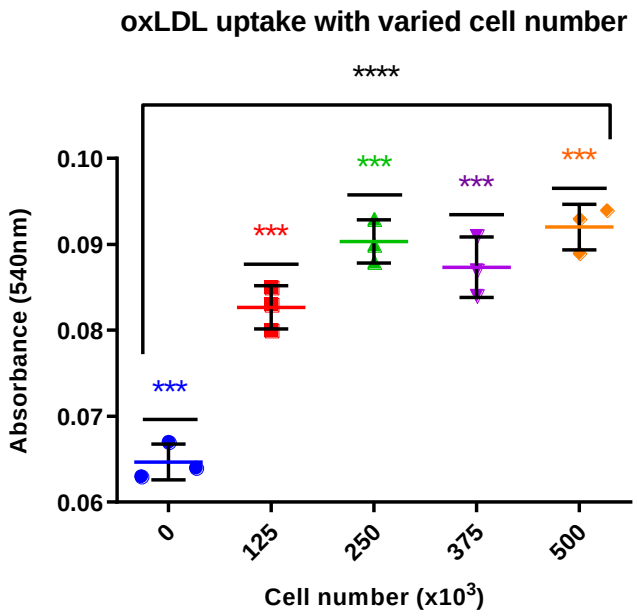

Figure 6-4: Seeding density effect on lipid uptake. 100µg/ml of oxLDL was used across all samples with an increasing density of seeded cells. Samples were incubated for 24 hours with oxLDL and internalised lipid was quantified using oil red-O. Statistical analysis was done using ordinary one-way ANOVA and two-way ANOVA, with significance identified between all cell densities (p <0.0001 ****), as well as one sample t-and Wilcoxon test, with significance identified for uptake for each cell density (p = 0.0003 ***, ***, ***, *** and p = 0.0005 ***). N=3.

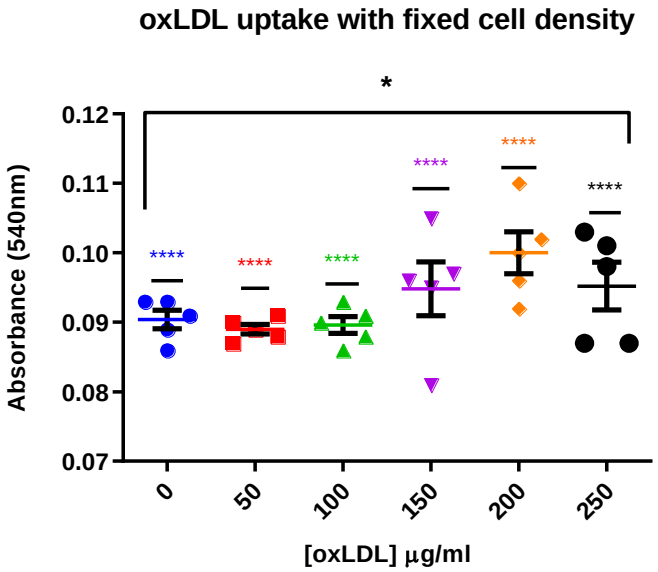

Figure 6-5: oxLDL concentration effect on total uptake. 250 x 10^3 cells were incubated with varying concentrations of oxLDL for 24 hours, followed by quantification of internalised lipid using oil red-O. Statistical analysis was carried out with one way ANOVA, with significance identified between the different oxLDL concentrations (p = 0.0421 * Bartlett test p = 0.0192 *). One sample t-test identified significance for all the concentrations of oxLDL (p <0.0001 ****, ****, ****, ****, ****, ****). N=5.

Cell density appears to have more of an effect on extent of oxLDL uptake than concentration of oxLDL added, which appears to have a maximum limit at 250 x 10^3, suggesting that lipid uptake by RAW264 is dependent on lipid availability, i.e., more cells would require more lipid. The findings in figure 6-5 support this in that as oxLDL concentration increased above 100µg/ml, the concentration within the cells increased, with a variation in absorbance of 0.01 between 100µg/ml and 200µg/ml. There does not appear to be much variation between 0 and 100µg/ml and between 150 and 250µg/ml. The final cell density settled on was 250 x 10^3 cells per well, to be incubated with 100µg/ml, as concentrations higher than this were demonstrated to trigger apoptosis in smooth muscle cells and are also toxic to macrophages and endothelial cells (Ding *et al.*, 2012; Reid and Mitchinson, 1993; Han and Pak, 1999).

6.1.11.4 RAW264 polarization and foam cell formation

The normal/steady state of RAW264 cells is that of inactivated or M0 macrophages. In order to promote RAW264 uptake of oxLDL, stimulation with LPS and IFN-γ was carried out to push these cells to an M1 phenotype. Cells were incubated with LPS and/or IFN-γ, both at a concentration of 100ng/ml, for 24 hours, followed by oxLDL or LDL incubation for a further 24 hours. Extent of lipid uptake was qualitatively evaluated using Nile red staining. The factors evaluated here include the shift of RAW264 from M0 to M1 based on stimulation protocols i.e., LPS vs. IFN-γ vs LPS + IFN-γ and effect of lipid oxidation state i.e., LDL vs. oxLDL. Images comparing extent of lipid uptake are shown in figure 6-6.

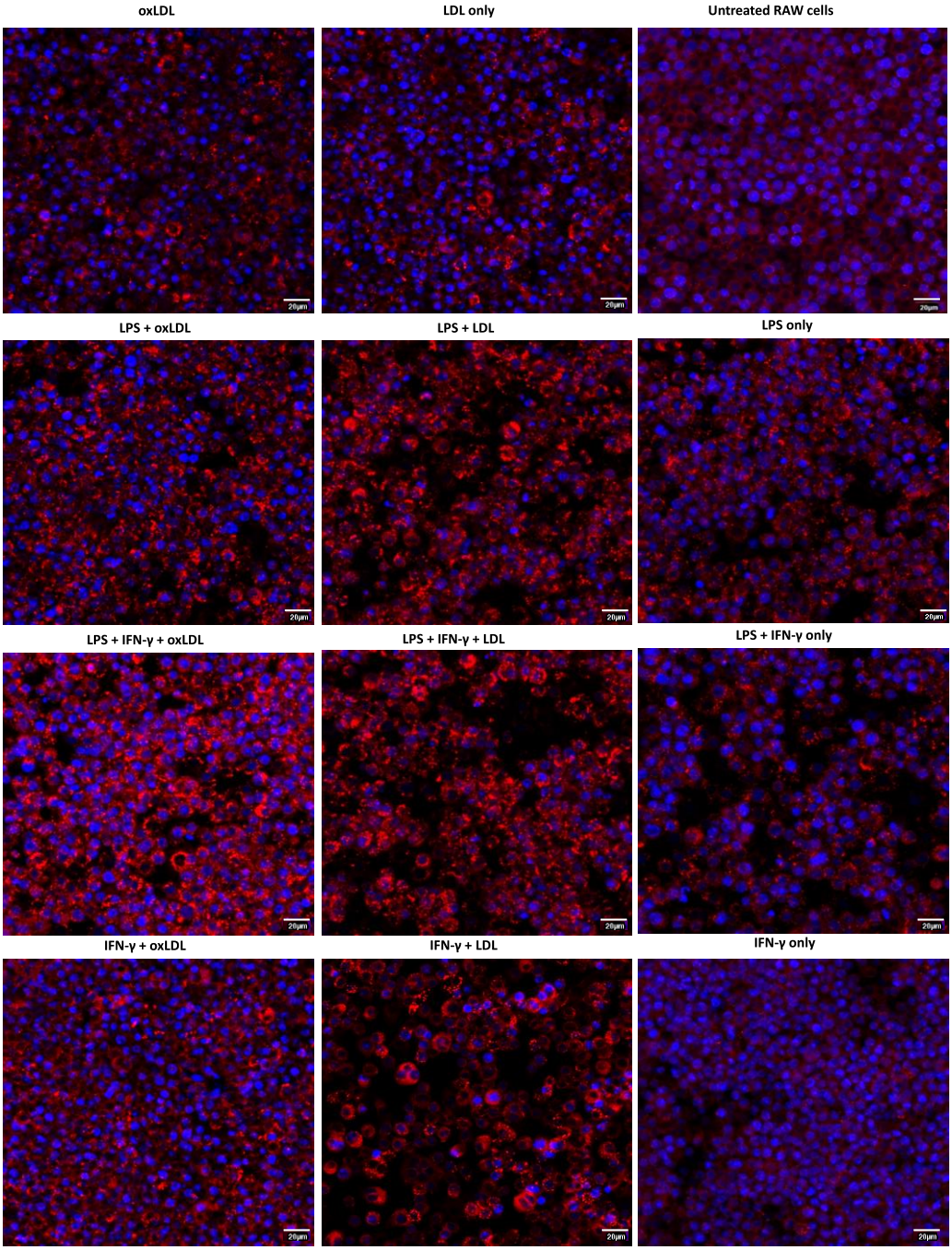

Figure 6-6: Stimulation of foam cell formation. To enhance the uptake of lipids, the RAW cells were treated with either LPS or IFN-γ or both, after which they were stained with Nile red. Untreated RAW264 were cultured under normal conditions. Images taken at 40x.

The images in figure 6-6 show droplets appearing denser with LDL versus oxLDL, and cell density also appears to be lower post incubation in the LDL loaded samples, supporting the observation that LDL has a negative effect on cell viability shown in figure 6-3, compared to oxLDL treated group. Samples stimulated with LPS also appear to have a denser accumulation of droplets than those without as

well as those with just IFN-γ stimulation. Co-stimulation with IFN-γ and LPS show the densest lipid uptake for both LDL and oxLDL. Given that LPS is in itself a lipid, samples incubated only with LPS had droplets present in amounts comparable to oxLDL or LDL only incubations. Samples treated with IFN-γ and either oxLDL and LDL have stronger indications of lipid uptake than the IFN-γ only treated samples. A comparative of IFN-γ only samples with LPS and IFN-γ treated samples, in the absence of either LDL or oxLDL, further demonstrates that LPS addition results in internalised lipid within RAW cells that is unrelated to uptake of either oxLDL or LDL. This resulted in the disqualification of LPS as a practical stimulant for foam cell formation, especially in light of the selected method of uptake quantification. Consequently, only IFN-γ stimulation was used in subsequent experiments to eliminate observed LPS influence.

6.1.11.4.1 Stimulant effect on RAW264 NO production

To characterise RAW264 NO production in response to various polarisation stimulants i.e., LPS, IFN-γ, LDL and oxLDL, RAW264 cells were treated as follows; first 25 x 10^4 RAW264 cells were seeded into individual wells of a 24 well plate, followed by addition of the stimulants. NO readings were taken at the end of the incubations. Quantification was done using Griess buffer mixed 1:1 with media samples, followed by absorbance measurements on a plate reader set at 546nm. [NO] was determined using a previously established standard curve. IFN-γ and LPS were both used at 100ng/ml and both LDL and oxLDL at 100µg/ml for all samples. The results of the cell stimulations are shown in figure 6-7.

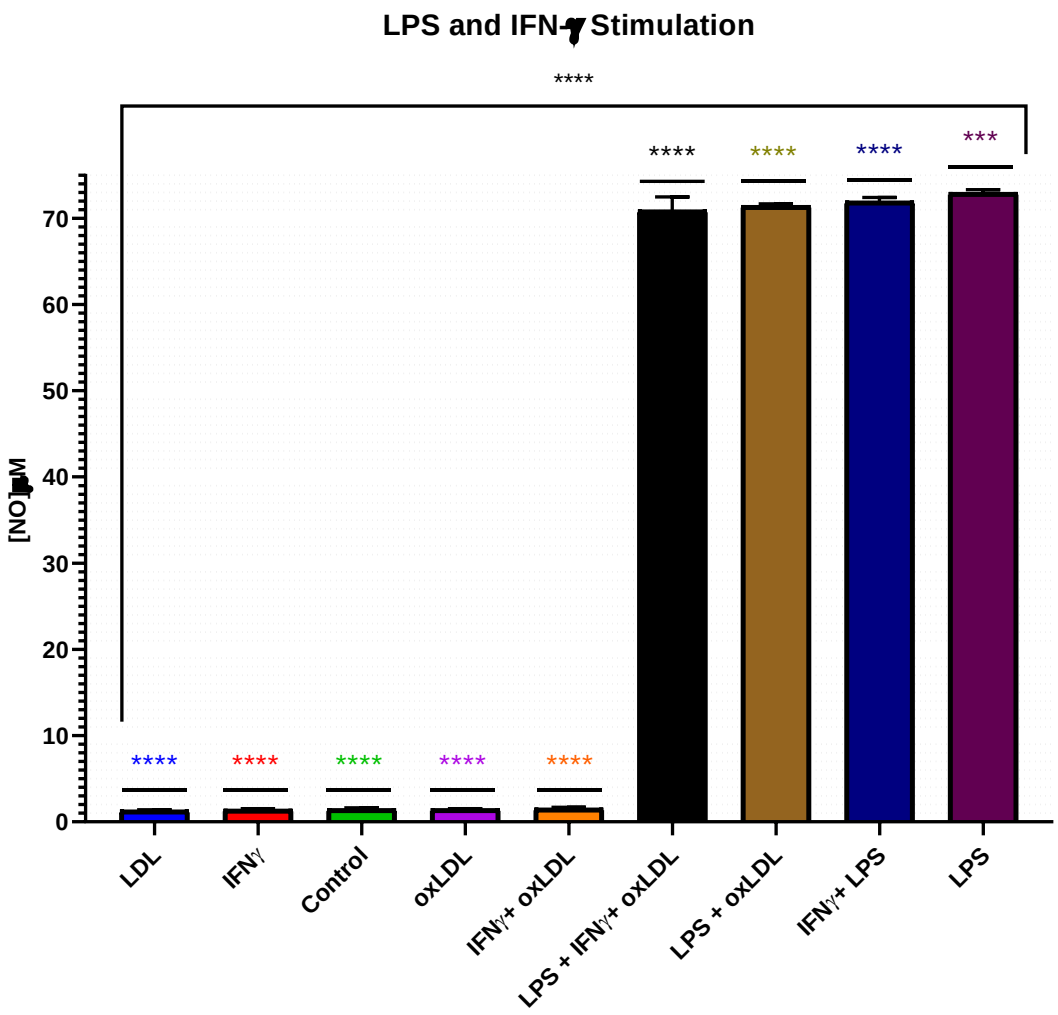

Figure 6-7: NO production in stimulated RAW264 cells. Summary of all stimulants' effect on NO production. All samples contained 250 x 10^3 cells, and were incubated with the stimulants for 24-hours before NO readings were taken. Statistical analysis was done using one-way ANOVA, and significance was identified between stimulants (P <0.0001 ***; Brown-Forsythe test p = 0.0029 **; Bartlett test p <0.0001 ****). One sample t-and-Wilcoxon test was also carried out, and significance was identified for [NO] for each stimulant evaluated (p <0.0001 ****, ****, ****, ****, ****, ****, ****, **** and p = 0.0005 ***. N=5. One-way ANOVA used for analysis. Statistical significance denoted by *. P < 0.0001.

The findings in figure 6-7 indicate that LPS is a far stronger stimulator, in respect to NO production, than the other stimulants, with the highest readings recorded in samples only treated with LPS. The findings here also suggest that IFN-γ has some limiting effect on NO production in that samples with IFN-γ inclusion, either with or without co-stimulation, generally have lower readings than those stimulated with LPS.

6.1.12 Atorvastatin dose effect on foam cell models

To evaluate the effect atorvastatin has on RAW264 polarization, its effect on cell viability and NO production were evaluated as detailed below.

6.1.12.1 LDL vs. oxLDL effect on cell viability under different doses of atorvastatin

To determine if there were functional differences between LDL and oxLDL with the inclusion of atorvastatin, a CCK8 assay was carried out to determine effect on cell viability. Cells were incubated with either 100µg/ml LDL or 100µg/ml oxLDL, and different doses of atorvastatin for 24 hours before readings were taken. The findings are represented in figure 6-8.

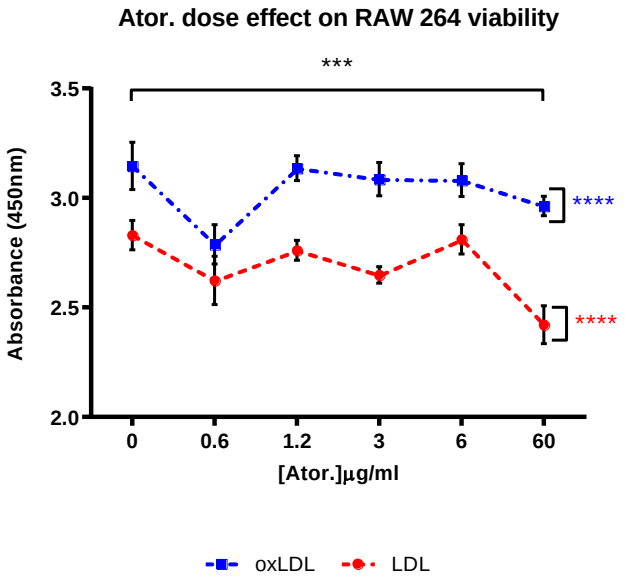

Figure 6-8: CCK8 cell viability assay. This plot compares both the effect of LDL oxidation state, and atorvastatin concentration on cell viability. 2.5 x 10^4 cells were first incubated with either LDL or oxLDL for 24 hours, followed by atorvastatin at the stipulated concentrations for 24 hours. Statistical analysis was done using two-way ANOVA, with significance identified between the concentrations of atorvastatin used (p = 0.0002 ***). Additional analysis was done with a one sample t-and Wilcoxon test, and significance was identified for each group i.e., oxLDL and LDL (p <0.0001 ****, ****(. N=6. Statistical significance denoted by *. P < 0.0001.

The overall trend regarding atorvastatin effect on cell viability is consistent for both LDL and oxLDL, with higher concentrations of atorvastatin consistently lowering cell viability. The reduction in cell viability observed at 0.6µg/ml atorvastatin was unexpected and a proper explanation for why this occurred has not been determined yet. LDL also appears to have a more negative effect on cell

viability than oxLDL, giving consistently lower absorbance readings across all doses of atorvastatin. This observation confirms that the oxidation process was successful. Two-way ANOVA was carried out on these data sets, significance was set at a p value lower than 0.05. Significance was found between doses as well as between LDL and oxLDL treated samples.

6.1.12.2 Atorvastatin effect on uptake of LDL vs. oxLDL

An evaluation was done to determine what effect atorvastatin has on uptake and retention of lipid by foam cells, qualitative analysis using Nile red staining and quantification using oil red-O staining was carried out. Samples were first incubated with IFN-γ for 24 hours, followed by another 24-hour incubation with either LDL or oxLDL, then a 24-hour incubation with atorvastatin at the following doses; 0.6µg/ml, 1.2µg/ml, 3µg/ml, 6µg/ml and 60µg/ml. Representative images are shown in figure 6-9 and 6-10.

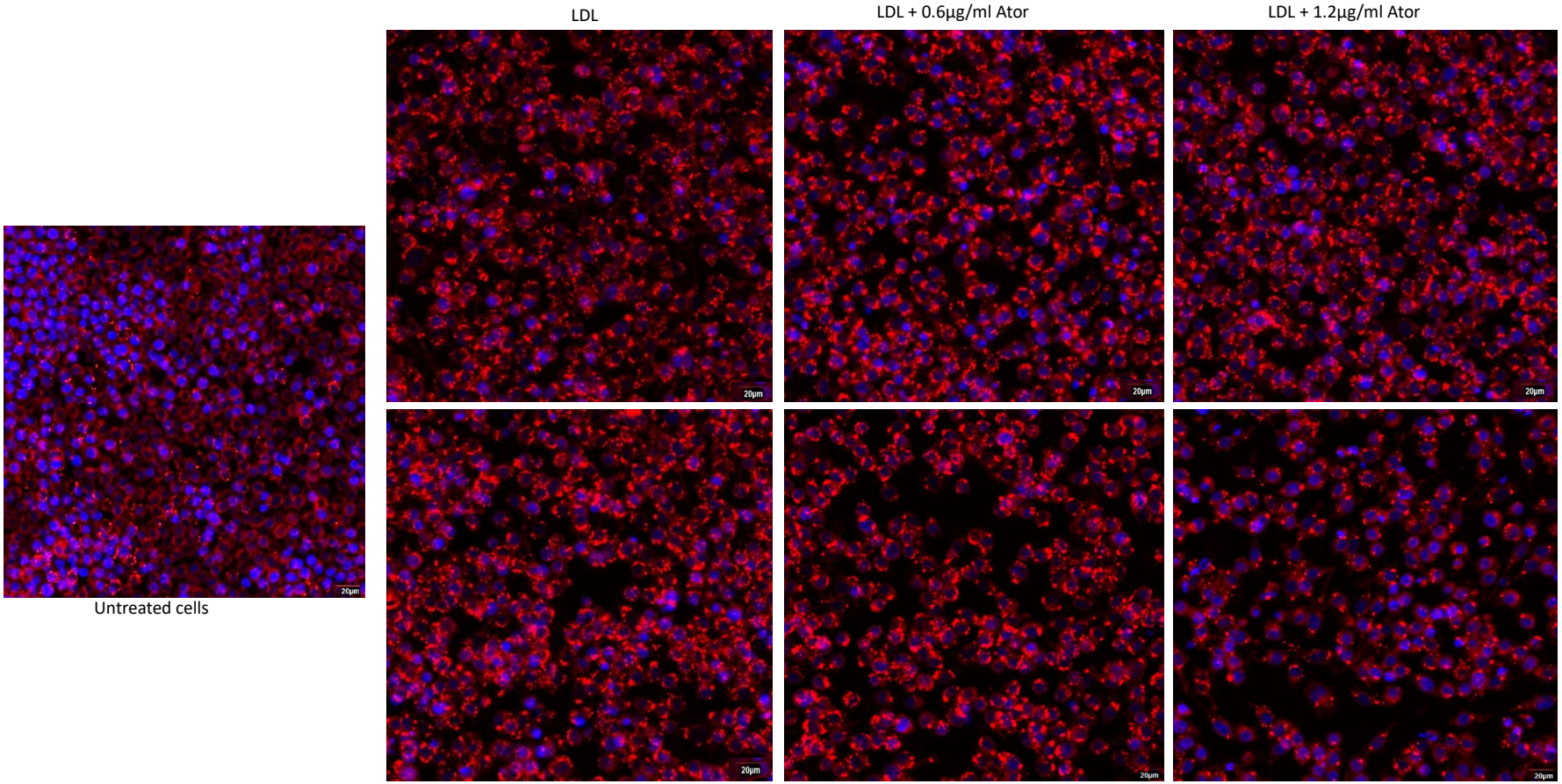

Figure 6-9: Atorvastatin dose effect on lipid (LDL) uptake and retention. Samples were stained with Nile red for droplet visualisation. Atorvastatin was added after addition of the stimulants. All images taken at 40x. DAPI, Nile red.

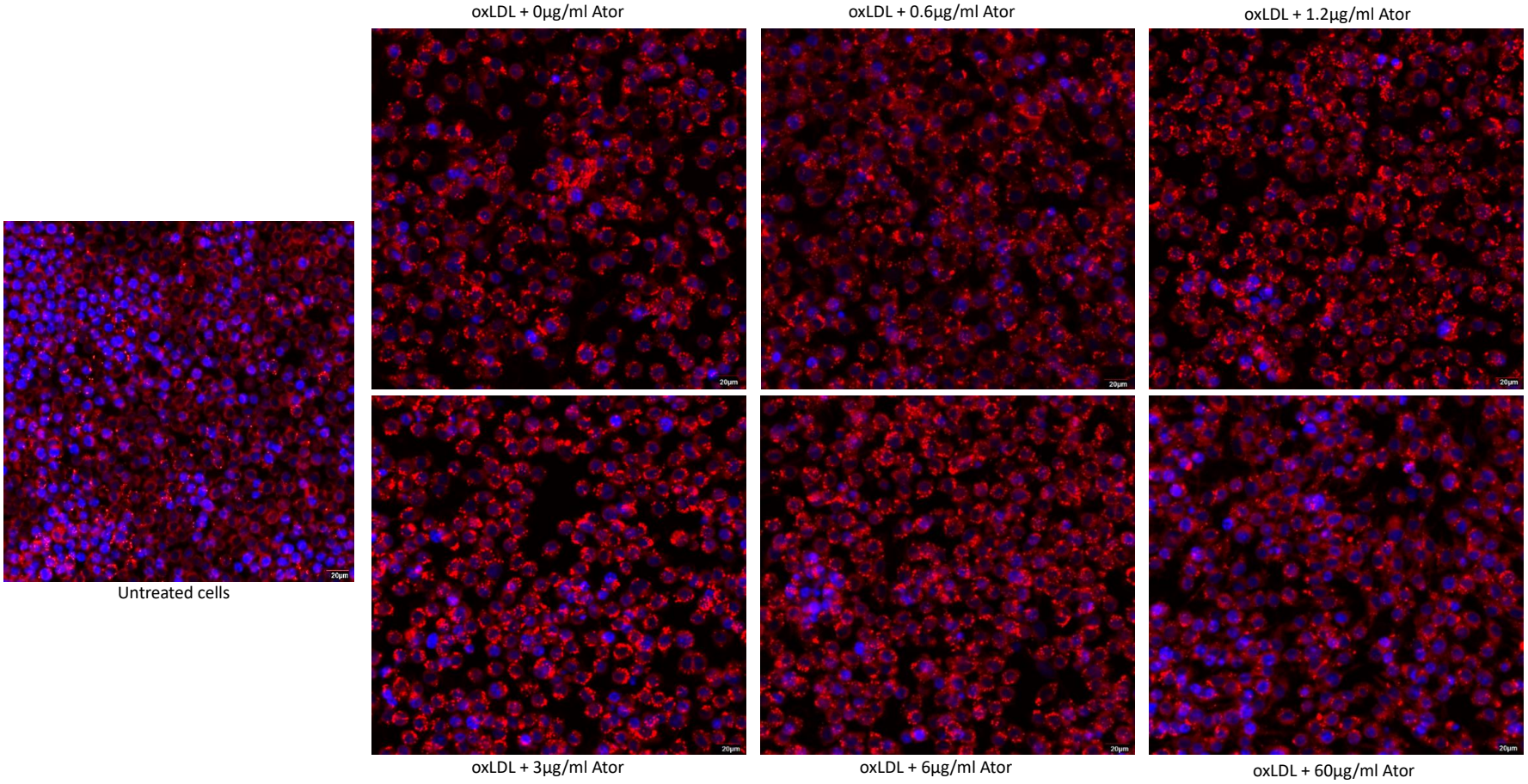

Figure 6-10: Atorvastatin dose effect on lipid (oxLDL) uptake and retention. Samples were stained with Nile red for droplet visualisation. Atorvastatin was added after addition of the stimulants. All images taken at 40x. DAPI, Nile red.

Comparing both LDL and oxLDL uptake, atorvastatin appears to reduce the amount of internalised lipid at the highest dose, 60µg/ml after just 24 hours of culture. Red lipid droplets are far fewer at this dose than other concentrations of atorvastatin. There also appear to be fewer cells present in the wells for both LDL and oxLDL treated cells compared to the untreated controls, with generally fewer cells seen in the LDL treated wells than the oxLDL treated ones, again, as expected due to LDLs impact on cell viability, demonstrated in both figure 6-3 and 6-8. Cells also appear larger and denser for the oxLDL treated samples compared to LDL, with brighter droplet staining in the LDL treated samples.

6.1.12.3 Atorvastatin effect on cholesterol efflux

To determine whether the reduction in lipid droplets observed at 60µg/ml in both figure 6-8 and 6-9 occurs at other concentrations of atorvastatin, the same treatment described in 6.3.1.5.2 was applied but the cells cultured for 24, 48 and 72 hours i.e., first IFN-γ (24h) then LDL/oxLDL (24h) and finally atorvastatin for 24, 48 or 72 hours. Media was changed daily and replenished with freshly made atorvastatin for the 48 and 72h samples. The drug free samples were replenished with untreated culture media. Representative images showing qualitative evaluation of lipid retention can be seen in figure 6-11 and 6-12.

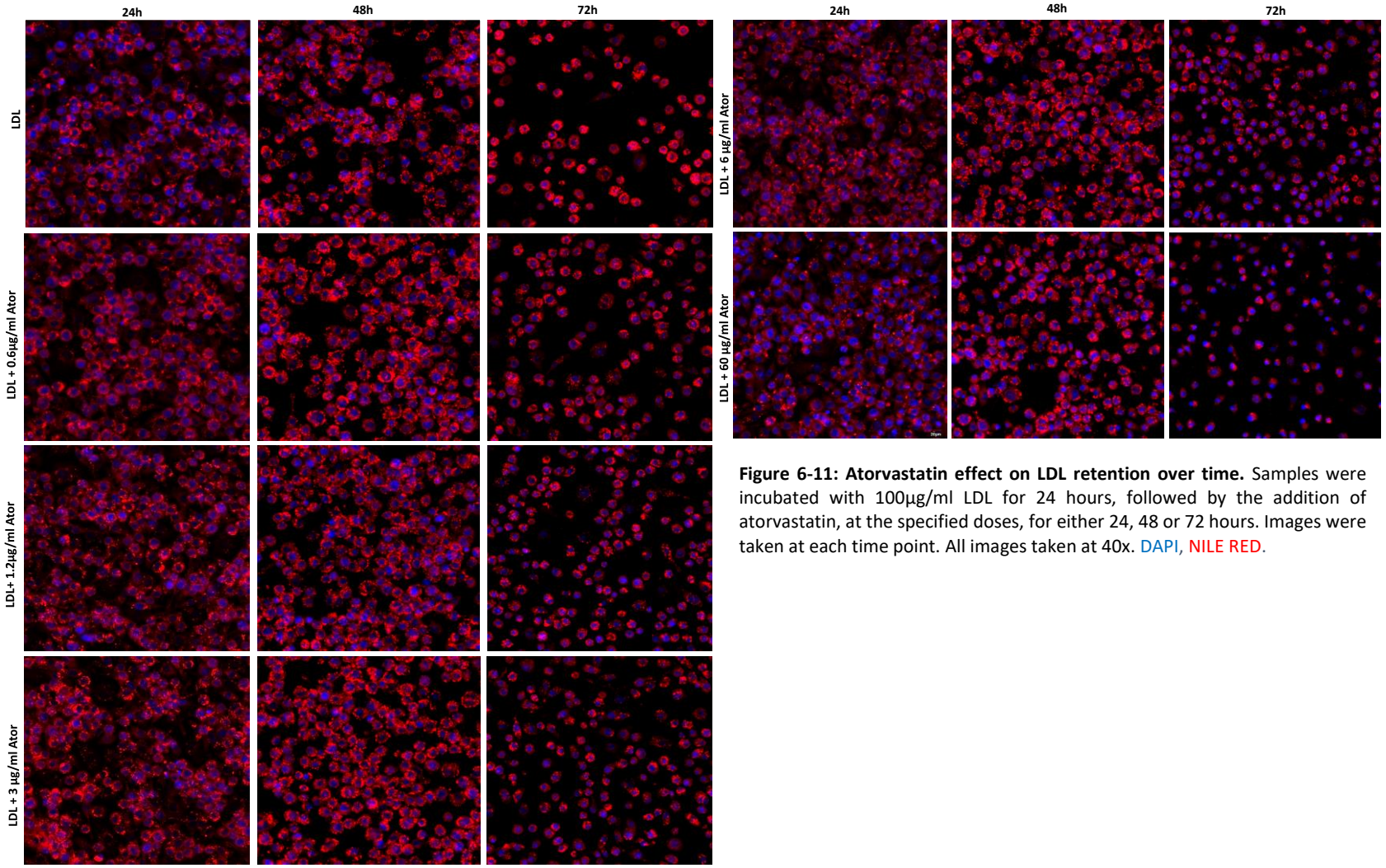

Figure 6-11: Atorvastatin effect on LDL retention over time. Samples were incubated with 100µg/ml LDL for 24 hours, followed by the addition of atorvastatin, at the specified doses, for either 24, 48 or 72 hours. Images were taken at each time point. All images taken at 40x. DAPI, NILE RED.

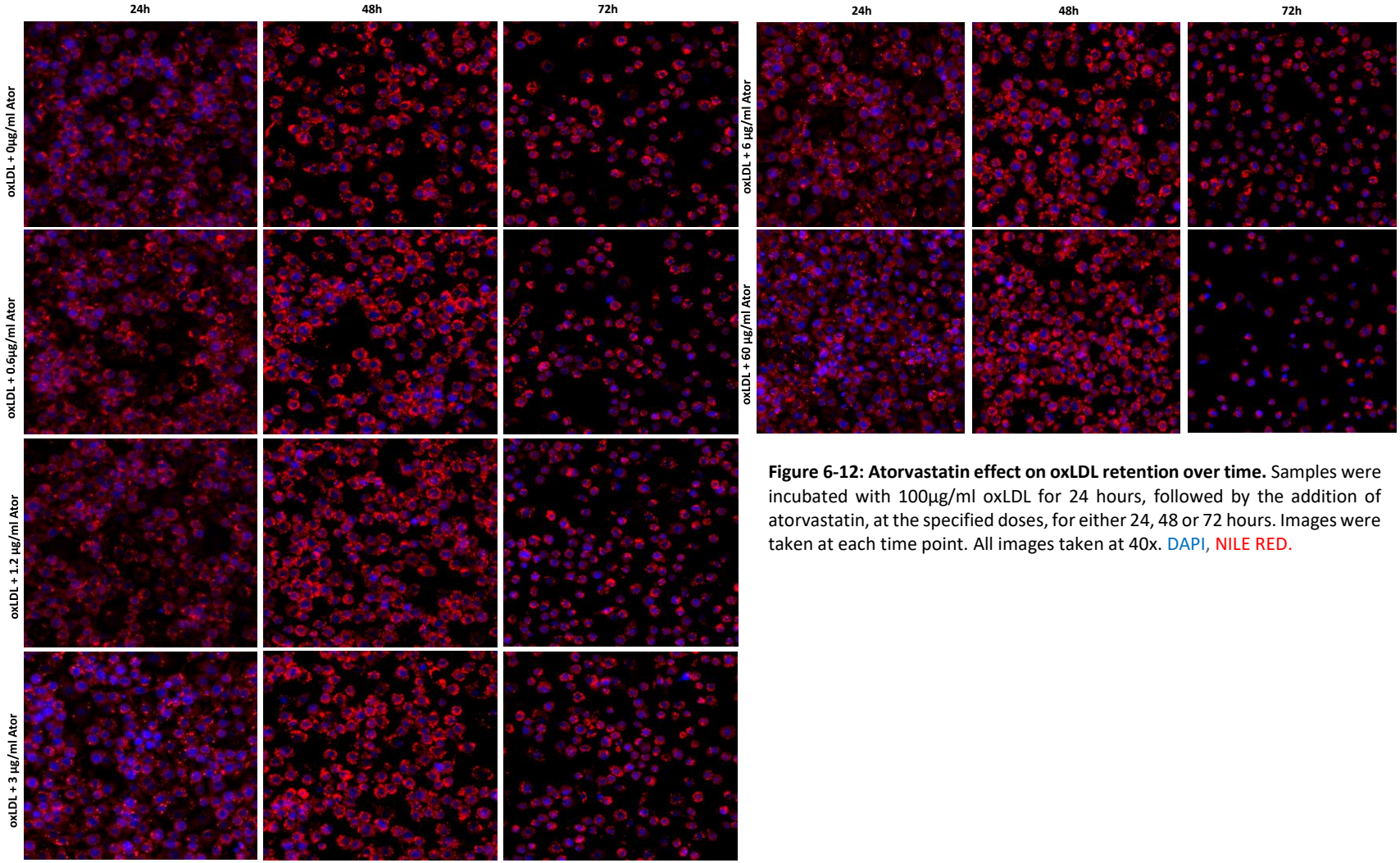

Figure 6-12: Atorvastatin effect on oxLDL retention over time. Samples were incubated with 100µg/ml oxLDL for 24 hours, followed by the addition of atorvastatin, at the specified doses, for either 24, 48 or 72 hours. Images were taken at each time point. All images taken at 40x. DAPI, NILE RED.

For both LDL and oxLDL incubated samples, prolonged culture results in a reduction in cell density, both with and without the inclusion of atorvastatin. Density of lipid droplets appears densest at the 48-hour mark, after which density of cells is markedly lower after 72 hours across all samples in both figure 6-11 and 6-12. Once again, density of lipid droplets is lower at the highest concentration of atorvastatin, 60μg/ml. Other concentrations also have fewer accumulated droplets after 72 hours compared to 48 hours and the control samples. As reduction in cell density was seen across all samples, it is likely due to an overabundance of cells within the culture flask due to the highly proliferative nature of RAW264. This over confluence may have resulted in cell death due to limited availability of space and nutrients.

6.1.12.3.1 Mode of stimulation effect on cholesterol efflux

A quantitative analysis based on the images in figure 6-11 and 6-12 was carried out to verify that atorvastatin triggers the observed ejection, or efflux, of internalised lipid. For this experiment, only oxLDL loading was done to RAW264 cells. Culture conditions were as follows; one batch was treated first with 100ng/ml IFN-γ (24h), followed by 100μg/ml oxLDL (24h) then by atorvastatin (24, 48 and 72h). The other batch was first treated with IFN-γ (24h), the atorvastatin (24h) then a combination of atorvastatin and oxLDL (24, 48 and 72h). After 24 hours, media was changed and replaced with fresh media containing only atorvastatin. After culture, samples were fixed with 4% PFA and internalised lipid content quantified using the previously described oil red-o method. Findings are represented in figure 6-13.

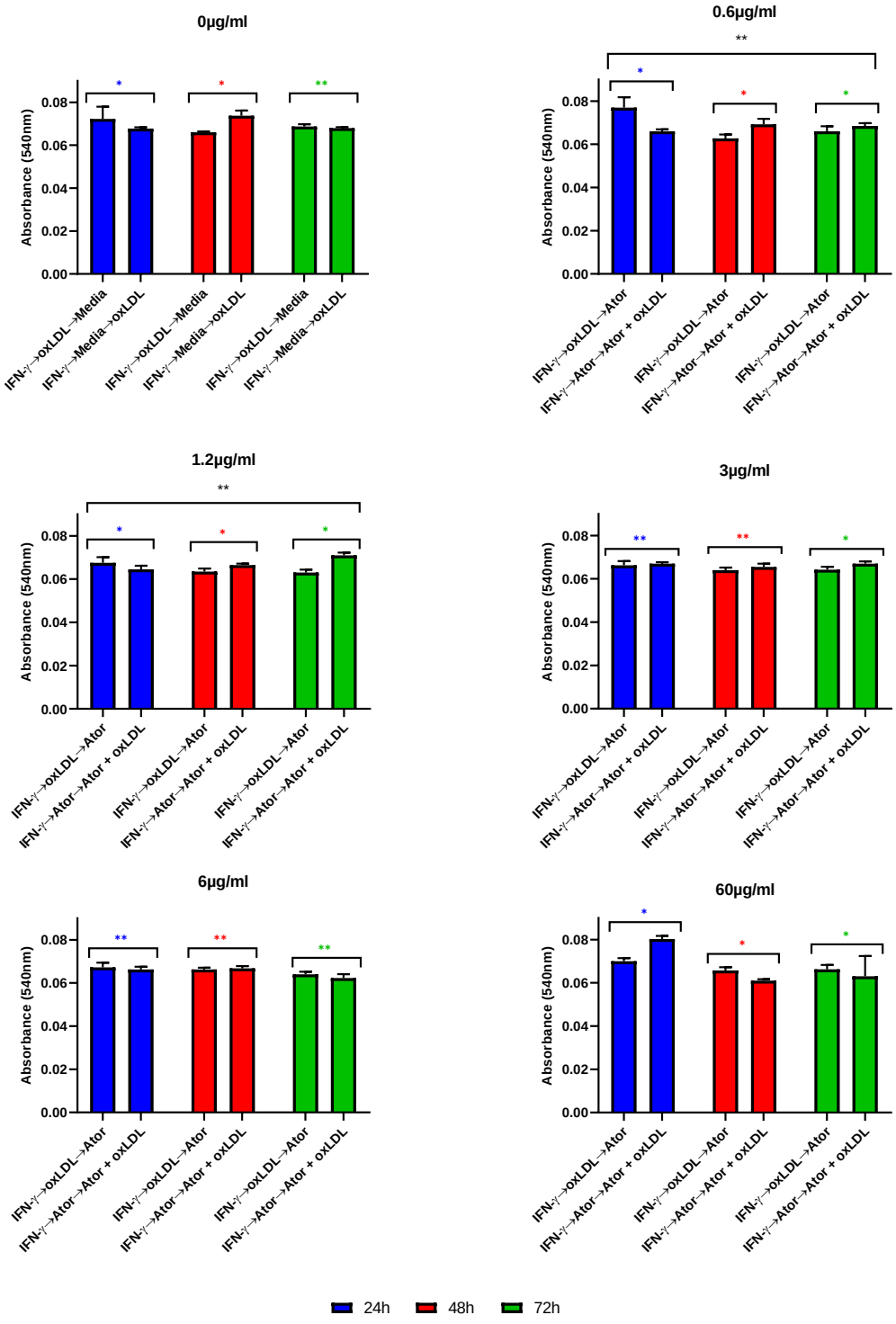

Figure 6-13: Effect of different doses of atorvastatin on OxLDL uptake over time: Extent of oxLDL uptake was evaluated using Oil Red-O staining. One set of samples was first incubated with IFN-γ, followed by oxLDL then atorvastatin (IFN-γ→oxLDL→Ator). The other set was first incubated with IFN-γ, then atorvastatin, then a combination of atorvastatin and oxLDL (IFN-γ→Ator→Ator + oxLDL). Samples were then cultured for 24, 48 and 72 hours. Statistical analysis was done using one-sample t-and Wilcoxon test, significance was identified for each time point i.e., 24h, 48h, and 72h ((0µg/ml; p = 0.0205 *, 0.0353 * and 0.0035 **), (0.6µg/ml; p = 0.0489 *, 0.0313 *, 0.0118 *) (1.2µg/ml; p = 0.0145 *, 0.0147 * and 0.0380 *) (3µg/ml; p = 0.0036 **, 0.0074 ** and 0.0133 *) (6µg/ml; p = 0.0048 **, 0.0024 **, and 0.0088 **) (60µg/ml; p = 0.0434 *, 0.0238 *, and 0.0160 *). Additional significance was also identified using two-way ANOVA for the interaction between mode of stimulation and time for 0.6µg/ml atorvastatin (p = 0.0013 **) and 1.2µg/ml (p = 0.0033). N=4.

From the data represented in figure 6-13, the dose that provided the most consistent reduction in amount of internalised oxLDL over time is 6µg/ml, which had little variation between modes of stimulation i.e., there was no significant difference between whether atorvastatin or oxLDL was added first, compared to the drug free control and other doses. This dose also demonstrated progressive lowering over time, with the 72-hour incubation showing the greatest reduction for this dose. Statistical significance for this dose was found between time points, suggesting that mode of administration of atorvastatin was not a determining factor in reducing amount of internalised lipid but instead the selected dose. For the other doses tested, peak effectiveness appears to be after 48 hours, with addition of atorvastatin after oxLDL proving the most effective at lowering internalised oxLDL.

It should also be noted that pre-treatment with atorvastatin before addition of oxLDL showed a greater reduction in amounts of internalised oxLDL after 72 hours only in the higher doses of atorvastatin (6µg/ml and 60µg/ml), with 60µg/ml showing the largest variation between pre-treatment with atorvastatin versus treatment after oxLDL addition. 3µg/ml appears to have a similar trend to 6µg/ml, however, given the lack of statistical significance, subsequent experiments were carried out with 6µg/ml.

6.1.12.4 NO production

The findings in figure 6-7 show the effect on the selected polarization stimulants on NO production, with LPS showing the greatest effect on NO production by RAW264. The effect of atorvastatin on NO production on stimulated RAW264 cells is detailed in figure 6-14. Stimulations were done as detailed in section 6.3.1.4.1 with atorvastatin being added either after the stimulations or at the same time as the stimulants.

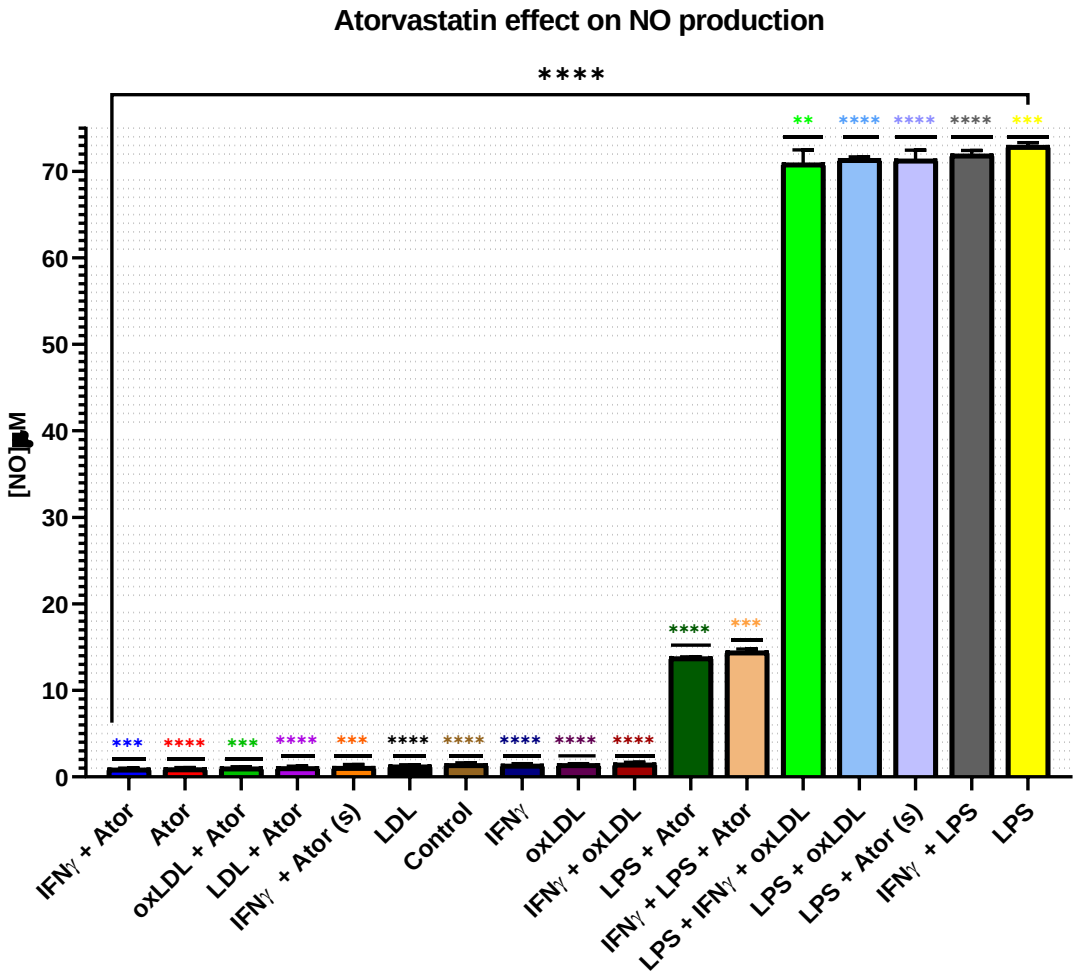

Figure 6-14: Atorvastatin effect on NO production after LPS and IFN-γ stimulation. (s) denotes samples where atorvastatin was added at the same time as the stimulant. In all other cases, atorvastatin was added after addition of either LPS or IFN-γ, or LPS and IFN-γ, or oxLDL or LDL. Statistical analysis was done using one sample t-and Wilcoxon test, significance was identified per variable (IFN-γ + Ator, p = 0.0002 ***; Ator, p <0.0001 ****; oxLDL + Ator, p = 0.0002 ***; LDL + Ator, p <0.0001 ****; IFN-γ + Ator (s), p = 0.0001 ***; LDL, p <0.0001 ****; control, p <0.0001****; IFN-γ, p <0.0001****; oxLDL, p <0.0001****; IFN-γ + oxLDL, p <0.0001****; LPS + Ator, p <0.0001****; IFN-γ + LPS + Ator, p = 0.0002 ***; LPS + IFN-γ + oxLDL, p = 0.0094 **; LPS + oxLDL, p <0.0001****; LPS + Ator (s), p <0.0001****; IFN-γ + LPS, p <0.0001****; LPS, p = 0.0005 ***). Two-way ANOVA also identified significance between all the variables (p <0.0001). N=5.

The data in figure 6-14 shows that atorvastatin has a negative effect on NO production by RAW264, especially when added after removal of the stimulants, suggesting a reversal of NO production triggered by LPS and IFN-γ either separately or in conjunction, thus implying that atorvastatin is a stronger inhibitor of NO production in inflammatory macrophages. This is also observed when only LDL or oxLDL are used as stimulants followed by the addition of atorvastatin. When atorvastatin is added simultaneously with either LPS or IFN-γ, there is also an observable reduction in [NO] but this is not as significant as the reduction observed after removal of the stimulants prior to addition of atorvastatin.

LPS also demonstrates the strongest capacity to stimulate NO production in RAW264, and also to limit the effect observed with atorvastatin.

6.1.13 The effect of HUVEC co-culture on foam cell models

After determining RAW264 responses to atorvastatin, the selected dose, 6µg/ml, was used in conjunction with HUVECs. In summation, RAW264 cells were either stimulated with 100ng/ml IFN-γ for 24 hours followed by a 24-hour incubation with oxLDL or just incubated with oxLDL for 24 hours. Following these stimulations, HUVECs seeded on nanofiber well inserts, at a density of 4 x 10^4 cells per insert, were placed atop the seeded RAW cells (figure 6-15). The nature of the insert allowed the use of individual cell media i.e., HUVECs were cultured with medium 200 supplemented with 2% LSGS while RAW264 were cultured with DMEM supplemented with 10% FBS, 1% LG and 1% AA. HUVECs were either lesioned with $FeCl_3$ or left intact. Atorvastatin treatment was also included for both lesioned and intact HUVECs and for both IFN-γ stimulated and unstimulated RAW264 cells. The $FeCl_3$ lesion was created by adding 0.2µl the solution to a 1mm^2 piece of filter paper, which was then placed on the HUVEC layer for 1 minute, followed by a PBS wash. The co-culture system was incubated at 37°C/5%CO_2 for 24 hours. Co-culture combinations are detailed in figure 6-16. NO readings were taken after final incubation and compared to control samples. Nile red imaging was done with both FITC and Texas red excitation on the confocal microscope. Oil red-O quantification was also carried out as previously described.

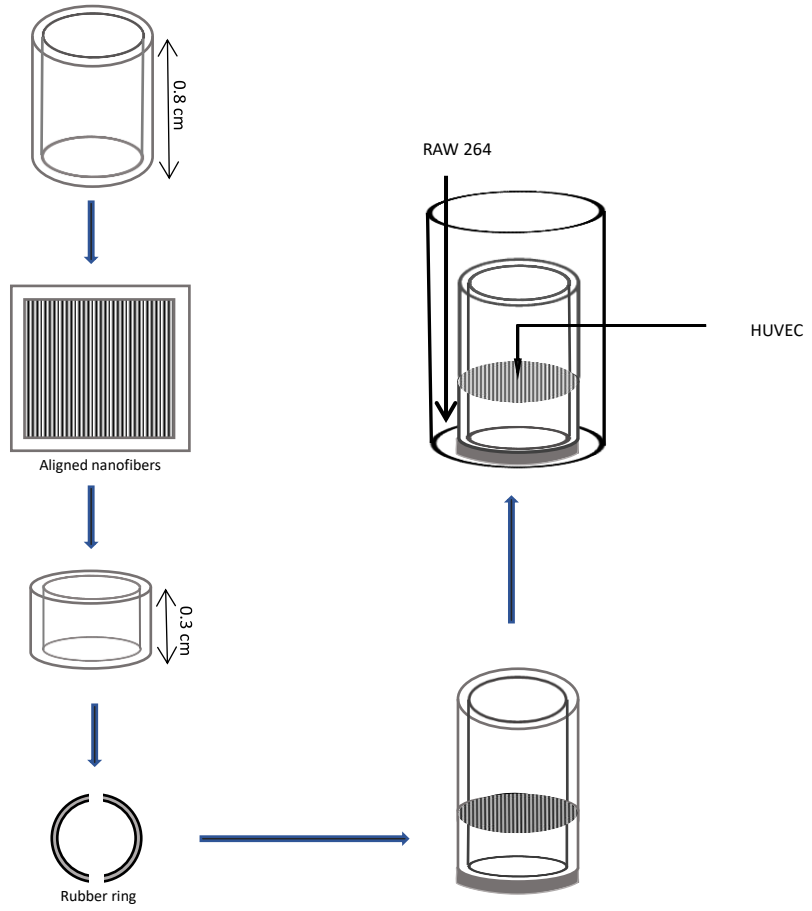

Figure 6-15: Nanofiber well insert assembly. The customised rings were fused together with the aligned nanofibers between. A split rubber ring was affixed to the bottom portion of the insert. After sterilisation, HUVECs are seeded onto the fibronectin coated nanofibers. The completed insert is placed inside a 24 well plate well seeded with RAW 264.

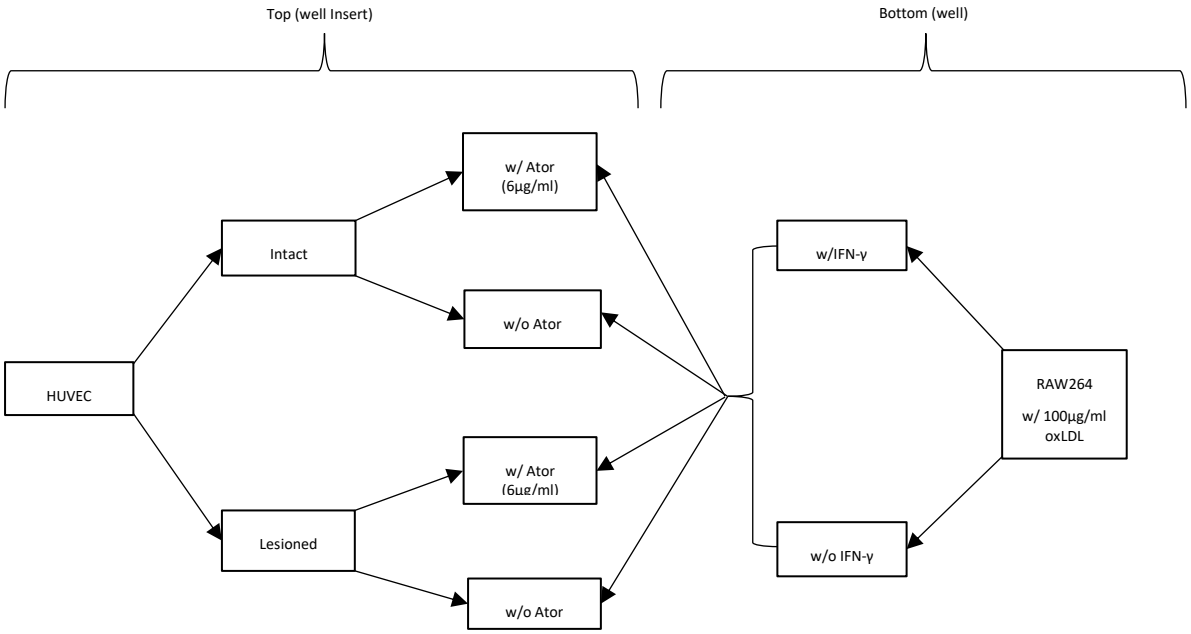

Figure 6-16: Flow chart of co-culture conditions. HUVECs were either lesioned or left intact and each group was cultured either with or without 6µg/ml atorvastatin. The HUVECs were then added to RAW264 either stimulated or unstimulated with IFN-γ. All RAW264 cells were cultured with 100µg/ml oxLDL.

6.1.13.1 HUVEC and Atorvastatin effect on oxLDL uptake

Extent of oxLDL uptake is visualised in figure 6-17 and 6-18. Representative images are overlays of green (495nm) and red (604nm). Yellow-gold represents internalised lipid, red denotes primarily membrane staining. The use of co-excitation was selected here as it provides a clearer distinction between membrane lipids versus internalised lipid, allowing better elucidation of the effect HUVECs and/or atorvastatin have on cholesterol efflux.

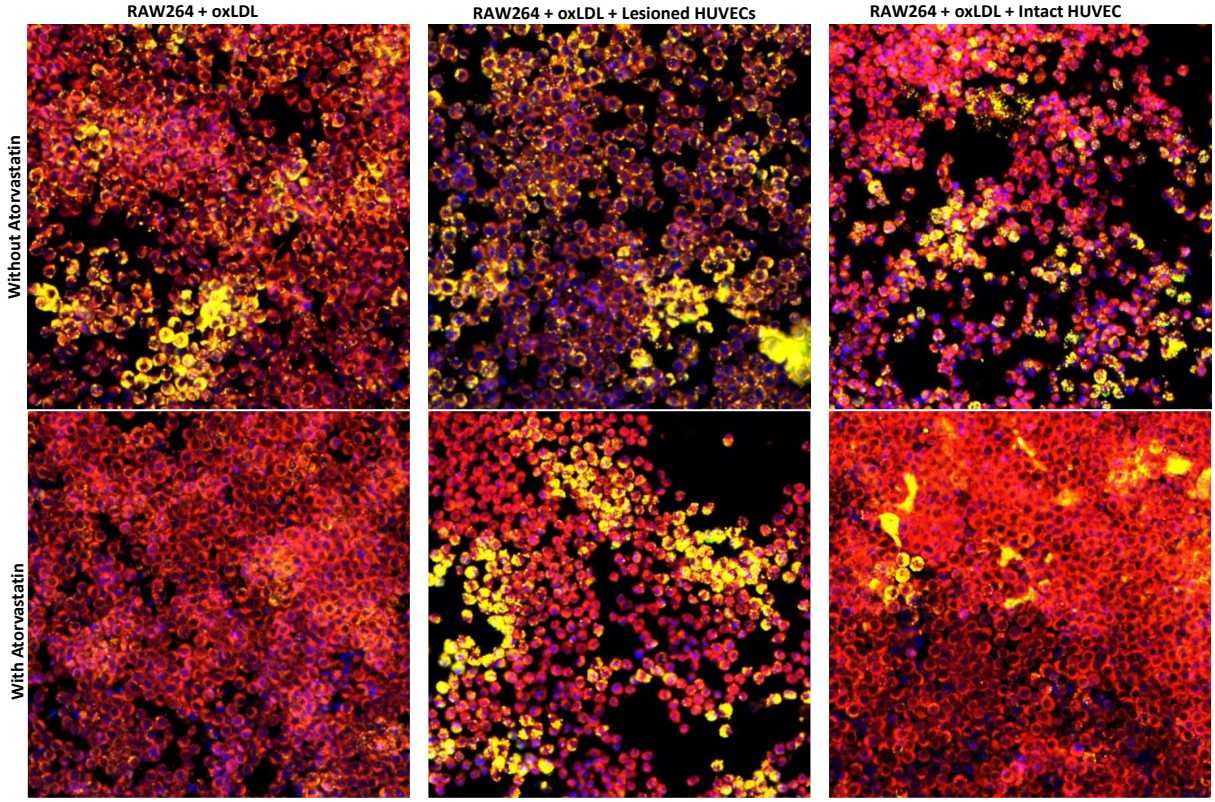

Figure 6-17: Qualitative evaluation of oxLDL uptake with IFN-γ stimulation. Images are of RAW264 cells co-cultured with HUVECs either with or without a lesion and either with or without 6µg/ml atorvastatin. RAW264 were all stimulated with IFN-γ for 24h followed by a further 24h incubation with 100µg/ml oxLDL. All images taken at 40x. Nile red, Nile red, DAPI.

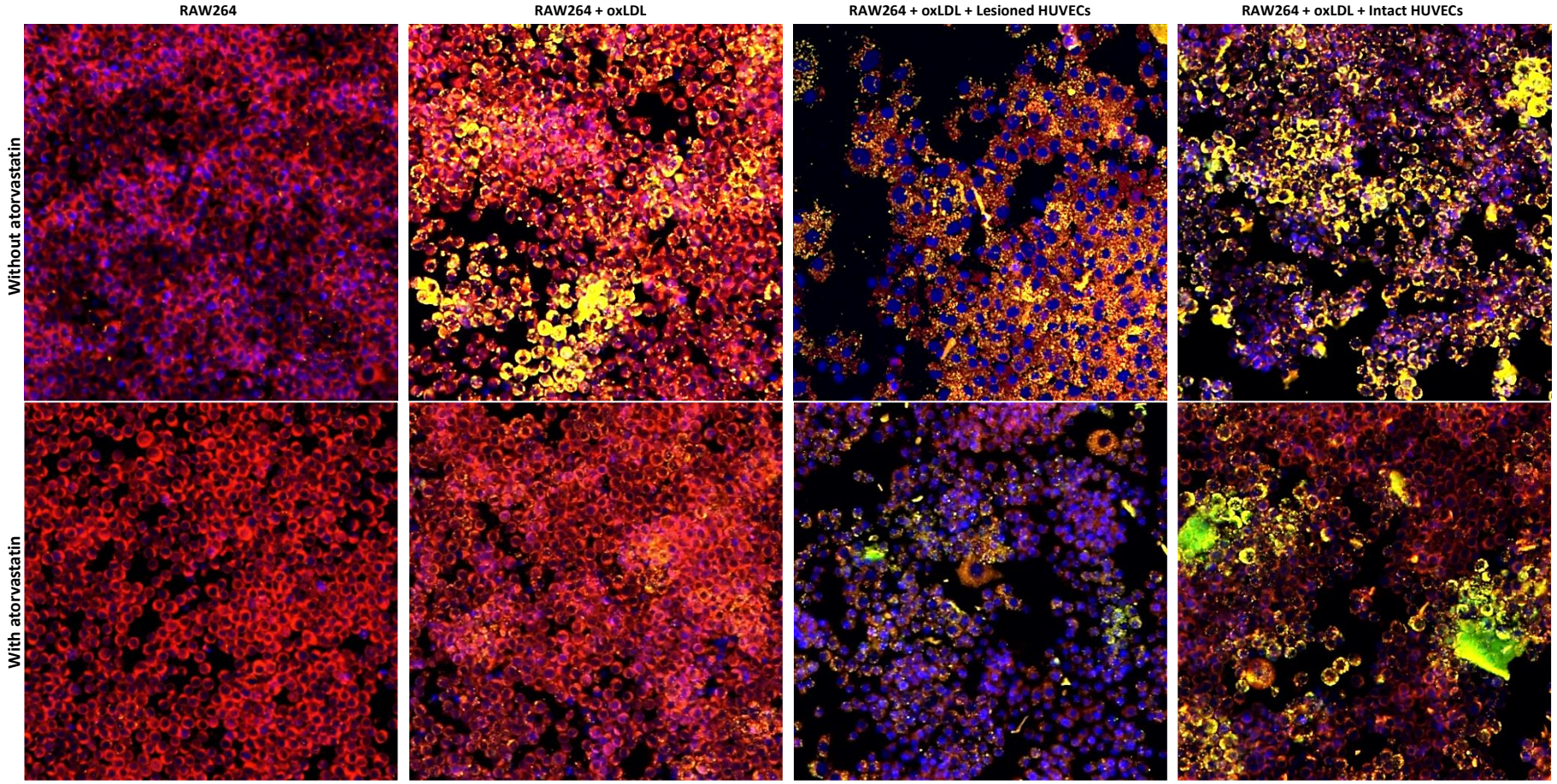

Figure 6-18: Qualitative evaluation of oxLDL uptake without IFN-γ stimulation. Images are of RAW264 cells co-cultured with HUVECs either with or without a lesion and either with or without 6µg/ml atorvastatin. RAW264 were only incubated with 100µg/ml oxLDL for 24h before addition of HUVEC seeded inserts. All images taken at 40x. Nile red, Nile red, DAPI.

From both figure 6-17 and 6-18, internalised oxLDL generates a strong yellow-gold colouration, with only a faint yellow tinge on the membrane observed in the presence of atorvastatin. Samples without both oxLDL and atorvastatin display a redder colouration. The alteration of membrane colouration from a red to a yellow-red colour in the presence of atorvastatin could be a result of lipid content being transferred to the extracellular space (cholesterol efflux), resulting in a blending of the stronger red and yellow-gold. This colour blending is more observable in the IFN-γ treated samples than the untreated ones. In figure 6-17, the RAW264 cells cultured with lesioned HUVECs and without atorvastatin have a redder membrane stain than the same group without IFN-γ, suggesting IFN-γ promotes retention of internalised lipid. A comparison of the same group without IFN-γ (figure 6-18) further shows the effect of IFN-γ on retention of internalised lipid i.e., blocking cholesterol efflux, as the cells imaged show far less yellow-gold staining, as well as less distinct red membrane staining, than the IFN-γ stimulated group. In the presence of IFN-γ, intact HUVECs appear to exert some protective effect on the maintenance of internalised lipid i.e., these samples appear to have fewer lipid droplets visible after 24 hours than those cultured with lesioned HUVECs. The presence of atorvastatin distinctly limits maintenance of internalised lipid as shown in both figure 6-17 and 6-18. The use of dual excitation/emission shows its value here, compared to earlier images that just show red, in that it's far easier to distinguish internalised lipid from membrane lipid content as well as giving an impression of lipid localisation between the inner and outer sections of the cell.

6.1.13.2 NO production

Following the protocol described in section 2.1.16, the effect of atorvastatin, IFN-γ and oxLDL stimulation on NO production was determined, and results are detailed in figure 6-19. HUVECs were stimulated with 100ng/ml IFN-γ and readings were taken after 24 hours. RAW264 were stimulated with either IFN-γ or oxLDL for 24 hours then analysed, or first stimulated with IFN-γ (24h) followed by a further 24-hour incubation with oxLDL before readings were taken. Cells here were not used in the co-culture system but cultured separately.

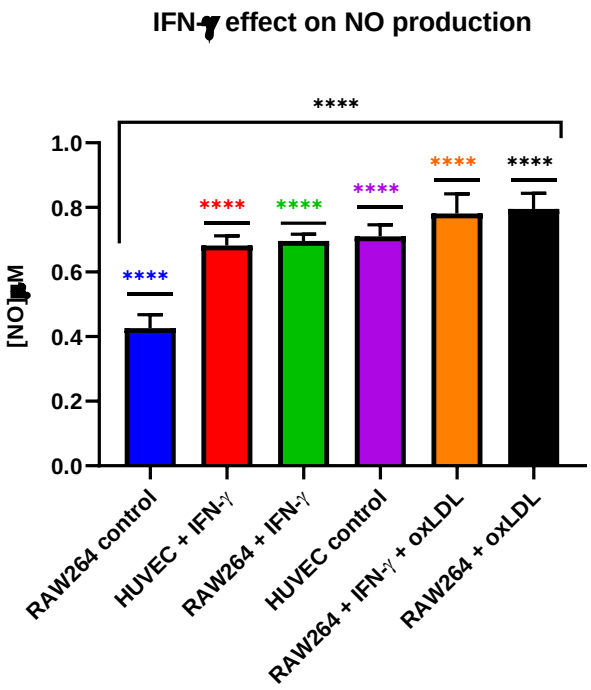

Figure 6-19: IFN-γ effect on NO production. The data represented here shows the impact of IFN-γ on the production of NO in HUVECs and RAW264. IFN-γ does trigger NO production in both cell types, but oxLDL has a stronger effect on NO production than IFN-γ alone, or IFN-γ in combination with oxLDL. Statistical analysis was done using both one sample t-and Wilcoxon test, and two-way ANOVA, with significance identified both for, and between the variables ($p < 0.0001$ **** for each variable analysis. N=8.

OxLDL has the strongest effect on RAW264 NO production, with IFN-γ stimulation also triggering an increase in NO production. IFN-γ had the opposite effect on HUVECs i.e., stimulation resulted in a reduction in NO production.

6.1.13.2.1 Atorvastatin effect on NO production

As detailed previously, RAW264 cells were stimulated with IFN-γ for 24 hours after which they were incubated with oxLDL for 24 hours, then co-cultured with either lesioned or intact HUVECs and either with or without atorvastatin as detailed in figure 6-16. Atorvastatin incubation was carried out for a further 24 hours, whereupon the media was collected and tested for NO. Media was collected from both the HUVEC insert and the RAW264 portion of the co-culture system (figure 6-15). Data collected is represented in figure 6-20 and 6-21.

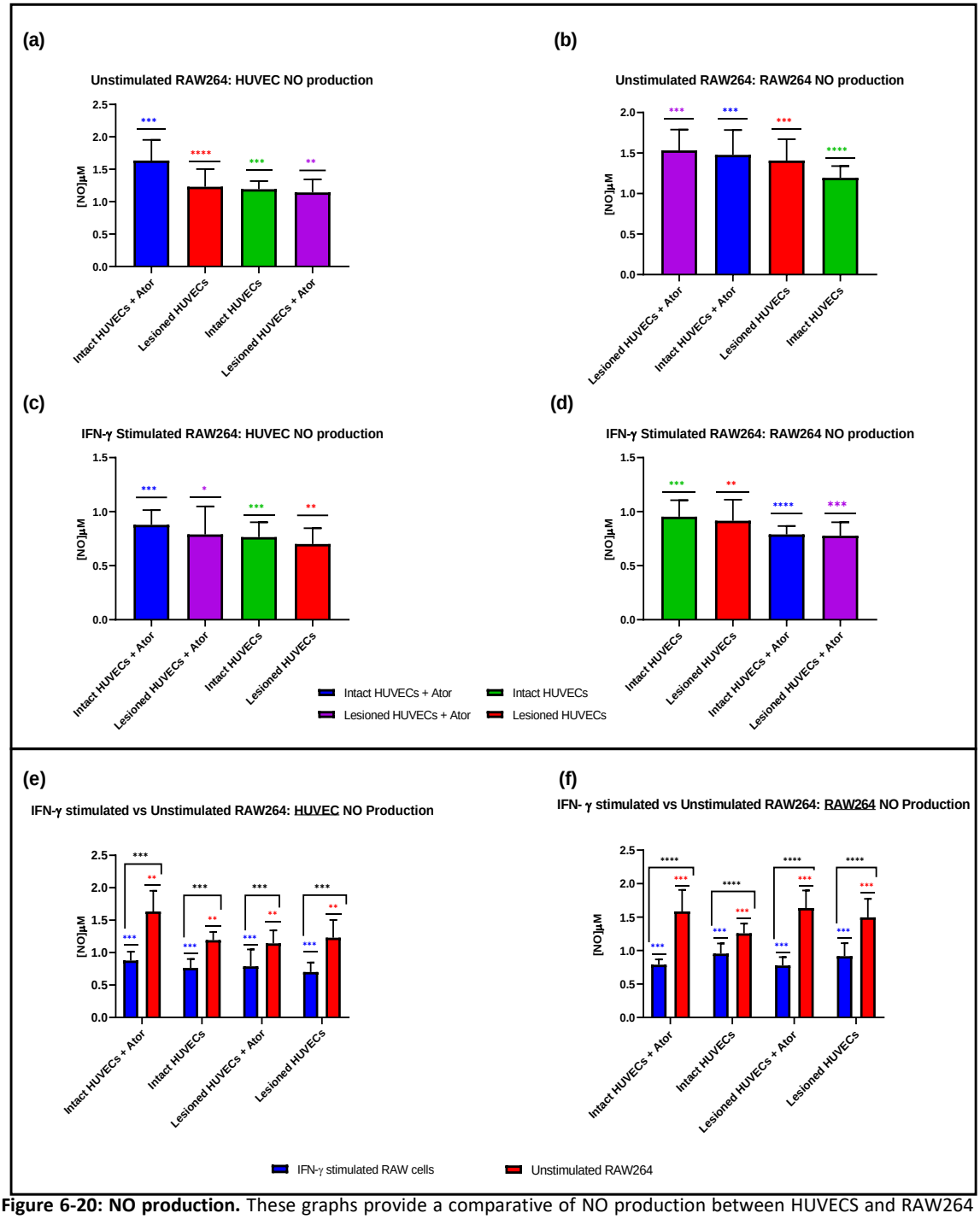

Figure 6-20: NO production. These graphs provide a comparative of NO production between HUVECS and RAW264 as well as the effect of IFN-γ stimulation on NO production in both HUVECs and RAW264. **(a)** compares NO production in lesioned and intact HUVECs cultured with unstimulated RAW264; media collected from HUVEC well insert. **(b)** compares NO production for unstimulated RAW264 cultured with HUVECs from **(a)**. **(c)** compares NO production in lesioned and intact HUVECs cultured with IFN-γ stimulated RAW264; media collected from HUVEC well insert. **(d)** compares NO production for IFN-γ stimulated RAW264 cultured with HUVECs from **(c)**. **(e)** is a combination of **(a)** and **(c)** comparing effect of IFN-γ on NO production in HUVECs. **(f)** is a combination of (b) and **(d)** comparing effect of IFN-γ on NO production in RAW264. Statistical significance was determined through one sample t-and Wilcoxon test, and significance identified per variable i.e., lesioned and intact HUVECS, with and without atorvastatin (**(a)** p = 0.0009 ***, <0.0001 ****, 0.0005 ***, 0.0019 *; **(b)** p = 0.0002 ***, 0.0009 ***, 0.0005 ***; <0.0001 ****; **(c)** p = 0.0002 ***, 0.0159 *, 0.0005 ***, 0.0013**; **(d)** p = 0.0002 ***, 0.0016 **, <0.0001 ****, 0.0003 ***; **(e)** p = 0.0002 ***, 0.0014 **; **(f)** p = 0.0003 ***, ***). Additional significance was identified through two-way ANOVA, between IFN-γ stimulated vs. unstimulated RAW264, for plot **(e)** and **(f)** (p = 0.0009 and <0.0001 respectively).

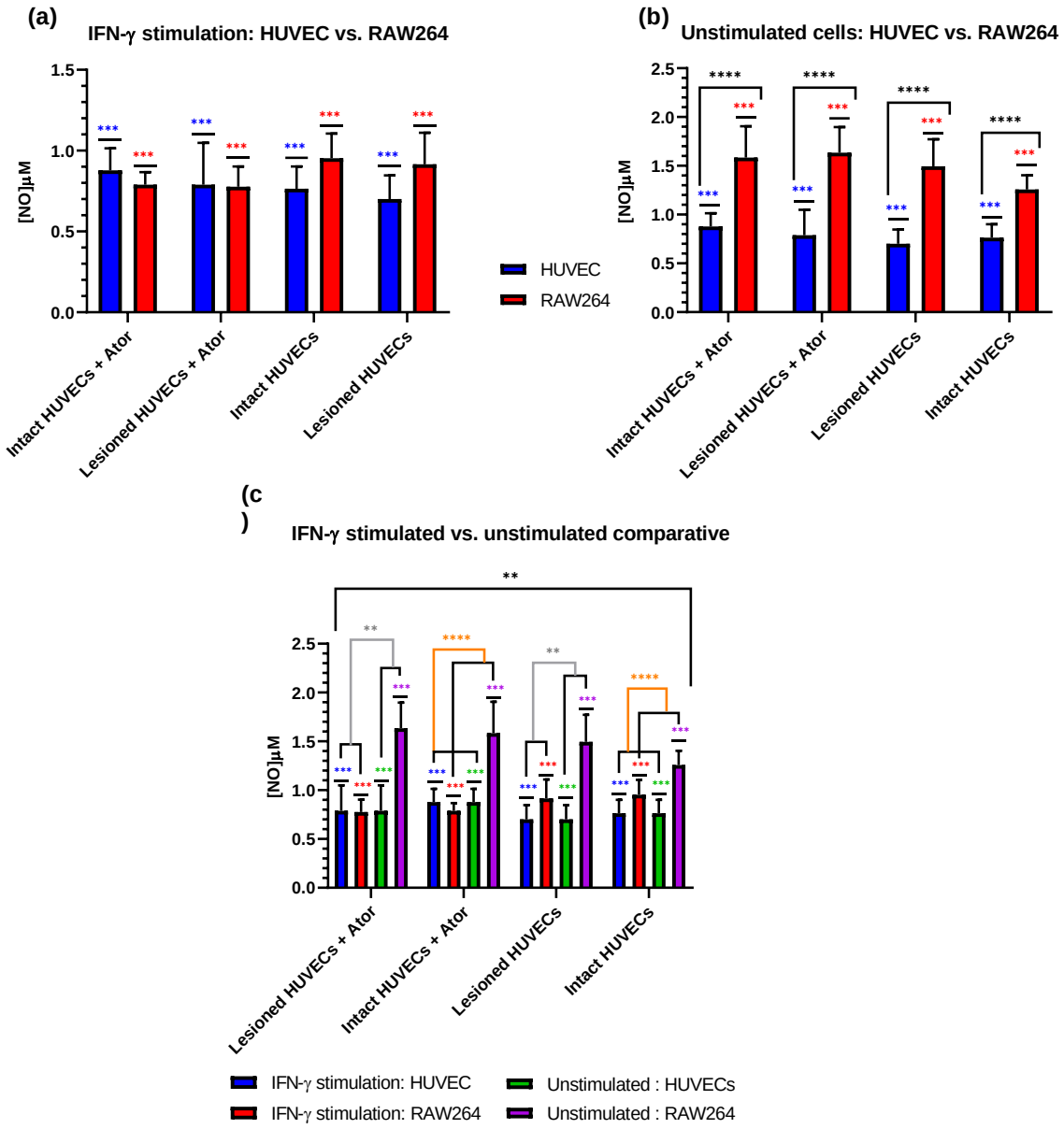

Figure 6-21: Cell comparative between IFN-γ stimulated and unstimulated HUVECs and RAW264. (a) compares NO production between HUVECs and RAW264, when RAW264 have been stimulated with IFN-γ. **(b)** compares NO production between HUVECs and RAW264 when RAW264 were not stimulated with IFN-γ. **(c)** is a comparative of **(a)** and **(b)**. Statistical significance was determined using one sample t-and Wilcoxon test, with significance identified for HUVECs and RAW264, both with and without IFN-γ stimulation (**(a)** p = 0.0002 *** (HUVEC); p = 0.0003 *** (RAW264); **(b)** p = 0.0002 *** (HUVEC); p = 0.0004 *** (RAW264); **(c)** p = 0.0002 *** (IFN-γ stimulated HUVEC); p = 0.0003 *** (IFN-γ stimulated RAW264); p = 0.0002 *** (unstimulated HUVEC); p = 0.0004 *** (unstimulated RAW264). Two-way ANOVA was carried out for all the data sets, no significance was identified for the data represented in **(a)**, significance was identified for the interaction between HUVECs and RAW264 in **(b)** (p <0.0001). Three-way ANOVA was also carried out for the data represented in **(c),** with significance identified between IFN-γ stimulated HUVECs and RAW264 (p = 0.0014 **), Unstimulated HUVEC and RAW264 (p = 0.0014 **), IFN-γ stimulated and unstimulated RAW264 (p <0.0001 ****), IFN-γ stimulated and unstimulated HUVECs (p <0.0001 ****), and the interaction between IFN-γ stimulated versus unstimulated cells (p = 0.0014 **). N=9

An evaluation of figure 6-20 and 6-21 shows that the concentration of IFN-γ used here attenuates production of NO across both cell types, but more so in HUVECs, and to a lesser extent when atorvastatin is included in culture. RAW cells appear to produce more nitric oxide when cultured with lesioned HUVECs, especially in the absence of IFN-γ stimulation, and in the presence of atorvastatin (figure 6-21). As expected, intact HUVECs have a better NO production profile in general than lesioned HUVECs and atorvastatin appears to ameliorate the limiting effect of IFN-γ observed. The data in figure 6-19 also support the observation that the selected concentration of IFN-γ used is not as effective a stimulator of NO production as oxLDL, especially on RAW264 cells and may not have fully pushed RAW264 cells to an M1 phenotype. Statistical significance for figure 6-21 (b) was found between RAW264 and HUVEC NO production but not between the lesioned and intact groups, either with or without atorvastatin. In figure 6-21 (c) significance was found between IFN-γ stimulated and unstimulated cells and again not between the lesioned and intact groups, either with or without atorvastatin. These analyses suggest that the more significant contributor to these differences observed is the inclusion of IFN-γ, rather than lesioning HUVECs or the inclusion of atorvastatin.

6.1.14 Cholesterol efflux

As described previously, oil red-O was used to quantify extent of lipid uptake with and without atorvastatin and IFN-γ stimulation. This method was used exclusively on RAW264. These cells were those used in co-culture with HUVECs as described in section 6.2.9 and 6.3.1.6 and figure 6-16. Briefly, fixed cells were first stained with oil red-O, after which the excess dye was removed, followed by extraction of bound oil red-O from the cells using isopropanol. The absorbance was read at 540nm and these readings were used to estimate extent of lipid uptake. Figure 6-22 details these findings.

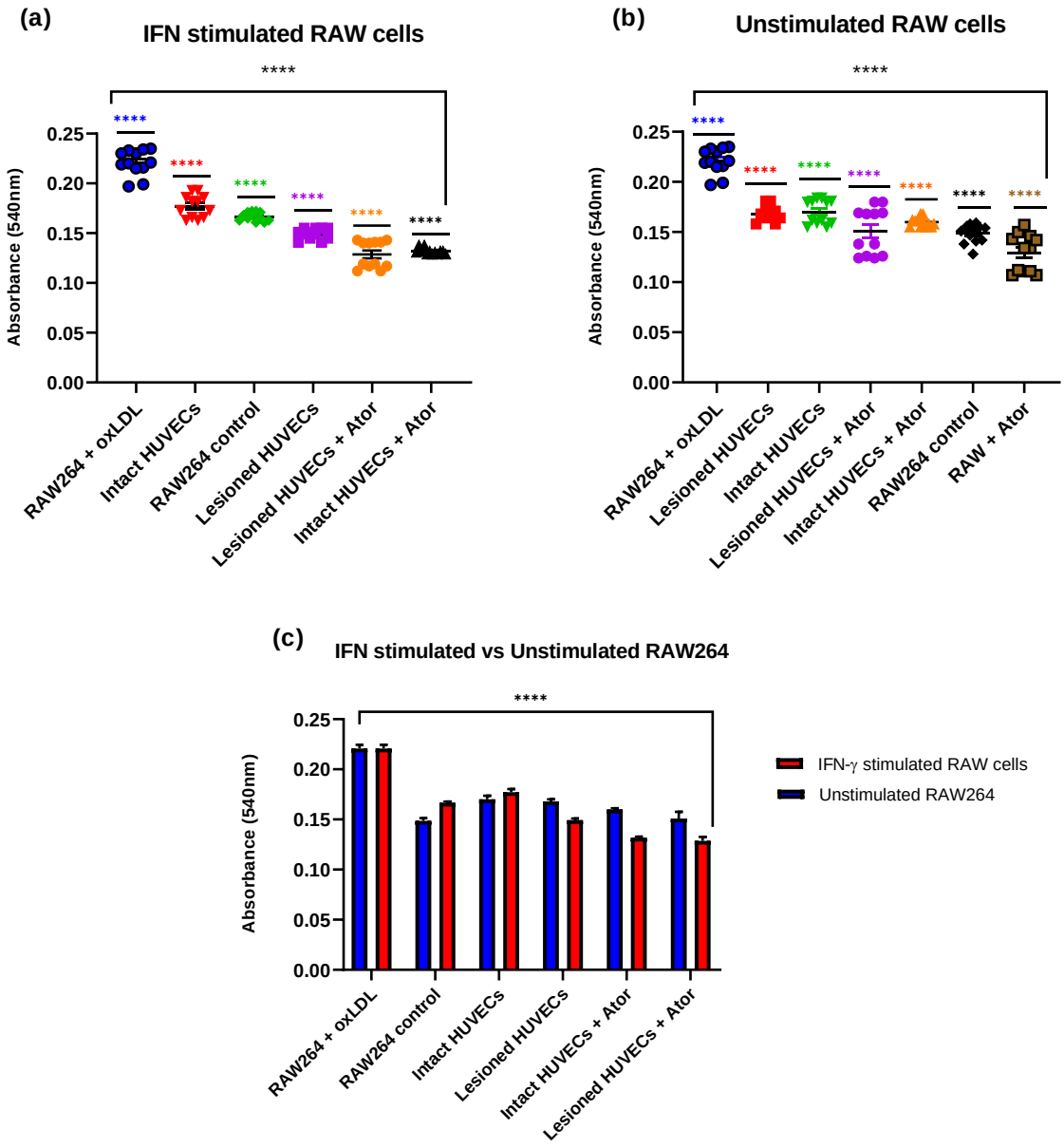

Figure 6-22: Co-culture oxLDL quantification. (a) oxLDL uptake in IFN-γ stimulated RAW264. **(b)** oxLDL uptake in unstimulated RAW264. **(c)** comparative between IFN-γ stimulation and no stimulation on oxLDL uptake in RAW264 cultured with lesioned and intact HUVECs and either with or without atorvastatin. One-way and two-way ANOVA, as well as one sample t-and Wilcoxon tests were carried out and they all showed significance for each variable, as well as between variables, and all having $p < 0.0001$ ****. N=12.

The findings in figure 6-22 demonstrate that atorvastatin inclusion results in a reduction of internalised lipids i.e., atorvastatin triggers cholesterol efflux. Both with and without IFN-γ stimulation, RAW264 cells show a distinct reduction in amounts of quantifiable oxLDL in the presence of atorvastatin. The

RAW264 controls were not incubated with any oxLDL, and their absorbance readings suggest there is a baseline amount of internalised lipid, likely obtained from FBS content in culture media. This lipid content is also affected by the presence of atorvastatin, given that samples not treated with oxLDL, followed by treatment with atorvastatin, showed lower absorbance values than the control. These findings also suggest that lesioned HUVECs are also able to marginally promote cholesterol efflux, both with and without atorvastatin, as the absorbance values are consistently lower than with intact HUVECs, especially in the presence of IFN-γ. Statistical analysis identified significance between the inclusion or exclusion of IFN-γ (figure 6-22 (c)), lesioned and intact HUVECs (figure 6-22 (a, b)), as well as the presence of atorvastatin (figure 6-22 (a, b and c)), suggesting an interaction of these factors in the uptake/efflux of oxLDL in RAW264, with each factor contributing in one way or another.

6.1.15 Immunostaining

Immunostaining was carried out to track the expression of CD36 and CD146. Briefly, the primary antibody was added to the samples following a 1-hour incubation with 5% BSA. 1° antibody was incubated with the sample for 2-hours at 37°C/5% CO_2. After 1° incubation, samples were washed twice each with 0.05% Tween20 and PBS. This was followed by a 1-hour incubation with the 2° antibody also at 37°C/5% CO_2. Two 0.05% Tween20 and two PBS washes followed. DAPI was then added to the samples and incubated for 10 minutes, followed by three PBS washes. Negative control samples were only incubated with the secondary antibody and DAPI for the same duration and without the BSA blocking stage. Representative images of staining, taken with a confocal microscope, are shown in figure 6-23 to 26.

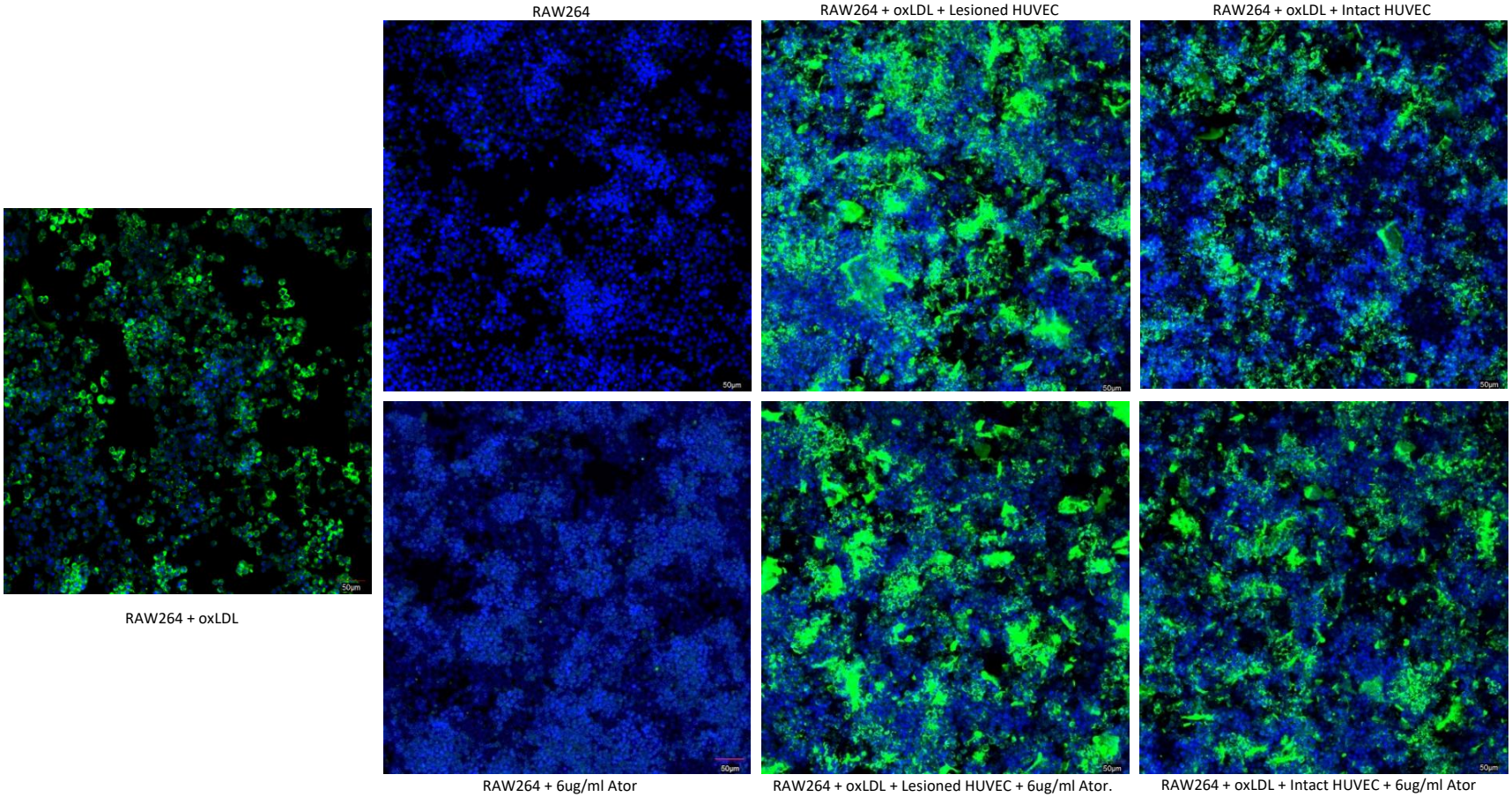

Figure 6-23: Unstimulated RAW264 CD36 staining. Samples used were RAW264 cells co-cultured with lesioned or intact HUVECs, either with or without atorvastatin. Images taken at 20x magnification. DAPI; CD36

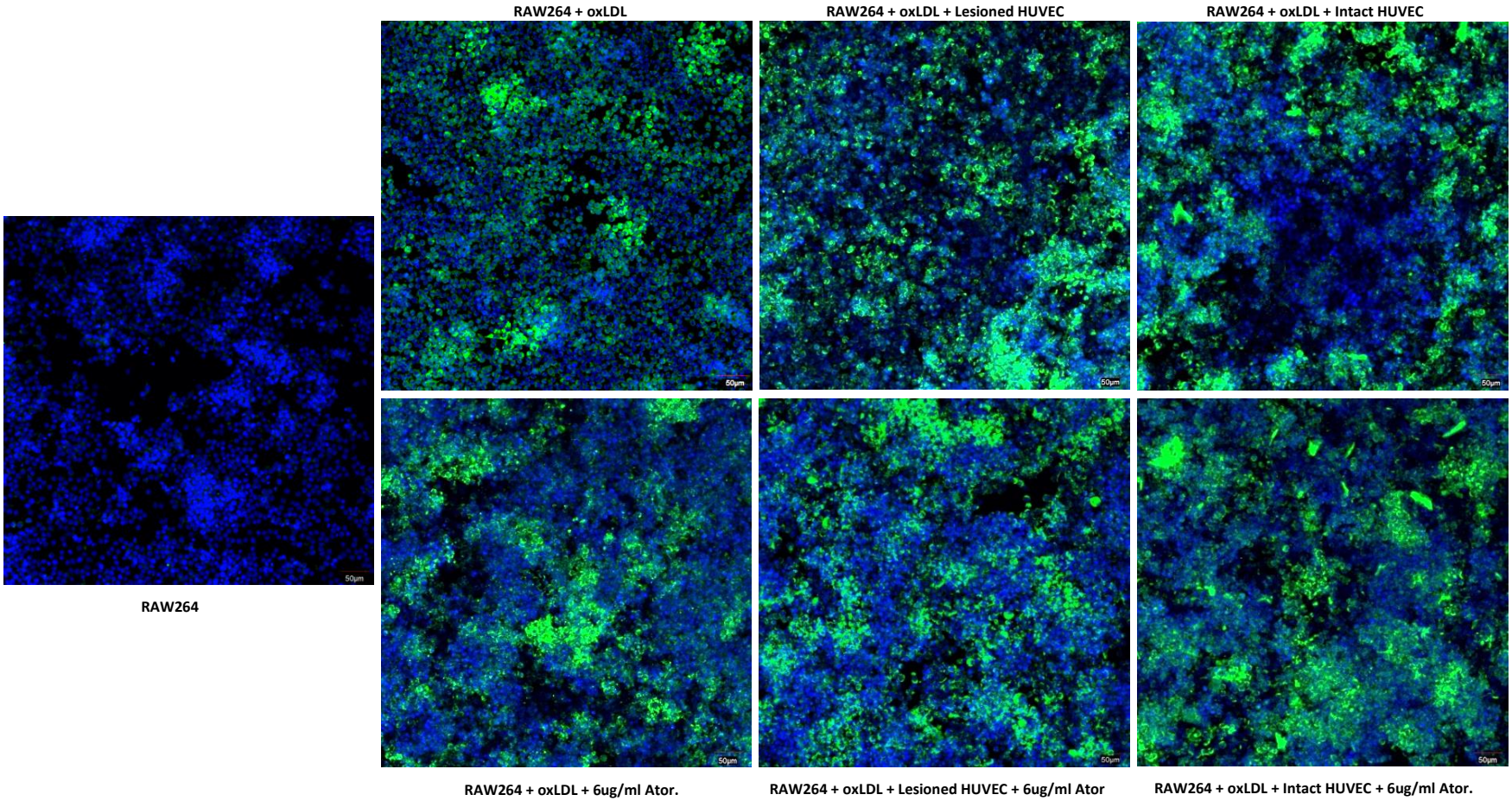

Figure 6-24: IFN-γ stimulated RAW264 CD36 staining. Samples used were RAW264 cells co-cultured with lesioned or intact HUVECs, either with or without atorvastatin. All images taken at 20x. DAPI; CD36

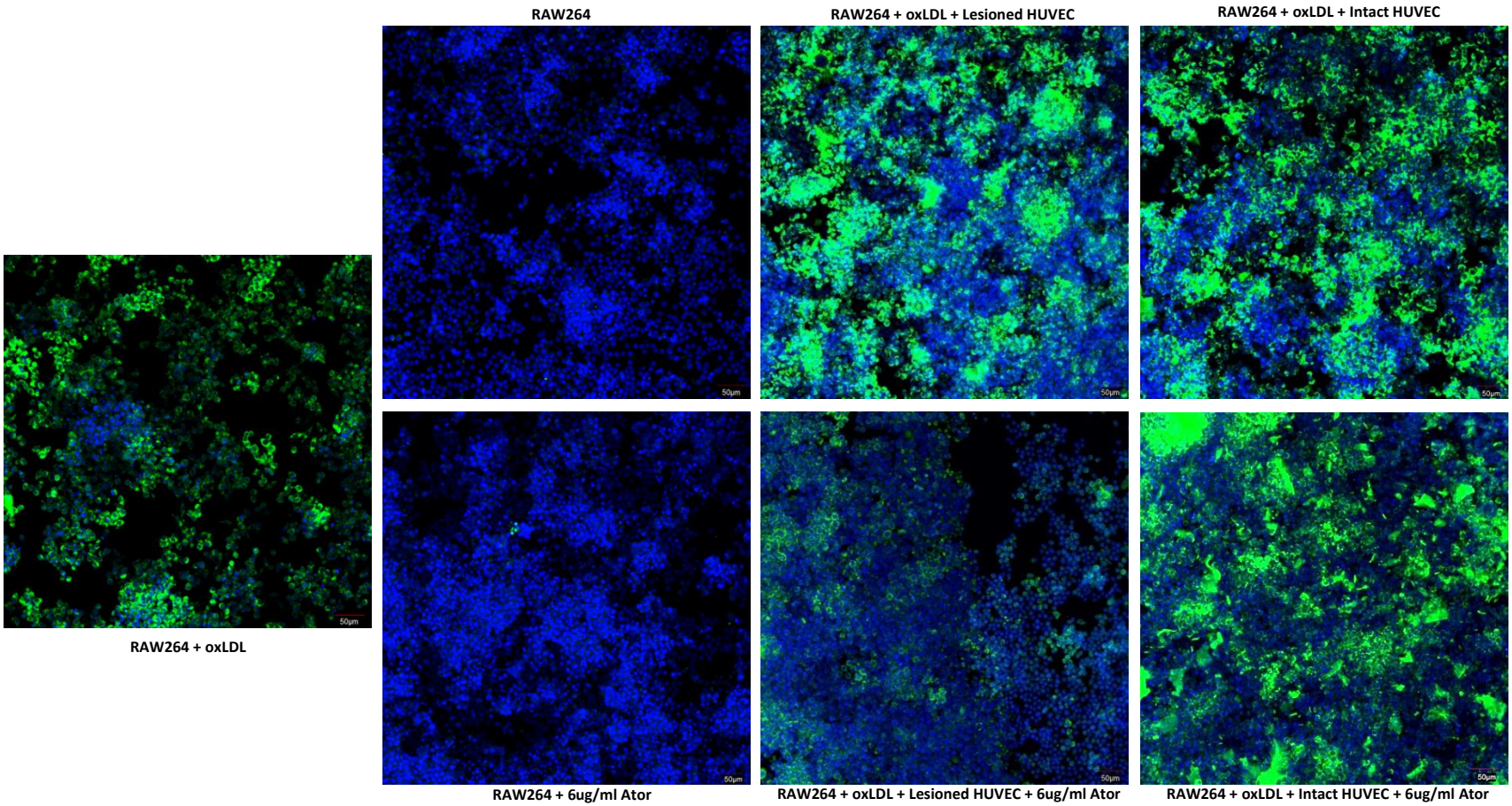

Figure 6-25: Unstimulated RAW264 CD146 staining. Samples used were RAW264 cells co-cultured with lesioned or intact HUVECs, either with or without atorvastatin. All images taken at 20x. DAPI; CD146.

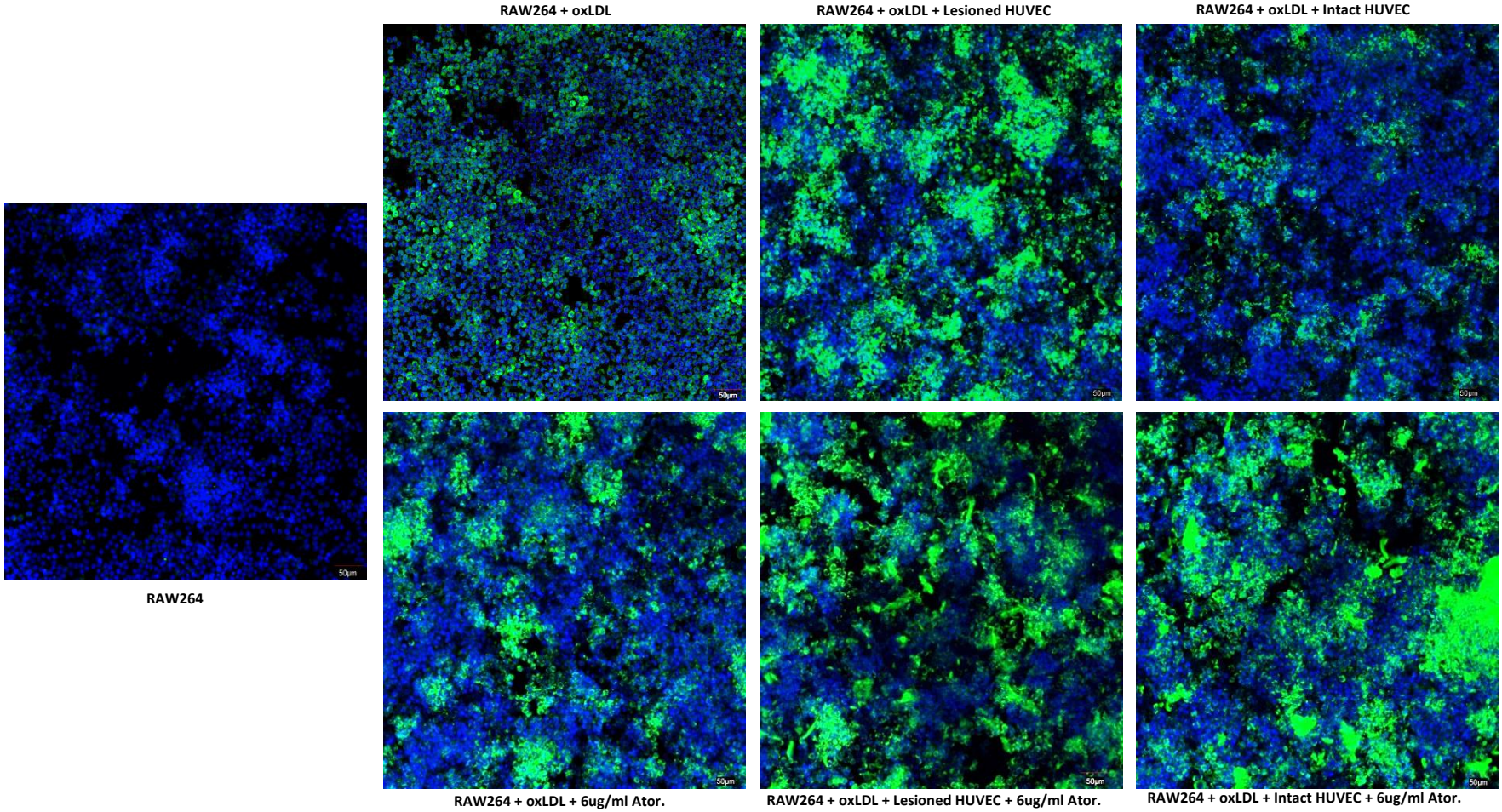

Figure 6-26: IFN-γ stimulated RAW264 CD146 staining. Samples used were RAW264 cells co-cultured with lesioned or intact HUVECs, either with or without atorvastatin. All images taken at 20x. DAPI; CD146.

Looking at figure 6-23, the expression of CD36 is triggered by the presence of oxLDL, and appears to be enhanced with atorvastatin, with no visually obvious difference between IFN-γ stimulated (figure 6-24) or unstimulated (figure 6-23) RAW264 cells. Lesioned HUVECs also appear to have a positive impact on CD36 expression when compared to intact HUVECs without atorvastatin. For the IFN-γ stimulated cells, CD36 expression seems elevated in samples co-cultured with lesioned HUVECs, with a slight reduction in the atorvastatin treated lesioned HUVEC co-culture. CD146 on the other hand, seems to be influenced by IFN-γ stimulation in that unstimulated samples (figure 6-25) showed an apparent reduction in extent of CD146 expression when atorvastatin was added, while those stimulated with IFN-γ (figure 6-26) show the opposite i.e., a stronger expression of CD146. Given the absence of a positive signal in samples not exposed to oxLDL, this suggests that the staining protocol was successful and only specific for the targeted receptors, which are selectively expressed on macrophages exposed to oxLDL.

6.1.16 3D atherosclerosis plaque model: Foam cells in plastically compressed collagen

After evaluating RAW264 behaviour in a 2D environment, the same was attempted for 3D culture. The selected density of cells i.e., 2.5 x 10^5, were seeded either individually or together with HCASMCs as described in section 6.2.10. Compressed gels were selected for culturing RAW264 due to the increased stiffness afforded by a compressed gel. Compression protocol is detailed further in figure 6-27. Image comparative of RAW264 growth in 2D and 3D is represented in figure 6-28.

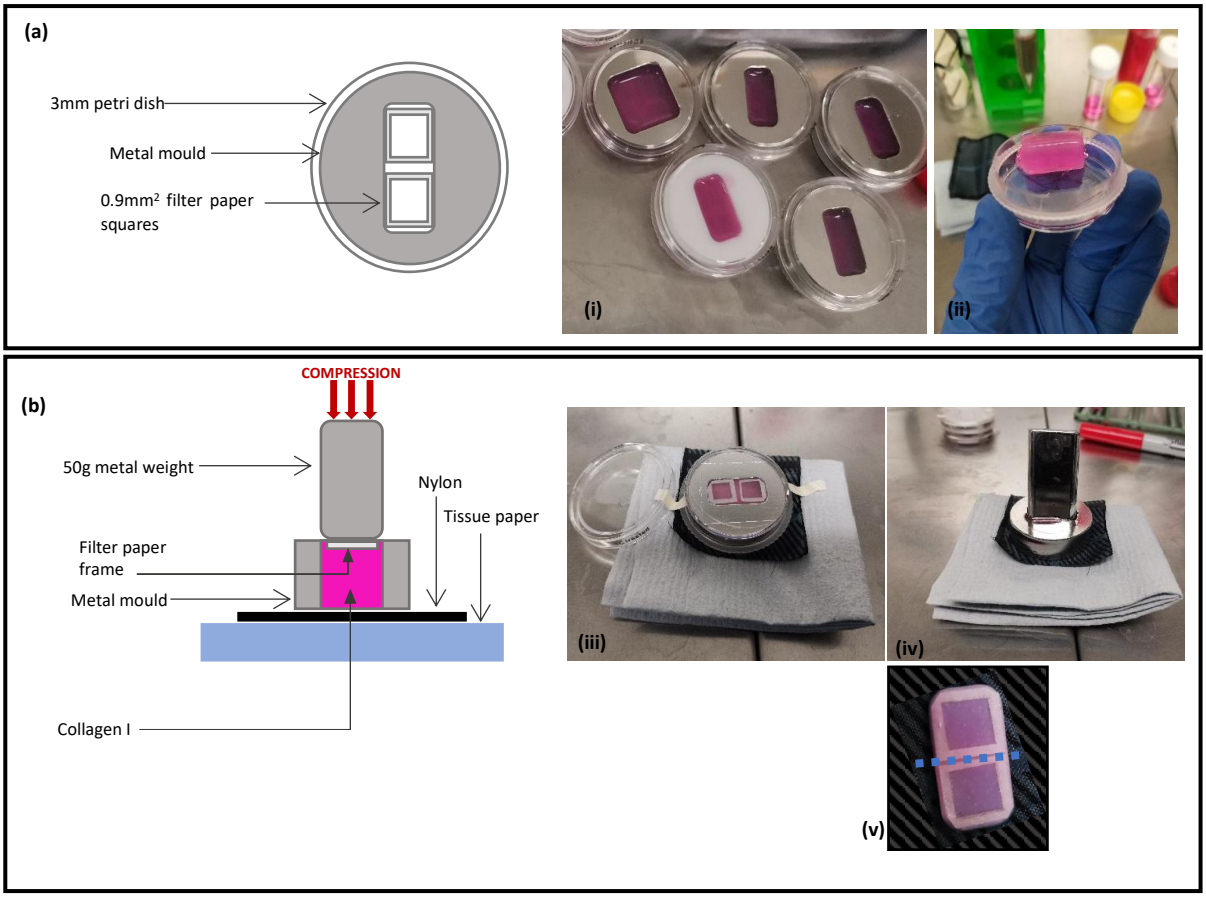

Figure 6-27: Collagen gel compression. (a) shows the preparation of the moulds before collagen addition. (i) shows the solidified collagen in the moulds and (ii) the gel removed from the mould. To compress and extract the gels (b), the mould was turned upside down on a piece of nylon placed on layered sterilised tissue (iii). Once inverted, the glass cover slip is carefully removed to avoid breakage, after which the weight, designed to fit into the mould, is placed on the gel (iv). The weight is left on the gel for 5 minutes until the majority of the water content is removed. The filter paper frames are separated using a scalpel (v), then transferred to a 24 well plate for culture.

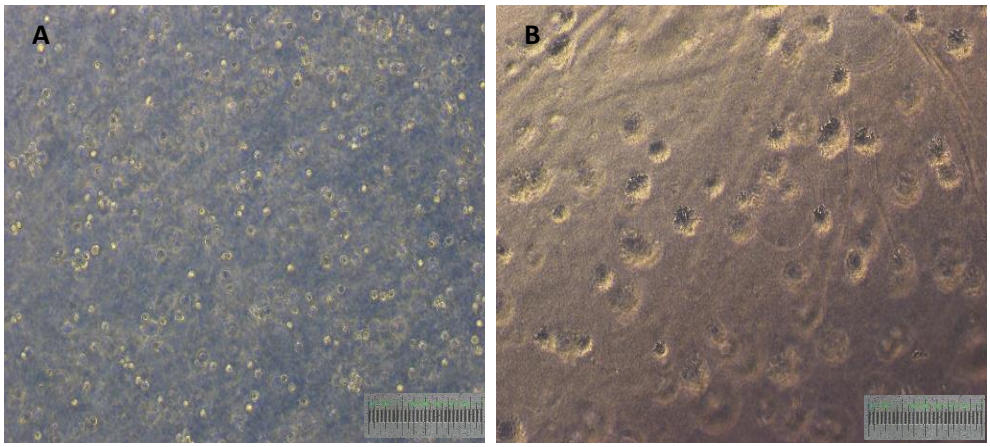

Figure 6-28: RAW264 in 3D culture. (A) RAW264 after compression (within an hour). (B) RAW264 after 48 hours in compressed collagen. All images taken at 10x.

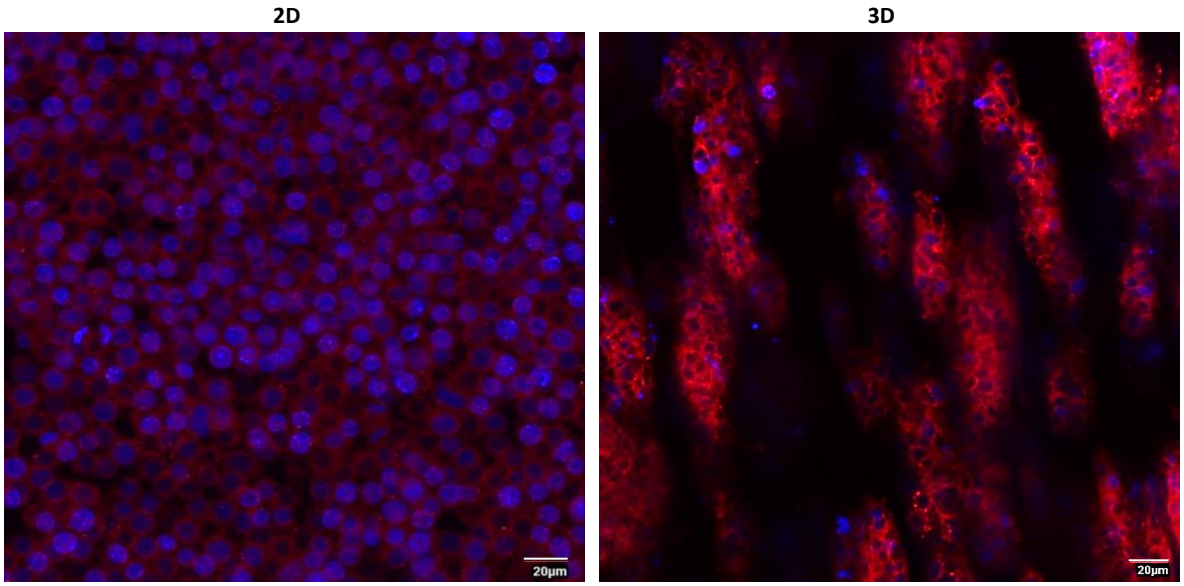

Figure 6-29: Comparison of 2D RAW264 culture and 3D RAW264 culture in compressed collagen hydrogel. RAW264 appearance in 2D (left) versus 3D culture (right). Samples stained with Nile red. For 3D culture, cells were seeded at 5 x 10^5 cells in 1500µl collagen (3mg/ml) before compression and separation into two gels. Compressed gels were cultured for at least 48 hours before imaging. Images taken at 40x. Nile red, DAPI.

The brightfield images shown in figure 6-28, showing 3D culture of RAW264 at different time points, and the fluorescent ones in figure 6-29 highlight the differences in appearance of cells in different environments. Compared to 2D culture, RAW264 adopted a more clustered growth pattern when cultured in 3D for at least 48 hours. After initial seeding and compression (figure 6-28 A), cells appear individual and diffused throughout the entire gel. After 48 hours (figure 6-28 B; figure 6-29 (right)), cells appear to have clustered together and the diffusion through the gel seen in panel A of figure 6-28 appears to have reversed and be replaced with larger clusters of cells that are not as densely distributed as they were immediately post seeding. The Nile red staining clearly denotes the differences in membranes between individuated and clustered cells while showing no uptake of lipid.

The polarization stimulations done for 2D RAW264 culture were also done for 3D culture as shown in figure 6-30. RAW264 cells were able to demonstrate oxLDL uptake, although extent of uptake is difficult to visualise due to the thickness of the gel and the clustered growth formation of the RAW264 cells.

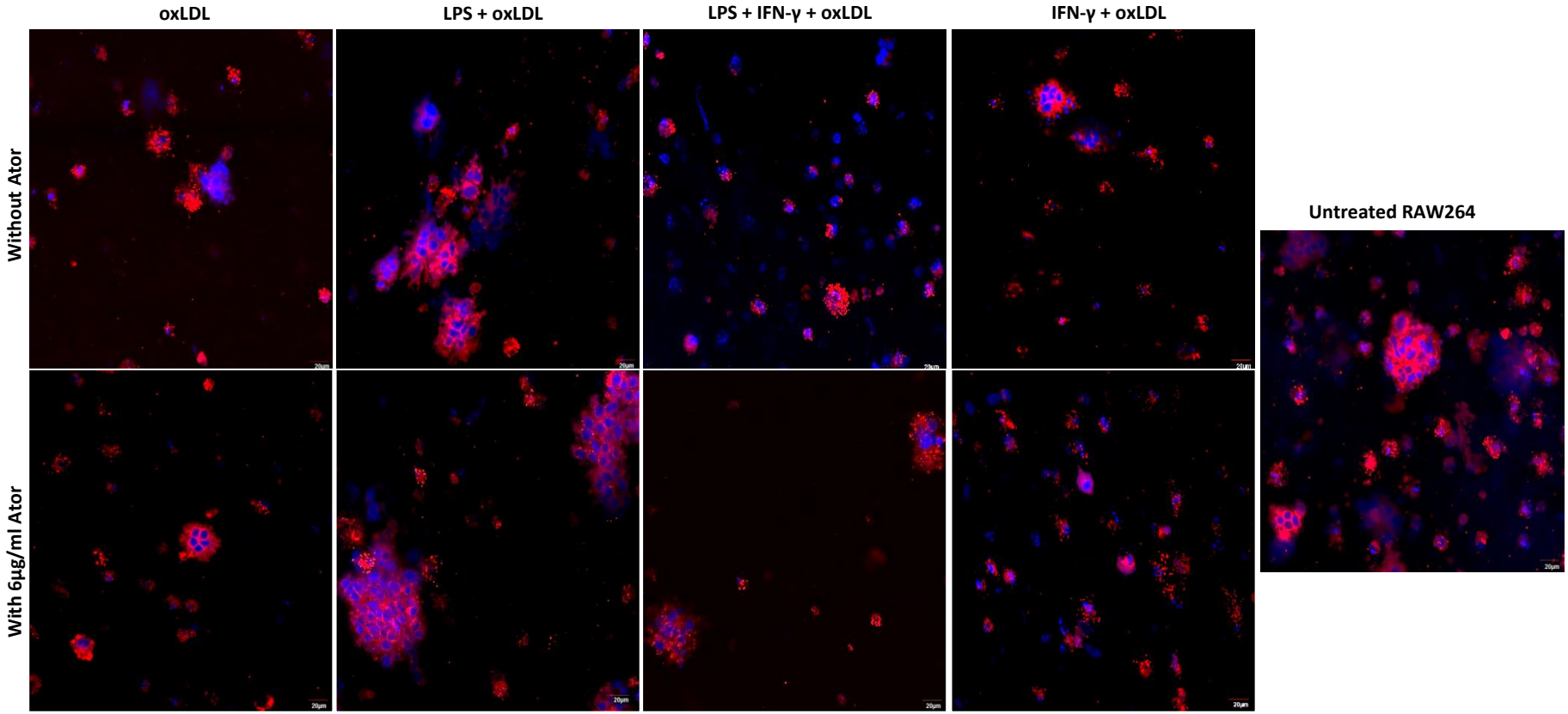

Figure 6-30: LPS and IFN-γ stimulation of RAW264 in 3D. The IFN-γ and LPS stimulations attempted on the 2D model were attempted here. Images taken at 40x. Nile red, DAPI.

As evidenced by figure 6-28, 6-29 and 6-30, the clustered growth of RAW264 adds complexity to the evaluation of extent of oxLDL uptake with either LPS or IFN-γ or both and also in the presence of atorvastatin. Atorvastatin does seem to have an effect on accumulation of lipid droplets and their retention within cells i.e., there appear to be fewer droplets in the drug treated samples and for the IFN-γ treated samples, the lipid droplets do not seem associated with an intact cell body but rather a ruptured cell. The clusters observed as a regular feature of 3D culture also appear to have dissociated into individual cells in the presence of IFN-γ and oxLDL (figure 6-30). This appears to be an effect unique to IFN-γ or oxLDL inclusion as this “clump dissociation” is more apparent in IFN-γ, and to a lesser extent oxLDL, treated samples. The same is observed in the live dead staining below (figure 6-31), in that the size of green bodies in the image are distinctly smaller and fewer in the IFN-γ and oxLDL treated samples, especially in the absence of atorvastatin. The Image of the untreated sample was taken immediately after compression as such the cells maintain the appearance seen in figure 6-29 (right).

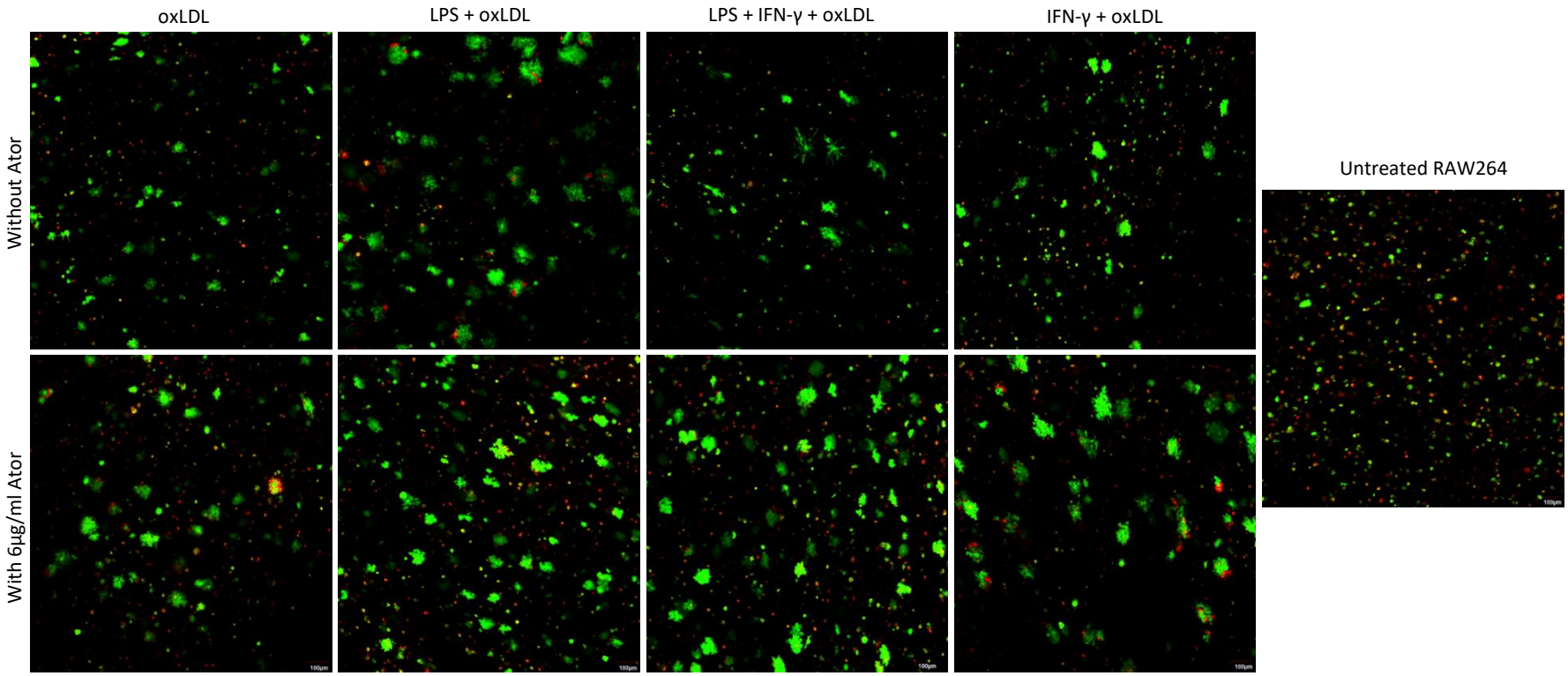

Figure 6-31: Live/dead viability evaluation: A live/dead (green/red) evaluation was carried out across 3D RAW264 culture samples. The RAW264 untreated sample was cultured in standard RAW264 media. Images taken at 10x.

The live/dead images in figure 6-31 suggest that atorvastatin has a positive impact on cell viability/proliferation, with treated samples showing large and numerous cell clusters, which indicate higher density of RAW264 cells. The images appear to indicate there more live cells in the presence of atorvastatin

than without. Given the density of clusters i.e., larger sized green stained bodies observed in the presence of atorvastatin, it can be suggested that atorvastatin has a positive impact on proliferation of RAW264 cells, resulting in larger and more numerous cell clusters.

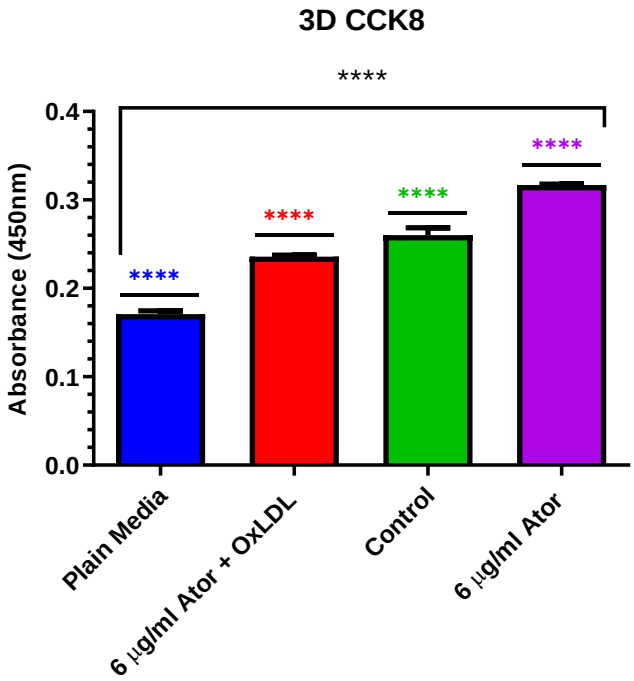

Figure 6-32: RAW264 in 3D - CCK8 cell viability. This plot compares cell viability of RAW264 embedded in a compressed collagen hydrogel. Samples were cultured for 24 hours before analysis with CCK8. Statistical analysis was done using one sample t-test as well as two-way ANOVA, with significance identified for each variable and between variables. For all analyses, the generated p value was <0.0001 ****. N=4.

The data represented in figure 6-32 shows that atorvastatin, in the presence of oxLDL, appears to result in a reduction in cell viability. With 6µg/ml atorvastatin, compared to the control sample, appearing to be more effective at promoting cell viability in 3D.

6.1.16.1 Effect of HCASMC co-culture on foam cell models

Attempts were made to culture both RAW264 and HCASMCs to create a lipid and macrophage rich "plaque". To accomplish this, different seeding techniques were applied. The first follows the protocol described for seeding RAW 264 cells in compressed gels. For the co-culture model, the acellular gel first dispensed into the compression moulds was replaced with a collagen-HCASMC mix, with HCASMCs seeded at 1 x 10^5 cells/gel. RAW264 cells suspended in collagen were then added to the mould and allowed to set, followed by compression. The main problem presented by this seeding method was that the thickness of the compressed gel does not permit visualisation of both cell types simultaneously (figure 6-33).

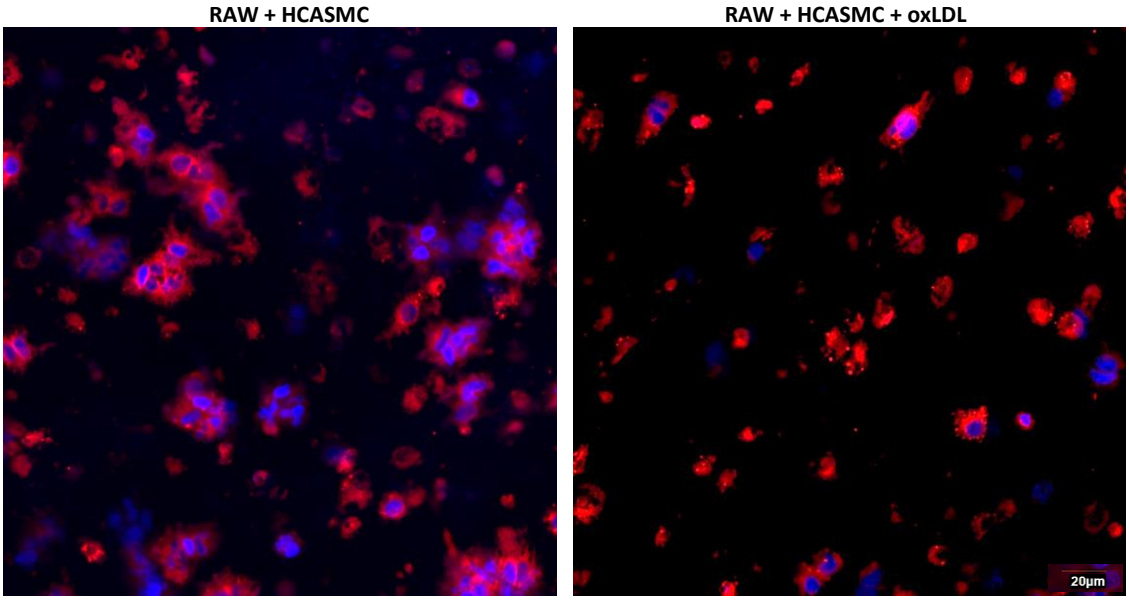

Figure 6-33*:* **HCASMC-RAW264 co-culture.** Nile red staining of RAW264 co-cultured with HCASMC in a compressed collagen gel. Samples here were not treated with any stimulants aside from oxLDL. Images taken at 40x. Nile red, DAPI.

As was observed in figure 6-30, there also appears to be some evidence of "clump dissociation" in the oxLDL treated samples (figure 6-33). This may be a feature specific to partially activated/polarized RAW264 cells, and may be reversed by the inclusion of atorvastatin. Given the challenge in visualisation of these gels, an alternative method was attempted to seed RAW264 cells on smaller un-compressed collagen gels seeded with HCASMCs. These alternative co-culture gels were made by first

dispensing 200µl HCASMCs suspended in collagen gel onto 1 x 1cm^2 filter paper frames to form a TEML. This primary gel was allowed to set for 20 minutes at 37°C/5% CO_2. This was followed by injecting RAW264 cells suspended in collagen into the centre of the TEML. The resultant hydrogel would, ideally, have a zone enriched with RAW264 cells that was separate from the HCASMCs while having a gel that can be examined microscopically. Versions of this alternative co-culture seeding method are represented in figure 6-34.

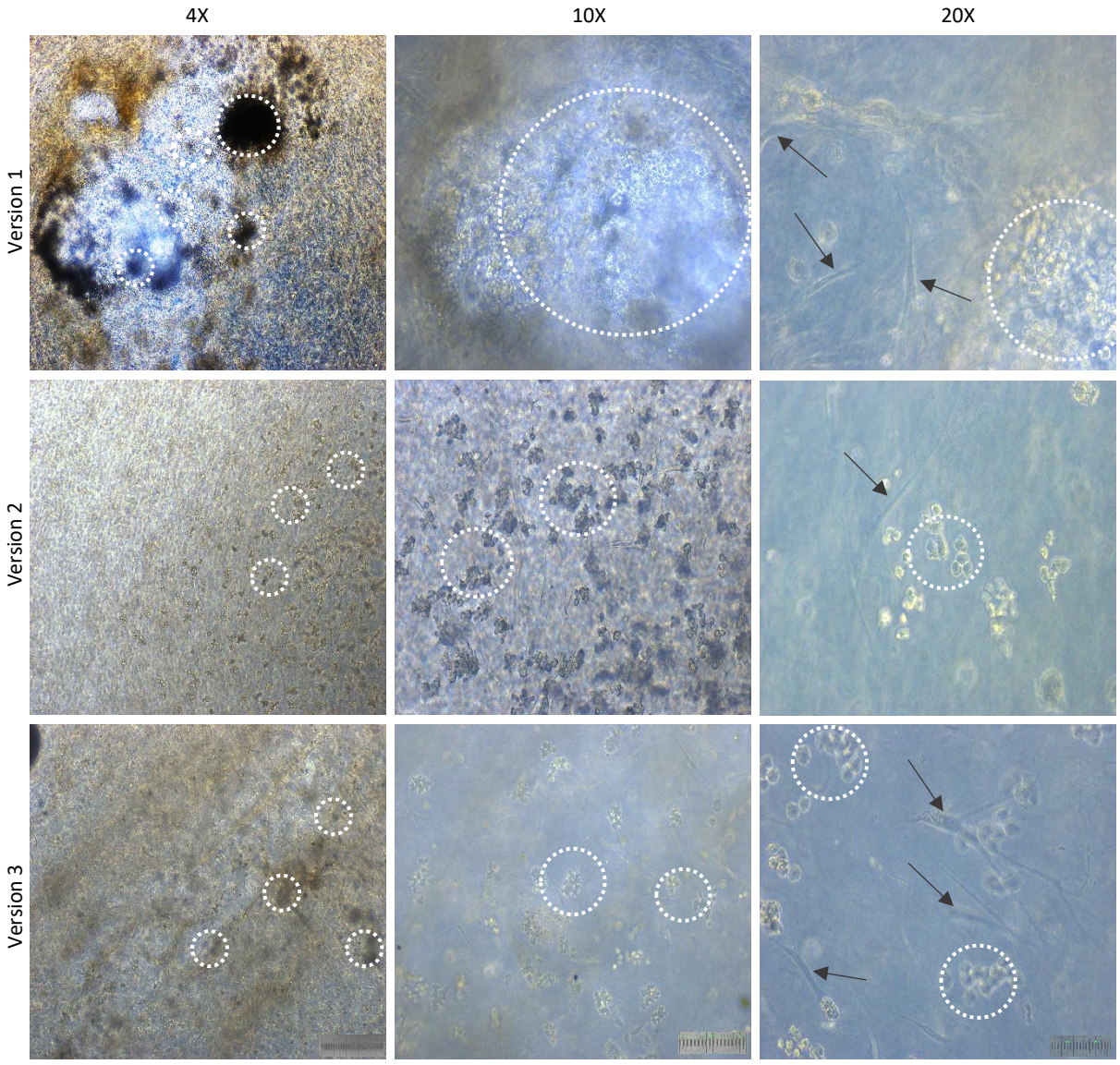

Figure 6-34: RAW264 and HCASMC co-culture. These images represent different attempts at injecting RAW264 into TEMLs. Version one involved the syringe being angled perpendicular to the TEML then injecting the RAW264 cells. Version two and three, the syringe was angled approximately 45 degrees to the TEML surface before injecting RAW264. White dotted circle denotes areas of RAW264 coverage/localization; arrows denote HCASMC localization.

Of the three attempts at an alternative seeding method represented in figure 6-34, version one gave the best expected result but with unwanted tearing of the TEML during injection. The resultant gel has distinct separation of the RAW264 and HCASMCs, and RAW264 cells permeated the depth of the gel versus only surface infiltration in versions 2 and 3, with version 3 having more scattered distribution of RAW264.

6.4 Discussion

6.1.17 IFN-γ is a weak inducer of macrophage polarization

Macrophages are involved in a number of regulatory functions in many organ systems such as innate and adaptive immunity, haematopoiesis, vasculogenesis and systemic metabolism. These numerous functions are also associated with varying cellular phenotypes with general classification under either M1 or M2. M1 or classically activated macrophages are associated with pro-inflammatory processes while M2, or alternatively activated macrophages, are associated with anti-inflammatory processes and tissue remodelling (Liu *et al.*, 2014). One of the objectives of this chapter was to switch RAW264 cells into an M1 phenotype which would result in increased uptake of oxLDL. This was attempted with both IFN-γ and LPS, but using only IFN-γ as a stimulant was the preferred method due to the quantification method being applied here. While we have observed uptake of both LDL and oxLDL here, quantification data suggests that the influence of IFN-γ does not trigger vastly stronger uptake of oxLDL. This could be explained by findings that state IFN-γ treatment can actually lower circulating amounts of cholesterol (Whitman *et al.*, 2000) as well as the lipid content within cells, resulting in the decrease of foam cell numbers in atherosclerotic plaques rich in T-cells secreting lesional IFN-γ (Young, Libby and Schönbeck, 2002). These variations in IFN-γ effect on foam cell formation could be a result of differing environmental signals that shift polarization along the M1/M2 spectrum. Macrophages are able to change their activation state in response to growth factors, cytokines and additional external cues such as any entity capable of being recognised by macrophages (Murray *et al.*, 2014). Here, the inclusion of HUVECs and/or atorvastatin appears to limit the expected effect IFN-γ has on oxLDL uptake/retention in that the quantification done shows lower oxLDL concentrations on the IFN-γ treated samples than the unstimulated ones, especially in lesioned HUVECs in the presence of atorvastatin (figure 6-22).

6.1.18 NO is a useful biomarker for foam cell models

In consideration of NO production data, the findings here do show that IFN-γ is able to stimulate NO

production in both HUVECs and RAW264, however they also indicate that IFN-γ stimulation results in lower NO production compared to unstimulated cells, and that oxLDL is a stronger stimulus for NO production than IFN-γ (figure 6-19 and figure 6-21). Figure 6-20 (e, f) shows that in regards to NO production, addition of IFN-γ appears to limit NO production in HUVECs and, to a lesser extent, in RAW264. The co-culture model shows expected responses in terms of NO production, with intact HUVECs consistently demonstrating higher NO levels than lesioned HUVECs. The highest NO readings were seen for cells cultured without IFN-γ stimulation and in the presence of 6µg/ml atorvastatin. Produced by endothelial cells, NO is a key regulator of vascular health and reduction in its production is related to oxidative stress, lipid infiltration, alteration of vascular tone and the expression of inflammatory factors (Chen *et al.*, 2018). In macrophages, production of NO is associated with their activation, along with the production of inflammatory mediators such as interleukin, tumour necrosis factor (TNF) and reactive oxygen species (ROS). This increase in production is to aid in destruction of internalised pathogens (Guo *et al.*, 2020). IFN-γ has been associated with triggering NO production in macrophages, through inducible nitric oxide synthase (iNOS), as part of native immunity (Hoeksema *et al.*, 2015). The data presented in figure 6-16 suggest that atorvastatin negatively affects NO production in RAW264 stimulated with IFN-γ, while the opposite effect is seen on IFN-γ stimulated HUVECs where the inclusion of atorvastatin promotes NO production, albeit in a somewhat lesser extent than without IFN-γ. This suggests that atorvastatin exerts some protective effect on maintaining vascular health in that it promotes the beneficial production of NO in endothelial cells, while limiting deleterious RAW264 NO production. This observation can be supported by findings that suggest that atorvastatin exerts some immunomodulatory effects and can promote a shift from a pro- to and anti-inflammatory profile.

6.1.19 oxLDL contributes to foam cell formation and macrophage polarization

oxLDL has also been associated with an increase in NO production in macrophages. Specifically, the increased production on iNOS which facilitates extended production of NO (Huang *et al.*, 2014). A key difference between this work and cited literature is the mode of macrophage stimulation. Traditionally,

this is done with IFN-γ (for an M1 phenotype) in conjunction with toll like receptor (TLR) activation with immunological substrates such as LPS for further activation (Hoeksema *et al.*, 2015; Guo *et al.*, 2020). oxLDL has been demonstrated as being able to stimulate toll like receptors (Chávez-Sánchez *et al.*, 2014), which would potentially explain the increased NO production seen when IFN-γ was used in conjunction with oxLDL (figure 6-19), versus just IFN-γ stimulation alone. These observations are corroborated by the data in figure 6-7, where LPS demonstrates a very strong effect on NO production on its own, and to a lesser extent with the inclusion of oxLDL.

6.1.20 Atorvastatin has a strong impact on cholesterol efflux

The experiments conducted here also demonstrate that atorvastatin has an effect on cholesterol efflux/reverse cholesterol transport. Nile red imaging and oil red-O quantification show the inclusion of atorvastatin results in fewer lipid droplets observed within samples (figure 6-9 to figure 6-12) and lower concentrations of quantified lipid content (Figure 6-13 and figure 6-22). There is a general lack of consensus on whether atorvastatin has an effect on cholesterol efflux, but it has been suggested as a strong possibility. The regulation of the scavenger receptor ATP-binding cassette transporter G1 (ABCG1) expression on macrophages has been linked to atorvastatin related cholesterol efflux (L. Xu *et al.*, 2019). The work by Xu et. al., 2019, related to advanced glycation end products (AGEs) in diabetes, showed that atorvastatin increased expression of ABCG1, a receptor that is associated with cholesterol efflux and maintaining cholesterol homeostasis, reversing the inhibition of this receptor done by AGEs. Counter to these findings, earlier work by Qui and Hill, 2008, suggested that atorvastatin inhibits expression of another variant of scavenger receptor, ATP-binding cassette transporter A1 (ABCA1), and thus cholesterol efflux. Their work, however, found this inhibition only on non-cholesterol loaded macrophages and this effect was compromised after acetylated LDL loading, suggesting that atorvastatin's efflux effect may be dependent on cells actually having internalised lipid in the first place (Qiu and Hill, 2008). The findings in this chapter also suggest that the efflux effect of atorvastatin is stronger in IFN-γ stimulated samples than unstimulated samples. This may be explained by the observation that atorvastatin is able to modulate immune responses, shifting from a pro- to an

anti-inflammatory profile. Cheng et. al., 2009 observed that levels of IFN-γ and the ratio of IFN-γ: Il-4 were significantly decreased with atorvastatin in patients suffering from chronic heart failure (Cheng *et al.*, 2009).

6.1.21 HUVEC integrity affects foam cell formation and cholesterol efflux

Lesioned HUVECs also appear to limit the efflux effect, suggesting that the cytokine profile/environmental cues associated with lesioned HUVECs, along with IFN-γ stimulation especially, also contribute to cholesterol efflux. HUVECs triggered into dysfunction produce a variety of pro-inflammatory mediators, adhesion molecules and pro-thrombotic factors. Some of these pro-inflammatory mediators include IFN-γ, tumour necrosis factor-alpha (TNF-α), tumour growth factor-beta (TGF-β) and macrophage colony stimulating factor (M-CSF) (Ramji and Davies, 2015). Findings from chapter 5 demonstrate that atorvastatin has an effect on increasing and sustaining SDF-1 production in both endothelial and smooth muscle cells. Li. et. al., 2020 identified SDF-1 (CXCL12) production by macrophages (THP-1 cells) as a promoter of atherosclerosis development. Cells were first stimulated with poly-methyl acrylate (PMA) then oxLDL to promote foam cell formation. oxLDL loaded cells were cultured with vascular smooth muscle cells (VSMC) and they found that the foam cells produced SDF-1, which in turn promoted VSMC uptake of oxLDL, resulting in their proliferation and their becoming foam cells (Li *et al.*, 2020). As stated previously, pro-inflammatory cytokines like IFN-γ and TNF-α are associated with driving foam cell formation in atherosclerosis, as such, it is likely that the lesioned HUVECs are producing these pro-inflammatory cytokines that are affecting cholesterol efflux.

6.1.22 Scavenger receptor (CD36) expression is affected by oxLDL and atorvastatin

CD36 is a scavenger receptor able to bind to a number of ligands, such as modified phospholipid, long chain fatty acids, oxLDL, oxidized and negatively charged phospholipids, collagen and apoptotic cells, and is found on the surface of a number of cell types such as platelets, endothelial cells, smooth muscle cells and macrophages (Collot-Teixeira *et al.*, 2007; Choromañska *et al.*, 2017). Binding of oxLDL to CD36 results in endocytosis of the receptor-ligand complex, which in turn induces an upregulation of

CD36 expression (Collot-Teixeira *et al.*, 2007). Animal studies have demonstrated that deletion of CD36 prevented the development of atherosclerosis despite a lipid rich diet and human studies based on autopsies of obese subjects have demonstrated increased expression of CD36 on plaque localised macrophages (Choromañska *et al.*, 2017; Lara-Guzmán *et al.*, 2018). The data presented here (figure 6-23), supports these observations in that the inclusion of oxLDL to RAW264 culture results in increased expression of CD36, compared to the absence of this receptor in untreated samples. The data here also suggests that atorvastatin may upregulate the expression of CD36, in that the staining shown in figure 6-23 and figure 6-24 appears marginally stronger than in the atorvastatin free samples. These observations are supported by Ruiz-Velasco et. al., 2004, who found that statins (lovastatin, Fluvastatin and atorvastatin) increased CD36 expression in THP-1 cells in a time and dose dependent manner. The doses used were between 2-10μM, which fits with the selected concentration used here (6μg/ml = 4.96μM) (Ruiz-Velasco, Domínguez and Vega, 2004). In regard to IFN-γ effect on expression of CD36, the comparative between lesioned and un-lesioned HUVEC co-culture, both with and without atorvastatin, for samples treated with or free of IFN-γ, there does not appear to be any significant effect of IFN-γ on the expression of CD36. Some works have suggested that IFN-γ decreases expression of CD36 (Geng and Hansson, 1992; Nakagawa *et al.*, 1998), but more recent works demonstrating the positive effect of IFN-γ on foam cell formation, rather than an inhibitory effect, suggest that this may not be the case (McLaren and Ramji, 2009) and also that IFN-γ may have a stronger effect on other scavenger receptors, triggering foam cell formation in a CD36 independent manner (Reiss *et al.*, 2004; Yu *et al.*, 2015). Intracellular levels of cholesterol do not regulate CD36 mediated uptake of cholesterol, leading to continuous uptake of oxLDL and the differentiation of macrophages into foam cells (Rios, Gidlund and Jancar, 2011). This observation may partially explain reduction in circulating LDL levels observed with administration of atorvastatin and in light of the data shown here suggesting that atorvastatin promotes expression of CD36.

6.1.23 CD146 expression is affected by atorvastatin and IFN-γ

CD146 has been associated with the development of a number of non-resolving inflammatory diseases such as rheumatoid arthritis, inflammatory bowel disease and inflammatory diseases associated with endothelial damage (Blin *et al.*, 2019), and has been found on activated inflammatory cells, suggesting it confers a pro-inflammatory profile on immune cells (Luo *et al.*, 2017). Its expression has been identified on infiltrated macrophages in atherosclerotic plaques and has been associated with plaque vulnerability. Its expression on macrophagic foam cells is upregulated by oxLDL, and mediates CD36 internalisation during lipid uptake (Luo *et al.*, 2017; Blin *et al.*, 2019). The data here supports observations that oxLDL promotes CD146 expression and suggests IFN-γ may promote expression of CD146 (figure 6-26) when compared to unstimulated cells (figure 6-25). The images in figure 6-25, specifically those of RAW264 cultured with lesioned HUVECs, indicate atorvastatin restricts expression of CD146, while having little to no effect on CD146 expression in intact HUVECs. There is not a lot of literature available discussing the role of CD146 in the context of atherosclerosis and in relation to atorvastatin, with only the work done by Luo et. al., 2017 being the most significant, but the effect seen here suggests that the increase in CD36 expression observed in the unstimulated RAW264 cells co-cultured with lesioned HUVECs is possibly a result of the decreased CD146 expression seen for the same variable combination. Further characterization of CD146 and its role in foam cell formation is required.

To truly verify the effect atorvastatin has on cholesterol efflux, further evaluation needs to be done here; for example, visualisation and quantification of additional scavenger receptor expression. Further characterization of the impact of individual variables, and these same variables in conjunction, would be ideal. A number of atorvastatin doses also need to be applied to determine conclusively the doses at which this effect on CD146 and CD36 is observed. Here we visualised efflux at 6µg and 60µg/ml atorvastatin, with stronger indications of efflux, possibly tied to reduced cell numbers, observed at 60µg/ml. It has been observed that a CD146 deficiency results in neutrophilia and the accumulation of neutrophils at sites of inflammation, implying an atheroprotective role for this

receptor. This did not impact LDL uptake but did result in an increase in atherosclerotic plaque size (Blin *et al.*, 2019). The work by Blin et. al., 2019 highlights a possible correlation between CD146 expression and RANTES (CCL5) expression and further emphasises the need for further work on the role of CD146 in atherosclerosis.

6.1.24 3D models demonstrate variations in foam cell behaviour compared to 2D culture

For the 3D culture of RAW264 cells, the primary challenge was in optimising conditions to allow clearer visualisation of foam cells and physiologically relevant inclusion of smooth muscle cells. It was possible to generate higher concentration collagen gels with RAW264 embedded within the gel but these cells displayed different growth profiles than 2D culture. Images in figure 6-28 to figure 6-31 show what appear to be cell clusters as these cells proliferated. This phenomenon has been described as fusion, which occurs when macrophages are implanted in a 3D environment, resulting in the formation of multinuclear cells called “foreign body giant cells”, which are commonly occurring in the foreign body reaction against implanted biomaterials (Fang, Yang and Han, 2020). Fang et. al., 2020 demonstrated that at different concentrations of collagen, affecting material stiffness, implanted RAW264 slowed their proliferation with increasing concentration (and thus stiffness) of collagen. These observations align with the CCK8 data represented here (figure 6-32), where readings for cells seeded at the same density in 2D and 3D were markedly different, with the 3D cultured cells having much lower readings which correlate with reduced proliferation. The live dead images (figure 6-31) indicate that seeding into collagen followed by compression did not negatively affect cell health and also provides evidence of RAW264 fusion with prolonged culture.

6.5 Conclusion

The data collected in this chapter have been successful at demonstrating RAW264 induction to promote LDL/oxLDL uptake as well as the effects of atorvastatin in reversing this effect in a time and dose dependent manner. It was also revealed that the production of NO is affected by numerous factors, most notable being LPS, and that atorvastatin was able to restrict production of NO by macrophages in an inflammatory state. The experiments caried out also demonstrated the positive effect of atorvastatin on cholesterol efflux, likely due to manipulation of scavenger receptor expression. It was also possible to demonstrate the effect atorvastatin has on scavenger receptor expression. It was possible to create an alternative co-culture model with HUVECs and RAW264, demonstrating a synergistic effect in regards to NO production and oxLDL retention in the presence of atorvastatin. The attempts at incorporating RAW264 into a 3D matrix showed that cell behaviour is affected by environmental cues and this work can be taken further through experimentation with material stiffness and incorporation of different cell types. With the possibility of combining various variables, it should be possible to characterise the contributions of other pro-inflammatory cytokines as well as cell types using this foam cell model to generate a clearer picture of foam cell formation and elimination in atherosclerosis.

Chapter 7:
Discussion

7.1 Background review

Cardiovascular disease is recognised as the leading cause of morbidity and mortality globally and atherosclerosis has been identified as the underlying cause for cardiovascular diseases, such as heart attacks and strokes (Gareus *et al.*, 2008). This has resulted in a lot of research into the pathophysiology of atherosclerosis to better understand the mechanisms involved in its initiation and progression, and thus provide better insights into better preventative and curative measures. Currently, it is accepted that atherosclerosis is associated with both metabolic disorder and chronic inflammation in the arterial wall, a process initiated by the deposition of apolipoprotein B-containing lipoproteins in the sub endothelial space (H. Xu *et al.*, 2019). The primary lipoprotein associated with atherosclerosis is LDL, which can trigger endothelial activation/dysfunction as well as being prone to oxidation (Badimon, Padró and Vilahur, 2012; Moriya, 2019). These oxidised LDLs, combined with an endothelial inflammatory response, result in the recruitment of immune cells, primarily macrophages/monocytes, neutrophils, T-and B-lymphocytes, which contribute further to disease progression (Moriya, 2019).

For a number of years, the primary prescribed treatment for atherosclerosis has been statins. Studies have demonstrated that patients prescribed statins show statistically significant and clinically important reductions in risk of cardiovascular disease manifestation (Hennekens, Schuttenberg and Pfeffer, 2019). Their primary application is in the regulation of cholesterol levels and they have demonstrated very good effects on lowering the incidence of cardiovascular events in patients, with atorvastatin being the main statin used for this kind of treatment (Peng *et al.*, 2018). Aside from the lipid lowering effect, this drug has demonstrated a capacity to affect the inflammatory process, with evidence showing treatment with atorvastatin significantly ameliorates the secretion of pro-inflammatory cytokines such as tumour necrosis factor-α (TNF-α) and interleukin-1β (IL-1β), as well as levels of C-reactive protein (CRP) which is a common inflammation marker (Sugiyama *et al.*, 2005; Sadowitz, Maier and Gahtan, 2010; Peng *et al.*, 2018). Of particular interest in recent years is the effect statins have on endothelial progenitor cells (EPCs). A number of studies have reported beneficial effects, including increasing numbers of circulating EPCs (Eisen *et al.*, 2015)(Sandhu, Mamas and

Butler, 2017), enhancing homing/recruitment of EPCs to sites of vascular injury (Oikonomou *et al.*, 2015)(Walter, Dimmeler and Zeiher, 2004) and improving EPC attachment/adhesion and differentiation (Liu *et al.*, 2012).

As pertains to the obtainment of the observations on factors contributing to the pathogenesis of atherosclerosis, and additional effects of statins, a significant number of studies rely on animal models to generate data. The obvious limitations of this, primarily cost, ethical considerations, species variability and the inhibitory effect of anaesthetic agents on platelet aggregation (Atkinson, Taylor and Chetty, 1985; Nakagawa *et al.*, 2002), which potentially limit reproducibility and relatability of results, highlight a need for an alternative mode of data collection. In vitro models have also played an important role in determining contributing factors and elucidating mechanisms of action, but in addition to being carried out in a two-dimensional context, they also lack a key component involved in the pathophysiology of atherosclerosis, which is shear stress. Flow based models that can incorporate functional three-dimensional models for cellular responses in drug screening studies would have tremendous value in providing insight for future development of ideal strategies against atherosclerosis (Khodabandehlou *et al.*, 2017).

The work carried out in this thesis aimed to develop and apply 3D tissue engineered vascular models to investigate the pleiotropic effects of statins. First, the work here attempted to define the differences in stem cells and progenitor cells' responses in homing towards a lesion, using cells from different species. The second objective was to highlight the differences observed in stem and progenitor cells' responses in 2D and 3D physiologically relevant environments i.e., with an injury and under shear stress. The third objective was to demonstrate the applicability and ease of use of the 3D blood vessel model to create complex systems such as the atherosclerosis model. For all the objectives listed, the central focus has been the dose dependent effect of atorvastatin.

7.2 Key findings

Through the experiments conducted within this thesis, it was possible to demonstrate the value of having 3D tissue models to study disease pathology, and these models were able to highlight the contributions of the intimal and medial layers, separately and in concert, to the recruitment of circulating cells and in response to different activation stimuli. The use of nanofiber inserts to create a novel HUVEC-RAW264 co-culture system provided a convenient, and rapid system to study atorvastatin's effect on cholesterol efflux, while evaluating the impact of intact or lesioned intimal layer on this process. These models were also useful in characterising cellular responses to atorvastatin, demonstrating both a time and dose dependent effect in regards to wound closure, EPC homing (under high and low shear stress), SDF-1 production, cholesterol efflux, inhibition of inflammatory effects of IFN-γ, and regulation of NO production. These models also manage to highlight the differences in relatability of responses between animal and human cells.

7.3 EPCs demonstrate different features of stemness compared to MSCs.

Characterisation of EPCs is a challenging task as since their discovery in 1997 by Asahara et.al., there has been a general lack of consensus regarding defining the characteristics that are used to identify this cell type (Chopra *et al.*, 2018c). Because of this lack of consensus, a general definition of EPCs can be used which identifies them as cells formed in either nonhematopoietic tissues or the bone marrow, and conceptually can be considered a heterogeneous group of cells, which can characteristically be detected at different phases of endothelial differentiation in the peripheral blood (Poay Sian Sabrina Lee and Kian Keong, 2014). Over the years, EPCs have been sourced either from umbilical cord blood, adult peripheral blood or bone marrow (Ii, 2010; Yoder, 2012; Chen *et al.*, 2021). As relates to their origin, one theory states that EPCs are derived from haemangioblasts, a precursor of both haematopoietic and endothelial cells (Chopra *et al.*, 2018c). Upon first discovery, these cells were initially identified through expression of CD34, a marker indicating haematopoietic lineage, and Flk-1 (KDR/VEGFR-2) which is an endothelial lineage marker and co expression of CD34 and Flk-1 have been associated with coronary artery disease (Schmidt-Lucke *et al.*, 2010; Fadini, Losordo and Dimmeler,

2012). To aid with increasing specificity for EPCs, inclusion of CD133 as a marker was done as it denotes a more immature haematopoietic cell (Urbich and Dimmeler, 2004). Another marker of interest is CXCR4 and its association with SDF-1, which contributes to the mobilisation and homing of bone marrow derived cells. Studies have indicated an importance of the SDF-1/CXCR4 axis in promoting the mobilisation and homing of EPCs, with disruption to the SDF-1/CXCR4 interaction resulting in impaired incorporation of EPCs into ischaemic sites (Yu and Feng, 2008). Cells that express CD34 have been shown to express low levels of CD45, and detection of this receptor has been suggested as an additional method of characterising EPCs (Fadini, Losordo and Dimmeler, 2012). CD31 has also been proposed, and used, as a potential marker for these cells even though it can also be expressed on mature endothelial cells (Poay Sian Sabrina Lee and Kian Keong, 2014; Melchiorri *et al.*, 2016).

For our purposes, the markers selected to verify the nature of the cultured cell type were CXCR4, CD34, Flk-1, CD45 and CD31, which proved sufficient to define these cells as endothelial progenitors. Further to surface marker expression, tube formation is an additional assay used to define cells as endothelial progenitors. This involves the seeding of isolated cells in Matrigel supplemented with factors such as vascular endothelial growth factor (VEGF), which stimulates vessel formation (Huang *et al.*, 2012; Zhao *et al.*, 2018). In our 2D aspect of this study, it was possible to observe spontaneous formation of tube-like structures, with cells joining end to end to form a closed loop structure, observed in both fibronectin and collagen coated plates, which provided additional evidence that the cells isolated from whole blood were progenitors. Additionally, it has been demonstrated that cells capable of colony formation would also result in the formation of tubes (Peters, 2018). The cells cultured in this study always formed colonies within the first 3-4 days of culture, further suggesting that they were the desired cell type given the subsequent spontaneous formation of the tube-like structures as well as the expression of a number of surface receptors that correlate with EPCs.

Aside from the characterisations done on the EPCs on their own, their responses to atorvastatin and interactions with the TE constructs is in line with published work (Petit, Jin and Rafii, 2007; Yu and Feng, 2008; Melchiorri *et al.*, 2016), in that we were able to demonstrate increased attachment of

perfused cells on atorvastatin treated and lesioned constructs, at both low and high shear stress in chapter 5.

7.4 Murine cells have different responses to atorvastatin compared to human cells

As relates to the beneficial effects of atorvastatin, the data collected here has demonstrated that murine cells had higher migration rates into a scratch wound compared to human derived MSCs (hMSCs) and EPCs, and more cells were present with increasing concentrations of atorvastatin, with peak infiltration observed at 120µg/ml. The methods applied here were a simple scratch wound which allowed rapid collection of data as well as providing a starting point for evaluating cellular responses to atorvastatin. In comparison, hMSCs showed reduced numbers of cells at all doses of atorvastatin compared to the drug free control. This model was also useful in showing that depending on cell combinations, the HUVEC response was also varied in that when co-cultured with rMSCs, HUVEC migration into the scratch wound followed the same trend, with increasing cell numbers with higher concentrations of atorvastatin, with peak cell numbers also achieved at 120µg/ml. When HUVECs were cultured with hMSCs, peak attachment was observed at the lowest concentration of atorvastatin applies, 30µg/ml. This was followed by a reduction in cells within the scratch wound, with a second smaller peak observed at 120µg/ml. As for the EPCs, they showed a positive response to atorvastatin up to 60µg/ml, however HUVECs were fewer in number with atorvastatin compared to the drug free control. They did demonstrate a small peak at the same point as the EPCs (60µg/ml), further highlighting that there are cellular interplays that influence the behaviour of surrounding cells. Exploration of a wider range of atorvastatin concentrations would have allowed clarification of the interaction between the endothelial cells used here and hMSCs, as numerous studies have explored the possibility of using MSCs from various locations as therapies and have shown promising results in regards to atorvastatin enhancing the migration and differentiation of MSCs, and improving incorporation of MSCs to injury sites and improving endothelial health (Song *et al.*, 2013b; Zhang *et al.*, 2014; Bing *et al.*, 2016). The variations observed between the work carried out here and the studies that reported positive findings could be because of species variation i.e., use of miniswine (Song *et al.*,

2013b) or rats (Cai *et al.*, 2014) could affect outcomes as well as differences in experimental design in that other pathways and cellular stimulations/activations were investigated (Zhang *et al.*, 2014).

To further explore these differences observed by using different cell types in culture, more work would be needed to clearly characterise the inter-relationship between endothelial cells and MSCs as the data here suggests that even between human cells, the cell types have different interactions with each other as is demonstrated by the EPC responses to atorvastatin versus the hMSC responses to the same, in conjunction with HUVECs. As previously mentioned, it is likely that the concentration of atorvastatin that would be ideal to enhance MSC homing is different to that observed with EPCs, with different studies reporting varying ranges of concentrations with similar results, for example Yu and Feng, 2008 reported that EPC migration was enhanced at low concentrations of atorvastatin i.e., 10 nM-100 nM, whereas the beneficail effect observed was significantly inhibited at concentrations higher that 1000 nM (Yu and Feng, 2008). It should be noted that these findings were based on a mouse model of ischaemia (Yu and Feng, 2008), so again, species variation may also be a contributing factor. Other works report the concentration in terms of weight (Song *et al.*, 2013b; Cai *et al.*, 2014; Zhang *et al.*, 2014), which makes it difficult to compare without the weights of the animals used or resorting to using animal models. It would also be interesting to compare adhesion molecule expression between these cell types i.e., other than the commonly expressed CXCR4, and determine if there are specific conditions that are not met by the parameters set out in this experiment, and also possibly determine if there is a concentration of atorvastatin that works equally for both cell types, improving the functionality of these cells together with endothelial cells.

7.5 Multiple factors affected 3D culture and perfusion outcomes.

Advancing from the established 3D tissue engineering blood vessel (TEBV) studies in which single and multi-cellular layers and extracellular matrix (ECM) can be included into TEBV models (Musa, Harper and Yang, 2016), the work in this study, has incorporated multiple factors to assess TEBV responses under physiologically relevant conditions. Under static culture, these models have been comprehensively characterised i.e., by using real-time spectrofluorimetry measurements of cytosolic

Ca2+ signalling (Musa, Harper and Yang, 2016). Their anti-platelet and pro-platelet activation features have been confirmed when the intimal layer is intact and absent respectively, replicating the anti- and pro-aggregatory properties of native arteries. Furthermore, it is evident that the neo-collagen formation in medial layer was pro-aggregatory, whilst collagen gel from rat tail used as the scaffold for medium layer didn't. To the end of replication of physiological relevant environment, multiple factors have been investigated including perfusion modes via commercially-available parallel-plate flow chamber versus rocker; different statin dose and incubation duration; lesion modes and TEBV models.

7.1.1 The effect of mode of perfusion

The data collected in chapter 4 suggested that hMSCs are not responsive to atorvastatin at the selected doses, possibly because additional factors such as shear are required to facilitate this (Rüster *et al.*, 2006). When shear was introduced using a parallel plate flow chamber in chapter 5, perfused hMSCs showed increased attachment over the TEBVs incubated with atorvastatin versus those without. The parallel plate flow chamber provided a defined flow pattern and enabled variable shear stress through changing the flow rate or the dimensions of the gasket which holds the sample. Using the attached cells as the readout, consistent observations across hMSC and EPC perfusion with $FeCl_3$ as the lesion model have been obtained. Contrastingly, even though the rocker model did show some difference between atorvastatin treated and drug free samples, the differences were not as significant as those seen under physiologic shear stress, although it was possible to evaluate cell attachment over a wider range of time points. These two modes of perfusion showed that peak attachment is generally attained at the 5-hour time point across models, with some variation between 5 and 7-hours, with the most noticeable difference being the number of attached cells on the surface of the constructs i.e., lower shear stresses resulted in higher numbers of attached cells, while maintaining the same trend denoting the impact of atorvastatin and duration of incubation on the same. The advantage of the parallel plate flow chamber is that the shear stress is physiologically relevant and adjustable, and the flow unidirectional and continuous, whereas with the rocker, the flow alters the directionality of shear stress during operation (Tucker *et al.*, 2014). The disadvantage of the parallel plate flow chamber is

that it limits the test sample number, while the rocker is ideal for high throughput testing (Zhou *et al.*, 2010).

7.1.2 The effect of statin incubation duration

To simulate a clinical scenario, the injured TE constructs were incubated with atorvastatin for different durations before perfusion of hMSCs and EPCs. Oral intake of atorvastatin would require time to circulate to the lesion site and enhance cytokine production for cell homing. Injured tissues themselves would have a time frame during which peak cytokine production would naturally be reached. What we were able to determine from the 3D models is that atorvastatin was able to increase density of attached cells on the surfaces of lesioned TE constructs. This effect was also seen to be time dependent as consistently across the TEIL, TEML and TEBV, longer incubations resulted in an increased density of attached cells, with the optimal time frame being around 5-hours post lesioning and incubation with atorvastatin. This effect was observed under different modes of perfusion i.e., dynamic flow within a parallel plate flow chamber and with a see-saw rocker, which were able to provide high (20.16 dyne/cm^2) and low (up to 2.2 dyne/cm^2) shear stress respectively.

In addition to the influence atorvastatin had on cell attachment onto the lesioned TEBV, the duration of incubation also contributed to an increase in the number of attached cells, with the 5-hour incubation having more cells attached onto the surface compared to the 3-hour incubation. The difference here could be because of shear or it could also be because the hMSCs were not also incubated with atorvastatin at the same dose or for the same duration, but rather only inoculated with atorvastatin immediately before perfusion. For further clarification, it would have been ideal to have a comparative of hMSCs also incubated with atorvastatin for 3 and 5-hours before perfusion.

Relative to the static incubation with hMSCs, despite a longer incubation period (24 hours versus 3 and 5-hours), and with the same density of cells used for both conditions i.e., 6 x 10^3 cells/ml, the samples subjected to shear showed overall higher numbers of cells attaching on the surface of the TEBV compared to the numbers of cells recorded within the scratch wound. This again highlights the differences between 2D and 3D evaluations as with the 3D environment, in addition to supplying shear

stress, it was also possible to incorporate smooth muscle cells, which would have their own separate effect on stimulating cell attachment. Another difference is the surface area for evaluation. The scratch wound provides a smaller surface area than the TEBV and does not accurately represent the conditions of the vasculature that the perfusion system does i.e., hMSCs would be in motion through the vasculature versus being suspended over the endothelial layer as happened in the scratch wound model. It was evidenced that the incubation duration of atorvastatin and the host blood vessel cells was an essential factor in triggering EPC or MSC homing, while the inclusion of hear stress and other cell types e.g., smooth muscle cells, were more a more important factor in affecting EPC migration than the atorvastatin incubation time.

7.1.3 The effect injury type

We were also able to examine the effect of injury type on cell responses and it was possible to determine that this too has an impact on observations. The injury types evaluated here were mechanical-representing mild denudation as can be seen with percutaneous transluminal coronary angioplasty (PTCA/balloon injury)- and $FeCl_3$ induced oxidative injury, which is more representative of the oxidative damage seen in atherosclerosis (Varghese, Patel and Yadav, 2017). The mechanical injury provided an opportunity to regulate the extent of injury, causing only a disruption in physical integrity and provides useful insight into vascular responses in a non-oxidation-based injury, and allowed the investigation of whether the potential damage caused by balloon injuries would need pharmaceutical intervention to aid in repair and trigger mild/moderate cellular responses. The data obtained with these injury models suggested that atorvastatin's beneficial effects are linked to oxidative stress, and thus $FeCl_3$ provides a more biomimetic model to represent native injury. The mechanical injury model did not generate consistent observations of cell migration. To take this a step further, characterizing NO and endothelial nitric oxide synthase (eNOS) production, along with other markers of oxidative stress by these different models, would also aid in giving a clearer understanding of the effect of oxidative state.

These observations again demonstrate the value of a 3D tissue model as it is fairly simple to simulate oxidative damage on the constructs, and regulate the extent of damage by adjusting parameters such as filter paper size and volume of $FeCl_3$ used, creating a zone with oxidative damage surrounded by healthy tissue.

7.1.4 The effect of TEBV models

In addition to facilitating the inclusion of shear stress, the various TE models also allowed the exploration of the roles of the intimal and medial layers separately and in concert on EPC and MSC homing. With this, it was possible to identify differences in extent of observed responses between the individual layers and the composite model, further supporting the observation that observations in monoculture are different from those in co-culture, underlining the value of 3D tissue models. As the TEBV is a composite model, it also appears as though the responses seen with the TEBV are also a composite of the responses seen in the TEIL and TEML.

From the data collected, especially the results obtained in chapter 5, it was determined ha the TEBV is a more appropriate blood vessel model to study the cellular interactions, as well as atorvastatin's enhancing effect between the blood vessel and the perfused EPCs. With 5-hour incubation with atorvastatin (figure 5-15-EPC and figure 5-5-hMSC), attached cells, both hMSC and EPCs, demonstrate a more than 50% increase compared to the drug free controls.

7.6 Atorvastatin promotes production of SDF-1 and expression of CXCR4

The data collected in chapter 4 showed that atorvastatin had an effect on expression of CXCR4, with an increase in expression on hMSCs noted with an increased concentration of atorvastatin, both with and without ECM disruption with the scratch wound. This observation, however, was not reflected in HUVECs, which showed an almost steady state expression of this receptor with a seeming increase at 120µg/ml atorvastatin in the presence of a scratch wound. CXCR4 has been identified as the primary receptor for the cytokine SDF-1, and they both are associated with migration and homing of stem cells (Liu *et al.*, 2011), with loss of either SDF-1 or its receptor resulting in defects in angiogenesis and organ

development (Hattermann *et al.*, 2014; Döring *et al.*, 2017). In chapter 5, the expression of CXCR4 appears to fluctuate over time and is also affected by mode of lesioning, with mechanically lesioned samples generally showing more expression of this receptor, and with sustained expression between the 1 and 9-hour time points evaluated. Given the observation that CXCR4 gets internalised upon binding to SDF-1 (Förster *et al.*, 1998; Hattermann *et al.*, 2014), it is likely that the reduced expression observed with $FeCl_3$ injury is as a result of this mode of injury triggering secretion of higher levels of SDF-1, which would in turn result in more internalisation of its receptor (Yu and Feng, 2008), and also because SDF-1 has been shown to reduce expression of CXCR4, likely through receptor consumption (Molino *et al.*, 2000; Hattermann *et al.*, 2014). These observations are suppoted by the exxpression of CXCR4 seen in chapter 5 where staining appeared higher at the 1-hour time point compared to the 9-hour time point in the presence of atorvastatin, and more so with $FeCl_3$ injury.

Recently, attention has fallen on CXCR7 which has been identified as another receptor for SDF-1 (Hao *et al.*, 2017) but its role in the context of atherosclerosis and cardiovascular disease has yet to be fully elucidated and it would be interesting to observe it's behaviour in the context of our models. The models used here have proven useful in providing a tool that allows tracking of SDF-1 production over time, and demonstrating the effect statins have on this. These models could be used to characterise an array of cytokines that are associated with inflammation and oxidative damage and aid the provision of more insight into the complex interplay of factors involved in these processes.

7.7 Atorvastatin promoted cholesterol efflux and restricted macrophage NO production

Because atherosclerosis and cardiovascular disease were the primary motivators for the contents of this thesis, an evaluation of foam cell formation and the generation of a plaque model were a natural follow-up to the other experiments carried out for this thesis. Metabolic syndrome, a collective term referring to hyperglycaemia, dyslipidaemia and hyperinsulinemia-the primary risk factors for the development of atherosclerosis-, has been shown to aid in the instigation of a hypoxic environment along with oxidative stress leading to the generation of reactive oxygen species, which in turn lead to the activation and augmentation of various inflammatory pathways. These in turn initiate endothelial

dysfunction, foam cell formation and smooth muscle cell proliferation and migration (Varghese, Patel and Yadav, 2017). The data in chapter 6 showed that atorvastatin contributes to reversal of foam cell formation through cholesterol efflux. RAW264 cells dosed with either LDL or oxLDL, then treated with atorvastatin, consistently displayed reduced amounts of cholesterol compared to drug free controls, showing up to a 13% reduction in amount of internalised cholesterol. We determined that the ideal dose that this can be observed within 24 hours was 6µg/ml and the dose used in previous chapters, 60µg/ml, also showed efficacy in this aspect but was accompanied by a significant reduction in cell numbers following the stipulated culture period. This aspect of cell death could be beneficial in terms of reducing plaque size and general uptake of LDL/oxLDL. On the other hand, atorvastatin, and statins in general, are primarily prescribed to lower circulating levels of LDL through inhibition of the cholesterol synthesis pathway, so in that context, concurrent reduction/death of lipid loaded macrophages i.e., foam cells may not have this potential detrimental effect.

One other effect noted with atorvastatin in chapter 6 is that it had an effect on reducing NO production in macrophages, which is associated with a non-inflammatory macrophage phenotype and, in this context, be beneficial in reducing inflammation associated with atherosclerotic plaques, thus easing the strain on the vasculature in dealing with inflammation. With the model created here incorporating HUVECs cultured together with RAW264 cells, it was possible to see, to an extent, the interplay between activated macrophages and endothelial cells. HUVECs were shown to have the ability to affect foam cell formation and behaviour depending on the presence or absence of oxidative damage induced by $FeCl_3$. Specifically, RAW264 foam cells cultured with lesioned HUVECs had lower levels of internalised cholesterol, and this reduction was more apparent in IFN-γ induced RAW264 cells, and even more so in the presence of atorvastatin. It was also interesting to note that atorvastatin limits the effects of IFN-γ on RAW264 lipid uptake (figure 6-22). As to what components are produced by lesioned HUVECs to cause this observation, further work needs to be done to define these parameters in terms of the cytokine profile present in the HUVEC-RAW264 co-culture model. As was previously discussed, it is also possible that the primarily 2D nature of the experiments carried out in this chapter

may not be truly representative of a 3D environment, providing insight but not conclusive evidence. This was further highlighted by the observation that RAW264 behave differently in 2D and 3D i.e., shifting from a monolayer sheet to cluster formation when incorporated into a 3D collagen matrix. As was discussed in chapter 6, material stiffness has been shown to impact macrophage behaviour (Fang, Yang and Han, 2020) so it would have been interesting to see if altering collagen stiffness from that generated by compressing collagen to that used in making the other TE constructs would have given us a model that was easier to visually characterise. Attempts were made to make such a model i.e., attempting to create a plaque zone within a collagen gel which could have smooth muscle and endothelial cells added to it but time and the current global situation were not on our side. The value of including both cell types here is shown by observations recorded in chapter 5 where it was noted that oxidative damage has differing effects on endothelial and smooth muscle cells, with more of an effect, in terms of cellular responses to the damage as well as the functioning of atorvastatin, being observed on endothelial cells.

Through the experiments carried out in chapter 6, it was possible to also see the effect atorvastatin and oxLDL have on expression of the scavenger receptor CD36. This identified the need to look at other scavenger receptors as it was not possible to definitively declare that atorvastatin has a strong effect on CD36 expression, even though atorvastatin did visibly and quantifiably result in reduced oxLDL within RAW264, suggesting that CD36 may not directly contribute to cholesterol efflux. Other published works point out the role of other scavenger receptors i.e., ABCA1 in contributing to cholesterol efflux, so it would be useful to determine the effect atorvastatin has on these receptors in the context of our model. The data collected here also highlighted a deficiency of information regarding the role of CD146 in atherosclerosis, with available information, two papers by Luo et.al, and Blin et. al., suggesting a role in retention of macrophage in atherosclerotic plaques as well as contributing to CD36 internalisation during cholesterol uptake (Luo *et al.*, 2017; Blin *et al.*, 2019). We have managed to show that atorvastatin has an effect on the expression of CD146 i.e., without IFN-γ, atorvastatin appears to restrict expression of CD146 on RAW264 cultured with lesioned HUVECs, which

may contribute to reduced uptake of cholesterol by CD36 given the role of CD146 in promoting CD36 internalisation (Luo *et al.*, 2017; Shu *et al.*, 2020). In the presence of IFN-γ, atorvastatin appears to have less of an influence on expression of CD146. This is interesting as Blin et.al., 2019 demonstrated that CD146 deficiency promoted plaque formation in a mouse model of atherosclerosis through promotion of RANTES production and resultant increased inflammatory responses (Blin *et al.*, 2019). This suggests that under the influence of inflammatory mediators such as IFN-γ, which is possibly stronger than that of lesioned HUVECs, the downstream effects of atorvastatin are altered, possibly due to the observation that IFN-γ increases ROS production (Voloshyna, Littlefield and Reiss, 2014) and as we have seen in other chapters, atorvastatin functions better/triggers cellular responses in an oxidative environment.

The data collected here, and supported by experiments done in chapter 4 and 5, also highlights the importance of evaluating experimental components individually and in concert. For this chapter, this was in evaluating the impact of foam cell stimulants IFN-γ and LPS. It was observed that in regards to NO production and quantification of oxLDL uptake, LPS is a far stronger promoter of NO production than IFN-γ due to its nature as a bacterial cell wall component, and can influence visual and quantitative evaluations of foam cell formation due to its being a lipid-based compound, again as it is a bacterial cell wall component.

7.8 Conclusions

What we have determined through the experiments carried out here is that atorvastatin has several effects aside form lowering cholesterol. Through the two modes of perfusion applied on the 3D constructs, atorvastatin was able to increase density of attached cells on lesioned TE constructs. This effect was observed to be time dependent as consistently across the TEIL, TEML and TEBV, longer incubations resulted in an increased density of attached cells, with optimal attachment being reached 5-hours post lesioning and incubation with atorvastatin. The parallel plate flow chamber was more physiologically relevant, and with adjustable parameters allowing the generation of unidirectional and continuous flow. Through a comparative of injury models, atorvastatin's beneficial effects appear

linked to oxidative stress, demonstrating that $FeCl_3$ is a more biomimetic injury model.

Atorvastatin has shown a capacity to increase secretion of SDF-1 and affect expression of CXCR4, likely through modulation of SDF-1 secretion. The models used to evaluate SDF-1 production highlight the concert effect of both smooth muscle cells and endothelial cells in terms of stabilising production over time. This concert effect is also demonstrated when evaluating cell recruitment to the surface of the injured TE constructs, with the TEBV showing responses that were a midway point between the intimal and medial layer constructs. It was also possible to observe differences in responses based on species of cells used, with murine cells showing better responses with higher doses of atorvastatin compared to human cells. There was also variation observed between human cells, suggesting that EPCs are more adapted to vascular repair than MSCs. Atorvastatin was also shown to positively influence recruitment of perfused cells at both high and low shear stress.

The EPC and MSC homing phenomenon have been studied by evaluating the SDF-1 CXCR4 axis. It was confirmed in both 2D and 3D that the extent of damage caused by both the mechanical means and oxidative damage were sufficient to trigger production of SDF-1, with the $FeCl_3$ induced oxidative damage resulting in higher SDF-1 levels than the mechanical injury. In the 3D TE models, production of SDF-1 increased with longer incubation duration with optimal expression once again being around 5 hours post lesioning and incubation with 60µg/ml atorvastatin. In the 2D model, CXCR4 expression increased in both hMSC and HUVEC with a scratch wound and increasing atorvastatin. In the 3D model, all TE models showed reduced CXCR4 expression after 9 hours incubation compared to the 1-hour incubation counterpart. The reduction in expression was more noticeable in the atorvastatin treated group, implying that the atorvastatin induced SDF-1 production resulted in complete binding and internalisation of available CXCR4, leading to reduced expression over time due to maximum internalisation. The expression pattern of SDF-1/CXCR4 axis potentially explains the higher attachment numbers observed with $FeCl_3$ injured models.

It was also possible to show that atorvastatin affects efflux of internalised cholesterol from foam cells, as well as restricting macrophagic production of NO. We were also able to define the effect of different

stimuli such as IFN-γ and LPS both individually and in concert, showing that LPS is a far stronger stimulator of NO production and as such is not an ideal tool to use in generating foam cells as the effects are more indicative of an infection versus an inflammatory disorder. The foam cell model, made with RAW264 cells dosed with either LDL or oxLDL, demonstrated that treatment with atorvastatin resulted in consistently reduced amounts of internalised cholesterol compared to the drug free controls, showing up to a 13% reduction in the amount of internalised cholesterol. The ideal dose at which this can be observed is 6µg/ml.

The use of a new prototype incorporating nanofibers into a well insert revealed the interplay between activated macrophages and endothelial cells. HUVECs were shown to have the ability to affect foam cell formation and behaviour, depending on the presence or absence of oxidative damage induced by $FeCl_3$. Specifically, IFN-γ stimulated RAW264 foam cells, cultured with lesioned HUVECs, showed higher efficacy at cholesterol efflux in the presence of atorvastatin. It was also interesting to note that atorvastatin was not as effective at stimulating efflux when IFN-γ was not used to induce RAW264 lipid uptake. The nanofiber well inserts also allowed the investigation of the role of endothelial cells in the expression of CD36 and CD146. Without IFN-γ induction, CD36 expression was higher in RAW264 cells cultured with lesioned HUVECs, and the presence of statin showed no change of CD36 expression. With IFN-γ stimulated RAW264 cells, there was no difference in CD36 expression between lesioned or intact HUVECs or with atorvastatin, indicating that IFN-γ is a strong trigger for CD36 expression. It was also possible to highlight the deficiency in information regarding the role of CD146 in atherosclerosis, generating data that suggests atorvastatin has an effect on expression of this receptor and that IFN-γ appears to negate this effect i.e., atorvastatin reduces expression of CD146 in oxLDL loaded RAW264 foam cells in the absence of IFN-γ. The versatility of these models was that they can be adjusted to different dimensions and could be used to evaluate different types of injury and gauge cellular responses both to the injury as well as the effects of atorvastatin in these contexts. Through this, it was possible to demonstrate that atorvastatin is more effective in a cellular environment affected by oxidative stress.

7.9 Future perspectives

As with any body of work, addressing research problems sheds light on additional avenues of investigation based on outputs generated and experimental parameters. For the experiments carried out here, we have evaluated directions this work could take to make some things clearer and address new questions raised through experimentation.

To further improve the relatability of chapter 6, switching to human cells i.e., human macrophages such as THP-1 cells would help in seeing of the observations recorded for RAW264 cells could be applied to human cells, the importance of this not only being the relatability to humans but also to confirm accuracy of observations as data collected in chapter 4 and the discussion earlier demonstrates the variability of responses between human and murine cells. It would also be interesting to investigate the effects of material stiffness on macrophage behaviour due to observations of differing behaviour in 2D versus 3D culture. As pertains to foam cell formation and cholesterol efflux, we identified an area lacking sufficient research, i.e., the specific role of CD146 in atherosclerosis. It was possible to identify an impact of both IFN-γ and atorvastatin on expression of this receptor, but the effect of a variety of other inflammatory mediators/cytokines on expression of this and other receptors associated with foam cell formation and potentially cholesterol efflux are still to be determined. The models used here were able to both quantify and track expression of SDF-1, as such it should be more than possible to quantify and track expression of others related to inflammation and atherosclerosis such as IFN-γ, the interleukin family of cytokines and TNF-α and compare the extent of expression both with and without atorvastatin, thus gaining a clearer picture of the interactions at play during atherosclerosis associated inflammation. This would also be ideal in determining redundancies between cytokines and their related receptors.

Further characterization of EPCs would also be beneficial as there is still disagreement in regards to specific characteristics that define this cell type. We used the receptors CXCR4, CD34, Flk-1, CD45 and CD31 which were deemed sufficient to define these cells as endothelial progenitors, and this definition

was supported further by observations that reflected previously published work. It would also be interesting to see if different isolation protocols, such as the use of antibody coated magnetic beads/magnetic activated cell sorting (MACS), flow cytometry and modified culture conditions could be applied to extract a purer fraction of cells with a more homogenous surface receptor profile (Urbich and Dimmeler, 2004; Yoder, 2012; Chong, Ng and Chan, 2016; Chopra *et al.*, 2018c). It would also be interesting to compare behaviour of a purer fraction with a more heterogenous cell mixture and possibly including platelets which have been shown to be able to transfer receptors such as Flk-1 and CD133 to other cells when cultured together (Medina *et al.*, 2010; Fadini, Losordo and Dimmeler, 2012; Chopra *et al.*, 2018b).

References

1. Abou-Saleh, H. *et al.* (2009) 'Endothelial Progenitor Cells Bind and Inhibit Platelet Function and Thrombus Formation', *Circulation*. PMC Canada manuscript submission, 120(22), p. 2230. doi: 10.1161/CIRCULATIONAHA.109.894642.
2. Afzal, M. R. *et al.* (2015) 'Adult Bone Marrow Cell Therapy for Ischemic Heart DiseaseNovelty and Significance', *Circulation Research*, 117(6), pp. 558–575. doi: 10.1161/CIRCRESAHA.114.304792.Adult.
3. Akata, T., Izumi, K. and Nakashima, M. (2001) 'Mechanisms of direct inhibitory action of ketamine on vascular smooth muscle in mesenteric resistance arteries', *Anesthesiology*. Lippincott Williams and Wilkins, 95(2), pp. 452–462. doi: 10.1097/00000542-200108000-00030.
4. Anisi, F. *et al.* (2014) 'Applying shear stress to endothelial cells in a new perfusion chamber: hydrodynamic analysis', *Journal of Artificial Organs*, 17(4), pp. 329–336. doi: 10.1007/s10047-014-0790-0.
5. Anton, D. *et al.* (2015) 'Three-dimensional cell culture: A breakthrough in vivo', *International Journal of Molecular Sciences*, 16(3), pp. 5517–5527. doi: 10.3390/ijms16035517.
6. Asahara, T. *et al.* (1997) 'Isolation of putative progenitor endothelial cells for angiogenesis', *Science*, 275(5302), pp. 964–967. doi: 10.1126/science.275.5302.964.
7. Atkinson, P. M., Taylor, D. I. and Chetty, N. (1985) 'Inhibition of platelet aggregation by ketamine hydrochloride', *Thrombosis Research*. Pergamon, 40(2), pp. 227–234. doi: 10.1016/0049-3848(85)90333-0.
8. Babczyk, P. *et al.* (2014) 'Stem Cells on Biomaterials for Synthetic Grafts to Promote Vascular Healing', *Journal of Clinical Medicine*, 3(1), pp. 39–87. doi: 10.3390/jcm3010039.
9. Babita Mahanta, R. N. (2014) 'An Overview of Various Biomimetic Scaffolds: Challenges and Applications in Tissue Engineering', *Journal of Tissue Science & Engineering*, 05(02). doi:

10.4172/2157-7552.1000137.

10. Badimon, L., Padró, T. and Vilahur, G. (2012) 'Atherosclerosis, platelets and thrombosis in acute ischaemic heart disease', *European Heart Journal: Acute Cardiovascular Care*. SAGE Publications, 1(1), pp. 60–74. doi: 10.1177/2048872612441582.
11. Bagno, L. *et al.* (2018) 'Mesenchymal Stem Cell-Based Therapy for Cardiovascular Disease: Progress and Challenges', *Molecular Therapy*. Elsevier Ltd., 26(7), pp. 1610–1623. doi: 10.1016/j.ymthe.2018.05.009.
12. Baker, S. K. and Tarnopolsky, M. A. (2001) 'Statin myopathies: Pathophysiologic and clinical perspectives', *Clinical and Investigative Medicine*, 24(5), pp. 258–272.
13. Bangalore, S. *et al.* (2018) 'Newer-Generation Ultrathin Strut Drug-Eluting Stents Versus Older Second-Generation Thicker Strut Drug-Eluting Stents for Coronary Artery Disease: Meta-Analysis of Randomized Trials', *Circulation*, 138(20), pp. 2216–2226. doi: 10.1161/CIRCULATIONAHA.118.034456.
14. Barbier, V. *et al.* (2020) 'Endothelial E-selectin inhibition improves acute myeloid leukaemia therapy by disrupting vascular niche-mediated chemoresistance', *Nature Communications*. Springer US, 11(1), pp. 1–15. doi: 10.1038/s41467-020-15817-5.
15. Basatemur, G. L. *et al.* (2019) 'Vascular smooth muscle cells in atherosclerosis', *Nature Reviews Cardiology*, 16(12), pp. 727–744. doi: 10.1038/s41569-019-0227-9.
16. Bashir, S. *et al.* (2016) 'Macrophage polarization: the link between inflammation and related diseases', *Inflammation Research*. Springer Basel, 65(1), pp. 1–11. doi: 10.1007/s00011-015-0874-1.
17. Bentzon, J. F. *et al.* (2014) 'Mechanisms of plaque formation and rupture', *Circulation Research*. Lippincott Williams and Wilkins, 114(12), pp. 1852–1866. doi: 10.1161/CIRCRESAHA.114.302721.
18. Bing, W. *et al.* (2016) 'Simvastatin improves the homing of BMSCs via the PI3K/AKT/miR-9 pathway', *Journal of Cellular and Molecular Medicine*, 20(5), pp. 949–961. doi:

10.1111/jcmm.12795.

19. Biros, E., Reznik, J. E. and Moran, C. S. (2021) 'Role of inflammatory cytokines in genesis and treatment of atherosclerosis', *Trends in Cardiovascular Medicine*. Elsevier Inc., (xxxx). doi: 10.1016/j.tcm.2021.02.001.
20. Biscetti, F. *et al.* (2019) 'The role of the stem cells therapy in the peripheral artery disease', *International Journal of Molecular Sciences*, 20(9). doi: 10.3390/ijms20092233.
21. Blin, M. G. *et al.* (2019) 'CD146 deficiency promotes plaque formation in a mouse model of atherosclerosis by enhancing RANTES secretion and leukocyte recruitment', *Journal of Molecular and Cellular Cardiology*. Elsevier, 130(March), pp. 76–87. doi: 10.1016/j.yjmcc.2019.03.017.
22. Boden, W. E., Sidhu, M. S. and Toth, P. P. (2014) 'The therapeutic role of niacin in dyslipidemia management', *Journal of Cardiovascular Pharmacology and Therapeutics*, 19(2), pp. 141–158. doi: 10.1177/1074248413514481.
23. Borén, J. *et al.* (2020) 'Low-density lipoproteins cause atherosclerotic cardiovascular disease: Pathophysiological, genetic, and therapeutic insights: A consensus statement from the European Atherosclerosis Society Consensus Panel', *European Heart Journal*, 41(24), pp. 2313–2330. doi: 10.1093/eurheartj/ehz962.
24. Bouitbir, J. *et al.* (2016) 'Statins Trigger Mitochondrial Reactive Oxygen Species-Induced Apoptosis in Glycolytic Skeletal Muscle', *Antioxidants & Redox Signaling*, 24(2), pp. 84–98. doi: 10.1089/ars.2014.6190.
25. Cai, A. *et al.* (2013) 'Atorvastatin Treatment of Rats with Ischemia-Reperfusion Injury Improves Adipose-Derived Mesenchymal Stem Cell Migration and Survival via the SDF-1α/CXCR-4 Axis', *PLoS ONE*. Edited by R. G. Katare. Public Library of Science, 8(12), p. e79100. doi: 10.1371/journal.pone.0079100.
26. Cai, J. *et al.* (2014) 'Atorvastatin improves survival of implanted stem cells in a rat model of renal ischemia-reperfusion injury', *American Journal of Nephrology*, 39(6), pp. 466–475. doi:

10.1159/000362623.

27. Camnitz, W. *et al.* (2012) 'Dose-dependent Effect of Statin Therapy on Circulating CXCL12 Levels in Patients with Hyperlipidemia', *Clinical and Translational Medicine*, 1(1), pp. 1–5. doi: 10.1186/2001-1326-1-23.
28. Castells-sala, C. *et al.* (2015) 'Current Applications of Tissue Engineering in Biomedicine', *Journal of Biochips & Tissue Chips*, s2(August 2015). doi: 10.4172/2153-0777.s2-004.
29. Cecchi, E. *et al.* (2011) 'Role of hemodynamic shear stress in cardiovascular disease', *Atherosclerosis*. Elsevier Ireland Ltd, 214(2), pp. 249–256. doi: 10.1016/j.atherosclerosis.2010.09.008.
30. Chávez-Sánchez, L. *et al.* (2014) 'The role of TLR2, TLR4 and CD36 in macrophage activation and foam cell formation in response to oxLDL in humans', *Human Immunology*, 75(4), pp. 322–329. doi: 10.1016/j.humimm.2014.01.012.
31. Chen, C. *et al.* (2021) 'Isolation and characterization of endothelial progenitor cells from canine bone marrow', *Biotechnic and Histochemistry*. Taylor & Francis, 96(2), pp. 85–93. doi: 10.1080/10520295.2020.1762001.
32. Chen, J. yi *et al.* (2018) 'Nitric oxide bioavailability dysfunction involves in atherosclerosis', *Biomedicine and Pharmacotherapy*. Elsevier, 97(October 2017), pp. 423–428. doi: 10.1016/j.biopha.2017.10.122.
33. Chen, Q., Liang, S. and Thouas, G. A. (2013) 'Elastomeric biomaterials for tissue engineering', *Progress in Polymer Science*. Elsevier Ltd, 38(3–4), pp. 584–671. doi: 10.1016/j.progpolymsci.2012.05.003.
34. Chen, X.-L. L. *et al.* (1997) 'E-Selectin Gene Expression in Vascular Smooth Muscle Cells', *Circulation Research*, 80(3), pp. 305–311. doi: 10.1161/01.res.80.3.305.
35. Cheng, C. *et al.* (2006) 'Atherosclerotic lesion size and vulnerability are determined by patterns of fluid shear stress', *Circulation*, 113(23), pp. 2744–2753. doi: 10.1161/CIRCULATIONAHA.105.590018.

36. Cheng, C. C. *et al.* (2013) 'Distinct angiogenesis roles and surface markers of early and late endothelial progenitor cells revealed by functional group analyses', *BMC Genomics*, 14(1). doi: 10.1186/1471-2164-14-182.
37. Cheng, X. *et al.* (2009) 'Atorvastatin Modulates Th1/Th2 Response in Patients With Chronic Heart Failure', *Journal of Cardiac Failure*. Elsevier Inc, 15(2), pp. 158–162. doi: 10.1016/j.cardfail.2008.10.001.
38. Chiang, K. H. *et al.* (2015) 'Statins, HMG-CoA reductase inhibitors, improve neovascularization by increasing the expression density of CXCR4 in endothelial progenitor cells', *PLoS ONE*, 10(8), pp. 1–18. doi: 10.1371/journal.pone.0136405.
39. Chong, M. S. K., Ng, W. K. and Chan, J. K. Y. (2016) 'Concise Review: Endothelial Progenitor Cells in Regenerative Medicine: Applications and Challenges', *STEM CELLS Translational Medicine*. Wiley, 5(4), pp. 530–538. doi: 10.5966/sctm.2015-0227.
40. Chong, P. P. *et al.* (2012) 'Human peripheral blood derived mesenchymal stem cells demonstrate similar characteristics and chondrogenic differentiation potential to bone marrow derived mesenchymal stem cells', *Journal of Orthopaedic Research*, 30(4), pp. 634–642. doi: 10.1002/jor.21556.
41. Chopra, H. *et al.* (2018a) 'Insights into endothelial progenitor cells: Origin, classification, potentials, and prospects', *Stem Cells International*. Hindawi Limited. doi: 10.1155/2018/9847015.
42. Chopra, H. *et al.* (2018b) 'Insights into endothelial progenitor cells: Origin, classification, potentials, and prospects', *Stem Cells International*, 2018. doi: 10.1155/2018/9847015.
43. Chopra, H. *et al.* (2018c) 'Insights into endothelial progenitor cells: Origin, classification, potentials, and prospects', *Stem Cells International*. Hindawi Limited. doi: 10.1155/2018/9847015.
44. Choromañska, B. *et al.* (2017) 'The role of CD36 receptor in the pathogenesis of atherosclerosis', *Advances in Clinical and Experimental Medicine*, 26(4), pp. 717–722. doi:

10.17219/acem/62325.

45. Collot-Teixeira, S. *et al.* (2007) 'CD36 and macrophages in atherosclerosis', *Cardiovascular Research*. Oxford Academic, pp. 468–477. doi: 10.1016/j.cardiores.2007.03.010.
46. Costa, S. *et al.* (2016) 'Statins and oxidative stress in chronic heart failure', *Revista Portuguesa de Cardiologia (English Edition)*. Sociedade Portuguesa de Cardiologia, 35(1), pp. 41–57. doi: 10.1016/j.repce.2015.12.016.
47. Cunningham, K. S. and Gotlieb, A. I. (2005) 'The role of shear stress in the pathogenesis of atherosclerosis', *Laboratory Investigation*, 85(1), pp. 9–23. doi: 10.1038/labinvest.3700215.
48. Dar, A., Kollet, O. and Lapidot, T. (2006) 'Mutual, reciprocal SDF-1/CXCR4 interactions between hematopoietic and bone marrow stromal cells regulate human stem cell migration and development in NOD/SCID chimeric mice', *Experimental Hematology*. Elsevier, pp. 967–975. doi: 10.1016/j.exphem.2006.04.002.
49. Davies, J. T. *et al.* (2016) 'Current and emerging uses of statins in clinical therapeutics: A review', *Lipid Insights*, 9(1), pp. 13–29. doi: 10.4137/LPI.S37450.
50. Davies, P. F. (2009) 'Hemodynamic shear stress and the endothelium in cardiovascular pathophysiology', *Nature Clinical Practice Cardiovascular Medicine*. NIH Public Access, pp. 16–26. doi: 10.1038/ncpcardio1397.
51. Deegan, A. J. (2013) *Novel tissue engineering approaches to enhance natural bone formation*, *Novel tissue engineering approaches to enhance natural bone formation*.
52. Desideri, G. and Ferri, C. (2005) 'Endothelial Activation. Sliding Door to Atherosclerosis', *Current Pharmaceutical Design*, 11(17), pp. 2163–2175. doi: 10.2174/1381612054367382.
53. Dimmeler, S. and Zeiher, A. M. (2004) 'Vascular repair by circulating endothelial progenitor cells: The missing link in atherosclerosis?', *Journal of Molecular Medicine*, 82(10), pp. 671–677. doi: 10.1007/s00109-004-0580-x.
54. Dimova, I. *et al.* (2019) 'SDF-1/CXCR4 signalling is involved in blood vessel growth and remodelling by intussusception', *Journal of Cellular and Molecular Medicine*. Blackwell

Publishing Inc., 23(6), pp. 3916–3926. doi: 10.1111/jcmm.14269.

55. Ding, Z. *et al.* (2012) 'Effect of oxidized low-density lipoprotein concentration polarization on human smooth muscle cells' proliferation, cycle, apoptosis and oxidized low-density lipoprotein uptake', *Journal of The Royal Society Interface*. Royal Society, 9(71), pp. 1233–1240. doi: 10.1098/rsif.2011.0436.
56. Döring, Y. *et al.* (2017) 'Vascular CXCR4 limits atherosclerosis by maintaining arterial integrity: Evidence from mouse and human studies', *Circulation*, 136(4), pp. 388–403. doi: 10.1161/CIRCULATIONAHA.117.027646.
57. Eisen, A. *et al.* (2015) 'Effect of High Dose Statin Pretreatment on Endothelial Progenitor Cells After Percutaneous Coronary Intervention (HIPOCRATES Study)', *Cardiovascular Drugs and Therapy*. Springer New York LLC, 29(2), pp. 129–135. doi: 10.1007/s10557-015-6575-8.
58. Elyasi, A. *et al.* (2020) 'The role of interferon-γ in cardiovascular disease: an update', *Inflammation Research*. Springer International Publishing, 69(10), pp. 975–988. doi: 10.1007/s00011-020-01382-6.
59. Evans, C. E., Iruela-Arispe, M. L. and Zhao, Y. Y. (2021) 'Mechanisms of Endothelial Regeneration and Vascular Repair and Their Application to Regenerative Medicine', *American Journal of Pathology*. American Society for Investigative Pathology, 191(1), pp. 52–65. doi: 10.1016/j.ajpath.2020.10.001.
60. Fadini, G. P., Losordo, D. and Dimmeler, S. (2012) 'Critical reevaluation of endothelial progenitor cell phenotypes for therapeutic and diagnostic use', *Circulation Research*, pp. 624–637. doi: 10.1161/CIRCRESAHA.111.243386.
61. Fang, J. Y., Yang, Z. and Han, B. (2020) 'Switch of macrophage fusion competency by 3D matrices', *Scientific Reports*, 10(1), pp. 1–12. doi: 10.1038/s41598-020-67056-9.
62. Fattori, R. and Piva, T. (2003) 'Drug-eluting stents in vascular intervention', *Lancet*, 361(9353), pp. 247–249. doi: 10.1016/S0140-6736(03)12275-1.
63. Félétou, M. (2011) 'The Endothelium, Part I: Multiple Functions of the Endothelial Cells --

Focus on Endothelium-Derived Vasoactive Mediators', *Colloquium Series on Integrated Systems Physiology: From Molecule to Function*. San Rafael (CA), 3(4), pp. 1–306. doi: 10.4199/C00031ED1V01Y201105ISP019.

64. Fisher, S. *et al.* (2016) 'Stem cell therapy for chronic ischaemic heart disease and congestive heart failure (Review) SUMMARY OF FINDINGS FOR THE MAIN COMPARISON', *Cochrane Library*, (4). doi: 10.1002/14651858.CD007888.pub3.www.cochranelibrary.com.
65. Förster, R. *et al.* (1998) 'Intracellular and surface expression of the HIV-1 coreceptor CXCR4/fusin on various leukocyte subsets: rapid internalization and recycling upon activation.', *Journal of immunology (Baltimore, Md. : 1950)*, 160(3), pp. 1522–31. Available at: http://www.ncbi.nlm.nih.gov/pubmed/9570576.
66. Förstermann, U. and Sessa, W. C. (2012) 'Nitric oxide synthases: Regulation and function', *European Heart Journal*. Oxford University Press, p. 829. doi: 10.1093/eurheartj/ehr304.
67. Gao, C. *et al.* (2020) 'Treatment of atherosclerosis by macrophage-biomimetic nanoparticles via targeted pharmacotherapy and sequestration of proinflammatory cytokines', *Nature Communications*. Springer US, 11(1). doi: 10.1038/s41467-020-16439-7.
68. Gao, J. H., Yu, X. H. and Tang, C. K. (2019) 'CXC chemokine ligand 12 (CXCL12) in atherosclerosis: An underlying therapeutic target', *Clinica Chimica Acta*. Elsevier, 495(April), pp. 538–544. doi: 10.1016/j.cca.2019.05.022.
69. Gareus, R. *et al.* (2008) 'Endothelial Cell-Specific NF-κB Inhibition Protects Mice from Atherosclerosis', *Cell Metabolism*, 8(5), pp. 372–383. doi: 10.1016/j.cmet.2008.08.016.
70. Gazzerro, P. *et al.* (2012) 'Pharmacological actions of statins: A critical appraisal in the management of cancer', *Pharmacological Reviews*, 64(1), pp. 102–146. doi: 10.1124/pr.111.004994.
71. Geng, Y. J. and Hansson, G. K. (1992) 'Interferon-γ inhibits scavenger receptor expression and foam cell formation in human monocyte-derived macrophages', *Journal of Clinical Investigation*, 89(4), pp. 1322–1330. doi: 10.1172/JCI115718.

72. Geovanini, G. R. and Libby, P. (2018) 'Atherosclerosis and inflammation: Overview and updates', *Clinical Science*, 132(12), pp. 1243–1252. doi: 10.1042/CS20180306.
73. Golia, E. *et al.* (2014) 'Inflammation and cardiovascular disease: From pathogenesis to therapeutic target', *Current Atherosclerosis Reports*, 16(9). doi: 10.1007/s11883-014-0435-z.
74. Gorabi, A. M. *et al.* (2020) 'Effects of statins on the biological features of mesenchymal stem cells and therapeutic implications', *Heart Failure Reviews*. Heart Failure Reviews. doi: 10.1007/s10741-020-09929-9.
75. Granger, D. N. and Senchenkova, E. (2010) *Inflammation and the Microcirculation*, *Colloquium Series on Integrated Systems Physiology: From Molecule to Function*. doi: 10.4199/c00013ed1v01y201006isp008.
76. Greenspan, P. and Fowler, S. D. (1985) 'Spectrofluorometric studies of the lipid probe, nile red', *Journal of Lipid Research*, 26(7), pp. 781–789. doi: 10.1016/S0022-2275(20)34307-8.
77. Guerrini, V. and Gennaro, M. L. (2019) 'Foam Cells: One Size Doesn't Fit All', *Trends in Immunology*, 40(12), pp. 1163–1179. doi: 10.1016/j.it.2019.10.002.
78. Guo, Q. *et al.* (2020) 'Immune activation of murine RAW264.7 macrophages by sonicated and alkalized paramylon from Euglena gracilis', *BMC Microbiology*, 20(1), pp. 1–10. doi: 10.1186/s12866-020-01782-y.
79. Gupta, R. *et al.* (2018) 'An overview of pleiotropic effect of statins in cardiovascular disease', *Pharmacy & Pharmacology International Journal*, 6(6), pp. 435–439. doi: 10.15406/ppij.2018.06.00214.
80. Han, C.-Y. and Pak, Y. K. (1999) *Oxidation-dependent effects of oxidized LDL: proliferation or cell death*, *EXPERIMENTAL and MOLECULAR MEDICINE*.
81. Hansen, M., Sonne, D. P. and Knop, F. K. (2014) 'Bile acid sequestrants: Glucose-lowering mechanisms and efficacy in type 2 diabetes', *Current Diabetes Reports*, 14(5). doi: 10.1007/s11892-014-0482-4.
82. Hao, H. *et al.* (2017) 'Loss of Endothelial CXCR7 Impairs Vascular Homeostasis and Cardiac

Remodeling after Myocardial Infarction: Implications for Cardiovascular Drug Discovery', *Circulation*, 135(13), pp. 1253–1264. doi: 10.1161/CIRCULATIONAHA.116.023027.

83. Hattermann, K. *et al.* (2014) 'Effects of the chemokine CXCL12 and combined internalization of its receptors CXCR4 and CXCR7 in human MCF-7 breast cancer cells', *Cell and Tissue Research*, 357(1), pp. 253–266. doi: 10.1007/s00441-014-1823-y.
84. Heidari, B. *et al.* (2013) 'Comparison of proliferative and multilineage differentiation potential of sheep mesenchymal stem cells derived from bone marrow, liver, and adipose tissue', *Avicenna Journal of Medical Biotechnology*, 5(2), pp. 104–117.
85. Heinke, S. *et al.* (2004) 'The influence of statins on the free intracellular calcium concentration in human umbilical vein endothelial cells', *BMC Cardiovascular Disorders*, 4, pp. 1–6. doi: 10.1186/1471-2261-4-4.
86. Hennekens, C. H., Schuttenberg, N. and Pfeffer, M. A. (2019) 'Prescription of Aspirin and Statins in Primary Prevention', *Primary Care - Clinics in Office Practice*, 46(1), pp. 13–25. doi: 10.1016/j.pop.2018.10.004.
87. Herrington, W. *et al.* (2016) 'Epidemiology of Atherosclerosis and the Potential to Reduce the Global Burden of Atherothrombotic Disease', *Circulation Research*, 118(4), pp. 535–546. doi: 10.1161/CIRCRESAHA.115.307611.
88. Hielscher, D. *et al.* (2018) 'Stem Cell Sources and Graft Material for Vascular Tissue Engineering', *Stem Cell Reviews and Reports*. Stem Cell Reviews and Reports, 14(5), pp. 642–667. doi: 10.1007/s12015-018-9825-x.
89. Hill, J. M. *et al.* (2003) 'Circulating Endothelial Progenitor Cells, Vascular Function, and Cardiovascular Risk', *New England Journal of Medicine*. Massachusetts Medical Society, 348(7), pp. 593–600. doi: 10.1056/nejmoa022287.
90. Hirase, T. and Node, K. (2012) 'Endothelial dysfunction as a cellular mechanism for vascular failure', *American Journal of Physiology - Heart and Circulatory Physiology*. American Physiological Society Bethesda, MD, pp. 499–505. doi: 10.1152/ajpheart.00325.2011.

91. Hoeksema, M. A. *et al.* (2015) 'IFN-γ Priming of Macrophages Represses a Part of the Inflammatory Program and Attenuates Neutrophil Recruitment', *The Journal of Immunology*, 194(8), pp. 3909–3916. doi: 10.4049/jimmunol.1402077.

92. Hristov, M. *et al.* (2007) 'Regulation of endothelial progenitor cell homing after arterial injury', *Thrombosis and Haemostasis*, 98(2), pp. 274–277. doi: 10.1160/TH07-03-0181.

93. Huang, H. *et al.* (2014) 'Induction of inducible nitric oxide synthase (iNOS) expression by oxLDL inhibits macrophage derived foam cell migration', *Atherosclerosis*. Elsevier Ltd, 235(1), pp. 213–222. doi: 10.1016/j.atherosclerosis.2014.04.020.

94. Huang, S. *et al.* (2012) 'Celastrol inhibits vasculogenesis by suppressing the VEGF-induced functional activity of bone marrow-derived endothelial progenitor cells', *Biochemical and Biophysical Research Communications*, 423(3), pp. 467–472. doi: 10.1016/j.bbrc.2012.05.143.

95. Huizer, K. *et al.* (2017) 'Improving the characterization of endothelial progenitor cell subsets by an optimized FACS protocol', *PLOS ONE*. Edited by F. Bertolini. Public Library of Science, 12(9), p. e0184895. doi: 10.1371/journal.pone.0184895.

96. Ii, M. (2010) 'Bone marrow-derived endothelial progenitor cells: Isolation and characterization for myocardial repair', *Methods in Molecular Biology*. Humana Press Inc., 660, pp. 9–27. doi: 10.1007/978-1-60761-705-1_2.

97. Janssen, B. J. A. *et al.* (2004) 'Effects of anesthetics on systemic hemodynamics in mice', *American Journal of Physiology - Heart and Circulatory Physiology*, 287(4 56-4), pp. 1618–1625. doi: 10.1152/ajpheart.01192.2003.

98. Jeevasankar, M. *et al.* (2008) 'Polycythemia in the newborn', *Indian Journal of Pediatrics*, 75(1), pp. 68–72. doi: 10.1007/s12098-008-0010-0.

99. Jötten, A. M. *et al.* (2019) 'Correlation of in vitro cell adhesion, local shear flow and cell density', *RSC Advances*, 9(1), pp. 543–551. doi: 10.1039/c8ra07416j.

100. Kachamakova-Trojanowska, N. *et al.* (2015) 'The real face of endothelial progenitor cells - Circulating angiogenic cells as endothelial prognostic marker?', *Pharmacological*

Reports. Institute of Pharmacology, Polish Academy of Sciences, 67(4), pp. 793–802. doi: 10.1016/j.pharep.2015.05.017.

101. Karantalis, V. and Hare, J. M. (2015) 'Use of Mesenchymal Stem Cells for Therapy of Cardiac Disease', *Circulation Research*, 116(8), pp. 1413–1430. doi: 10.1161/CIRCRESAHA.116.303614.

102. Karp, J. M. and Leng Teo, G. S. (2009) 'Mesenchymal Stem Cell Homing: The Devil Is in the Details', *Cell Stem Cell*. Elsevier Inc., 4(3), pp. 206–216. doi: 10.1016/j.stem.2009.02.001.

103. Kartz, G. A. *et al.* (2014) 'SR-BI/CD36 chimeric receptors define extracellular subdomains of SR-BI critical for cholesterol transport', *Biochemistry*, 53(39), pp. 6173–6182. doi: 10.1021/bi500706x.

104. Kattoor, A. J. *et al.* (2017) 'Oxidative Stress in Atherosclerosis', *Current Atherosclerosis Reports*. Current Atherosclerosis Reports, 19(11). doi: 10.1007/s11883-017-0678-6.

105. Khan, M., Adil, S. E. R. and Olson, A. L. (2017) 'The role of mesenchymal stem cells in oncology and regenerative medicine', *Future Oncology*, 13(9), pp. 821–831. doi: 10.2217/fon-2016-0264.

106. Khodabandehlou, K. *et al.* (2017) 'Targeting cell adhesion molecules with nanoparticles using in vivo and flow-based in vitro models of atherosclerosis', *Experimental Biology and Medicine*, 242(8), pp. 799–812. doi: 10.1177/1535370217693116.

107. Klabunde, R. (2011) *Cardiovascular Physiology Concepts*. Lippincott Williams & Wilkins/Wolters Kluwer. Available at: https://books.google.co.uk/books?id=27ExgvGnOagC.

108. Kouzbari, K. *et al.* (2019) 'Oscillatory shear potentiates latent TGF-β1 activation more than steady shear as demonstrated by a novel force generator', *Scientific Reports*, 9(1), pp. 1–8. doi: 10.1038/s41598-019-42302-x.

109. Kucia, M. *et al.* (2005) 'Trafficking of Normal Stem Cells and Metastasis of Cancer Stem Cells Involve Similar Mechanisms: Pivotal Role of the SDF-1-CXCR4 Axis', *Stem Cells*. Wiley, 23(7), pp. 879–894. doi: 10.1634/stemcells.2004-0342.

110. Kunz, G. A. *et al.* (2006) 'Circulating endothelial progenitor cells predict coronary artery disease severity', *American Heart Journal*, 152(1), pp. 190–195. doi: 10.1016/j.ahj.2006.02.001.

111. Kuo, T. T., Huang, Y. Bin and Hsieh, C. J. (2020) 'Consumption and market share of cholesterol-lowering drugs in high-risk patients before and after the release of the 2013 ACC/AHA cholesterol guidelines: A retrospective observational study', *BMJ Open*, 10(11), pp. 1–8. doi: 10.1136/bmjopen-2020-036769.

112. Kurebayashi, N. and Ogawa, Y. (2001) 'Depletion of Ca2+ in the sarcoplasmic reticulum stimulates Ca2+ entry into mouse skeletal muscle fibres', *Journal of Physiology*. John Wiley & Sons, Ltd, 533(1), pp. 185–199. doi: 10.1111/j.1469-7793.2001.0185b.x.

113. L'Heureux, N. *et al.* (2006) 'Human tissue-engineered blood vessels for adult arterial revascularization', *Nature Medicine*, 12(3), pp. 361–365. doi: 10.1038/nm1364.

114. Lamalice, L., Le Boeuf, F. and Huot, J. (2007) 'Endothelial cell migration during angiogenesis', *Circulation Research*. Lippincott Williams & Wilkins, pp. 782–794. doi: 10.1161/01.RES.0000259593.07661.1e.

115. Lara-Guzmán, O. J. *et al.* (2018) 'Oxidized LDL triggers changes in oxidative stress and inflammatory biomarkers in human macrophages', *Redox Biology*. Elsevier B.V., 15(September 2017), pp. 1–11. doi: 10.1016/j.redox.2017.11.017.

116. Lee, D. H. and Hernandez, J. M. d. la T. (2018) 'The newest generation of drug-eluting stents and beyond', *European Cardiology Review* , 13(1), pp. 54–59. doi: 10.15420/ecr.2018:8:2.

117. Lee, J. H. and Kim, H. W. (2018) 'Emerging properties of hydrogels in tissue engineering', *Journal of Tissue Engineering*, 9, pp. 0–3. doi: 10.1177/2041731418768285.

118. Lee, P. S. S. *et al.* (2014) 'Abstract 13054: Thymosin Beta-4-Treated Endothelial Progenitor Cells Improve Cardiac Function and Vasculogenesis in Diabetic Obese Rats with Myocardial Infarction', *Circulation*, 130(suppl_2), pp. A13054–A13054. doi:

10.1161/circ.130.suppl_2.13054.

119. Lehoux, S. and Jones, E. A. (2016) 'Shear stress, arterial identity and atherosclerosis', *Thrombosis and Haemostasis*, 115(03), pp. 467–473. doi: 10.1160/th15-10-0791.

120. Leong, D. P. *et al.* (2017) 'Reducing the global burden of cardiovascular disease, part 2: Prevention and treatment of cardiovascular disease', *Circulation Research*, 121(6), pp. 695–710. doi: 10.1161/CIRCRESAHA.117.311849.

121. Leroyer, A. S. *et al.* (2019) 'CD146 (Cluster of Differentiation 146): An Adhesion Molecule Involved in Vessel Homeostasis', *Arteriosclerosis, Thrombosis, and Vascular Biology*, 39(6), pp. 1026–1033. doi: 10.1161/ATVBAHA.119.312653.

122. Levitt, J. A., Chung, P.-H. and Suhling, K. (2015) 'Spectrally resolved fluorescence lifetime imaging of Nile red for measurements of intracellular polarity', *Journal of Biomedical Optics*. SPIE-Intl Soc Optical Eng, 20(9), p. 096002. doi: 10.1117/1.jbo.20.9.096002.

123. Li, B. R. *et al.* (2017) 'miR-758-5p regulates cholesterol uptake via targeting the CD36 3'UTR', *Biochemical and Biophysical Research Communications*, 494(1–2), pp. 384–389. doi: 10.1016/j.bbrc.2017.09.150.

124. Li, D. and Mehta, J. L. (2005) 'Oxidized LDL, a critical factor in atherogenesis', *Cardiovascular Research*, 68(3), pp. 353–354. doi: 10.1016/j.cardiores.2005.09.009.

125. Li, L. *et al.* (2020) 'Foam cells promote atherosclerosis progression by releasing CXCL12', *Bioscience Reports*, 40(1), pp. 1–12. doi: 10.1042/BSR20193267.

126. Li, W., Nieman, M. and Sen Gupta, A. (2016) 'Ferric chloride-induced murine thrombosis models', *Journal of Visualized Experiments*, 2016(115), pp. 1–12. doi: 10.3791/54479.

127. Li, Y. F. *et al.* (2015) 'Endothelial progenitor cells in ischemic stroke: An exploration from hypothesis to therapy', *Journal of Hematology and Oncology*. ???, 8(1), pp. 1–17. doi: 10.1186/s13045-015-0130-8.

128. Li, Z. and Cui, Z. (2014) 'Three-dimensional perfused cell culture', *Biotechnology*

Advances. Elsevier Inc., 32(2), pp. 243–254. doi: 10.1016/j.biotechadv.2013.10.006.

129. Libby, P. *et al.* (2019) 'Atherosclerosis', *Nature Reviews Disease Primers*, 5(1), pp. 1–18. doi: 10.1038/s41572-019-0106-z.

130. Libby, P. and Theroux, P. (2005) 'Pathophysiology of coronary artery disease', *Circulation*, 111(25), pp. 3481–3488. doi: 10.1161/CIRCULATIONAHA.105.537878.

131. Liesveld, J. L., Sharma, N. and Aljitawi, O. S. (2020) 'Stem cell homing: From physiology to therapeutics', *Stem Cells*, 38(10), pp. 1241–1253. doi: 10.1002/stem.3242.

132. Lillis, A. P. *et al.* (2015) 'LDL receptor-related protein-1 (LRP1) regulates cholesterol accumulation in macrophages', *PLoS ONE*. Public Library of Science, 10(6). doi: 10.1371/journal.pone.0128903.

133. Lin, Y. T. *et al.* (2016) 'Visfatin promotes foam cell formation by dysregulating CD36, SRA, ABCA1, and ABCG1 expression in RAW264.7 macrophages', *Shock*, 45(4), pp. 460–468. doi: 10.1097/SHK.0000000000000529.

134. Linton, M. F. *et al.* (2019) 'The role of lipoproteins in atherogenesis', in. Available at: https://www.ncbi.nlm.nih.gov/books/NBK343489/.

135. Lisek, M., Zylinska, L. and Boczek, T. (2020) 'Ketamine and calcium signaling—a crosstalk for neuronal physiology and pathology', *International Journal of Molecular Sciences*, 21(21), pp. 1–26. doi: 10.3390/ijms21218410.

136. Liu, X. *et al.* (2011) 'SDF-1/CXCR4 axis modulates bone marrow mesenchymal stem cell apoptosis, migration and cytokine secretion', *Protein and Cell*, 2(10), pp. 845–854. doi: 10.1007/s13238-011-1097-z.

137. Liu, Y. *et al.* (2012) 'Beneficial effects of statins on endothelial progenitor cells', *American Journal of the Medical Sciences*. Lippincott Williams and Wilkins, pp. 220–226. doi: 10.1097/MAJ.0b013e31824998f9.

138. Liu, Y. C. *et al.* (2014) 'Macrophage polarization in inflammatory diseases', *International Journal of Biological Sciences*, 10(5), pp. 520–529. doi: 10.7150/ijbs.8879.

139. Liu, Z. J. *et al.* (2016) 'SDF-1α-induced dual pairs of E-selectin/ligand mediate endothelial progenitor cell homing to critical ischemia', *Scientific Reports*. Nature Publishing Group, 6(July), pp. 1–11. doi: 10.1038/srep34416.

140. Lovett, M. *et al.* (2009) 'Vascularization Strategies for Tissue Engineering', *Tissue Engineering Part B: Reviews*, 15(3), pp. 353–370. doi: 10.1089/ten.teb.2009.0085.

141. Luo, J. *et al.* (2018) 'Nitric oxide functions in stromal cell-derived factor-1-induced cytoskeleton changes and the migration of Jurkat cells', *Oncology Letters*. Spandidos Publications, 16(5), pp. 6685–6690. doi: 10.3892/ol.2018.9429.

142. Luo, Y. *et al.* (2017) 'Macrophagic CD146 promotes foam cell formation and retention during atherosclerosis', *Cell Research*. Nature Publishing Group, 27(3), pp. 352–372. doi: 10.1038/cr.2017.8.

143. Lusis, A. J. (2000) 'Atherosclerosis', *Nature*, 407(6801), pp. 233–241. doi: 10.1038/35025203.

144. Maan, R., Menon, G. I. and Pullarkat, P. A. (2017) 'Quantifying cell adhesion dynamics using a custom-made fluid shear device: experiments and model', *bioRxiv*. Available at: https://www.biorxiv.org/content/early/2017/07/21/166371.

145. Maeng, Y. S. *et al.* (2009) 'Endothelial progenitor cell homing: Prominent role of the IGF2-IGF2R-PLC 22 axis', *Blood*. Â© 2009 by The American Society of Hematology, 113(1), pp. 233–243. doi: 10.1182/blood-2008-06-162891.

146. Mahmoud, M. M. *et al.* (2016) 'TWIST1 integrates endothelial responses to flow in vascular dysfunction and atherosclerosis', *Circulation Research*, 119(3), pp. 450–462. doi: 10.1161/CIRCRESAHA.116.308870.

147. Malek, A. M., Alper, S. L. and Izumo, S. (1999) 'Hemodynamic shear stress and its role in atherosclerosis', *Journal of the American Medical Association*, 282(21), pp. 2035–2042. doi: 10.1001/jama.282.21.2035.

148. Mannarino, E. and Pirro, M. (2008) 'Endothelial injury and repair: A novel theory for

atherosclerosis', *Angiology*, 59(2_suppl), pp. 69S-72S. doi: 10.1177/0003319708320761.

149. Marchetti, V. (2015) 'Endothelial Progenitor Cells and Endothelial Cells', *Stemcell technologies*, (June), pp. 1–4.

150. Mayorga, M. E. *et al.* (2018) 'Role of SDF-1:CXCR4 in Impaired Post-Myocardial Infarction Cardiac Repair in Diabetes', *STEM CELLS Translational Medicine*. John Wiley and Sons Ltd., 7(1), pp. 115–124. doi: 10.1002/sctm.17-0172.

151. McLaren, J. E. and Ramji, D. P. (2009) 'Interferon gamma: A master regulator of atherosclerosis', *Cytokine and Growth Factor Reviews*. Pergamon, pp. 125–135. doi: 10.1016/j.cytogfr.2008.11.003.

152. Medina, R. J. *et al.* (2010) 'Outgrowth endothelial cells: Characterization and their potential for reversing ischemic retinopathy', *Investigative Ophthalmology and Visual Science*. The Association for Research in Vision and Ophthalmology, 51(11), pp. 5906–5913. doi: 10.1167/iovs.09-4951.

153. Medina, R. J. *et al.* (2017) 'Endothelial Progenitors: A Consensus Statement on Nomenclature', *STEM CELLS Translational Medicine*, 6(5), pp. 1316–1320. doi: 10.1002/sctm.16-0360.

154. Meiliana, A. and Wijaya, A. (2009) 'Endothelial Progenitor Cells in Diabetic Vasculopathy', *The Indonesian Biomedical Journal*, 1(2), p. 4. doi: 10.18585/inabj.v1i2.89.

155. Melchiorri, A. J. *et al.* (2016) 'In Vitro Endothelialization of Biodegradable Vascular Grafts Via Endothelial Progenitor Cell Seeding and Maturation in a Tubular Perfusion System Bioreactor', *Tissue Engineering - Part C: Methods*. Mary Ann Liebert Inc., 22(7), pp. 663–670. doi: 10.1089/ten.tec.2015.0562.

156. Michael A., G. J. and Guillermo, G.-C. (2016) 'Endothelial cell dysfunction and the pathobiology of atherosclerosis.', *Circulation Research*, 176(1), pp. 139–148. doi: 10.1161/CIRCRESAHA.115.306301.Endothelial.

157. Milstone, D. S. *et al.* (2000) 'E-selectin expression and stimulation by inflammatory

mediators are developmentally regulated during embryogenesis', *Laboratory Investigation*, 80(6), pp. 943–954. doi: 10.1038/labinvest.3780097.

158. Mobasheri, A. and Lewis, M. (2013) 'Tissue Engineered Animal Sparing Models for the Study of Joint and Muscle Diseases', *Regenerative Medicine and Tissue Engineering*, (January). doi: 10.5772/55563.

159. Molino, M. *et al.* (2000) 'CXCR4 on human endothelial cells can serve as both a mediator of biological responses and as a receptor for HIV-2', *Biochimica et Biophysica Acta - Molecular Basis of Disease*, 1500(2), pp. 227–240. doi: 10.1016/S0925-4439(99)00110-6.

160. Moore, K. J., Sheedy, F. J. and Fisher, E. A. (2013) 'Macrophages in atherosclerosis: A dynamic balance', *Nature Reviews Immunology*, pp. 709–721. doi: 10.1038/nri3520.

161. Moriya, J. (2019) 'Critical roles of inflammation in atherosclerosis', *Journal of Cardiology*. Japanese College of Cardiology, 73(1), pp. 22–27. doi: 10.1016/j.jjcc.2018.05.010.

162. Murray, P. J. *et al.* (2014) 'Macrophage Activation and Polarization: Nomenclature and Experimental Guidelines', *Immunity*. Elsevier, 41(1), pp. 14–20. doi: 10.1016/j.immuni.2014.06.008.

163. Musa, F. I., Harper, A. G. S. and Yang, Y. (2016) 'A Real-Time Monitoring System to Assess the Platelet Aggregatory Capacity of Components of a Tissue-Engineered Blood Vessel Wall', *Tissue Engineering - Part C: Methods*. Mary Ann Liebert Inc., 22(7), pp. 691–699. doi: 10.1089/ten.tec.2015.0582.

164. Nakagami, H. *et al.* (2006) 'Model of vasculogenesis from embryonic stem cells for vascular research and regenerative medicine', *Hypertension*, 48(1), pp. 112–119. doi: 10.1161/01.HYP.0000225426.12101.15.

165. Nakagawa, T. *et al.* (1998) 'Oxidized LDL increases and interferon-γ decreases expression of CD36 in human monocyte-derived macrophages', *Arteriosclerosis, Thrombosis, and Vascular Biology*, 18(8), pp. 1350–1357. doi: 10.1161/01.ATV.18.8.1350.

166. Nakagawa, T. *et al.* (2002) 'Ketamine suppresses platelet aggregation possibly by

suppressed inositol triphosphate formation and subsequent suppression of cytosolic calcium increase', *Anesthesiology*. American Society of Anesthesiologists, 96(5), pp. 1147–1152. doi: 10.1097/00000542-200205000-00018.

167. Nemeno-Guanzon, J. G. *et al.* (2012) 'Trends in tissue engineering for blood vessels', *Journal of Biomedicine and Biotechnology*, 2012. doi: 10.1155/2012/956345.

168. Nigro, P., Abe, J. I. and Berk, B. C. (2011) 'Flow shear stress and atherosclerosis: A matter of site specificity', *Antioxidants and Redox Signaling*, 15(5), pp. 1405–1414. doi: 10.1089/ars.2010.3679.

169. Njoroge, W. *et al.* (2021) 'The Combination of Tissue - Engineered Blood Vessel Constructs and Parallel Flow Chamber Provides a Potential Alternative to In Vivo Drug Testing Models', pp. 1–18.

170. Oikonomou, E. *et al.* (2015) 'Atorvastatin treatment improves endothelial function through endothelial progenitor cells mobilization in ischemic heart failure patients', *Atherosclerosis*. Elsevier Ireland Ltd, 238(2), pp. 159–164. doi: 10.1016/j.atherosclerosis.2014.12.014.

171. Oppi, S., Lüscher, T. F. and Stein, S. (2019) 'Mouse Models for Atherosclerosis Research—Which Is My Line?', *Frontiers in Cardiovascular Medicine*, 6(April), pp. 1–8. doi: 10.3389/fcvm.2019.00046.

172. Owida, H. A. *et al.* (2017) 'Co-culture of chondrons and mesenchymal stromal cells reduces the loss of collagen VI and improves extracellular matrix production', *Histochemistry and Cell Biology*. Springer Berlin Heidelberg, 148(6), pp. 625–638. doi: 10.1007/s00418-017-1602-4.

173. Pahan, K. (2006) 'Lipid-lowering drugs', *Cellular and Molecular Life Sciences*, 63(10), pp. 1165–1178. doi: 10.1007/s00018-005-5406-7.

174. Papaioannou, T. G. *et al.* (2019) '3D bioprinting methods and techniques: Applications on artificial blood vessel fabrication', *Acta Cardiologica Sinica*, 35(3), pp. 284–289. doi:

10.6515/ACS.201905_35(3).20181115A.

175. Papaioannou, T. G. and Stefanadis, C. (2005) 'Vascular wall shear stress: basic principles and methods.', *Hellenic journal of cardiology : HJC = Hellenike kardiologike epitheorese*, 46(1), pp. 9–15. Available at: http://www.ncbi.nlm.nih.gov/pubmed/15807389.

176. Park, D. W. *et al.* (2020) 'Ten-Year Outcomes after Drug-Eluting Stents Versus Coronary Artery Bypass Grafting for Left Main Coronary Disease: Extended Follow-Up of the PRECOMBAT Trial', *Circulation*, pp. 1437–1446. doi: 10.1161/CIRCULATIONAHA.120.046039.

177. Parvin Zafar, R. (2015) 'An insight into pathogenesis of cardiovascular diseases', *Journal of Integrative Cardiology*, 1(4), pp. 79–81. doi: 10.15761/jic.1000123.

178. Patton, K. T. and Thibodeau, G. A. (2018) *Anthony's Textbook of Anatomy & Physiology - E-Book*. Elsevier Health Sciences. Available at: https://books.google.co.za/books?id=_n1_DwAAQBAJ.

179. Pearson, J. D. (2000) 'Normal endothelial cell function', *Lupus*, 9(3), pp. 183–188. doi: 10.1191/096120300678828299.

180. Peng, S. *et al.* (2018) 'Atorvastatin inhibits inflammatory response, attenuates lipid deposition, and improves the stability of vulnerable atherosclerotic plaques by modulating autophagy', *Frontiers in Pharmacology*, 9(MAY), pp. 1–17. doi: 10.3389/fphar.2018.00438.

181. Peters, E. B. (2018) 'Endothelial Progenitor Cells for the Vascularization of Engineered Tissues', *Tissue Engineering - Part B: Reviews*. Mary Ann Liebert Inc., pp. 1–24. doi: 10.1089/ten.teb.2017.0127.

182. Petit, I., Jin, D. and Rafii, S. (2007) 'The SDF-1-CXCR4 signaling pathway: a molecular hub modulating neo-angiogenesis', *Trends in Immunology*. Howard Hughes Medical Institute, 28(7), pp. 299–307. doi: 10.1016/j.it.2007.05.007.

183. Pi, X. *et al.* (2014) 'NADPH oxidase-generated reactive oxygen species are required for stromal cell-derived factor-1α-stimulated angiogenesis', *Arteriosclerosis, Thrombosis, and Vascular Biology*, 34(9), pp. 2023–2032. doi: 10.1161/ATVBAHA.114.303733.

184. Di Pietro, N., Formoso, G. and Pandolfi, A. (2016) 'Physiology and pathophysiology of oxLDL uptake by vascular wall cells in atherosclerosis', *Vascular Pharmacology*, 84, pp. 1–7. doi: 10.1016/j.vph.2016.05.013.

185. Pinal-Fernandez, I., Casal-Dominguez, M. and Mammen, A. L. (2018) 'Statins: pros and cons', *Medicina Clínica*, 150(10), pp. 398–402. doi: 10.1016/j.medcli.2017.11.030.

186. Poay Sian Sabrina Lee and Kian Keong (2014) 'Endothelial progenitor cells and cardiovascular disease', *Journal of Stem Cells*. Nova Science Publishers, Inc., 9(2), pp. 93–106. doi: 10.4252/wjsc.v6.i3.355.

187. Polak, D. J. (2010) 'Regenerative medicine. Opportunities and challenges: A brief overview', *Journal of the Royal Society Interface*, 7(SUPPL. 6). doi: 10.1098/rsif.2010.0362.focus.

188. Prieto-Bermejo, R. *et al.* (2018) 'Reactive oxygen species in haematopoiesis: Leukaemic cells take a walk on the wild side', *Journal of Experimental and Clinical Cancer Research*. Journal of Experimental & Clinical Cancer Research, 37(1), pp. 1–18. doi: 10.1186/s13046-018-0797-0.

189. Qiu, G. and Hill, J. S. (2008) 'Atorvastatin Inhibits ABCA1 Expression and Cholesterol Efflux in THP-1 Macrophages by an LXR-dependent Pathway', *Journal of Cardiovascular Pharmacology*. doi: 10.1097/FJC.0b013e318167141f.

190. Qiu, L. *et al.* (2020) 'Activation of CXCR7 promotes endothelial repair and reduces the carotid atherosclerotic lesions through inhibition of pyroptosis signaling pathways', *Aging Cell*, 19(9), pp. 1–13. doi: 10.1111/acel.13205.

191. Rabito, M. J. and Kaye, A. D. (2013) 'Complementary and alternative medicine and cardiovascular disease: An evidence-based review', *Evidence-based Complementary and Alternative Medicine*, 2013. doi: 10.1155/2013/672097.

192. Rahaman, S. O. *et al.* (2006) 'A CD36-dependent signaling cascade is necessary for macrophage foam cell formation', *Cell Metabolism*, 4(3), pp. 211–221. doi:

10.1016/j.cmet.2006.06.007.

193. Rahbari, M. *et al.* (2017) 'H2O2 dynamics in the malaria parasite Plasmodium falciparum', *PLoS ONE*, 12(4). doi: 10.1371/journal.

194. Ramji, D. P. and Davies, T. S. (2015) 'Cytokines in atherosclerosis: Key players in all stages of disease and promising therapeutic targets', *Cytokine and Growth Factor Reviews*. Elsevier Ltd, 26(6), pp. 673–685. doi: 10.1016/j.cytogfr.2015.04.003.

195. Ratajczak, M. Z. *et al.* (2006) 'The pleiotropic effects of the SDF-1–CXCR4 axis in organogenesis, regeneration and tumorigenesis', *Leukemia*, 20(11), pp. 1915–1924. doi: 10.1038/sj.leu.2404357.

196. Ravishankar, P., Zeballos, M. A. and Balachandran, K. (2017) 'Isolation of endothelial progenitor cells from human umbilical cord blood', *Journal of Visualized Experiments*, 2017(127), pp. 1–9. doi: 10.3791/56021.

197. Reid, V. C. and Mitchinson, M. J. (1993) 'Toxicity of oxidised low density lipoprotein towards mouse peritoneal macrophages in vitro', *Atherosclerosis*, 98(1), pp. 17–24. doi: 10.1016/0021-9150(93)90219-K.

198. Reiss, A. B. *et al.* (2004) 'Interferon-γ impedes reverse cholesterol transport and promotes foam cell transformation in THP-1 human monocytes/macrophages', *Medical Science Monitor*, 10(11), pp. 420–425.

199. Renna, N. F. *et al.* (2017) 'Vascular Repair and Remodeling: A Review', *Physiologic and Pathologic Angiogenesis - Signaling Mechanisms and Targeted Therapy*. doi: 10.5772/67485.

200. Richardson, M. R. and Yoder, M. C. (2011) 'Endothelial progenitor cells: Quo Vadis?', *Journal of Molecular and Cellular Cardiology*. Academic Press, pp. 266–272. doi: 10.1016/j.yjmcc.2010.07.009.

201. Rios, F. J. O., Gidlund, M. and Jancar, S. (2011) 'Pivotal role for platelet-activating factor receptor in CD36 expression and oxLDL uptake by human monocytes/macrophages', *Cellular Physiology and Biochemistry*, 27(3–4), pp. 363–372. doi: 10.1159/000327962.

202. Ross, S. *et al.* (2015) 'Effect of Bile Acid Sequestrants on the Risk of Cardiovascular Events: A Mendelian Randomization Analysis', *Circulation: Cardiovascular Genetics*, 8(4), pp. 618–627. doi: 10.1161/CIRCGENETICS.114.000952.

203. Rozanski, A., Blumenthal, J. A. and Kaplan, J. (1999) 'Impact of psychological factors on the pathogenesis of cardiovascular disease and implications for therapy', *Circulation*, 99(16), pp. 2192–2217. doi: 10.1161/01.CIR.99.16.2192.

204. Ruiz-Velasco, N., Domínguez, A. and Vega, M. A. (2004) 'Statins upregulate CD36 expression in human monocytes, an effect strengthened when combined with PPAR-γ ligands Putative contribution of Rho GTPases in statin-induced CD36 expression', *Biochemical Pharmacology*, 67(2), pp. 303–313. doi: 10.1016/j.bcp.2003.09.006.

205. Rumin, J. *et al.* (2015) 'The use of fluorescent Nile red and BODIPY for lipid measurement in microalgae', *Biotechnology for Biofuels*. BioMed Central Ltd., p. 42. doi: 10.1186/s13068-015-0220-4.

206. Rüster, B. *et al.* (2006) 'Mesenchymal stem cells display coordinated rolling and adhesion behavior on endothelial cells', *Blood*, 108(12), pp. 3938–3944. doi: 10.1182/blood-2006-05-025098.

207. Sadowitz, B., Maier, K. G. and Gahtan, V. (2010) 'Basic science review: Statin therapy-part I: The pleiotropic effects of statins in cardiovascular disease', *Vascular and Endovascular Surgery*, pp. 241–251. doi: 10.1177/1538574410362922.

208. Sainz, J. and Sata, M. (2007) 'CXCR4, a key modulator of vascular progenitor cells', *Arteriosclerosis, Thrombosis, and Vascular Biology*. Lippincott Williams & Wilkins, pp. 263–265. doi: 10.1161/01.ATV.0000256727.34148.e2.

209. Sandhu, K., Mamas, M. and Butler, R. (2017) 'Endothelial progenitor cells: Exploring the pleiotropic effects of statins', *World Journal of Cardiology*. Baishideng Publishing Group Inc., 9(1), p. 1. doi: 10.4330/wjc.v9.i1.1.

210. Sashindranath, M. *et al.* (2019) 'The mode of anesthesia influences outcome in mouse

models of arterial thrombosis', *Research and Practice in Thrombosis and Haemostasis*, 3(2), pp. 197–206. doi: 10.1002/rth2.12184.

211. von Scheidt, M. *et al.* (2017) 'Applications and Limitations of Mouse Models for Understanding Human Atherosclerosis', *Cell Metabolism*. doi: 10.1016/j.cmet.2016.11.001.

212. Schmidt-Lucke, C. *et al.* (2010) 'Quantification of circulating endothelial progenitor cells using the modified ISHAGE Protocol', *PLoS ONE*, 5(11), pp. 1–7. doi: 10.1371/journal.pone.0013790.

213. Selden, C. and Fuller, B. (2018) 'Role of bioreactor technology in tissue engineering for clinical use and therapeutic target design', *Bioengineering*, 5(2), pp. 1–10. doi: 10.3390/bioengineering5020032.

214. Shah, T. Z. *et al.* (2013) 'Effect of nicotinic acid (vitamin B3 or niacin) on the lipid profile of diabetic and non - Diabetic rats', *Pakistan Journal of Medical Sciences*, 29(5), pp. 1259–1264. doi: 10.12669/pjms.295.4193.

215. Shimoni, S. *et al.* (2016) 'Circulating endothelial progenitor cells and clinical outcome in patients with aortic stenosis', *PLoS ONE*, 11(2), pp. 1–16. doi: 10.1371/journal.pone.0148766.

216. Shu, H. *et al.* (2020) 'The role of CD36 in cardiovascular disease', *Cardiovascular Research*, pp. 1–14. doi: 10.1093/cvr/cvaa319.

217. Silva, M., Videira, P. A. and Sackstein, R. (2018) 'E-selectin ligands in the human mononuclear phagocyte system: Implications for infection, inflammation, and immunotherapy', *Frontiers in Immunology*, 8(JAN). doi: 10.3389/fimmu.2017.01878.

218. Sima, A. V., Stancu, C. S. and Simionescu, M. (2009) 'Vascular endothelium in atherosclerosis', *Cell and Tissue Research*, 335(1), pp. 191–203. doi: 10.1007/s00441-008-0678-5.

219. Sirtori, C. R. (2014) 'The pharmacology of statins', *Pharmacological Research*. Elsevier Ltd, 88, pp. 3–11. doi: 10.1016/j.phrs.2014.03.002.

220. Smith, H. *et al.* (2018) 'Interactions of helminths with macrophages: therapeutic potential for inflammatory intestinal disease', *Expert Review of Gastroenterology and Hepatology*. Taylor & Francis, 12(10), pp. 997–1006. doi: 10.1080/17474124.2018.1505498.

221. Sobti, N. *et al.* (2018) 'Evaluation of acellular dermal matrix efficacy in prosthesis-based breast reconstruction', *Plastic and Reconstructive Surgery*, 141(3), pp. 541–549. doi: 10.1097/PRS.0000000000004109.

222. Solanki, A., Bhatt, L. K. and Johnston, T. P. (2018) 'Evolving targets for the treatment of atherosclerosis', *Pharmacology and Therapeutics*. Elsevier Inc., 187, pp. 1–12. doi: 10.1016/j.pharmthera.2018.02.002.

223. Song, H. H. G. *et al.* (2018) 'Vascular Tissue Engineering: Progress, Challenges, and Clinical Promise', *Cell Stem Cell*. Elsevier Inc., 22(3), pp. 340–354. doi: 10.1016/j.stem.2018.02.009.

224. Song, L. *et al.* (2013a) 'Atorvastatin Enhance Efficacy of Mesenchymal Stem Cells Treatment for Swine Myocardial Infarction via Activation of Nitric Oxide Synthase', *PLoS ONE*. Public Library of Science, 8(5). doi: 10.1371/journal.pone.0065702.

225. Song, L. *et al.* (2013b) 'Atorvastatin Enhance Efficacy of Mesenchymal Stem Cells Treatment for Swine Myocardial Infarction via Activation of Nitric Oxide Synthase', *PLoS ONE*, 8(5), pp. 1–12. doi: 10.1371/journal.pone.0065702.

226. Stancu, C. and Sima, A. (2001) 'Statins: Mechanism of action and effects', *Journal of Cellular and Molecular Medicine*. Journal of Cellular and Molecular Medicine, 5(4), pp. 378–387. doi: 10.1111/j.1582-4934.2001.tb00172.x.

227. Stefani, I. *et al.* (2018) 'A double chamber rotating bioreactor for enhanced tubular tissue generation from human mesenchymal stem cells: a promising tool for vascular tissue regeneration', *Journal of Tissue Engineering and Regenerative Medicine*, 12(1), pp. e42–e52. doi: 10.1002/term.2341.

228. Sugiyama, M. *et al.* (2005) 'Effects of atorvastatin on inflammation and oxidative

stress', *Heart and Vessels*, 20(4), pp. 133–136. doi: 10.1007/s00380-005-0833-9.

229. Toh, Y. C. *et al.* (2007) 'A novel 3D mammalian cell perfusion-culture system in microfluidic channels', *Lab on a Chip*, 7(3), pp. 302–309. doi: 10.1039/b614872g.

230. Toulassi, I. A. *et al.* (2021) 'A Paradigm Shift in the Management of Atherosclerosis: Protective Role of Sirtuins in Atherosclerosis', *Cureus*, 13(1), pp. 1–9. doi: 10.7759/cureus.12735.

231. Tresoldi, C. *et al.* (2019) 'Shear-resistant hydrogels to control permeability of porous tubular scaffolds in vascular tissue engineering', *Materials Science and Engineering C*. Elsevier, 105(July), p. 110035. doi: 10.1016/j.msec.2019.110035.

232. Truskey, G. A. and Pirone, J. S. (1990) 'The effect of fluid shear stress upon cell adhesion to fibronectin-treated surfaces', *Journal of Biomedical Materials Research*, 24(10), pp. 1333–1353. doi: 10.1002/jbm.820241006.

233. Tucker, R. P. *et al.* (2014) 'See-saw rocking: An in vitro model for mechanotransduction research', *Journal of the Royal Society Interface*, 11(97). doi: 10.1098/rsif.2014.0330.

234. Urbich, C. and Dimmeler, S. (2004) 'Endothelial progenitor cells: Characterization and role in vascular biology', *Circulation Research*, pp. 343–353. doi: 10.1161/01.RES.0000137877.89448.78.

235. Varghese, J. F., Patel, R. and Yadav, U. C. S. (2017) 'Novel Insights in the Metabolic Syndrome-induced Oxidative Stress and Inflammation-mediated Atherosclerosis', *Current Cardiology Reviews*, 14(1), pp. 4–14. doi: 10.2174/1573403x13666171009112250.

236. Voloshyna, I., Littlefield, M. J. and Reiss, A. B. (2014) 'Atherosclerosis and interferon-γ: New insights and therapeutic targets', *Trends in Cardiovascular Medicine*, 24(1), pp. 45–51. doi: 10.1016/j.tcm.2013.06.003.

237. Wagenseil, J. E. and Mecham, R. P. (2009) 'Vascular ECM and arterial mechanics', *Physiological reviews*, 89(3), pp. 957–989. doi: 10.1152/physrev.00041.2008.Vascular.

238. Walter, D. H., Dimmeler, S. and Zeiher, A. M. (2004) 'Effects of Statins on Endothelium

and Endothelial Progenitor Cell Recruitment', *Seminars in Vascular Medicine*, 4(04), pp. 385–393. doi: 10.1055/s-2004-869595.

239. Wang, W. *et al.* (2013) 'HMG-CoA Reductase Inhibitors, Simvastatin and Atorvastatin, Downregulate ABCG1-mediated Cholesterol Efflux in Human Macrophages', *Journal of Cardiovascular Pharmacology*, 62(1), pp. 90–98. doi: 10.1097/FJC.0b013e3182927e7c.

240. Wang, Y. X. *et al.* (2016) 'A multi-component parallel-plate flow chamber system for studying the effect of exercise-induced wall shear stress on endothelial cells', *BioMedical Engineering Online*. BioMed Central, 15(s2), pp. 659–672. doi: 10.1186/s12938-016-0273-z.

241. Whitman, S. C. *et al.* (2000) 'Exogenous interferon-γ enhances atherosclerosis in apolipoprotein E-/- mice', *American Journal of Pathology*. American Society for Investigative Pathology, 157(6), pp. 1819–1824. doi: 10.1016/S0002-9440(10)64820-1.

242. Williams, P. A. and Silva, E. A. (2015) 'The Role of Synthetic Extracellular Matrices in Endothelial Progenitor Cell Homing for Treatment of Vascular Disease', *Annals of Biomedical Engineering*, 43(10), pp. 2301–2313. doi: 10.1007/s10439-015-1400-x.

243. Wiśniewski, A. *et al.* (2020) 'Endothelial Progenitor Cells as a Marker of Vascular Damage But not a Predictor in Acute Microangiopathy-Associated Stroke', *Journal of Clinical Medicine*, 9(7), p. 2248. doi: 10.3390/jcm9072248.

244. Wong, A. K. *et al.* (2016) 'A Parallel-Plate Flow Chamber for Mechanical Characterization of Endothelial Cells Exposed to Laminar Shear Stress', *Cellular and Molecular Bioengineering*, 9(1), pp. 127–138. doi: 10.1007/s12195-015-0424-5.

245. Woollard, K. J. *et al.* (2009) 'Erythrocyte hemolysis and hemoglobin oxidation promote ferric chloride-induced vascular injury', *Journal of Biological Chemistry*. Â© 2009 ASBMB. Currently published by Elsevier Inc; originally published by American Society for Biochemistry and Molecular Biology., 284(19), pp. 13110–13118. doi: 10.1074/jbc.M809095200.

246. Xu, H. *et al.* (2019) 'Vascular Macrophages in Atherosclerosis', *Journal of Immunology Research*, 2019, pp. 1–14. doi: 10.1155/2019/4354786.

247. Xu, J. *et al.* (2017) 'Vascular CXCR4 expression promotes vessel sprouting and sensitivity to sorafenib treatment in hepatocellular carcinoma', *Clinical Cancer Research*, 23(15), pp. 4482–4492. doi: 10.1158/1078-0432.CCR-16-2131.

248. Xu, L. *et al.* (2019) 'Atorvastatin blocks advanced glycation end products induced reduction in macrophage cholesterol efflux mediated with ATP-binding cassette transporters G 1', *Circulation Journal*, 83(9), pp. 1954–1964. doi: 10.1253/circj.CJ-19-0153.

249. Yang, Y., Wimpenny, I. and Ahearne, M. (2011) 'Portable nanofiber meshes dictate cell orientation throughout three-dimensional hydrogels', *Nanomedicine: Nanotechnology, Biology, and Medicine*. Elsevier Inc., 7(2), pp. 131–136. doi: 10.1016/j.nano.2010.12.011.

250. Yoder, M. C. (2012) 'Human endothelial progenitor cells', *Cold Spring Harbor Perspectives in Medicine*. Cold Spring Harbor Laboratory Press. doi: 10.1101/cshperspect.a006692.

251. Young, J. L., Libby, P. and Schönbeck, U. (2002) 'Cytokines in the pathogenesis of atherosclerosis', *Thrombosis and Haemostasis*, 88(4), pp. 554–567. doi: 10.1055/s-0037-1613256.

252. Yu, H. and Feng, Y. (2008) 'The potential of statin and stromal cell-derived factor-1 to promote angiogenesis', *Cell Adhesion & Migration*, 2(4), pp. 254–257. doi: 10.4161/cam.2.4.6818.

253. Yu, X. H. *et al.* (2015) 'Interferon-γ in foam cell formation and progression of atherosclerosis', *Clinica Chimica Acta*. Elsevier B.V., 441, pp. 33–43. doi: 10.1016/j.cca.2014.12.007.

254. Zeman, M. *et al.* (2015) 'Niacin in the treatment of hyperlipidemias in light of new clinical trials: Has niacin lost its place?', *Medical Science Monitor*, 21, pp. 2156–2162. doi: 10.12659/MSM.893619.

255. Zhang, M., Malik, A. B. and Rehman, J. (2014a) 'Endothelial progenitor cells and vascular repair', *Current Opinion in Hematology*. Lippincott Williams and Wilkins, pp. 224–228.

doi: 10.1097/MOH.0000000000000041.

256. Zhang, M., Malik, A. B. and Rehman, J. (2014b) 'Endothelial progenitor cells and vascular repair', *Current Opinion in Hematology*, 21(3), pp. 224–228. doi: 10.1097/MOH.0000000000000041.

257. Zhang, Q. *et al.* (2014) 'Atorvastatin treatment improves the effects of mesenchymal stem cell transplantation on acute myocardial infarction: The role of the RhoA/ROCK/ERK pathway', *International Journal of Cardiology*, 176(3), pp. 670–679. doi: 10.1016/j.ijcard.2014.07.071.

258. Zhao, J. *et al.* (2016) 'Disrupted Endothelial Cell Layer and Exposed Extracellular Matrix Proteins Promote Capture of Late Outgrowth Endothelial Progenitor Cells', *Stem Cells International*, 2016. doi: 10.1155/2016/1406304.

259. Zhao, P. *et al.* (2018) 'Fabrication of scaffolds in tissue engineering: A review', *Frontiers of Mechanical Engineering*, 13(1), pp. 107–119. doi: 10.1007/s11465-018-0496-8.

260. Zhao, Y., Vanhoutte, P. M. and Leung, S. W. S. (2015) 'Vascular nitric oxide: Beyond eNOS', *Journal of Pharmacological Sciences*. Elsevier Ltd, 129(2), pp. 83–94. doi: 10.1016/j.jphs.2015.09.002.

261. Zhao, Z. *et al.* (2018) 'Naringin enhances endothelial progenitor cell (EPC) proliferation and tube formation capacity through the CXCL12/CXCR4/PI3K/Akt signaling pathway', *Chemico-Biological Interactions*. Elsevier Ireland Ltd, 286, pp. 45–51. doi: 10.1016/j.cbi.2018.03.002.

262. Zheng, Shuzhan MD, P. *et al.* (2020) 'Atorvastatin enhances foam cell lipophagy and promotes cholesterol efflux through the AMPK/mTOR pathway', *Journal of Cardiovascular Pharmacology*. doi: 10.1097/FJC.0000000000000942.

263. Zhou, X. *et al.* (2010) 'Quantifying fluid shear stress in a rocking culture dish', *Journal of Biomechanics*, 43(8), pp. 1598–1602. doi: 10.1016/j.jbiomech.2009.12.028.